

Numerical Analyses of Liquefaction-Induced Building Settlement

By

Roberto Xavier Luque Nuques

A dissertation submitted in partial satisfaction of the
requirements for the degree of
Doctor in Philosophy

in

Engineering – Civil and Environmental Engineering

in the

Graduate Division

of the

University of California, Berkeley

Committee in charge:

Professor Jonathan D. Bray, Chair
Professor Raymond B. Seed
Professor Douglas S. Dreger

Summer 2017

Abstract

Numerical Analyses of Liquefaction-Induced Building Settlement

By

Roberto Xavier Luque Nuques

Doctor in Philosophy - Civil and Environmental Engineering

University of California, Berkeley

Professor Jonathan D. Bray, Chair

Liquefaction-induced settlement of shallow-founded buildings continues to produce significant damage during earthquakes. The state-of-the-practice for estimating liquefaction-induced settlements relies on simplified procedures that do not capture the important shear-induced mechanisms that often control structural settlements. Consequently, building settlement is often underestimated. Performance-based design requires an improved assessment of liquefaction-induced building settlement. Nonlinear dynamic soil-structure-interaction (SSI) effective stress analyses can capture shear-induced liquefaction building settlement mechanisms. However, they are not commonly used in engineering practice due to their lack of validation. Well-documented field case histories of building performance at sites with liquefiable soil provide the opportunity to validate available analytical tools. In this study, five significant buildings with shallow foundations affected by 2010-2011 Canterbury earthquake sequence are back-analyzed to evaluate the capabilities of dynamic SSI effective stress analysis and to gain insights into the mechanisms controlling liquefaction-induced building settlement.

Before the back-analyses of field case histories are performed, 36 model case histories of structural performance from a series of geotechnical centrifuge experiments are analyzed. The centrifuge experiments provide a wealth of quantitative time-varying parameters (e.g., pore water pressure, acceleration, and displacements) for detailed examination of the capabilities of the employed analytical model and procedures. The free-field responses measured in the centrifuge experiments are captured well in the numerical analyses, especially in terms of acceleration-time histories and pore water pressure generation during strong shaking. The analyses also captured liquefaction-induced building settlement in the centrifuge experiments reasonably well, although there was a tendency for it to overestimate the amount of measured building settlement. The tendency for and amount of overestimation were greater for cases in which the ground motions induced relatively small settlements (< 200 mm).

Although the field case histories contain significantly more uncertainty in terms of the earthquake ground motions, soil properties, and structural response than the centrifuge

experiments, they provide important insights not captured commonly in the centrifuge experiments (e.g., effects of sediment ejecta, variable ground conditions, and naturally deposited soil). Importantly, advanced analytical methods will not be employed in engineering practice until they can be shown to capture key aspects of building performance during earthquakes in the field. Thus, the primary objective of this research effort is to perform back-analyses of well documented case histories of liquefaction-induced building settlement in the Central Business District (CBD) of Christchurch, New Zealand. The Christchurch case histories include vast amounts of detailed information about the earthquake ground motions, site characterization, structural configurations, and observed seismic performance. Back-analyses were performed for three events of the Canterbury sequence of earthquakes: (1) the 4-SEP-2010 M_w 7.1 Darfield earthquake that produced peak ground accelerations (PGA) in the CBD of 0.16-0.28 g, (2) the 22-FEB-2011 M_w 6.2 Christchurch earthquake that produced PGAs of 0.35-0.55 g in the CBD, and (3) the 13-JUN-2011 M_w 6.0 earthquake that produced PGAs of 0.18-0.30 g in the CBD. In addition to having different intensities of strong shaking, the earthquakes also produced ground motions with different frequency contents and significant durations. The careful documentation of the effects of a sequence of three major earthquakes on the ground and structures in a modern city is unprecedented. Hence, these field case histories represent a unique opportunity to evaluate the capabilities of advanced numerical simulations of liquefaction effects on buildings.

The field case histories analyzed in this study consist of multi-story buildings with shallow foundations over soil deposits which include soil layers prone to liquefaction. Site-specific cone penetration tests (CPT) and laboratory test data, especially for loose-to-medium dense soil units that control the seismic response of the ground and building, are essential in refining the calibration of the PM4Sand model. Understanding site geology is also critically important when developing the FLAC model. The CPT investigations confirmed that shallowly buried streams were beneath parts of some of the buildings. Thus, the buried stream channels had to be included in the heterogeneous soil profiles modelled in the back-analyses. During the model calibration process, the free-field ground response was shown to compare well with field observations and the results of established simplified procedures in terms of pore water pressure ratios, shear strains, and factors of safety against liquefaction. The 5%-damped acceleration response spectra for the motions calculated at the ground surface also compared favorably with the response spectra of the nearby recorded free-field motions.

The CTUC building was a reinforced-concrete, six-story structure founded on footings connected with tie-beams. The site conditions include a buried stream that crosses underneath a corner of the building where most of the damaged was observed. Analyses show that the building underwent a bearing capacity-type of failure during the Christchurch earthquake, which led to significant differential settlement whose magnitude was consistent with field observations. The FTG-7 building was a moment resisting steel-frame structure founded on strip footings in one direction that were tied together with grade beams in the other direction. The soil deposit has fairly uniform, thick liquefiable layers. After the earthquakes, differential settlement, tilting, and structural damage were observed. The analyses indicated that SSI-induced ratcheting is the primary mode of deformation, which is observed by the rocking of the building's perimeter columns moving vertically in opposite directions during the same cycle of loading. The PWC building and CTH auditorium, which are located close to the Avon river, are also analyzed. Having a free-face near the structures added lateral and vertical movements associated with lateral spreading. The performance of the PWC building is influenced by several factors including the shape of the basement, a medium dense sandy soil layer located close to the base of

the foundation, lateral movements towards the river, etc. The performance of the CTH building was affected by shear-induced settlements that produced differential settlement of adjacent columns, as well as soil-ejecta-induced and volumetric-induced settlements, and vertical movements resulting from lateral spreading. For these two buildings, a single controlling mechanism is not clearly identified; it is likely that the observed building movements resulted from a combination of ground deformation mechanisms. In the last case, the difference in weight and bearing pressures of each side of the C building in the west and east direction and the unintended consequence of soil improvement due to installing tie-downs to resist static buoyant water pressures under the western part of the facility that did not have a structure atop of the basement caused differential settlement that induced structural cracking of some elements. The nonlinear dynamic SSI effective stress analyses were able to capture the tendencies of the basement mat to uplift on its western end and to settle on its eastern end.

Good agreement between the calculated and measured building settlements was obtained for these buildings for the Christchurch earthquake, which shook them most intensely. The analyses overestimated building settlements for the lower intensity Darfield and 13-JUN-11 earthquakes. The overestimation of building settlements for the Darfield earthquake was relatively minor. The overestimation of building settlements for the 13-JUN-11 event was more significant, and it was judged to occur because the analyses overestimated the free-field response recorded at nearby strong motion stations for this event.

The back-analyses of field case histories provide valuable insights into the mechanisms causing liquefaction-induced building settlements. The satisfactory comparison of the calculated and measured responses provides confidence in the use of nonlinear dynamic SSI effective stress analyses as a decision-making tool in performance-based design. One of the shortcomings of these continuum-based analyses of liquefaction-related phenomena is their inability to capture the effects of soil ejecta.

TABLE OF CONTENTS

ABSTRACT.....	1
TABLE OF CONTENTS.....	i
ACKNOWLEDGEMENTS.....	v
CHAPTER 1: INTRODUCTION.....	1
1.1. OVERVIEW	1
1.2. PREVIOUS RESEARCH.....	1
1.3. ORGANIZATION	3
CHAPTER 2: DYNAMIC SOIL-STRUCTURE INTERACTION ANALYSES OF CENTRIFUGE EXPERIMENTS WITH SHALLOW FOUNDED STRUCTURES ON LIQUEFIABLE SOILS	5
2.1. INTRODUCTION	5
2.2. PREVIOUS RESEARCH	5
2.3. CENTRIFUGE TESTING OVERVIEW.....	6
2.4. NUMERICAL MODEL.....	7
2.4.1. Model Construction and Boundary Conditions.....	7
2.4.2. PM4Sand constitutive model: Brief Description	8
2.4.3. Calibration process.....	9
2.4.4. Modeling of the structures.....	11
2.5. FREE-FIELD RESPONSE	12
2.6. BUILDING RESPONSE	13
2.7. SUMMARY OF RESULTS	13
2.8. CONCLUSIONS.....	14
CHAPTER 3: DYNAMIC ANALYSES OF TWO BUILDINGS FOUNDED ON LIQUEFIABLE SOILS DURING THE CANTERBURY EARTHQUAKE SEQUENCE.....	30
3.1. INTRODUCTION	30
3.2. EARTHQUAKE GROUND SHAKING.....	31
3.3. SITES DESCRIPTIONS AND PERFORMANCE OBSERVATIONS	32
3.3.1. CTUC Building.....	32

3.3.1.1.	Building Description.....	32
3.3.1.2.	Site Conditions	33
3.3.1.3.	Seismic Performance	34
3.3.2.	FTG-7 Building.....	34
3.3.2.1.	Building Description.....	34
3.3.2.2.	Site Conditions	35
3.3.2.3.	Seismic Performance	35
3.4.	CALIBRATION OF THE CONSTITUTIVE MODEL	36
3.5.	FREE-FIELD RESPONSE ANALYSES	38
3.6.	BUILDING RESPONSE ANALYSES	39
3.6.1.	General	39
3.6.2.	CTUC Building	39
3.6.3.	FTG-7 Building.....	41
3.7.	CONCLUSIONS.....	42
CHAPTER 4: DYNAMIC SOIL-STRUCTURE INTERACTION ANALYSES OF TWO IMPORTANT STRUCTURES AFFECTED BY LIQUEFACTION DURING THE CANTERBURY EARTHQUAKE SEQUENCE		62
4.1.	INTRODUCTION	62
4.2.	CANTERBURY EARTHQUAKE SEQUENCE	63
4.2.1.	Earthquake ground shaking in Christchurch	63
4.2.3.	Input ground motions	63
4.3.	STRUCTURE & SITE DESCRIPTIONS AND PERFORMANCE OBSERVATIONS..	64
4.3.1.	PWC building.....	64
4.3.1.1.	Building description	64
4.3.1.2.	Site conditions	65
4.3.1.3.	Seismic performance	66
4.3.2.	CTH auditorium	67
4.3.2.1.	Building description	67
4.3.2.2.	Site conditions	68
4.3.2.3.	Seismic performance	68
4.4.	NUMERICAL ANALYSES OF THE PWC AND CTH BUILDINGS	69

4.4.1.	General considerations	69
4.4.2.	Calibration of the constitutive model	71
4.4.3.	Building response	72
4.4.3.1.	PWC building	73
4.4.3.2.	CTH auditorium.....	74
4.5.	CONCLUSIONS.....	75
CHAPTER 5: SEISMIC PERFORMANCE OF A BUILDING AFFECTED BY MODERATE LIQUEFACTION DURING THE CHRISTCHURCH EARTHQUAKE.....		94
5.1.	INTRODUCTION	94
5.2.	LIQUEFACTION-INDUCED BUILDING MOVEMENTS	94
5.3.	BUILDING C CASE HISTORY DESCRIPTION	95
5.3.1.	Structural Configuration.....	95
5.3.2.	Subsurface Conditions.....	96
5.3.3.	Canterbury Earthquake Sequence and Ground Shaking	96
5.3.4.	Post-Canterbury Earthquake Sequence Condition	97
5.3.5.	Pre-Canterbury Earthquake Sequence Ground Movements.....	98
5.4.	EVALUATION OF LIQUEFACTION-INDUCED BUILDING MOVEMENTS	98
5.4.1.	Recommended Approach	98
5.4.2.	Liquefaction Triggering Assessment	99
5.4.3.	Liquefaction-Induced Reconsolidation Volumetric Settlements	100
5.4.4.	Sediment Ejecta-Induced Settlements.....	100
5.4.5.	Shear-Induced Settlements.....	101
5.4.6.	Simplified Liquefaction-Induced Building Settlement Assessment Summary	101
5.5.	DYNAMIC SOIL-STRUCTURE-INTERACTION (SSI) ANALYSIS	102
5.5.1.	Numerical Model.....	102
5.5.2.	Results	103
5.6.	OVERALL ASSESSMENT OF LIQUEFACTION-INDUCED BUILDING SETTLEMENT.....	104
5.7.	CONCLUSIONS.....	105
CHAPTER 6: CONCLUSIONS		125
6.1.	SUMMARY	125

6.2. FINDINGS.....	126
6.3. FUTURE RESEARCH.....	129
REFERENCES.....	131
Appendix A - Building “C”: Supporting information.....	138
Appendix A.1 - Building “C”: Subsurface Characterization Data.....	139
Appendix A.2 - Building “C”: Static Settlement Analyses.....	180
Appendix A.3 - Building “C”: Simplified Liquefaction Triggering and Volumetric-Induced Deformation Analyses.....	184
Appendix B - Condominium “Los Presidentes”: Case History Documentation.....	221
Appendix B.1. Introduction.....	222
Appendix B.2. Seismological and Ground Motions Aspects.....	222
Appendix B.3. Site Investigation.....	223
Appendix B.4. Description of the Buildings.....	224
Appendix B.5. Performance Observations and Analyses.....	225
Appendix B.6. Conclusions.....	226
Appendix B.7. References.....	226
Appendix C - Ground Motions for use in Numerical Soil-Structure-Interaction (SSI) Dynamic Analyses of case histories in Christchurch, New Zealand.....	245
Appendix C.1. Description of Procedure.....	246
Appendix C.2. Source Parameters for each Event.....	246
Appendix C.3. Site Parameters for each Site.....	247
Appendix C.4. Path Parameters: Source to Site Distance (R_{RUP}).....	247
Appendix C.5. Scaling Factor.....	247

ACKNOWLEDGEMENTS

This research has been funded by the National Secretary of Higher Education, Science and Technology (SENESCYT) from Ecuador. Additional funding was provided by the National Science Foundation (NSF) under award number CMMI-1332501. The financial support of both institutions, SENESCYT and NSF, is greatly appreciated. Any opinions, findings and conclusions or recommendations expressed in this thesis do not necessarily reflect the views of either SENESCYT or the NSF.

The support, encouragement, advice and lessons from my advisor, Prof. Jonathan Bray, were invaluable for this work to be completed, and I am very thankful for his valuable lessons during my years at Berkeley. Other professors in Berkeley helped shape my views not only on geotechnical and earthquake engineering but also as a person. I am very thankful to Prof. Raymond Seed, Prof. Juan Pestana, Prof. Nicholas Sitar, and Prof. Michel Riemer.

During these years in Berkeley, I have been fortunate enough to know many smart people, who now I am glad to call my friends. The support and friendship of Christopher Markham, Zee Beyzaei, Nathan Wagner, Michael Gardener, Julien Cohen-Weber, Jorge Macedo, Robert Lanzafame, Maggie Parks, Mike George, Stephan Garcia, and Chukwuebuka Nweke are greatly appreciated.

Although I quickly called Berkeley my home, being away from my home country and my family was not always easy. However, their continuous support was instrumental to my success. Both sides of our families were always supportive and helping us through every step of the way. Specifically, I would like to mention my parents for their tremendous support and encouragement.

Last but not least, I would like to thank my beautiful wife Fabiana. She has supported me entirely through this journey and without her, this achievement would literally not be possible. During our years at Berkeley, she gave me the two most beautiful gifts a man can receive, our beloved kids Obe and Fabi.

CHAPTER 1: INTRODUCTION

1.1. OVERVIEW

Recognizing the important effects of soil liquefaction on structures has been a critical part of advancing geotechnical earthquake engineering. The loss of bearing capacity due to soil liquefaction experienced by buildings in the 1964 Niigata earthquake is one of the most mentioned examples of the damaging effects of soil liquefaction. This earthquake, together with the 1964 Alaska earthquake, initiated important research and study of this phenomenon. Since 1964, several advancements have been achieved in the field of geotechnical earthquake engineering, including the evaluation of triggering, susceptibility of fined-grained or gravelly soils to liquefaction, estimation of liquefaction-induced free-field settlements, evaluation of lateral spreading, constitutive modeling of liquefaction, effects of liquefaction on piled foundations, etc. The effects of liquefaction on shallow-founded buildings have also been widely studied as will be described in the next section of this chapter. However, performance-based design requires advancements to better estimate liquefaction-induced settlements of buildings. The current state of the practice largely relies on estimating liquefaction-induced building movements using one-dimensional (1D) post-liquefaction reconsolidation empirical procedures as described by Ishihara and Yoshimine (1992), Tokimatsu and Seed (1987), and Zhang et al. (2002). However, these procedures do not take into account shear-induced movements which play an important role in building movements as explained by Dashti et al. (2010a,b). The alternative is to use numerical modeling to estimate the displacements for a structure at a site given a suite of acceleration-time histories for a specified earthquake scenario. This latter approach requires the use of an advanced constitutive model, which is able to reproduce liquefaction stress-strain behavior and pore water pressure generation. In this research, this approach is taken to back-analyze centrifuge experiments and selected case histories from Christchurch, New Zealand, where a sequence of earthquakes during 2010-2011 yielded different responses in several shallow-founded buildings on top of liquefiable soils.

1.2. PREVIOUS RESEARCH

Several approaches have been used for studying the effects of liquefaction on shallow-founded buildings. These approaches include the use of case histories, shaking table tests, centrifuge experiments, numerical modeling, or a combination of two or more approaches. Yoshimi and Tokimatsu (1977) combined observations from shaking table tests and field observations from the 1964 Niigata earthquake. They observed: (1) that the excess pore water pressure ratio beneath the structure was usually smaller than its value in the free-field, (2) that the pore water pressure ratio decreases as the weight of the structure increases, (3) that the settlements of the structure decreases as the width of the foundation increases, and (4) that a value of pore water pressure ratio (r_u) of 0.6 in the zone beneath the structure is sufficient for building settlement to increase sharply. They also were the first to publish their results in a plot of settlement ratio (observed settlement divided by the thickness of liquefiable layer) vs. building foundation width ratio (width of foundation divided by the thickness of liq. layer).

Based on the results of centrifuge testing, Whitman and Lambe (1982) agreed with the observations of Yoshimi and Tokimatsu (1977) but noted that “...*the complexity of the phenomena is evident in these new results and there is need to study the phenomenon of liquefaction-related settlement for a wider range of pertinent variables...*”

Ishi and Tokimatsu (1988), based on the work of Yoshimi and Tokimatsu (1977), presented a procedure for estimating liquefaction-induced displacements of buildings. They suggested that structures with foundation width ratios larger than about 2 to 3 suffered mainly volumetric strains and the settlements can be calculated using the Tokimatsu and Seed (1987) procedure. However, if the foundation width ratio is less than 2 or 3, the primary cause of settlements of the structure is shear deformation, and the settlement is calculated as the volumetric strain (estimated from the Tokimatsu and Seed (1987) procedure) multiplied by a scaling factor greater than one.

Rollins and Seed (1990) presented an extension to the simplified liquefaction procedure type of analyses, where the induced cyclic stress ratio (CSR) beneath the building is estimated as a function of the ratio of the spectral acceleration to the maximum ground surface acceleration (S_a/a_{max}) and compare it to the cyclic resistance ratio (CRR) to obtain a factor of safety that will be different from the one under free field conditions.

Liu (1995) proposed a simplified procedure to estimate liquefaction-induced displacements of buildings based on finite element analyses and observations from the 1964 Niigata, 1983 Nihonkai, 1976 Tangshan, 1975 Heichen, and 1966 Shintain earthquakes. Finite element analyses were performed of a site with a 15-m thick liquefiable layer overlying bedrock. The soil's relative density (D_R), building contact pressure (q), and width of foundation (B) were changed to study the effects of these parameters on the building settlement. A simplified formula was proposed based on the intensity of the ground motion (based on a Mercalli-type of intensity from China), width ratio, contact pressure, and relative density.

Liu and Dobry (1997) performed a series of centrifuge experiments to study the mechanism of liquefaction-induced settlement of shallow foundations and the effects of compaction under the foundation. They also discussed observations from the 1964 Niigata and 1990 Dagupan, Philippines earthquakes. The centrifuge experiments were performed on a 6-m thick, 50% relative density sand over bedrock. The results of these tests fell within the range of observed settlement ratios (S/H_L) in the previously mentioned earthquakes. Consequently, the authors noted that increasing the building's width ratio decreased the foundation settlement.

Hausler (2002) compiled case histories with different mitigation techniques and investigated through centrifuge experiments the effects that the depth and degree of soil improvement of the liquefiable material below the foundation had on building settlement. They found that for low levels of shaking, partial improvement of the liquefiable layer may be satisfactory. However, for strong shaking, leaving an unimproved liquefiable layer below the improved material can result in a high concentration of shear strains within the liquefied layer, which can lead to significant building settlement.

Dashti et al. (2010 a,b) performed a series of centrifuge experiments with different soil profile configurations (e.g., varying relative density, thickness of liquefiable layer, and fill material) where three single degree of freedom (SDOF) structures (with different widths, bearing pressures, and fixed-base periods) were shaken by different ground motions (with varying intensities, frequency contents, and durations). They also investigated the performance of one of the buildings with two mitigation techniques. The results helped to identify and understand the mechanisms involved in liquefaction-induced building settlement as well to validate observations

from previous studies. They found that the primary settlement mechanisms were: (1) volumetric strains as a result of partial drainage during strong shaking, sedimentation, and consolidation; and (2) deviatoric strains as a result of bearing capacity failure and SSI-induced building ratcheting. They also found that the normalization done in several of the previous studies (wherein building settlement and width were normalized by the thickness of the liquefiable layer) was not fundamentally correct, and some of the observed ranges in previous studies were unconservative for thin liquefiable layers.

Cetin et al. (2012) proposed a simplified way to estimate the induced cyclic stress ratio from the earthquake with the adding effect of the structure such that it can be used for liquefaction triggering in the stress-based liquefaction methodology. Unutmaz and Cetin (2012) took advantage of this methodology to estimate volumetric and deviatoric strains based on the cyclic stress ratios (considering the effects of the structure) estimated from their relationship and a capacity parameter ($N_{1,60,cs}$ for cohesionless soils and S_u , LL and PI for cohesive soils). Then the strains are integrated over depth to get the liquefaction-induced building settlements.

Karamitros et al. (2013a) performed a parametric study using sine waves with different amplitudes, periods, and numbers of cycles as input motions, several thicknesses of the liquefiable layer from 5 to 21 meters, and a rigid structure with different widths and bearing pressures. They proposed a formula for estimating liquefaction-induced building displacement based on the maximum ground surface acceleration, period of the ground motion, number of cycles, thickness of liquefiable layer, width of the building, and the degraded factor of safety. The procedure for estimating the degraded factor of is described in detail in a companion paper by Karamitros et al. (2013b).

Bertalot et al. (2013) compiled a database of building case histories from the 2010 Maule earthquake and analyzed the width of the foundation and its bearing pressure and compared them to the previous database from the Niigata and Luzon earthquakes. They showed that the Liu and Dobry (1997) type of approach (settlement ratio vs. width ratio) is not appropriate for cases with thin liquefiable layers as found in Concepcion, Chile. Their findings were more consistent with the results of the centrifuge experiments of Dashti et al. (2010 a,b). Bertalot and Brennan (2015) studied through centrifuge experiments the effects of stress distribution and bearing pressure on building settlement. They concluded that high bearing pressures and correspondingly high initial static shear stresses (i.e., high K_α values) will prevent stress reversal to occur, and thus, it will limit the pore water pressure generation (i.e., low r_u values) and the resulting building settlement.

1.3. ORGANIZATION

This thesis is organized in the following chapters:

- Chapter 2 describes the numerical analyses of a set of centrifuge experiments performed by different researchers over the past decade. All the experiments involved an isolated shallow-founded building over a non-liquefiable crust, followed by liquefiable sand and then a dense non-liquefiable layer to the base of the centrifuge model. The results of the numerical analyses are compared to the measurements in the centrifuge experiments, and key issues are discussed.
- Chapter 3 focuses on the dynamic numerical soil-structure interaction analyses of two multi-story shallow founded buildings located in Christchurch, New Zealand. These two buildings were severely damaged during the 2010-2011 Canterbury earthquake sequence

resulting in the demolition of the two buildings. The FTG-7 building is a 7-story steel-frame structure founded on reinforced concrete (RC) spread footings. The soil profile was fairly uniform throughout the building and it included loose silty sand layer (SM/ML) beneath the foundation that was found to be the main cause of the observed settlements. The CTUC building is a 6-story RC structure founded on RC isolated footings interconnected with grade beams. The soil profile beneath this building was not uniform because of the presence of an old-buried stream near the south of the building. This material was responsible for the significant damage that occurred in the southern zone of the building, which led to significant structural damage due to differential settlement. The results of numerical analyses of the two buildings for the three main earthquakes of the Canterbury earthquake sequence are discussed.

- Chapter 4 describes the numerical analyses of two landmark buildings in Christchurch, NZ, which suffered liquefaction-related damage. These two structures were also affected by lateral spreading, as they were close to the Avon River. This effect was also captured in the numerical model. The first structure is a 21-story RC building with one basement level and founded on a shallow mat foundation placed directly over a dense gravel. To the sides of the basement, a loose liquefiable sandy-silt material exists. Also, a medium dense gravelly sand layer was also found within the dense gravel beneath the mat foundation, which affected site and building performance. The second structure was also influenced by loose soils beneath its foundation.
- Chapter 5 describes a case history of a building with a one-story basement in Christchurch, New Zealand. The building and the site are described. Simplified and advanced finite element analyses are performed, and their results are compared to the observed performance.
- Chapter 6 provides a summary of the key findings presented in this research and provides recommendations for future research.
- Appendix A provides relevant information about Building "C", which is described in Chapter 5.
- Appendix B describes a case history of 4 identical buildings damaged by the 2010 Maule earthquake in Concepcion, Chile.
- Appendix C describes the method used for scaling the deconvolved ground motions for numerical analyses in the Christchurch Business District.

CHAPTER 2: DYNAMIC SOIL-STRUCTURE INTERACTION ANALYSES OF CENTRIFUGE EXPERIMENTS WITH SHALLOW FOUNDED STRUCTURES ON LIQUEFIABLE SOILS

2.1. INTRODUCTION

Liquefaction-induced settlement has caused severe damage in buildings in several earthquakes. The current state of the practice is to estimate liquefaction building movements using 1D post-liquefaction reconsolidation empirical procedures as described by Ishihara and Yoshimine (1992), Tokimatsu and Seed (1987), and Zhang et al. (2002). However, these procedures do not take into account shear-induced movements which play an important role in building movements as explained by Dashti et al. (2010 a,b). The other alternative is to use numerical modeling to estimate the displacements for the structure given a suite of acceleration-time histories for a specified earthquake scenario. This latter procedure requires the use of an advanced constitutive model that is able to reproduce liquefaction stress-strain behavior and pore water pressure generation. This approach has been used in this research to replicate results of centrifuge experiments involving SDOF structures founded on soils containing liquefiable layers with different thicknesses. The numerical simulations performed in this research includes some of the centrifuge experiments performed by Dashti et al. (2010 a,b) that were already modeled numerically by Dashti and Bray (2013) and Karimi and Dashti (2016 a,b), with additional cases from other centrifuges experiments, such as Almond and Kutter (2012, 2013), Zupan et al. (2013), and Hayden et al. (2014, 2015). The constitutive model PM4Sand Version 3 (Boulanger and Ziotopoulou, 2015), which is implemented in FLAC 7.0 (Itasca, 2009), was used.

2.2. PREVIOUS RESEARCH

Several approaches have been used for studying the effects of liquefaction on shallow-founded buildings. These approaches include the use of case histories, shaking table tests, centrifuge experiments, numerical modeling, or a combination of two or more approaches.

Yoshimi and Tokimatsu (1977) combined observations from shaking table tests and field observations from the Niigata earthquake, observing that the excess pore water pressure ratios beneath the structure are usually smaller than those in the free-field and that the settlement of the structure decreases with an increasing width of the foundation. They published their results in a plot of settlement ratio (observed settlement/thickness of liq. layer) vs. building foundation width ratio (width of foundation/thickness of liq. layer). Whitman and Lambe (1982) agreed with the observations of Yoshimi and Tokimatsu (1977) based on centrifuge test results, but noted that “...the complexity of the phenomena is evident in these new results and there is need to study the phenomenon of liquefaction-related settlement for a wider range of pertinent variables...”. Ishi and Tokimatsu (1988) presented a procedure for estimating liquefaction induced displacements on buildings that involved estimating volumetric strain multiplied by a scaling factor greater than one, when shear deformation controls the settlement. Rollins and Seed (1990) presented an extension of the simplified procedure for liquefaction evaluation taking into consideration the effects of the building on the seismic demand (i.e., cyclic stress ratio, CSR) as a function of the ratio of the spectral acceleration to the maximum ground surface acceleration (S_a/a_{max}). Liu

(1995) proposed a simplified procedure to estimate liquefaction-induced displacements on buildings based on the relative density, contact pressure and width of foundation, and the intensity of the motion.

Liu and Dobry (1997) performed a series of centrifuge experiments and validated their data with observations from past earthquakes. The results of their tests fell within the range of observed settlement ratios (S/H_L) in the 1964 Niigata and 1990 Dagupan earthquakes. They concluded that foundation settlement decreased with increasing width ratio (similar to the findings of Yoshimi and Tokimatsu (1977)). Dashti et al. (2010 a,b) performed a series of centrifuge experiments with several soil profile configurations and five different SDOF structures shaken by different earthquake motions. They found that the primary settlements mechanisms were: (1) volumetric strains as a result of partial drainage during strong shaking, sedimentation, and consolidation; and (2) deviatoric strains as a result of bearing capacity failure and SSI-induced building ratcheting. They also found that the previously described normalization (S/H_L) was not correct fundamentally. Building settlement is not just governed by the thickness of the liquefiable soil layer. Instead, shear-induced deformations govern for thin-layers of liquefiable soil. Cetin et al. (2012) and Unutmaz and Cetin (2012) proposed a simplified method to estimate the induced cyclic stress ratio from the earthquake, which included the effect of the structure. They then used that CSR to estimate shear and volumetric strains, and by integrating the strains, the liquefaction-induced building settlements could be obtained.

Using their results of numerical analyses, Karamitros et al. (2013a,b,c) proposed a formula for estimating liquefaction-induced building settlement based on the maximum ground surface acceleration, period of the ground motion, number of cycles, thickness of liquefiable layer, width of the building, and the degraded factor of safety. Bertalot et al. (2013) show that the Liu and Dobry (1997) type of approach (settlement ratio vs. foundation width ratio) is not appropriate for thin liquefiable layers as found in Concepcion, Chile, after the 2010 Maule earthquake. Bertalot and Brennan (2015) concluded that high bearing pressures and correspondingly high initial static shear stresses will prevent stress reversal to occur and thus it will limit pore water pressure generation and the foundation settlement.

Several researchers (e.g., Popescu and Prevost 1993, Elgamal 2005, Popescu et al. 2005, Lopez-Caballero and Farahmand-Razavi 2008, Shahir and Pak 2010, Adrianopoulos et al. 2010, Dashti and Bray 2013, Karamitros et al. 2013a,b,c, Karimi and Dashti 2016a,b) have used numerical analyses to replicate the results of centrifuge experiments involving liquefiable ground with a structure. They have used different numerical methods (finite element or finite difference methods), a wide variety of constitutive models and different modeling techniques for the structures (rigid structures, SDOF systems, or a surface load). They have been generally successful in capturing the key experimental observations with their numerical simulations.

2.3. CENTRIFUGE TESTING OVERVIEW

All centrifuge experiments that have been modeled in this research have been performed on the 9 m radius centrifuge at the Center for Geotechnical Modeling (CGM) facility at UC Davis at a centrifugal acceleration of 55 g. A summary of the centrifuge experiments that were modeled can be found in Allmond et al. (2014, 2015), where a new Foundation-Liquefaction Database (FLIQ) has been collected of centrifuge experiments involving structures on liquefiable sands. The centrifuge experiments modeled herein were performed by more than one researcher, each with different goals. As mentioned in the previous section, Dashti et al. (2010 a,b) investigated

liquefaction-induced building settlement mechanisms by modeling different shallow founded structures with different soil configurations, including an experiment with possible techniques to mitigate liquefaction-induced settlements. Almond and Kutter (2012, 2013) performed experiments to evaluate rocking foundations on liquefiable soils. Zupan et al. (2013) and Hayden et al. (2014, 2015) investigated structure-soil-structure interaction (SSSI) of adjacent structures, such as those found in city blocks. However, from the experiments of Zupan et al. (2013) and Hayden et al. (2014), only the cases of isolated buildings were analyzed in this study.

Dimensions and properties such as bearing pressure and fixed-base period are different for each building and are listed in Table 2.1. The soil configurations and layering of each centrifuge experiment is also different. The nomenclature adopted was the same as Allmond et al. (2015), which describes the thickness of the liquefiable layer and its relative density (e.g., T3-50 for an experiment with a 3-m thick liquefiable layer and a relative density of 50%). Table 2.2 summarizes the different soil configurations modeled in this study, relevant information for each soil layer, including which building was modeled in that particular configuration as well as which input ground motion was used in each configuration, and their intensity. Figure 2.1 shows the soil configuration of a typical test with the five buildings modeled in this study. The two ground motions used were the Port Island (PI) and TCU ground motions scaled at different amplitudes between 0.15 to 0.7g. The PI event refers to the motion recorded in the down-hole array at a depth of 83 m during the 1995 M_w 6.9 Kobe, Japan earthquake. The TCU ground was recorded in the TCU-078 station during 1999 M_w 7.6 Chi-Chi, Taiwan earthquake. Figure 2.2 shows the typical shape of the time history, normalized arias intensity and normalized response spectra at 5% structural damping for both ground motions.

2.4. NUMERICAL MODEL

2.4.1. Model Construction and Boundary Conditions

The base of the model was considered as a rigid base which is an appropriate condition for the rigid box subjected to the motions in the centrifuge experiments. The input ground motion was directly obtained from the accelerometers installed on the base of the centrifuge experiments. The sides of the model were attached to each other using FLAC's attach command to ensure equal horizontal movements of the lateral sides replicating the rigid container box from the centrifuge. Damping was provided through hysteretic damping from the constitutive model and also a small amount of typically 0.5 – 1.0 % Rayleigh damping was specified at an average frequency between the input ground motion and the fundamental site frequency. After each event, volumetric strains are expected to occur with a consequent increase in relative density, which was considered in the analyses. The basis for the increase on the relative density were found in Dashti (2009), who estimated the increase based on the amount of volumetric strain measured during shaking and it usually involved an increase of the relative density by 3 to 5% for the moderate ground motion levels and about 5 to 7% increase in relative density for large intensity motions. These values were typically adopted for the other centrifuge experiments different than from those from Dashti (2009). The element size was selected to be less than one tenth of the wavelength associated with the maximum frequency from the input motion, which usually yielded maximum length values of about 1 m but for the analyses the elements were typically modeled with length element sizes of about 0.5 m.

2.4.2. PM4Sand constitutive model: Brief Description

The user-defined model PM4Sand Version 3 (Boulanger and Ziotopoulou, 2015) was employed. The model follows the basic framework of the stress-ratio controlled, critical-state compatible, bounding surface plasticity model for sand presented by Dafalias and Manzari (2004). The model defines the critical state line in the D_R - p' space and uses the concept of the relative state parameter index (ξ_R), which is given in Equation 2.1.

$$\xi_R = D_{R,cs} - D_R \quad (2.1)$$

$$D_{R,cs} = \frac{R}{Q - \ln\left(100 \frac{p'}{p_a}\right)} \quad (2.2)$$

where D_R is the relative density at the current state and $D_{R,cs}$ is the relative density at the critical state. The critical state line (CSL) is defined in equation 2.2 as a function of model parameters Q and R , which were empirically obtained from several sands by Bolton (1986), which suggest Q and R values of 10 and 1, respectively for quartzitic sands. However, Boulanger and Ziotopoulou (2012) recommend a value of 1.5 for R to better approximate the CSL for direct simple shear.

The behavior of the soil largely depends on the relative state parameter, as it defines the tendency of the soil to contract or dilate during shearing, thus it also defines the generation of positive or negative pore water pressure in undrained conditions. The model includes bounding, dilation, and critical state surfaces (M_b , M_d , and M_c , respectively). The bounding and dilation surfaces are related to the critical state surface through equations 2.3 and 2.4, respectively.

$$M_b = M_c \exp(-n^b \xi_R) \quad (2.3)$$

$$M_d = M_c \exp(n^d \xi_R) \quad (2.4)$$

$$M_c = 2 \sin(\varphi_{cv}) \quad (2.5)$$

Additionally, a rotated dilatancy line is used in the model to capture early dilation at low stress ratios under certain loading paths. Equation 2.5 defines the critical stress ratio (M_c) as a function of the constant-volume friction angle (φ_{cv}), which is an input parameter. For stress ratios less than M_d , the soil is contracting, until it reaches M_d , when it starts to dilate. Under static loading and for soils dense from critical, the bounding surface ratio (M_b) will be higher than the critical state ratio, resulting in a peak friction angle and strain softening to the critical state friction angle after the peak stress ratio is reached. If the soil is looser than critical, the bounding surface will be close to the critical state ratio, providing peak friction angles similar to critical state ratio (i.e. the soil will contract mostly).

The yield surface is a cone in stress (q - p') space. The center of the yield surface is defined by the back-stress ratio tensor and the diameter of the cone is defined by the parameter “ m ”. The fabric-dilatancy tensor included in Dafalias and Manzari (2004) was modified to depend on plastic deviatoric strains rather than plastic volumetric strains. The elastic shear and bulk modulus are dependent on the mean effective stress (p') and they account for stress ratio effects and they degrade as cumulative plastic deviatoric strain increases (controlled by the fabric tensor).

The main parameters of the model are: Relative Density (D_R), Normalized Shear Modulus (G_o) and the Contraction Parameter (h_{po}). Secondary parameters include: R and Q , which define the critical-state line in D_R - p' space; n_b and n_d , which control peak friction angle and “phase transformation” stress ratio, respectively; critical-state or constant-volume friction angle (ϕ_{cv}), maximum and minimum void ratios (e_{max} , e_{min}), poison’s ratio, and other parameters. The other parameters usually involved terms that are incorporated into the fabric equation, and they were developed to capture important liquefaction response observed in laboratory testing.

2.4.3. Calibration process

Before performing numerical simulations of the centrifuge experiments, the constitutive model has to be calibrated to capture the liquefaction behavior of Nevada Sand, which was used as the liquefiable sand in the experiments modeled. For doing this, several data sets were used: Arulmoli et al. (1992), Chen (1995), Kammerer et al. (2000), Hsu and Vucetic (2002), Kano (2007) and Doygun (2009). It is important to note that Nevada Sand varies between each batch, so the sand tested by different researchers is likely to be different with each other and with the sand used for each centrifuge experiment. However, the amount of data available for the sand batches that were used for each centrifuge experiment is not enough to calibrate the constitutive model, therefore, the laboratory testing at the element level were used to calibrate the model.

The critical state line (CSL) of Nevada Sand has been determined before by a few researchers. Jefferies and Been (1992) showed parameters of the CSL for Nevada Sand in e - p' space to be $\Gamma_1 = 0.91$ and $\lambda_{10} = 0.045$, where Γ_1 and λ_{10} define the CSL in e - p' space. These parameters were based on isotropically consolidated drained and undrained triaxial tests (CID and CIU) and direct simple shear tests (DSS) performed by Arulmoli et al. (1992) for the VELACS project. Kamai and Boulanger (2013) approximated the CSL in D_R - p' space from Castro (2001) CIU tests with $Q = 9.5$ and $R = 0.7$, where Q and R define the CSL in D_R - p' space as shown in Equation (2.2). In this research, the two datasets as processed by the two mentioned researchers were combined and a CSL with parameters $Q = 9.5$ and $R = 0.8$ was found to give the best fit to the data as presented in Figure 2.3, which is very similar to the found by Kamai and Boulanger (2013).

The critical-state (or constant-volume) friction angle was obtained by analyzing monotonic drained and undrained triaxial tests performed by Arulmoli et al. (1992). For each test, the relative state parameter and the bounding stress ratio was calculated, plotted and fitted with an exponential function as the one shown in Equation (2.3). The fitted data shows a constant-volume friction angle $\phi_{cv} = 31.6^\circ$ (at relative state parameter, $\xi_R = 0$) and a value of n_b of 0.4.

The normalized shear modulus (G_o) is related to the overburden-normalized shear wave velocity (V_{S1}) through Equation (2.6). V_{S1} has been correlated to Relative Density (D_R) based on a compiled data set of shear wave velocity measurements in centrifuge experiments as presented by Armstrong (2010) and Arulnathan et al. (2000), and laboratory testing as presented by Arulmoli et al. (1992) and Hsu and Vucetic (2000). Equation 2.7 is the calibrated relation between V_{S1} and D_R . This estimation is similar to the one found by Armstrong (2010).

$$G_o = \frac{\rho V_{S1}^2}{p_a \left(\frac{1+K_o}{2}\right)^{1/2}} \quad (2.6)$$

$$V_{S1} = 125 (D_R + 1)^{0.1} \quad (2.7)$$

The liquefaction behavior was calibrated by adjusting the parameter h_{po} , which controls liquefaction triggering and according to Boulanger and Ziotopoulou (2015) should be changed if the triggering correlation is significantly different than the proposed by Boulanger and Idriss (2016). The triggering correlation for Nevada Sand was obtained from several datasets and includes cyclic triaxial (CTX) testing, cyclic simple shear (CSS) testing, and torsional hollow cylinder (THC) testing. For each laboratory test, the number of cycles to trigger liquefaction was counted. The criterion for liquefaction triggering varies for each test and differs according to each research team. In this study, the criterion for liquefaction triggering was considered to be 3% single amplitude for CTX (which is consistent with Bray & Sancio 2006, among several other researchers), 3% single amplitude strain for the CSS (which is consistent with the recommendations of Boulanger and Ziotopoulou (2015)), and 3% double amplitude for THC (which is roughly consistent with the use of 5% double amplitude for the data set employed). For each test, the cyclic stress ratio (CSR) values were corrected for overburden (K_σ effect) using the Idriss and Boulanger (2008) correction factors. The CSR values were also corrected for the in-situ stress ratio (K_o) and over-consolidation ratio (OCR) effects using equations (2.8) and (2.9), respectively, assuming that the centrifuge testing will consolidate the soil at a K_o value of around 0.55 with an OCR value of 1.5. The value of $(K_o)_{lab}$ was assumed to be 0.45 for CSS. Most of the researchers used normally consolidated samples ($OCR = 1$) except for Chen (1995), who investigated the effect of OCR in the cyclic resistance ratio (CRR) of Nevada Sand. The exponent “m” in Equation (2.9) was obtained from the CTX performed by Chen (1995) and was found to be 0.33. Thus, the final CSR values for the calibration process corresponds to an initial effective stress (σ'_{vo}) of 1 atm., no static shear stress ($\alpha=0$), an at-rest lateral pressure coefficient (K_o) of 0.55, and an over-consolidation ratio (OCR) of 1.5.

$$\frac{CSR_{(K_o)centrifuge}}{CSR_{(K_o)lab}} = \frac{1+2 (K_o)_{centrifuge}}{1+2 (K_o)_{lab}} \quad (2.8)$$

$$\frac{CSR_{(OCR)centrifuge}}{CSR_{(OCR)lab}} = \left[\frac{(OCR)_{centrifuge}}{(OCR)_{lab}} \right]^m \quad (2.9)$$

The data were compiled in a plot of number of cycles (N) vs. CRR and organized by different relative densities groupings. For a given relative density grouping, a power function of the form of Equation (2.10), where A and B are coefficients, used to fit the data.

$$CRR = A (N)^{-B} \quad (2.10)$$

The values of A and B are shown in Table 2.3 for the different relative densities groupings. With the fitted equations, the value of CSR required to cause 15 number of cycles was obtained and a liquefaction triggering curve (in $D_R - CSR$ space) was obtained. The parameter h_{po} was calibrated to obtain both the laboratory based cyclic resistance curve (N vs. CSR) and the triggering curve (D_R vs. CSR) as presented in Figures 2.4 (a) and (b), respectively. As observed in Figure 2.4(a) the fitted data (dotted lines) follow fairly close the fitted data (solid lines). However, it can be observed the significant existing scatter for each relative density bin. Judgment, rather than perfect curve fitting to minimize error, has to be used when interpreting triggering curves, especially using data from several researchers considering the probably

differing properties of the Nevada Sand used by different researchers. It was decided to give more importance to the general trends, for example to obtain higher CRR values across all the ranges of number of cycles (N_{cycles}) when increasing relative density and also to obtain higher slopes of the CRR-N curve as the relative density increases when fitting the laboratory tests data points presented in Figure 2.4(a). Figure 2.4(b) shows CRR at N_{cycles} equal to 15 (equivalent to magnitude $M_w = 7.5$) for the different relative densities groupings for both the fitted data and the numerical-based triggering curve. The final calibration for the contraction rate parameter (h_{po}) was found to be a function of the relative density and is specified in equation form in Table 2.4, which also shows a list of geotechnical properties and model parameters that were used in this study and their respective values or equations.

Importantly, the calibration was also checked to capture the decrease in CRR with increasing effective confining pressure for a given relative density (K_σ effect) as well as the change in CRR with sustained static shear stress for a given relative density (K_α effect). These effects are important in the behavior of the soils below shallow founded structures, because the structure will increase the confining pressure of the soil as well as impose a static shear stress near the edges of the building. The numerical model captures the trends of the K_σ and K_α effects as shown in Figure 2.5(a) and (b), which compare the numerically obtained K_σ and K_α responses with the recommended by the Idriss and Boulanger (2008) simplified procedure.

The normalized shear modulus degradation curve was calibrated against data from Arulmoli et al. (1992) for small strains and the Menq (2003) generic curves at larger strains. The calibration was obtained by applying a 0.75 multiplier to the default value of the model parameter h_o . Model parameters not listed in Table 2.4 were considered as the default values of the PM4 Sand constitutive model (see Boulanger and Ziotopoulou, 2015).

Previous work (e.g., Manzari and Arulanandan 1992, Popescu and Prevost 1993, and Shahir and Pak 2010) suggests that the hydraulic conductivity of the liquefiable sand increases as strong shaking occurs and liquefaction is triggered. They recommended modeling this increase in hydraulic conductivity during shaking to obtain analytical results that matched those of the centrifuge experiments. Moreover, Dashti and Bray (2013) showed that free-field settlements are sensitive to changes in hydraulic conductivity. In this study, the calibrated final values of hydraulic conductivity provided in Dashti and Bray (2013) were adopted and shown in equation form in Table 2.4; they were used as a constant during shaking. The effect of not increasing the hydraulic conductivity after the onset of liquefaction will likely affect the post-liquefaction dissipation of pore water pressures and consequently the post-liquefaction consolidation settlements. However, this assumption will not affect significantly the shear-induced deformations beneath the structures.

A contraction rate parameter (h_{po}) of 0.4 for Monterey Sand was found to produce results that were in agreement with laboratory triggering curves obtained by Kammerer et al. (2004) at relative densities between 80 and 90% which is the range of relative densities at which Monterey Sand were used in the centrifuge experiments. The other parameters for Monterey Sand were default parameters specified for the PM4Sand model (Boulanger and Ziotopoulou, 2015).

2.4.4. Modeling of the structures

The structures were modeled using beam elements in FLAC 2D (Itasca, 2009). The general properties were obtained from the geometry and material properties of the experimented buildings. Because the structural elements have no physical thickness in the numerical model,

the height, elastic modulus, and material density of the structural elements were changed slightly to capture the bearing pressure (q) and the natural fixed-base period (T_n) of the structure, which were measured before spinning and are shown in Table 1. The natural fixed-base period in the numerical model was tested by applying a unit velocity in the top corner of an undamped model of the structure and recording the displacement response. These two parameters (q and T_n) were judged to be most important, as settlement is expected to increase with increasing bearing pressure and a higher rocking response of the building is expected to increased shear-induced settlements near the edges of the building. The latter effect depends on the frequency content of the input ground motion. Previous work by Popescu and Prevost (1993) recommends the use of a lower bearing pressure when analyzing 3D structures under 2D plane strain conditions, based on the fact that a lower bearing pressure results in the same static consolidation settlement obtained in a 3D model of a particular centrifuge experiment with a rigid structure. The buildings modeled herein are not rigid, they are single-degree-of-freedom (SDOF) systems and their inertial response could affect the response of the ground beneath it as well as affect its settlement. Thus, bearing pressure and natural period of the system were matched by using realistic values of masses and stiffness of the structural elements. Figure 2.6 shows an example of the finite difference mesh for soil configuration T3.9-50 and the J_S building.

2.5. FREE-FIELD RESPONSE

The free field response has been evaluated in terms of acceleration-time histories, 5% damped acceleration response spectra, arias intensity and excess pore water pressures generation during shaking. Figure 2.7 shows representative results of the T3-50 experiment for the free-field conditions. The two left columns show the response for the moderate Port Island event (MPI) with a PGA of 0.19 g and the two columns to the right show the response for the large Port Island event (LPI2) with a PGA of 0.66 g. The graphs also show the acceleration-time history and Husid plots at the surface of the model, the excess pore water pressure (Δu) generation in the middle of the liquefiable layer, and the input acceleration-time history.

For the MPI event, the acceleration-time history is captured well including the dilations spikes typical in records over liquefiable soils. The Husid plots are also similar in shape and intensity for the MPI motion. The pore water pressure response is similar, although the numerical model develops pore water pressure more rapidly than the observed in the centrifuge experiment and at 25 seconds approximately the excess pore water pressures starts dissipating in the centrifuge experiments but remains constant in the numerical analyses. For the LPI2 motion, the intensity of the surface motion is captured well, but not as good as for the MPI motion. In the latter part of the record (time > 10 seconds), the recorded acceleration in the centrifuge experiment has some significant acceleration spikes that are not in the simulated surface motion. This is also shown in the arias intensity plot observing that at 10 seconds the arias intensity is similar for the experiment and the simulation but later in the record more energy is being transmitted in the experiment compared to what is estimated by the numerical simulation. The pore water pressure generation is captured in terms of its magnitude, but how the ultimate value of pore water pressure develops differs between the simulation and experiment. The numerical simulation develops excess pore water pressure more quickly, and it also oscillates more than the centrifuge experiments measurements.

Figure 2.8 shows the comparison between the 5%-damped acceleration response spectra at the surface of the model for the recorded motions in the centrifuge experiment and the

calculated values in the numerical analyses for the same T3-50 experiment and the same MPI and LPI2 motions. The MPI motion is captured reasonably well but the LPI2 motion is significantly underestimated at long periods. The centrifuge recorded acceleration response spectrum shows a clear lengthening of the two periods where the two peaks in spectral acceleration exist in the input motions (i.e., at 0.8 s and 2 s, approximately). This lengthening of the period of the motion does not occur as dramatically as in the numerical analysis. These types of responses shown in Figure 2.8 are representative of other experiments with different configurations.

2.6. BUILDING RESPONSE

The model building performance in the centrifuge experiments is evaluated in terms of the liquefaction-induced structural vertical displacement. A few representative cases are selected to show how the constitutive model with the calibrated parameters was able to capture important mechanisms controlling liquefaction-induced movement of buildings.

The building A_D was tested in three configurations (T3-50, T3-30 and T6-30), A_{ZH} was tested under two configurations (T4.6-40 and T4.5-50) and the K building was tested under the T4.6-40 configuration. Geometrically the three buildings are similar, however the buildings had different weights and consequently different bearing pressures and natural fixed-base periods (see Table 1). Figure 2.9 shows the structural vertical displacements of these buildings under different configurations and shaken by different ground motions.

In general, the trends are captured well in the numerical analyses, especially in terms of the amount of total vertical settlement. The results from Figure 2.9 provide confidence in the sense that a well calibrated constitutive model is able not only to capture reasonable values of settlements but also capture key trends. For example, all other things being equal, changing the relative density from combination T350-AD-MPI to T330-AD-MPI increases settlement by a factor of 3 in the centrifuge testing. In the numerical analyses the factor was about two. Also, increasing building weight and ground motion intensity generally resulted in more settlement, with the latter having a greater effect.

However, there are details within the displacement-time history that vary between calculated and measured responses. For example, in some cases (e.g., T4.6-40- A_{ZH} -LPI), there is significant rocking of the building apparent in the displacement-time histories measured in the centrifuge experiments, which are not captured in the numerical simulations. Instead, the calculated response steadily develops vertical settlement without much variation in vertical settlement within each cycle. The calculated vertical settlements of the model structures for LPI and TCU motions (i.e., strong and small levels of shaking, respectively) are generally higher than those measured in the centrifuge experiment (but still within 25%). For MPI ground motions the calculated response agrees well with the observed response.

2.7. SUMMARY OF RESULTS

A total of 36 cases in the centrifuge experiments were back-analyzed with FLAC 7.0 using the PM4Sand model, wherein each case consisted of one building, one soil configuration, and one ground motion. The analytical results are compared to the centrifuge test results in

Figure 2.10, which shows a plot of estimated building settlement vs. measured building settlement. In Figure 2.10, the shape of the symbol represents the soil configuration, the color of the symbol represents the building, and the filling of the symbol represents the ground motion. Figure 2.10 shows two plots: one plot shows cases with up to 1000 mm of building settlement and the other plot is a close-up view of those cases that go up to 400 mm of building settlement.

Although most of the analytical results fall within the anticipated range of 2:1 to 1:2 (estimated-to-measured building settlement), there is a clear bias towards calculating larger building settlements than what was measured in the centrifuge experiments, with only 7 out of 36 cases falling below the 1:1 line. This bias is more pronounced in the low settlement range of values (i.e., from 0 to 150 mm). The cases found within this lower range include several of the low intensity motions (PIM or TCU motions), the J-type of buildings, and soil configurations T6-30 and T3-50. In these cases, the estimated building settlement is usually above the 1:3/2 line. The over-estimation of building settlement for the low intensity motions can be attributed to the fact that the numerical analyses estimated triggering of liquefaction when in the centrifuge experiments, some of the soils developed high pore pressure ratios but they often did not reach the $r_u = 1$ condition. Thus, in these cases, the numerical model overly softened the ground, which led to an over-estimation of shear sand volumetric strains and a consequently over-estimation of building settlement.

The over-estimation of J-type of building settlement is explained by the observation in the centrifuge tests that there was significant soil movement during shaking from the zone adjacent to the footing to the zone below the footing. This happens usually with rocking foundations, where there is a high amplitude of vertical motion of the edges of the foundation, which opens a gap between the foundation and the soil which in turn allows for that space to fill up with nearby soil. This was not captured in the numerical analyses, and it is likely the main reason why the numerical analyses over-estimated building settlement for the J-type structures, which rocked the most. The other data points shown in Fig. 2.10 indicate normally expected variations in calculated and measured values of building settlement. They usually range between the 1:2/3 and 1:3/2 lines shown in Fig. 2.10.

2.8. CONCLUSIONS

A total of 36 cases in the centrifuge experiments were back-analyzed with FLAC 7.0 using the PM4Sand model, wherein each case consisted of one building, one soil configuration, and one ground motion. The buildings had different weight and geometry resulting in different bearing pressures and fixed-based periods. The soil configuration consisted generally on three-layer systems, where the middle layer was liquefiable with varying relative densities and thickness. The ground motions had different intensities, frequency content, and durations.

The presented analytical results show that the calibration of the constitutive model is important to capture key mechanisms that control free-field response and building response. All available laboratory test data available were considered in the calibration process. The data had to be interpreted and modified to obtain the likely liquefaction triggering curve ($CRR-N_{cycles}$) that is expected in the centrifuge experiments. Developing a CRR curve from several points obtained by different researchers for different tests (e.g., triaxial and simple shear test) on a variable sand (i.e., Nevada Sand is an unprocessed mined sand that has natural variability) is challenging. When the data exhibit contradictions, priority was given to capturing key trends and reasonable

values of liquefaction triggering resistance. Moreover, sensitivity analyses become a necessary tool when performing numerical analyses, so that one understands what parameters are most important.

After completing the element level calibration, it is useful to examine the calculated free-field response. The calculated free-field response can be evaluated in terms of pore water pressure ratios, shear strains, and cyclic shear stresses. In the absence of centrifuge testing (which is the usual case), these quantities can be compared (at least qualitatively) to the results of simplified liquefaction triggering procedures, with terms such as the factor of safety against liquefaction. The free-field response can also be evaluated by comparing the calculated surface motions to those recorded in terms of 5%-damped acceleration response spectra. In this study, the free-field responses observed in the centrifuge experiments were captured well in most cases by the calibrated numerical simulations.

Capturing building response is most important. The structural analytical model should capture the key response characteristics of the physical model building. For single-degree-of-freedom systems (as was the case in these centrifuge experiments), capturing the fixed-based period and the weight of the building are most important. These two properties have an important influence on the amount of vertical settlement of the structure. In this study, the analytical model was adjusted and calibrated to obtain measured or best-estimated values for the physical model building, even if this required changing slightly some of the dimensions of some of the structural elements comprising the model.

The calibrated numerical model provided reasonable estimates of the liquefaction-induced building settlement measured in the centrifuge experiments. Responses were also compared in terms of acceleration-time histories, and acceleration response spectra, and in addition through comparison of other quantities, such as excess pore water pressures and shear strains (which were not shown here, but were found to be in good agreement with the results of the centrifuge experiments). Therefore, after this careful examination of the capabilities of the selected numerical model to capture element response, free-field response, and building response, the numerical model is used to back-analyze field case histories developed following the 2010-2011 Canterbury earthquake sequence.

Table 2.1. Properties and dimensions of the different buildings modeled in this study.

Name	Width B (m)	Length L (m)	Height H (m)	Foundation thickness, t (m)	Embedment Depth, d_f (m)	Bearing Pressure , q (kPa)	Fixed-Base Period, T_n (s)
A _D	6	9	2.12	0.7	1.0	80	0.21
A _{Z&H}	6	9	2.12	0.7	0.7	65	0.33
B	12	18	2.12	0.7	1.0	80	0.26
C	6	9	4.20	0.7	1.0	130	0.33
K	6	9	2.42	0.7	0.7	180	0.38
J _S	7.5	7.5	10.45	1.4	0	179	0.87
J _E	7.5	7.5	10.45	1.4	1.4	179	0.87
J _{E,IM}	7.5	7.5	10.45	1.4	1.4	269	1.1

Table 2.2. Geometry and properties of the soils for each configuration modeled in this study.

Name	Bldg	Water Depth (m)	Soil Layer	Soil Type ^a	Layer Thick. (m)	Relative Dens. (%)	G _S	e _{min}	e _{max}	Ground Motions Name ^b PGA _b (g)	
T3-50	A _D	1.1	L3	M	2	85	2.64	0.536	0.843	PIM	0.15
			L2	N	3	50	2.65	0.52	0.78	TCU	0.13
			L1	N	21	90	2.65	0.52	0.78	PIL1 PIL2	0.38 0.66
T3-30	A _D	1.1	L3	M	2	90	2.64	0.541	0.855	PIM PIL	0.15 0.50
	B		L2	N	3	30	2.67	0.533	0.888		
	C		L1	N	21	90	2.67	0.533	0.888		
T6-30	A _D	1.1	L3	M	2	86	2.64	0.541	0.855	PIM PIL	0.19 0.50
	B		L2	N	6	30	2.67	0.533	0.888		
	C		L1	N	18	86	2.67	0.533	0.888		
T4.5-50	A _{Z&H}	0.7	L3	M	1.9	85	2.64	0.536	0.843	PIM	0.21
			L2	N	4.5	50	2.66	0.516	0.774	TCU	0.16
			L1	N	19.4	90	2.66	0.516	0.774	PIL	0.49
T4.6-40	A _{Z&H} K	0.2	L3	M	1.7	85	2.64	0.536	0.843	PIM	0.2
			L2	N	4.6	40	2.66	0.516	0.774	TCU	0.17
			L1	N	19.3	90	2.66	0.516	0.774	PIL	0.58
T3.9-50	J _S J _E	-0.7	L3	N	2.8	80	2.66	0.52	0.77	PIM1	0.16
			L2	N	3.9	50	2.66	0.52	0.77	PIM2	0.19
			L1	N	16.8	80	2.66	0.52	0.77	PIL	0.55
T2.5-55	J _E J _{E,IM}	0.0	L3	N	2.6	80	2.66	0.52	0.77	PIM1	0.18
			L2	N	2.5	55	2.66	0.52	0.77	PIM2	0.20
			L1	N	20.7	80	2.66	0.52	0.77	PIL	0.60

^a "M" for Monterey Sand and "N" for Nevada Sand

^b "PIM" and "PIL" refers to moderate and large Port Island motions respectively.

Table 2.3. Regression parameter for power function used to fit laboratory testing data in Number of cycles (N) – CSR space.

Relative Density (%)	A	B
30	0.165	0.23
40	0.21	0.25
55	0.26	0.28
60	0.33	0.30
85	1.5	0.5

Table 2.4. Properties and parameters used for this study for Nevada Sand

General Parameters	Value or equation
D_R	Varies
G_s^a	2.67
e_{max}^b	0.89
e_{min}^b	0.53
e	$e_{max} - D_R \cdot (e_{max} - e_{min})$
ρ_d	$(G_s \cdot \rho_w)/(1 + e)$
ρ_{sat}	$\rho_d \left(1 + \frac{e}{G_s}\right)$
k (m/s) ^c	$6.79 \times 10^{-5} - 6.15 \times 10^{-7}(D_R)$
PM4 - Parameters	Value or equation
V_{S1}^d	$125 (D_R + 1)^{0.1}$
G_o	$\frac{\rho V_{S1}^2}{p_a \left(\frac{1 + K_o}{2}\right)^{1/2}}$
h_{po}^d	0.15 for $D_R \leq 40\%$ 0.05 for $50 \leq D_R \leq 65$ 20.0 for $D_R \geq 80\%$
ϕ_{cv}^d	31.6
Q^d	9.5
R^d	0.8
n_b^d	0.3 for dense of critical 0.1 for loose of critical

^a Amuroli et al. (1992), ^b Dashti (2009), ^c Dashti and Bray (2013), ^d Obtained or calibrated in this study

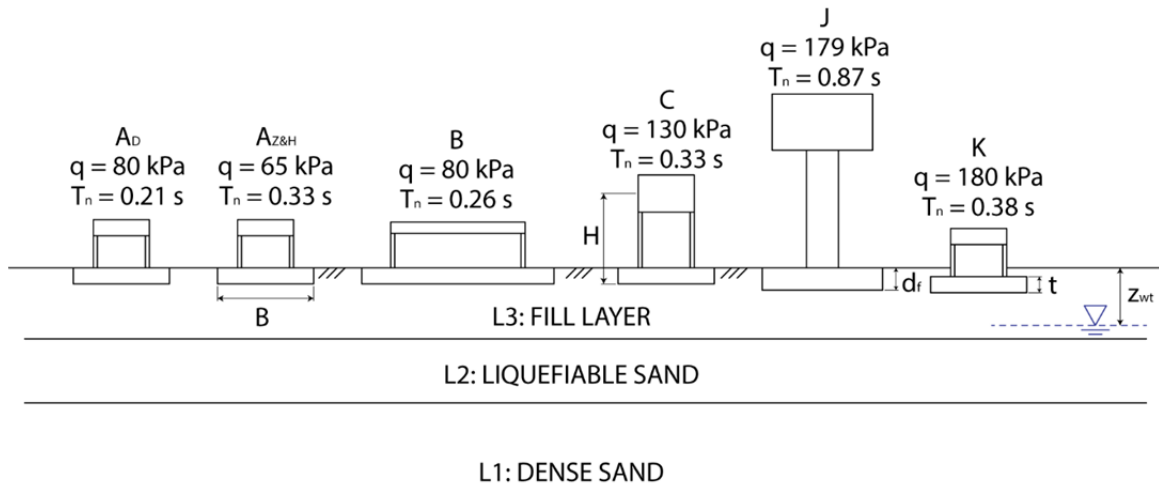


Figure 2.1. Different buildings modeled in this study with a typical soil configuration.

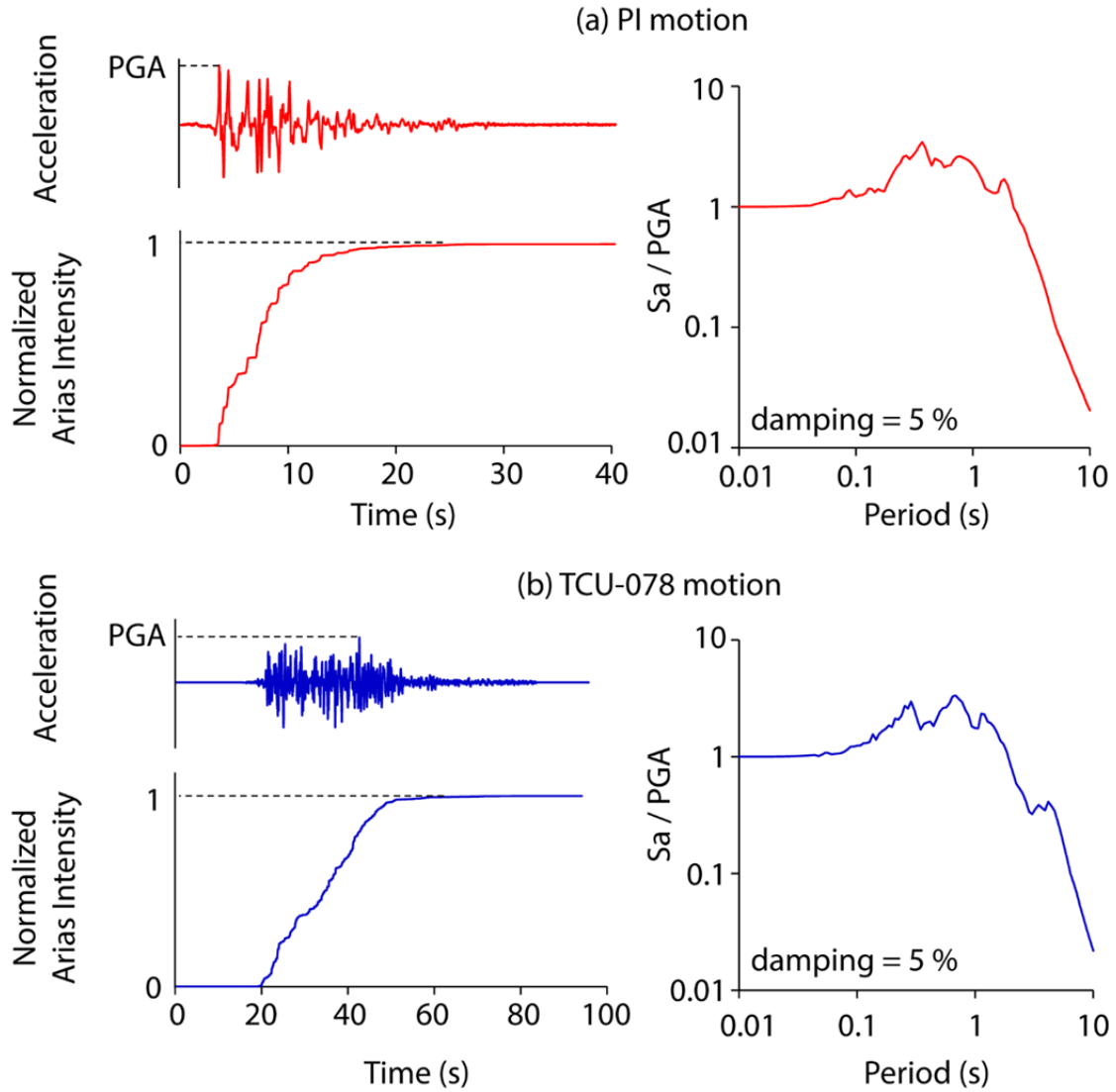


Figure 2.2. Ground motion acceleration time history, normalized arias intensity and normalized spectral acceleration for the two ground motions used in this study: (a) PI event and (b) TCU event.

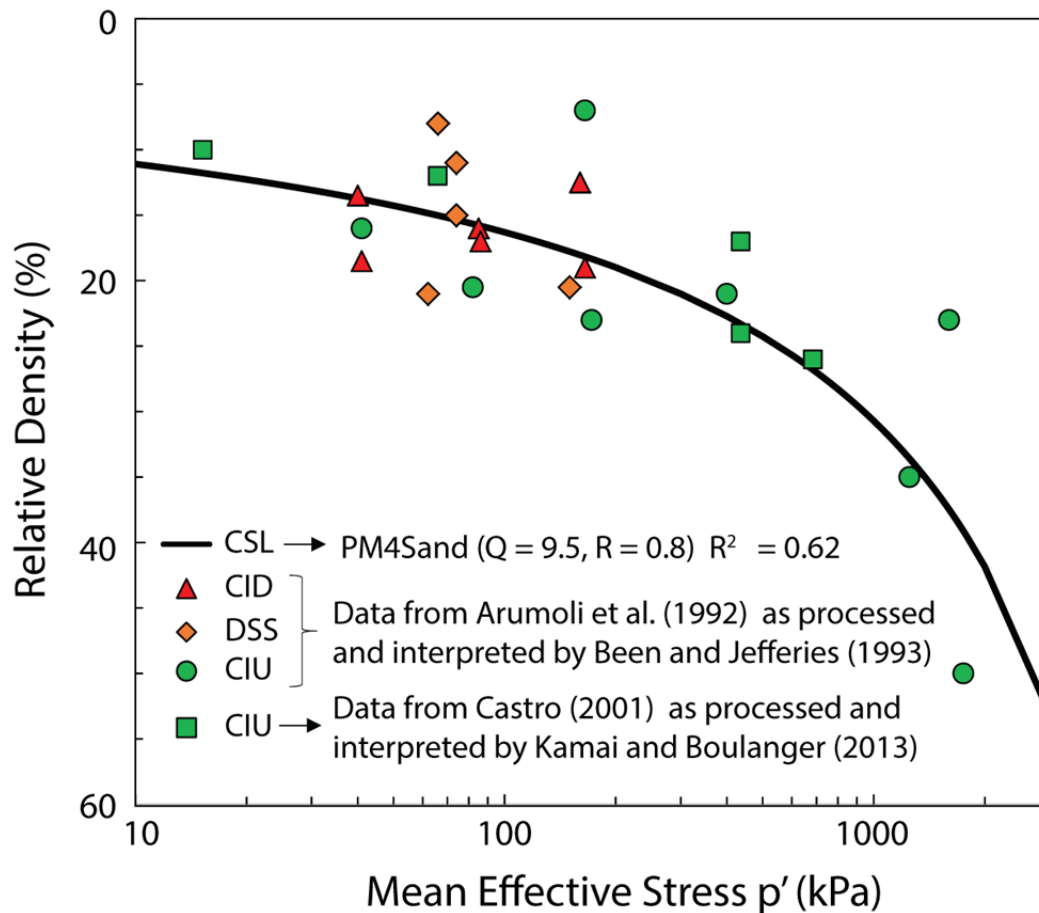


Figure 2.3. Critical State Line (CSL) used in this research based on previous data.

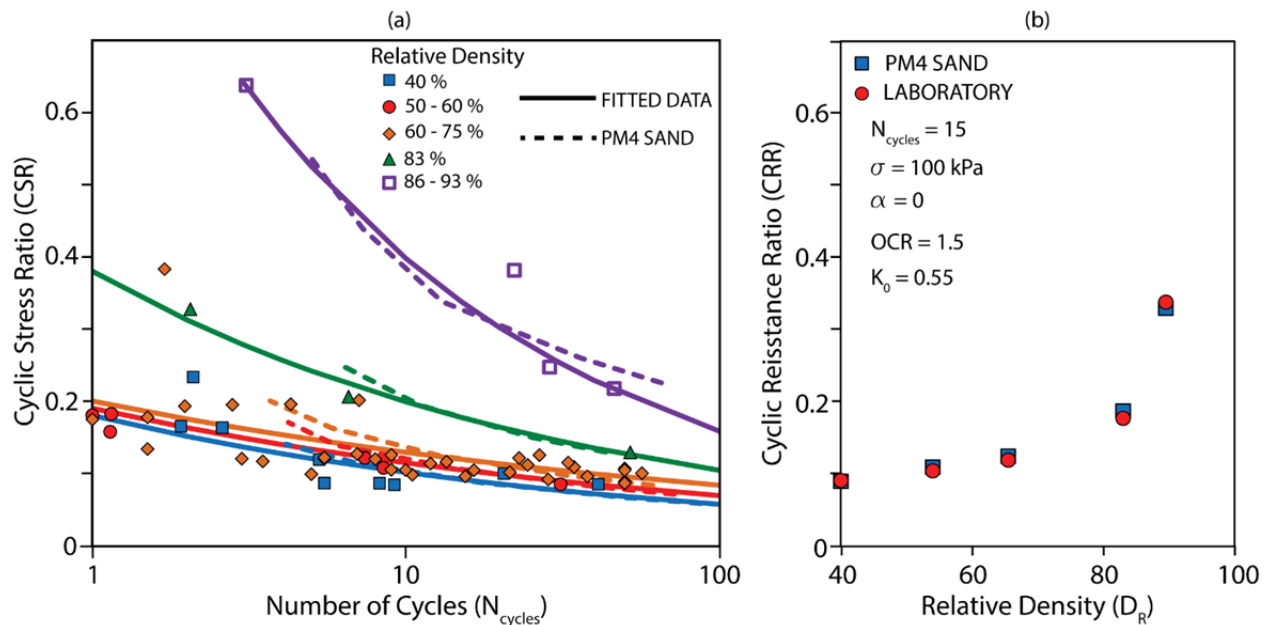


Figure 2.4. Liquefaction triggering curves based on laboratory testing for Nevada Sand: (a) CRR vs. Number of Cycles showing different relative densities, fitted data and numerical simulation, (b) CRR vs. Relative Density for $N_{cycles} = 15$

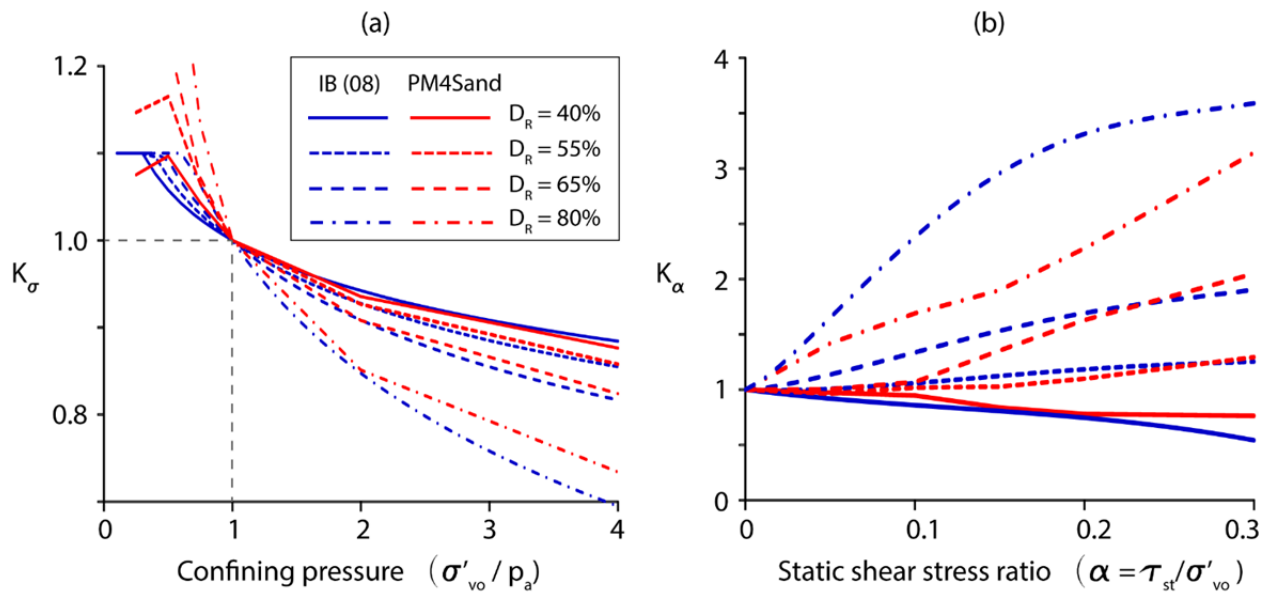


Figure 2.5. (a) K_σ and (b) K_α responses obtained from Idriss & Boulanger (2008) liquefaction triggering procedure (blue) and from the PM4Sand constitutive model (red) for different relative densities.

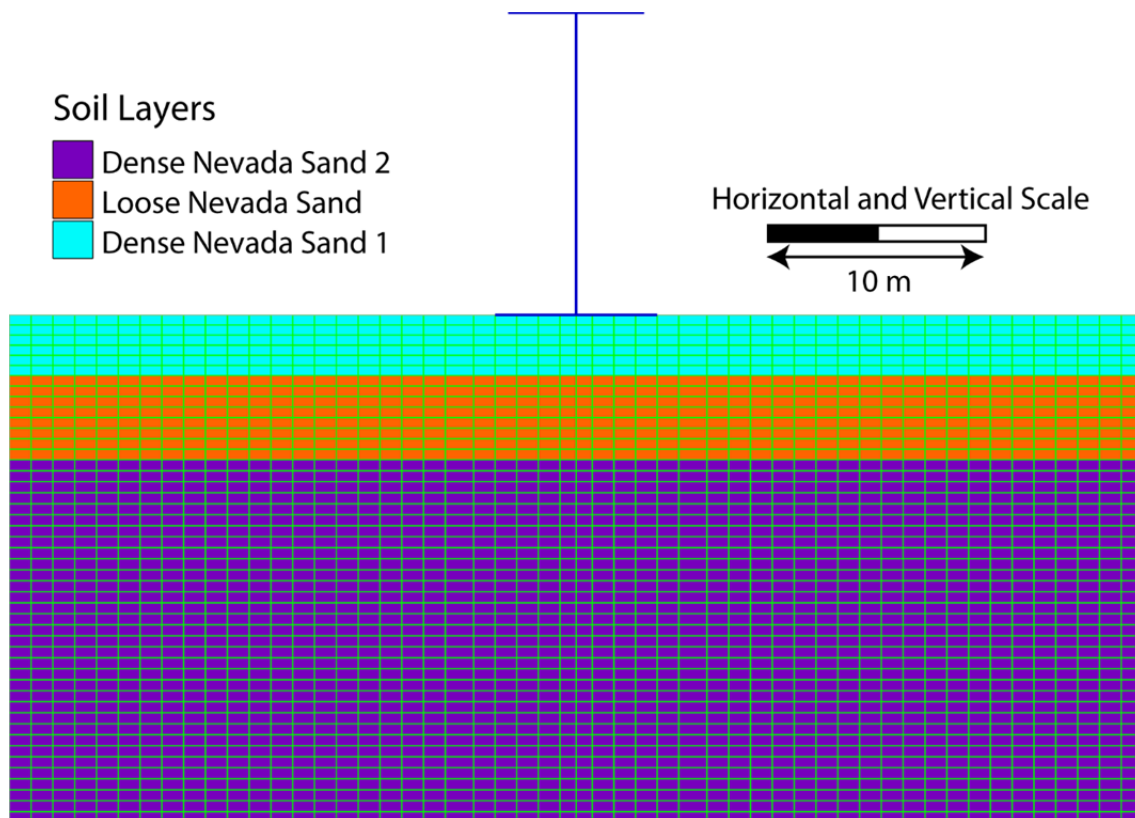


Figure 2.6. Finite difference mesh for configuration T3.9-50 and Building J_s

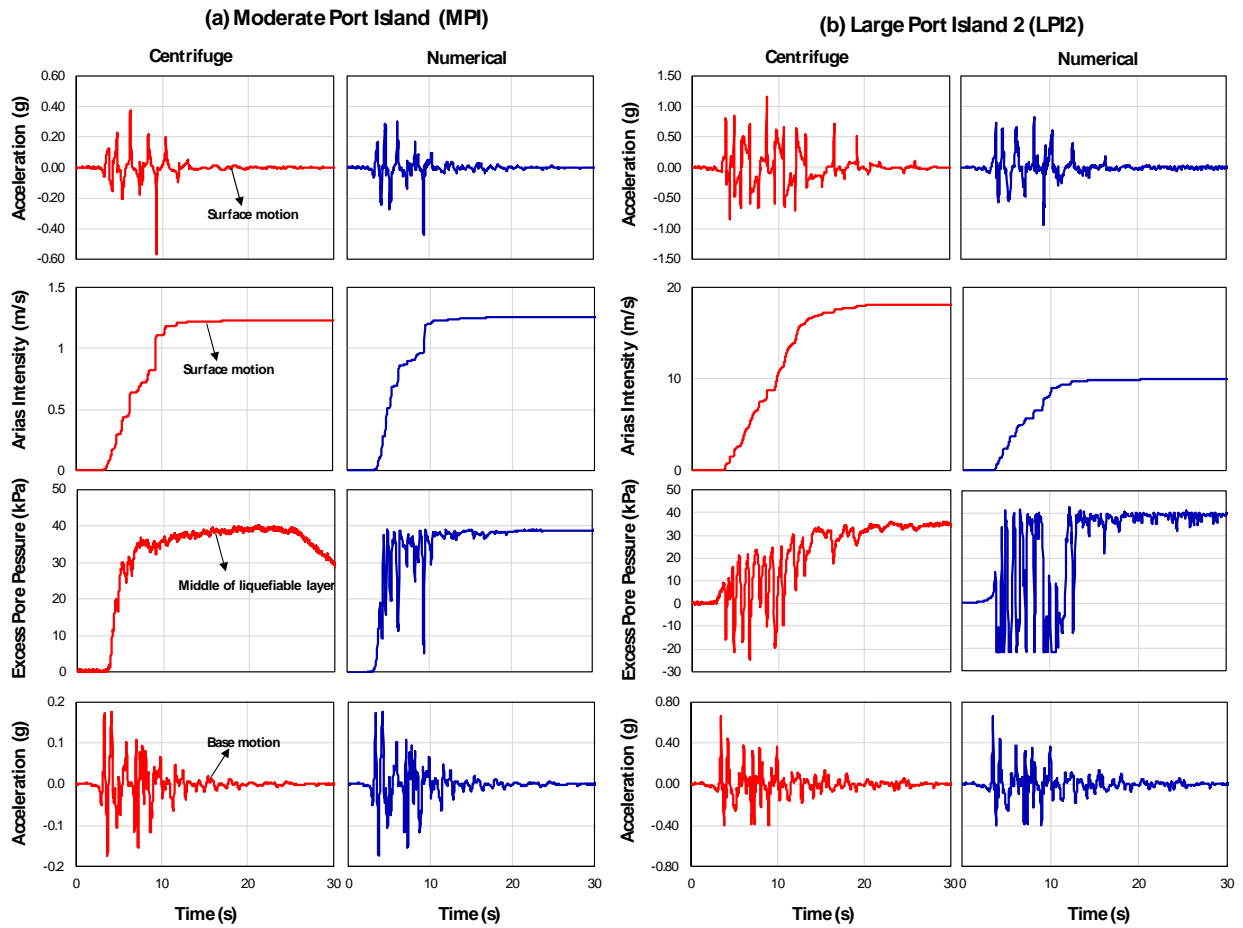


Figure 2.7. Free-field response comparison of centrifuge test and numerical simulations for the T3-50 experiment for: (a) the moderate Port Island event (MPI) and (b) the large Port Island event (LPI2)

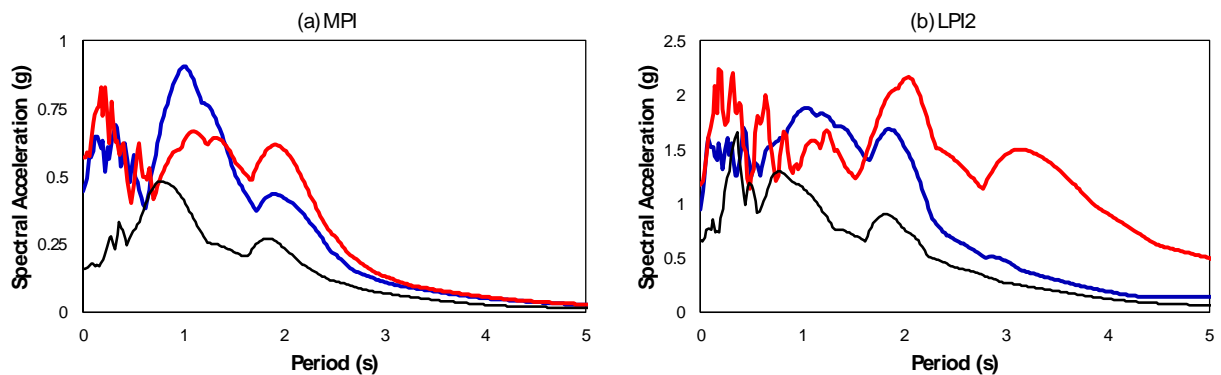


Figure 2.8. Free-field 5%-damped acceleration response spectra comparison between the recorded surface motion in the centrifuge (shown in red) and the numerical calculated surface response (shown in blue) for the MPI and LPI2 motions and the T3-50 experiment. The input response spectra are shown in black.

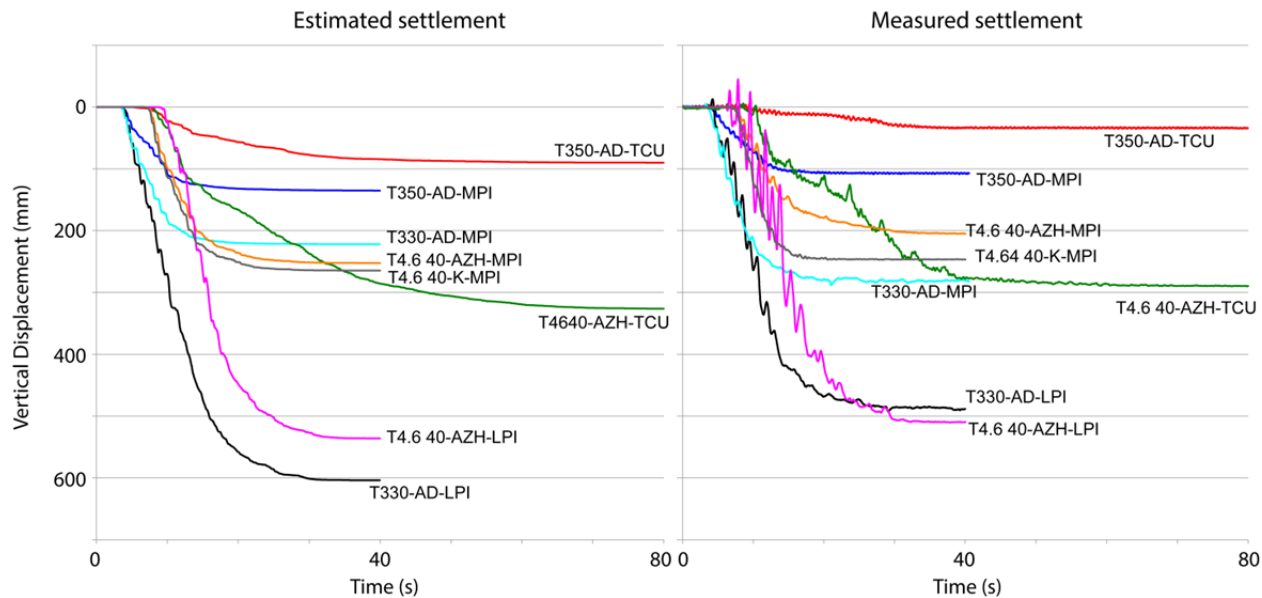


Figure 2.9. Estimated and measured structural vertical displacement for a few representative cases of different buildings, soil configurations and ground motions used in the centrifuge experiments.

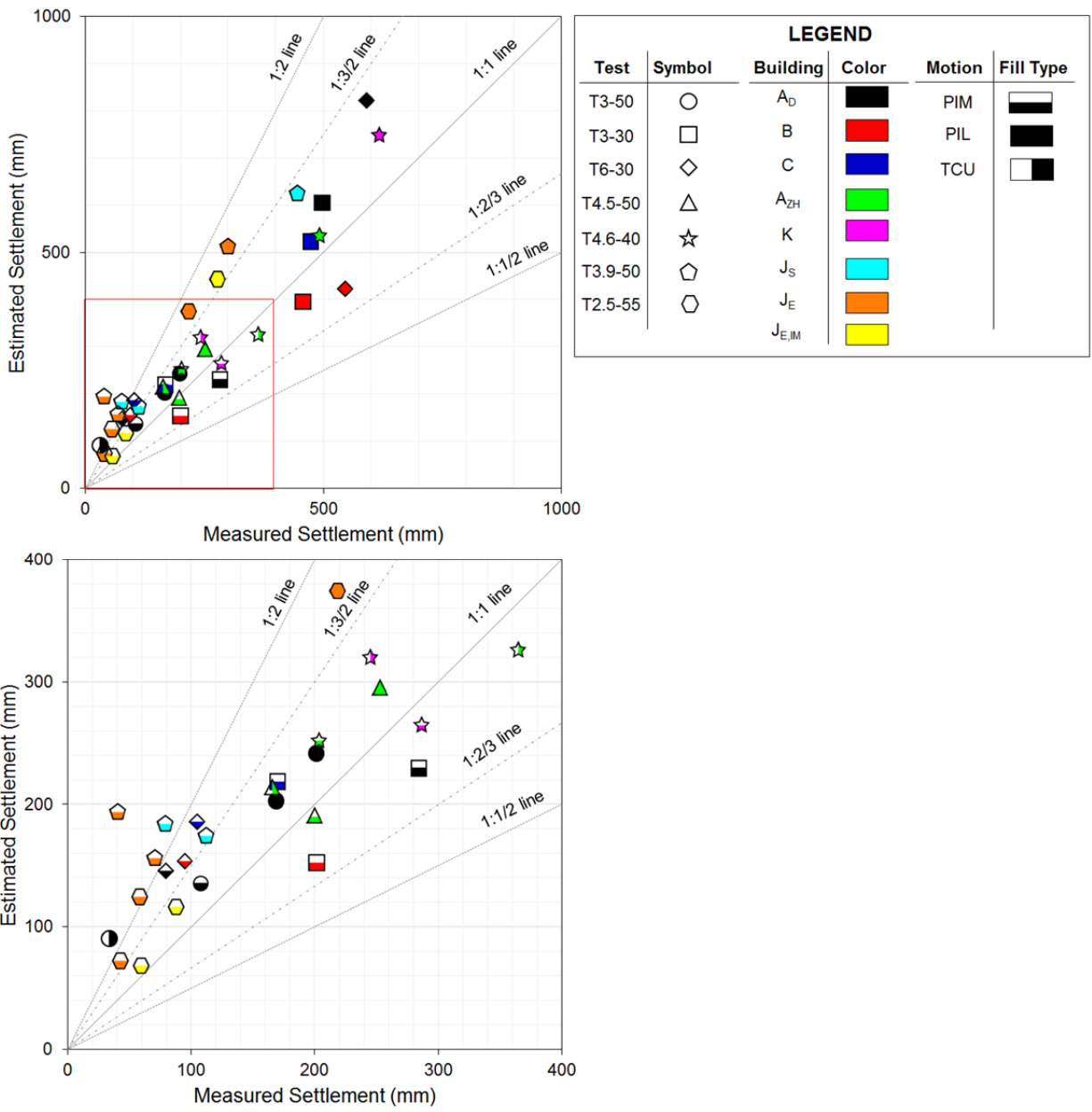


Figure 2.10. Comparison between measured and estimated vertical structural settlements

CHAPTER 3: DYNAMIC ANALYSES OF TWO BUILDINGS FOUNDED ON LIQUEFIABLE SOILS DURING THE CANTERBURY EARTHQUAKE SEQUENCE

The contents of this chapter are primarily from a journal article submitted to the Journal of Geotechnical and Geoenvironmental Engineering from the American Society of Civil Engineers (ASCE) by Luque, R. and Bray, J.D. entitled: “Dynamic Analyses of two Buildings Founded on Liquefiable Soils during the Canterbury Earthquake Sequence”, which has been accepted.

3.1. INTRODUCTION

The estimation of liquefaction-induced settlement of structures is still often based on empirical procedures that estimate post-liquefaction, one-dimensional (1D) reconsolidation settlements in the free-field. These 1D volumetric-induced settlement procedures (e.g., Tokimatsu and Seed 1987, and Zhang et al. 2002) neglect the important effects of the presence of a structure. The free-field methods are used, because alternative simplified procedures that capture shear-induced deformation due to the presence of buildings are currently lacking. However, it is known that seismically induced building movements are often controlled primarily by shear-induced ground deformations as a result of soil-structure interaction (SSI)-induced ratcheting and bearing capacity-type movements (e.g., Dashti et al. 2010 a,b, and Dashti and Bray 2013). Volumetric-induced ground deformations resulting from localized partial drainage, sedimentation, and post-liquefaction reconsolidation can also contribute in addition to the removal of materials beneath a structure due to the formation of sediment ejecta. Liquefaction-induced displacement mechanisms are illustrated in Figure 3.1. The previously mentioned 1D empirical procedures can only capture the settlements as a result of the cumulative effect of volumetric strains related to sedimentation and post-liquefaction reconsolidation mechanisms.

Analytical procedures that are able to capture shear-induced ground deformations are required to evaluate liquefaction-induced building settlement. Numerical analyses have been used by researchers to replicate the measured responses of the ground or structures during physical experiments, which are commonly centrifuge tests. Popescu and Prevost (1993), Elgamal et al. (2005), Popescu et al. (2006), Lopez-Caballero and Farahmand-Razavi (2008), Shakir and Pak (2010), Adrianopoulos et al. (2010), Dashti and Bray (2013), and Karimi and Dashti (2016a,b) performed nonlinear effective stress dynamic analyses to capture the response of buildings on top of a soil deposit that commonly include a liquefiable soil layer. These analyses vary widely in terms of the numerical method used (i.e., finite element or finite difference method), soil constitutive model used, model geometry employed (i.e., 2D or 3D), and structure representation (i.e., rigid, single-degree-of-freedom, or surface load). Travararou et al. (2008) and Karamitros et al. (2013a) performed numerical analyses of buildings that suffered liquefaction-induced damage in the 1999 Kocaeli earthquake. However, papers that describe the back-analysis of liquefaction-induced building movement case histories are scarce.

In this chapter, the results of the numerical analysis of two buildings that suffered different levels of liquefaction-induced settlement damage in several events during the 2010-2011 Canterbury earthquake sequence are presented to advance the profession’s understanding

of liquefaction-induced building settlement. The dynamic SSI analyses were performed using the program FLAC 2D (Itasca 2009) and the user-defined model PM4Sand-Version 3 (Boulanger and Ziotopoulou 2015). The calibration of the model was performed by capturing the key soil units' likely Cyclic Resistance Ratio (CRR) vs. Number of Load Cycles (N_{cycles}) relationships as defined by the results of advanced laboratory testing or field liquefaction triggering procedures when laboratory test data were not available. The structure and the underlying soil were modeled, and the calculated building displacements were compared to the observed displacements after three of the Canterbury earthquakes to investigate this phenomenon and to develop recommendations for performing dynamic SSI analyses to estimate liquefaction-induced building movements.

3.2. EARTHQUAKE GROUND SHAKING

The Canterbury earthquake sequence included seven events with $M_w \geq 5.5$, three of which had $M_w \geq 6.0$. Ground shaking was recorded at four strong motion stations within the Central Business District (CBD). The 22 February 2011 Christchurch M_w 6.2 earthquake produced the most intense ground shaking in the CBD, because the source-to-site distances (R) were only 3-6 km. Its peak ground acceleration (PGA) values were twice those recorded during the larger, but more distant 4 September 2010 Darfield M_w 7.1 event ($R = 18$ -20 km). The PGAs recorded in the CBD during the Darfield event are similar to those recorded during the 13 June 2011 M_w 6.0 and 23 December 2011 M_w 5.9 events. The PGA values of the dozens of other earthquakes events are lower than those recorded during these events. This chapter focuses on the seismic performance of two multi-story office structures supported on shallow foundations (i.e., the CTUC and FTG-7 buildings) during the three primary events: 4 September 2010 M_w 7.1 Darfield, 22 February 2011 M_w 6.2 Christchurch, and 13 June 2011 M_w 6.0 earthquakes.

PGA values were required for the simplified liquefaction evaluations as well as to calibrate ground motions for the dynamic SSI analyses. Free-field ground surface median PGA values at the building sites were estimated using Bradley (2014) to be 0.22 g, 0.45 g, and 0.24 g for the Darfield, Christchurch, and 13 June 2011 earthquakes, respectively. As the Bradley (2014) model was conditioned to capture recorded ground-motion intensities at strong motion stations, it is not surprising that these estimated median PGAs values were consistent with the PGA values recorded at the four CBD strong motion stations (i.e., REHS, CCCC, CHHC, and CBGS stations) surrounding the building sites (Bray et al. 2014a,b). Liquefaction was not observed at these stations for the Darfield and June 2011 events, but it was observed at some of the stations for the Christchurch event. However, in the latter case, the PGA values occurred before liquefaction effects are observed in the records. Thus, the estimated PGA values are not likely influenced by liquefaction.

There are no "outcropping rock" site recordings to use directly in the dynamic SSI analysis (Markham et al. 2016a). Additionally, the Canterbury basin is hundreds of meters deep, and most of its soil layers are not well characterized. Even if an "outcropping rock" site recording existed, the results of seismic site response analyses of the very deep soil profiles that extended to bedrock would be uncertain. However, there is a significant impedance contrast between the near surface soils and the pervasive, dense Riccarton Gravel layer, which is at a depth of about 20-24 m in the CBD (Markham et al. 2016a). Thus, recorded ground motions at shallow, stiff (non-liquefiable) soil sites west of the CBD were used by Markham et al. (2016a)

to deconvolve “within” motions for the top of the dense Riccarton Gravel layer using the Silva (1988) deconvolution procedure. The Markham et al. (2016a) deconvolved Riccarton Gravel motions were modified in this study to consider the differences of the rupture distance (R_{rup}) and the stiffness of the Riccarton Gravel between the deconvolution sites and the CBD sites. The deconvolved motions were scaled linearly with a factor derived from the Bradley (2013) New Zealand-specific ground motion prediction equation (GMPE). The scaling factor was calculated as the average of the ratio of the 5% damped response spectra from the GMPE estimated using the different R_{rup} and Riccarton Gravel V_{s30} values for the CBD site and the deconvolution site. The deconvolved, modified “within” Riccarton Gravel motions were assigned at the rigid base of the numerical model as input motions.

Figure 3.2 shows the input “within” North-South (NS) component acceleration–time histories at the top of the dense Riccarton Gravel layer for the CTUC building for the three events, with their respective acceleration response spectra and Husid plots as well as other important ground motion parameters, such as peak ground acceleration (PGA), significant duration (D_{5-95}), arias intensity (I_a), mean period (T_m) and shaking intensity rate (SIR). The “within” Riccarton Gravel ground motions for these three earthquakes differ significantly in terms of the intensity, frequency content, and duration. The Christchurch earthquake produces an intense, short-duration motion in the CBD compared to the larger magnitude, larger source-to-site distance Darfield event which produces a less intense (half the amplitude) but longer duration motion. The 13 June 2011 motion intensity is between those of the Darfield and Christchurch motions with a similar duration to the Christchurch motion.

3.3. SITES DESCRIPTIONS AND PERFORMANCE OBSERVATIONS

3.3.1. CTUC Building

3.3.1.1. Building Description

The CTUC office building (S43.529 E172.642) was a 6-story (21-m high) RC frame structure, which was 20 m wide (EW) and 25 m long (NS), supported on individual footings connected with tie beams (Zupan 2014). The building foundation and the eastern NS-oriented structural frame are shown in Figure 3.3. A majority of the foundation consisted of 2.44-m square footings that were embedded 0.46 m or 0.6 m, which supported 0.5-m wide square RC columns. There were also a large 9-m square footing where two columns, the elevator, and stair core were founded on the west side of the building, a 0.9-m thick, 1.3-m wide, and 15.44-m long EW-oriented footing, which supported a RC block wall, on the north side of the building, and two 0.46-m thick, 0.91-m wide, and 4.88-m long footings that supported southern 0.45 m x 1.5 m RC columns. RC tie beams (0.3 m x 0.38 m) connected the NS-oriented structural frames. In the NS direction, RC tie beams of the same dimension connected the three southern spans, whereas 0.61 m x 1.22 m RC tie connected the two northern spans. The embedment depths of the footings were 1.2-1.3 m. The spacing between columns was 4.9 m to 5.2 m in the NS direction and 9.15 m in the EW direction.

The columns of the building had a square section with a width of 0.5 m from ground level to the third floor, where they transition to 0.45-m wide square columns to the 5th story. The columns were connected on each floor with 0.4 m x 0.6 m beams in the EW direction. In the NS

direction, only the eastern frame was connected through beams of the same size. The floor consisted of 0.075-m thick uni-span precast concrete floor with 0.075-m thick RC topping. The top floor was a composition of four EW oriented steel frames connected in the NS direction with steel beams. Footing pressures, including dead load and 20% of the live load, were estimated to be 190–250 kPa.

3.3.1.2. Site Conditions

Six CPTs and one soil boring were advanced to characterize subsurface conditions (shown in Figure 3.3 except CPT Z4-10, which is located to the north). The subsurface profile along the building's east side is shown in Figure 3.4. The groundwater depth was estimated to be 2.5 m for the Darfield and Christchurch events, and 2.0 m for the 13 June 2011 event (New Zealand Geotechnical Database 2016). There is fill at the surface which is underlain by a shallow silty sand/sandy silt (SM/ML) layer that extends down to a depth of 2.5 m across the site, except for at the building's south side where this layer extends to 5 m depth. Its CPT tip resistance (q_t) is generally less than 5 MPa ($D_r \approx 35 - 45\%$), and its Soil Behavior Type Index (I_c) is generally between 2.2 and 2.4. Thus, the loose SM/ML layer below the groundwater table is likely to liquefy when strongly shaken. A dense gravelly sand with q_t values of 20-30 MPa ($D_r \approx 80-90\%$) underlies the shallow SM/ML layer and extends to 7.5-9 m depth. The gravelly sand is underlain by a medium dense sand and silty sand with q_t values of 10-20 MPa ($D_r \approx 60-70\%$) and I_c values of 1.6-1.9 which extends down to a depth of 16-17 m. There are thin layers of silts and clayey soil layers, with $I_c = 2.9-3.2$ within this layer of medium dense sand and silty sand. They are more closely spaced at the south side of the building, and CPT Z4-5 estimates their undrained shear strength (s_u) to be about 150 kPa. A dense sand soil layer with $q_t = 25-30$ MPa ($D_r \approx 80-90\%$) and $I_c = 1.6-1.8$ is below a depth of 16-17 m and extends down to 21 m. An overconsolidated silty clay ($I_c > 2.6$ and $s_u = 100-200$ kPa) underlies this unit down to a depth of 21 m to 24 m. The dense Riccarton Gravel unit underlies the overconsolidated clay unit. The red and orange shaded zones in Figure 3.4 correspond to silty and sandy soils, respectively, with factor of safety against liquefaction (FS_l) less than 1.0 for the Christchurch event using the Robertson and Wride (1998) liquefaction evaluation procedure.

Markham (2015) performed classification and advanced testing on soil samples retrieved with the Dames & Moore hydraulic fixed-piston sampler and found that the critical layer at the south side of the CTUC building (i.e., the shallow, loose material identified in CPT Z4-5) could be divided in two distinct layers; a silty sand (SM) between 2.7 and 3.4 m and a sand or sand with silt (SP or SP-SM) between 3.4 and 4.0 m. The lower material (SP and SP-SM) had sufficiently low density (i.e., $q_{c1ncs} < 60$) that it is believed that the retrieved clean to only slightly silty sand samples were densified during the sampling process (Markham et al. 2016a). Siltier materials, like the SM between 2.7 and 3.4 m, or denser materials ($q_{c1n} > 60$), such as the medium dense SP/SM material between the depths of 10-15 m were retrieved without evidence of disturbance and tested by Markham (2015). The laboratory tests provide useful information on the medium dense soils and loose silty sands (SM) at the site, but they cannot be relied upon to characterize the shallow, loose SP and SP/SM material at the CTUC building site.

3.3.1.3. Seismic Performance

Damage to the CTUC building was negligible during the Darfield earthquake and minor during the 13 June 2011 earthquake, but severe liquefaction in the foundation soils during the Christchurch earthquake induced differential settlements that produced structural deformation and cracking (Bray et al. 2014a, Zupan 2014). Figure 3.3 shows measured differential settlements in each column relative to the adjacent building to the north which did not appear to settle relative to the surrounding ground. The SE column settled significantly more than the other columns. The differential settlement led to angular distortions of 1/50 in the southern span. Large amounts of sediment ejecta were observed at the SE corner of the building and limited ejecta occurred at the column directly north of the SE column. Bray et al. (2014a) performed bearing capacity calculations of the SE footing using the residual undrained strength of the liquefiable sand and calculated its static factor of safety (FS) to be less than one.

Table 3.1 summarizes the author's best interpretation and estimation of settlements that occurred in the NE and SE corners of the CTUC building during the Christchurch earthquake. Building settlements were not noticed after the Darfield earthquake and were negligible after the 13 June 2011 earthquake. Settlement estimates are categorized by the type of settlement (i.e., shear-induced, volumetric-induced, and sediment ejecta-induced settlement). Differential building punching settlements were measured to be 60 mm and 310 mm in the NE and SE corners, respectively. Sediment ejecta were only observed in the Christchurch event near the SE corner of the building, and sediment ejecta-induced settlement was estimated to be 70-150 mm based on observations of the amount of soil removed below the foundation. Volumetric-induced ground settlements were estimated using the Zhang et al. (2002) procedure with FS_I obtained from Robertson and Wride (1998). Shear-induced building settlements were estimated by comparing the estimated volumetric and sediment ejecta settlements with the measured differential settlement. Total liquefaction-induced settlements of about 160-300 mm and 320-600 mm were estimated for the NE and SE corners of the CTUC building, respectively, which are consistent with the measured differential settlement across the building of 250 mm on average.

3.3.2. FTG-7 Building

3.3.2.1. Building Description

The FTG-7 building (S43.526 E 172.638) was also demolished after the Canterbury earthquake sequence. It was a 7-floor (23.9-m high) steel frame structure, which was 29.1 m wide (EW) by 31.8 m long (NS), that was supported on reinforced concrete (RC) strip footings (Zupan 2014). Figure 3.5 shows the foundation plan view with the CPT locations and also a typical interior frame of the structure. In the NS direction, the foundation consisted of two perimeters RC strip footings, which were 0.6 m thick, 2.4 m wide, and 29 m long, with an embedment depth of 1.2 m. The four interior RC strip footings were 0.6 m thick, 3.3 m wide, 25 m long, and embedded 0.6 m into the ground. The distances between the centerlines of the NS-oriented footings and columns were between 5.5 m and 6.3 m. The interior and perimeter footings were interconnected in the EW direction through 0.6 m by 0.6 m RC tie beams. The EW-oriented perimeter footings were 0.6 m thick, 2.0 m wide, 34 m long, and embedded 1.2 m. The EW perimeter footings were connected to the NS-oriented footings through 0.6 m by 0.6 m

tie beams. The distances between the centerlines of the EW-oriented tie beams and columns were between 6.0 m and 6.8 m.

The columns were wide-flange steel sections with their web aligned parallel to the NS direction. The dimensions of the W sections depend on the building floor and column location. Primary beams (W section) connected columns in the NS direction. Secondary (smaller) beams connected columns and primary beams in the EW direction. The size of the beams depends on the building floor and whether is an interior or perimeter beam as shown in Figure 3.5. The ground floor consisted of a 0.1-m thick unreinforced concrete slab, and floors 2 through 7 consisted of 0.12-m thick RC slab over 0.75 mm galvanized steel decking. The pressure at the base of a representative footing was estimated to be 80–100 kPa, which includes 100% of the dead load and 20% of the live load.

3.3.2.2. Site Conditions

Five CPTs, which were located near the building corners and along its northern perimeter, and three soil borings, which were located along its southern perimeter, were used to characterize the subsurface conditions at the FTG-7 site (as shown in Figure 3.5). The site conditions are not as variable as typically found in Christchurch (see soil profile shown in Figure 3.6). There is fill with relative density (D_r) \approx 65% from the ground surface to 1-1.5 m depth. A sandy silt/silty sand unit with variable fines content (FC) and soil behavior type index (I_c) generally between 2.2–2.4 underlies the fill and extends to a depth of 7–8.5 m. The “clean sand” equivalent relative density for this deposit is 35-55% (based on Idriss and Boulanger 2008). Below this layer, a medium dense sand ($I_c \approx$ 1.8 and 2.1) with $D_r \approx$ 60–70% is found that extends down to a depth of around 14-16.5 m. Below the medium dense sand, very dense sand ($D_r \approx$ 90%) is encountered. The CPT typically reaches refusal in this unit.

The red and orange shaded zones correspond to silty and sandy soils, respectively, with factor of safety against liquefaction (FS_l) less than 1.0 for the Christchurch event using the Robertson and Wride (1998) liquefaction evaluation procedure. Taylor (2015) estimated the depth of the Riccarton Gravel as 22 m based on a soil boring near the SE corner of the FTG-7 building. A 1–2-m thick clayey silt (ML/MH) layer with some peat overlies the Riccarton Gravel. The groundwater table depth was about 2.0 m throughout the Canterbury earthquake sequence (New Zealand Geotechnical Database 2016).

3.3.2.3. Seismic Performance

The seismic performance of the FTG-7 building was assessed in the reconnaissance efforts after several of the key earthquakes as well as detailed floor-level and verticality surveys and LiDAR data performed after the Christchurch and 13 June 2011 earthquakes. The observed seismic performance presented in Bray et al. (2014a) is summarized herein with the addition of an assessment of the LiDAR data performed by M. Jacka (personal communication). The LiDAR data proved useful in estimating the vertical movements of the building and surrounding ground, which in turn enabled estimates of settlements produced by sediment ejecta and volumetric deformations mechanisms.

There was only minor surficial evidence of liquefaction at the site after the Darfield earthquake (see van Ballegooy et al. 2014 for descriptions of minor, moderate, and severe liquefaction). The Christchurch earthquake caused severe liquefaction at the site, and the 13 June

2011 earthquake caused moderate liquefaction. The building was damaged significantly by the Christchurch earthquake (e.g., the columns at the ground level were structurally damaged). Floor levels and building verticality surveys (Eliot Sinclair and Partners Limited 2011 and Beca Carter Hollings & Ferner Ltd. 2011) indicated tilting of the building towards the SE. One of the surveys indicated a downward displacement of 100 mm of the SE corner of the building relative to its NW corner. Additional surveys were performed following the 13 June 2011 event, which found an additional 35 mm of differential settlement of the SE corner relative to the NW corner. Total settlements relative to the city benchmarks were estimated as 550 mm and 700 mm for the NW and SE corner, respectively. These measurements include tectonic settlement as a result of the Christchurch earthquake which is in the order of 100–150 mm according to regional tectonic models by GNS (New Zealand Geotechnical Database 2016). LiDAR data indicate free-field ground settlements, which result from volumetric and sediment ejecta mechanisms, of 300 mm and 200 mm for the Christchurch and 13 June 2011 events, respectively. Additionally, LiDAR data indicate building settlements of 400 mm and 100 mm for the Christchurch and 13 June 2011 events, respectively, after removal of the tectonic ground movement. Table 3.2 summarizes the author's best interpretation of the measured settlement values as well as the best estimated values of the different liquefaction-induced displacement mechanisms (shear-induced, volumetric, and sediment-ejecta settlements). The total liquefaction-induced building settlement values were 300–550 mm and 450–700 mm for the NW and SE corners, respectively, which agree with measured values of 400–450 mm and 550–600 mm for the same two building corners.

3.4. CALIBRATION OF THE CONSTITUTIVE MODEL

The PM4Sand Version 3 (Boulanger and Ziotopoulou 2015) constitutive model was used to capture the cyclic response of sandy soils. The model was calibrated using advanced laboratory testing and simplified liquefaction triggering procedures. PM4Sand model parameters were developed using best-estimated median values of unit weights (γ), relative densities (D_r), and shear wave velocities (V_s). The use of median values of relative density is consistent with the recommendations of Montgomery and Boulanger (2017) who found characteristic values for uniform models to be within the 30th and 70th percentiles when estimating liquefaction-induced ground displacements. Estimating displacement was judged to be more important than capturing pore water pressure response, which was the focus of the Popescu et al. (1997) study that suggested using lower percentiles for characterizing uniform sand deposits. Median values of these parameters were obtained through correlations with the CPT (e.g., Robertson 2010) for unit weight; Idriss and Boulanger (2008), here called IB-08, Kulhawy and Mayne (1990), and Jamiolkowski (1991) with weights of 0.4, 0.3, and 0.3, respectively, for D_r ; and the McGann (2015) Christchurch-specific correlation between CPT data and V_s , which then was used to obtain the normalized shear modulus (G_o). Additional parameters found from laboratory testing in the two sites (Markham 2015 and Taylor 2015) include critical state line parameters ($Q = 8.0$ and $R = 1.0$), critical state friction angle (ϕ_{cv}), bounding surface parameter (n_b) and maximum and minimum void ratios (e_{max} and e_{min}). Keeping these parameters fixed and using the confining pressure of the different units, element tests were modeled in FLAC 2D (Itasca, 2009) and the contraction rate parameter (h_{po}) was varied to obtain the cyclic resistance ratio (CRR) at 15 cycles obtained from the advanced laboratory testing or the Boulanger and Idriss (2016) simplified liquefaction procedure (herein called BI-16). The soil parameter values selected for

the PM4Sand model used for sandy soils at the FTG-7 and CTUC buildings are provided in Table 3.3. Default PM4Sand model parameter values (Boulanger and Ziotopoulou 2015) were used for those parameters not listed in Table 3.3.

Markham (2015) retrieved “undisturbed” samples using the Dames & Moore sampler and after careful transportation and extrusion, some specimens were isotropically consolidated to values of vertical effective stress comparable to field conditions including an estimated increment of stress due to the building’s load and then stress-controlled triaxial tests were performed using a sinusoidal pattern at a frequency of 0.1 Hz under undrained conditions. For the CTUC building, the constitutive model was calibrated against laboratory-based liquefaction resistance curves for the SM shallow material. This material (and the other soil units which did not have a laboratory-based CRR curve) was also calibrated based on the 50% probability of liquefaction (P_L) CRR curve at 15 cycles from the BI-16 liquefaction triggering procedure method. The reason for doing two calibrations for the loose SM material was to explore potential differences, which were found to be insignificant for this case. Advanced laboratory testing by Markham (2015) and Taylor (2015) was available for the FTG-7 building. Tests performed by Markham (2015) on the medium dense sand (SP/SM) specimens, which could be retrieved without significant sample disturbance, provided a reliable liquefaction resistance curve. Gel-push samples tested by Taylor (2015) produced reliable liquefaction resistance curves for both the loose SM/ML and medium dense SP/SM units. These two soil units at the FTG-7 building site were calibrated using the laboratory testing data and then using the simplified liquefaction procedure to explore potential differences, which again were insignificant.

Figure 3.7 shows the calibration for the loose SM/ML shallow layers for the CTUC building and the FTG-7 building. The $CRR-N_{cycles}$ curve from the element test simulations is compared with the plus and minus one standard deviation range of the $CRR-N_{cycles}$ curves implied by the MSF relationships from the IB-08 liquefaction triggering method and they also show the laboratory-based cyclic resistance curves. The data from Markham (2015) and Taylor (2015) are also shown for the CTUC and the FTG-7 building sites in Figures 3.7a and 3.7b respectively. The position of the $CRR-N_{cycles}$ curve in the PM4Sand model is controlled primarily by the parameter h_{po} , which was changed until the CRR at 15 cycles from either laboratory testing or the desired simplified relationship was achieved. Once the position of the curve is determined, the slope of the curve is controlled primarily by the n_b parameter, which defines the change in the peak stress ratio as a function of the relative state parameter (ξ_R) (Boulanger and Ziotopoulou 2015). This relationship was obtained from the results of isotropically consolidated drained triaxial compression (CIDC) tests performed by Taylor (2015). With these two parameters calibrated (i.e., h_{po} to capture CRR_{15} and n_b to capture the results of CIDC tests), the resulting curves from the numerical model can be compared to the $CRR-N_{cycles}$ curves implied by the magnitude scaling factor (MSF) relationships. For the cases shown in Figure 3.7, the curves from the numerical model are in good agreement with IB08 MSF relationship. However, the modeling of other soil units with different h_{po} and n_b values can have slopes that are in more agreement with the updated density-dependent MSF relationship implied by the BI-16 MSF relationship. Representative comparisons of the numerical simulations and the laboratory test results are presented in Figure 3.8 and in Luque and Bray (2015). The Mohr-Coulomb model was used for clayey soils, with parameters presented in Table 3.4.

3.5. FREE-FIELD RESPONSE ANALYSES

The free-field soil responses at the sites were studied first. The seismic site responses in terms of PGA, pore water pressure ratio (r_u), and shear strain were computed at several locations and compared to the results of the factor of safety against liquefaction (FS_l) from the BI-16 simplified liquefaction procedure in Figure 3.9. The numerical analyses calculate zones of high pore water pressures ratio and shear strain in zones where the simplified procedure estimated $FS_l < 1$. The differing levels of calculated shear strain highlight the differences in the soil response during each of these events. Shear strains of $< 0.2\%$, $1-1.5\%$, and $< 0.7\%$ are calculated at the CTUC site for the Darfield, Christchurch, and 13 June 2011 events, respectively. The Christchurch earthquake also produces the largest calculated shear strains among these three events for the FTG-7 site. Shear strains of $3-4\%$ and r_u values of 1 are calculated in a large part of the upper, loose SM/ML layer. Significant r_u values of about 0.5 are also calculated in the deeper medium dense sand but the shear strains are less than 1% . The CPT-based simplified liquefaction triggering evaluation indicates that the performances of the sites during the Darfield and 13 June 2011 events should be similar. However, more liquefaction-induced damage was observed at these sites for the 13 June 2011 event. Loss of the beneficial effect of soil ageing (Seed 1979) is the most likely explanation of the larger amounts of liquefaction observed after the 13 June 2011 event, which followed the intense Christchurch event that produced moderate to severe liquefaction in the CBD. The PM4Sand model does calculate higher r_u values at the CTUC site for the 13 June 2011 event than for the Darfield event, which is more consistent with the observations. Lastly, relatively high values of pore water pressure ratios (i.e., > 0.5) do not necessarily translate into high shear strains as shown at the CTUC site for the 13 June 2011 event.

The computed 5%-damped acceleration response spectrum at the ground surface was compared to the acceleration response spectra recorded at the four strong ground motion stations in the CBD in Figure 3.10. For both sites the results show good agreement between calculated and recorded response spectra for the Christchurch and Darfield events. The 13 June 2011 event analyses computed higher response spectra than the recorded spectra, especially for the FTG-7 site, where significant amplification is calculated because of the relatively small amount of hysteretic damping due to computed shear strains being less than 0.2% . The difference in the computed spectrum and recorded ground motion spectra for the 13 June 2011 event is most likely due to the uncertainty in the input “within” ground motion. The adjusted deconvolved motion derived from recordings in the western part of Christchurch likely overestimated the intensity of the ground motion in the CBD. There are also differing site characteristics between each of the strong motion stations and the studied sites. Considering all of the above, the calculated response spectra are reasonable.

Therefore, given the calibration with the lab and field liquefaction triggering data, the reasonable comparison between the computed responses and established simplified liquefaction triggering procedures, and these favorable comparisons of computed and record acceleration response spectra, there is confidence that the calibrated PM4Sand model can provide useful insights. These calibration and comparison checks are important steps to undertake before performing the dynamic SSI analyses that follow.

3.6. BUILDING RESPONSE ANALYSES

3.6.1. General

Figure 3.11 shows the computational models employed in the dynamic SSI analyses performed in this study. The location of the lateral boundaries of the models was selected after a sensitivity analysis to minimize their effects on the structural performance while minimizing calculation time. The final models were approximately 2.5 to 3 times wider than the width of the building. The Riccarton Gravel was modeled as a rigid base and the input motions were applied as “within” acceleration time-histories obtained from the deconvolution process. Rayleigh damping of about 0.5% at frequencies between 1.5 to 2 Hz was used (corresponding to the average between the natural frequency of the building and the mean frequency of the input motion). The maximum element size was one tenth of the wavelength associated to the maximum frequency, which in this case was limited to 15 Hz by the Silva (1988) deconvolution procedure. The maximum element size was typically 1.2-1.5 m in the loose materials.

Popescu and Prevost (1993b) and Adrianopoulos et al. (2010) recommended reducing the bearing pressure of a 3D structure when analyzing the building 2D plain strain conditions. These recommendations were based on numerical simulations of rigid structures, but the structures modelled herein are not rigid, and the inertial response of the structure is important and may significantly influence the response of the system. Thus, modeling the structure with realistic mass and stiffness to obtain reasonable values of natural undamped period (T_n) was required in these analyses to capture the SSI-induced mechanism. However, the influence of out-of-plane drainage that occurs in the field is not captured in 2D analyses (e.g., Popescu et al. 2005). This mechanism is expected to play a less important role for cases involving a structure, where shear-induced mechanisms control the response (Dashti et al. 2010a,b). Dashti and Bray (2013) were able to capture the key response characteristics of 3D model buildings shaken in centrifuge experiments with 2D analyses. The uncertainty in the value of the horizontal hydraulic conductivity of the liquefied soil is likely larger than the modeling error introduced by using 2D analyses of a problem that includes some 3D water flow.

3.6.2. CTUC Building

The NS-oriented eastern structural frame of the CTUC building is analyzed. The elasticity young's modulus and unit weight of concrete were 2.35×10^7 kPa and 24 kN/m^3 , respectively. The flexural cracking of the structural elements was considered by applying a factor of 0.35 and 0.7 to the inertia of beams and columns, respectively (ACI 318-14, 2014). Beams oriented in the direction of the analysis were modelled considering the contribution to the stiffness of the floor slab by using an effective width following the recommendations of the ACI 318-14 (2014). The distribution of beams in the out-of-plane direction was taken into account by using a typical frame spacing of 9.1 m.

The dynamic SSI analyses helped to identify the primary mechanisms of building settlement during the Canterbury earthquake sequence (other than sediment ejecta-induced settlement which was not captured in these continuum analyses). The CTUC building performance during the damaging Christchurch earthquake was driven primarily by a bearing capacity-type of failure of the foundations near the SE corner of the building. The SE exterior column is founded on a 4.88 m x 0.91 m spread footing that has loose silty sand/sandy silt just

1.3 m below it. This mechanism led to excessive shear-induced settlements, illustrated by the shear strain contours shown in Figure 3.12. It is apparent that there is a large concentration of shear strains within the liquefiable soil just below the SE corner of the building. Shear strains on the order of 8% are calculated within the shallow, loose silty sand/sandy silt layer under the SE corner of the building; whereas shear strains on the order of 1-2% are computed within this shallow liquefiable layer in the free-field south of the building. In this area of large shear strains beneath the southern part of the building foundation the soil displaces laterally and upwards. Large shear strains do not develop under the middle and NE corner of the building, because the shallow, loose silty sand/sandy silt was not present below the groundwater table at these locations (see Figure 3.6). The differing responses of the soils directly beneath the shallow foundations of the CTUC building are the primary reasons for the 250-mm differential settlement observed across the building.

The accumulation of vertical displacements calculated at the southern and northern corners of the CTUC model during the Christchurch earthquake are presented in Figure 3.13(a). The comparisons of the calculated and measured vertical settlement profile are shown in Figure 3.13(b). The settlements shown in Figure 3.13 represent the seismic settlement that occurred during strong shaking, which is mostly shear-induced settlement. Some volumetric-induced settlement that occurs during strong shaking is also included. However, these results do not show the majority of volumetric post-liquefaction reconsolidation settlements that occur after strong shaking due to dissipation of excess pore water pressure as the FLAC analyses were terminated after shaking ended to minimize computational time. Version 3.0 of the PM4Sand model has been calibrated to calculate post-liquefaction reconsolidation settlements consistent with accepted simplified empirical procedures. The continuum analyses do not capture settlement due to the formation of sediment ejecta. Thus, the calculated settlements shown in Figure 3.13 are comparable to the estimated shear-induced settlement presented in Table 3.3, which is largely a result of the mechanism shown in Figure 3.12. The analytical results show how the different soil conditions under the southern and northern ends of the building affect the seismic performance of the building. There is a shallow loose silty sand layer from a buried stream channel present only under the southern side of the building. This layer causes significantly more shear-induced ground settlement under the southern side of the building. The differential settlement across the building footprint, which is most important in evaluating the seismic performance of the structure, is captured well by the numerical analyses.

The sensitivity of the calculated CTUC building displacements due to the input ground motion and the characteristics of the loose SM/ML liquefiable layer were studied, and the resulting range of displacements is shown in the red shaded zone shown in Figure 3.13. The range of calculated shear-induced settlement settlements is 80–130 mm and 30–80 mm in the SE and NE corners of the CTUC building, respectively; whereas the estimated values for this mechanism are 100–200 mm and 60 mm for the SE and NE building corners, respectively. Thus, the amount of shear-induced settlement measured after the Christchurch event is well captured in the dynamic SSI analyses if one remembers that part of the observed differential building settlement was due to the formation of sediment ejecta, which is not captured in these analyses. Less seismically induced settlements are calculated for the CTUC building for the Darfield and 13 June 2011 earthquakes relative to those calculated for the Christchurch earthquake; however, differential building settlements are overestimated for these two events. The calculated differential settlements were 30 mm and 70 mm for the Darfield and 13 June 2011 events, respectively, which exceed the lack of observed differential settlements during the Darfield event

and the less than 20 mm observed differential settlement for the 13 June 2011 event. The overestimation of the settlement for the 13 June 2011 event is attributable largely to the uncertainty in the input ground motion. As discussed previously, the free-field response for this event is overestimated, resulting also in larger calculated settlements. When the 13 June 2011 input ground motion is scaled down by a factor that would yield a calculated free-field response spectra in accordance to recorded spectra within the CBD, the liquefaction-induced building settlements were also less than 20 mm.

3.6.3. FTG-7 Building

The EW-oriented southern structural frame of the FTG-7 building was also analyzed. The elasticity modulus and unit weight of steel used for the analyses were 2.0×10^8 kPa and 77 kN/m^3 , respectively. In elements where the stiffness of the system came from different materials (steel and concrete), an equivalent steel section was estimated such that the actual stiffness and weight of the system was obtained for the analysis. The area and second moment of inertia of the W sections were obtained directly from AISC (2014). The distribution of beams in the out-of-plane direction was taken into account by using a typical frame spacing of 6.4 m.

Shear strain contours calculated in the soils beneath the FTG-7 building at the end of the Christchurch earthquake shaking are shown in Figure 3.14(a). The dynamic SSI analyses calculate large shear strains at the edges of the buildings in addition to smaller, but still substantial, shear strains under the building and in the free-field in the loose SM/ML layer that was found between 2 and 7.5 m depth (see also Figure 3.9). A primary mechanism for building settlement in this case is SSI-ratcheting (see Figure 3.1), where the rocking of the building induces high seismic demands in the soils beneath the edge of the building. The rocking of the building is captured in the displacement-time histories calculated at the two exterior columns and one interior column shown in Figure 3.14(b). In every cycle of shaking as one of the exterior column displaces upward the other exterior column displaces downward, indicating building rocking. The interior column displaces steadily downward without the oscillation observed for the exterior columns. The high seismic demands induced by the building displace the soil laterally from beneath the edges of the building toward the free-field, which produces downward cyclic movement of the building. Consequently, vertical displacements were larger under the exterior columns than under the interior columns. Shear-induced partial bearing capacity and volumetric-induced mechanisms also contributed to building settlement.

The dynamic SSI analyses of the FTG-7 building estimated punching settlements in its SE corner of 50, 190, and 80 mm for the Darfield, Christchurch, and 13 June 2011 events, respectively. These settlements are overestimated for the Darfield and 13 June 2011 events, but they are in good agreement with observed settlements for the Christchurch event. More importantly for evaluating distortion induced in the structural frame and hence structural damage, the differential settlements calculated across the EW-oriented structural frames of the FTG-7 building are in good agreement with measured differential settlements after the Christchurch and 13 June 2011 events as shown in Table 3.5. The amount of differential settlement was sufficient to cause cracking in some of the structural members. The observed (and calculated) differential settlements of the FTG-7 building were considerably less than those of the CTUC building, primarily because of the uniformity of the soil profile underlying the FTG-7 building compared to the highly variable shallow soil profile under the CTCU building, with a liquefiable soil only present under one of its corners. Additionally, the CTUC building

foundation had a fairly narrow isolated spread footing supported on this soil with weak tie beams extending out to this corner footing; whereas the FTG-7 building had a more robust, stiff foundation with interconnected larger spread footings in both directions, which minimized differential building movements.

3.7. CONCLUSIONS

Soil liquefaction-induced building displacements cannot be estimated directly using simplified empirical procedures that only estimate 1D post-liquefaction volumetrically-induced settlement, because these procedures do not capture the important shear mechanisms involved in building movements. Dynamic SSI nonlinear effective stress analysis can capture the critically important liquefaction-induced shear deformations. The dynamic SSI analyses of the CTUC and FTG-7 buildings were able to capture the observed trends in the seismic differential settlement measured in the three primary earthquakes of the Canterbury earthquake sequence; albeit, the building performances during the more intense Christchurch earthquake were captured better than those during the less intense Darfield and 13 June 2011 events wherein liquefaction-induced settlements were overestimated. The satisfactory comparisons of field observations and analytical results of the two buildings analyzed herein were only accomplished after calibrating the soil constitutive model, which including using laboratory and field tests and ensuring the response of free-field 1D seismic site response analyses were in general agreement with the results from established simplified liquefaction evaluation procedures. Thus, achieving reliable analytical results required sound characterizations of the site and earthquake shaking.

The relative magnitudes of the shear-induced and volumetric-induced ground deformation mechanisms that contributed to the total building settlement were captured well in the dynamic SSI analyses. The variation of the soil profile across the CTUC building footprint, which at one end of the building included a shallow loose, saturated sand and silty sand deposit from a buried stream channel, produced the observed differential settlement of the building. The dynamic SSI analyses also indicated that the observed significant differential settlement was largely a result of a bearing capacity-type of failure in these soils that were only present under the SE corner of the building. The highlighting of the importance of the bearing-capacity mechanism for the CTUC building performance through the dynamic SSI analyses is consistent the results from conventional bearing capacity analyses that indicate a bearing failure. The dynamic SSI analyses of the FTG-7 building indicated that the SSI-ratcheting mechanism was important for this case. The rocking of the 7-story building displaced the soil beneath the edges of the building outward laterally away from the building, which in turn produced vertical building displacement. This type of shear-induced settlement is judged to be reasonable, because bearing capacity calculations do not indicate a low factor of safety for the soils directly beneath the FTG-7 building foundation components. The inability of continuum-based soil models to capture the effects of sediment ejecta should be recognized as an important limitation for cases wherein this important mechanism governs performance.

Table 3.1: Settlement of the CTUC building during the Christchurch earthquake

Type of Settlement	NE corner		SE corner	
	Measured (mm)	Estimated (mm)	Measured (mm)	Estimated (mm)
Differential Settlement ^a	60		310	
Shear-Induced Settlement ^b		60		100 – 200
Volumetric-Induced Settlement ^c		100 – 200		150 – 250
Sediment Ejecta Settlement ^d		0		70 – 150
Total Liquefaction-Induced Settlement		160 – 260		320 – 600

^a Settlement measured relative to the adjacent building to the north, which did not appear to settle relative to the surrounding ground.

^b Shear-induced settlement estimated by comparing the estimated volumetric and sediment ejecta settlements with the measured differential settlement.

^c Volumetric-induced settlement estimated using Zhang et al. (2002) procedure based on Zupan (2014).

^d Sediment ejecta settlements were estimated based on photographic evidence of ejecta amount.

Table 3.2: Settlement of the FTG-7 building

Type of Settlement	Event	NW corner		SE corner	
		Measured (mm)	Estimated (mm)	Measured (mm)	Estimated (mm)
Total Building Settlement ^a	-	550		700	
Tectonic Movement ^b	-	100 – 150		100 – 150	
Total Liquefaction-Induced Settlement	-	400 – 450	300 – 550	550 – 600	450 – 700
Shear-Induced Settlement ^c	Darfield		0		0
	Christchurch		90 – 130		170 – 210
	13 June 2011		10 – 20		30 – 40
	Total		100 – 150		200 – 250
Volumetric-Induced Settlement ^d	Darfield		16		16
	Christchurch		120 – 260		170 – 310
	13 June 2011		20 – 30		20 – 30
	Total		150 – 300		200 – 350
Sediment Ejecta Settlement ^e	Darfield		0		0
	Christchurch		40 – 80		40 – 80
	13 June 2011		10 – 20		10 – 20
	Total		50 – 100		50 – 100

^a Total building settlement was measured accurately with surveys.

^b Tectonic movement based on calibrated seismological model developed by the GNS Science, New Zealand.

^c Settlement estimated from photographic evidence after the 13 June 2011 event, from detailed measurements of differential settlements relative to the NW corner, and from LiDAR data.

^d Volumetric-induced settlement of ground was estimated from nearby measured values, LiDAR data, and judgment.

^e Sediment ejecta settlements were estimated based on photographic evidence of ejecta amounts and judgment.

Table 3.3: PM4Sand model parameters for cohesionless soils at FTG-7 and CTUC building sites

Parameter	CTUC					FTG-7				Source
	Fill	SM/ML	SP/GP	SP/SM	SP	Fill	SM/ML	SP/SM	SP	
γ (kN/m ³)	17	16.6	19.7	19.3	20.3	18.8	17.3	18.8	20.3	CPT ^a
D_r (%)	50	40	85	65	85	63	43	63	89	CPT ^a
G_o	500	400	1500	900	2000	400	360	760	1350	CPT ^a
h_{po}	1.0	1.2	3	0.3	7.0	1.2	2.2	0.55	20	Calib.
ϕ_{cv}	35	35	35	35	35	35	35	35	35	T(15)
Q	8	8	8	8	8	8	8	8	8	M(15)
R	1	1	1	1	1	1	1	1	1	M(15)
n_b	1.4	1.4	1.4	1.4	1.4	0.8	0.8	0.6	0.6	T(15)
e_{max}	1.3	1.25	1.1	1	1	1.2	1.3	1	1	T(15)- CPT ^a
e_{min}	0.6	0.6	0.6	0.6	0.6	0.6	0.6	0.6	0.6	
k (m/s)	1.1e-5	2.0e-6	3.8e-4	4.8e-5	9.5E-5	6.2e-6	1.0e-6	1.6e-5	1.1e-4	CPT ^a

Note: T(15) stands for Taylor (2015), and M(15) for Markham (2015)

^a Robertson (2010) correlation for unit weight. Idriss and Boulanger (2008), Kulhawy and Mayne (1990) and Jamiolkowski (1991) correlations with weights of 0.4, 0.3, and 0.3, respectively for D_r . McGann (2015) correlation for shear wave velocity (V_s) to get G_o . CPT-FC correlation from Robinson (2013) and then FC- e_{max} and FC- e_{min} data from Taylor (2015). Robertson (2015) for hydraulic conductivity.

Table 3.4: Model parameters for cohesive soils for FTG-7 and CTUC building sites.

Parameter	CTUC		FTG-7
	ML/CL “shallow ”	ML/CL	ML/CL “deep”
γ (kN/m ³) ^a	17.5	18.5	18.5
Porosity	0.45	0.45	0.45
Cohesion (kPa) ^a	150	200	200
Friction angle (degrees)	0	0	0
Poisson's ratio	0.3	0.3	0.3
Shear Modulus (MPa) ^a	70	100	100
Bulk Modulus (MPa)	150	216	216
Tension (kPa)	1	1	1
Dilation angle (degrees)	0	0	0
k (m/s) ^a	8×10^{-8}	1×10^{-9}	1×10^{-9}

^aObtained from CPT correlations

Table 3.5: Comparison of differential settlements from numerical simulations and measured displacements after different events for EW oriented frames of the FTG-7 building.

Event	Calculated Differential Settlements (mm)	Measured Differential Settlements (mm)					
		Line A	Line B	Line C	Line D	Line E	Line F
Darfield	5 – 10	No measurements taken for this event					
Christchurch	20 – 50	23	20	11	13	27	27
13 June 2011	10 – 20	20	18	5	21	1	3

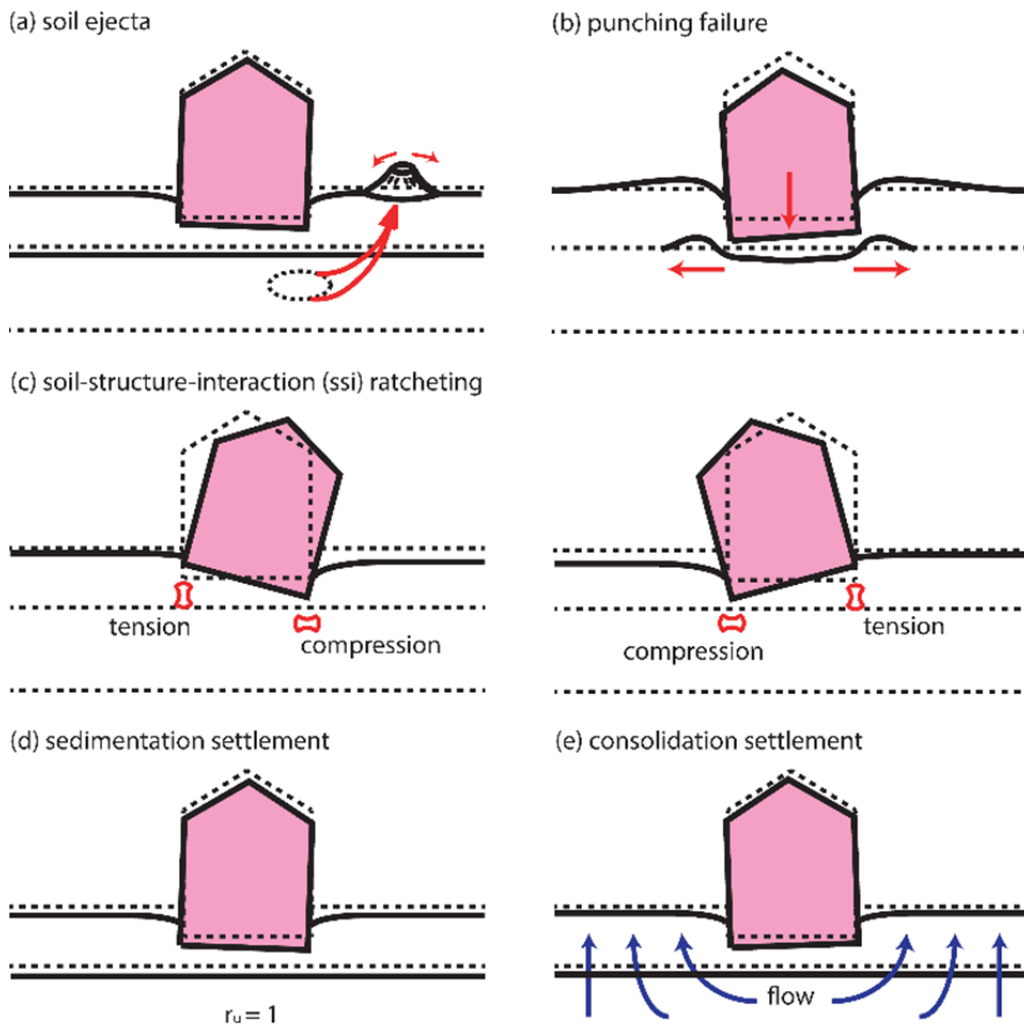


Figure 3.1. Liquefaction-induced displacement mechanisms: (a) ground loss due to soil ejecta; shear-induced settlement from (b) punching failure, or (c) soil-structure-interaction (SSI) ratcheting; and volumetric-induced settlement from (d) sedimentation, or (e) post-liquefaction reconsolidation (modified from Bray and Dashti 2014).

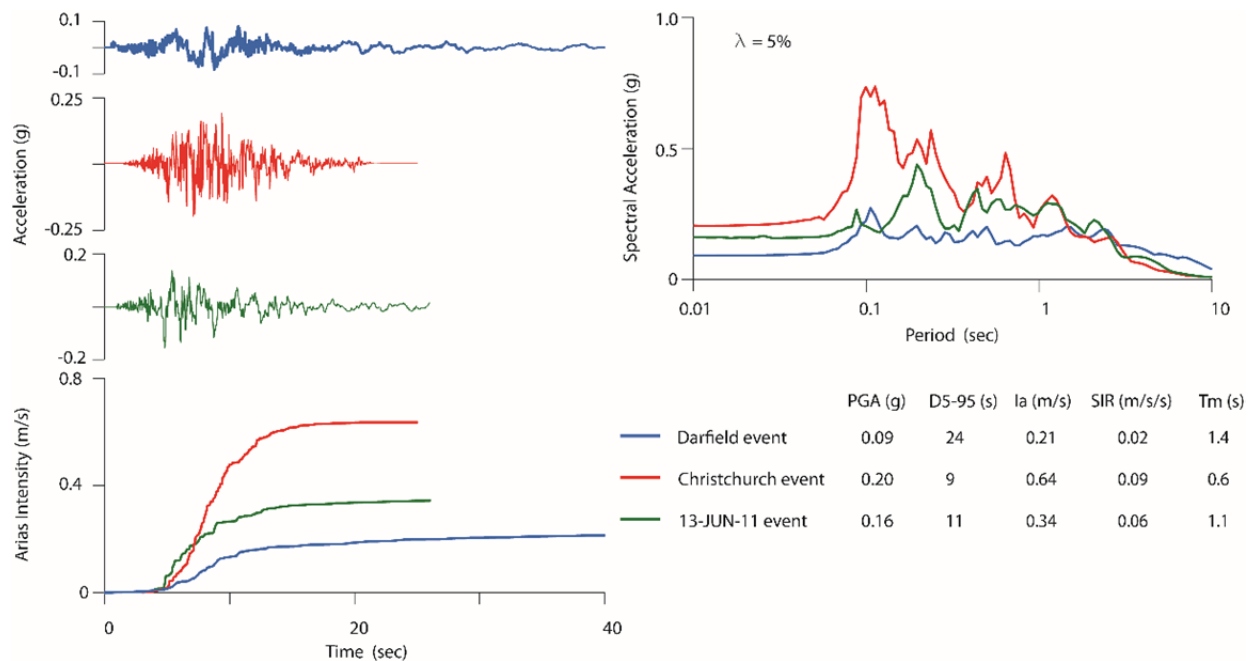


Figure 3.2. Input deconvolved “within” ground motions from the RHSC station for the NS component for the three primary earthquakes of the Canterbury earthquake sequence.

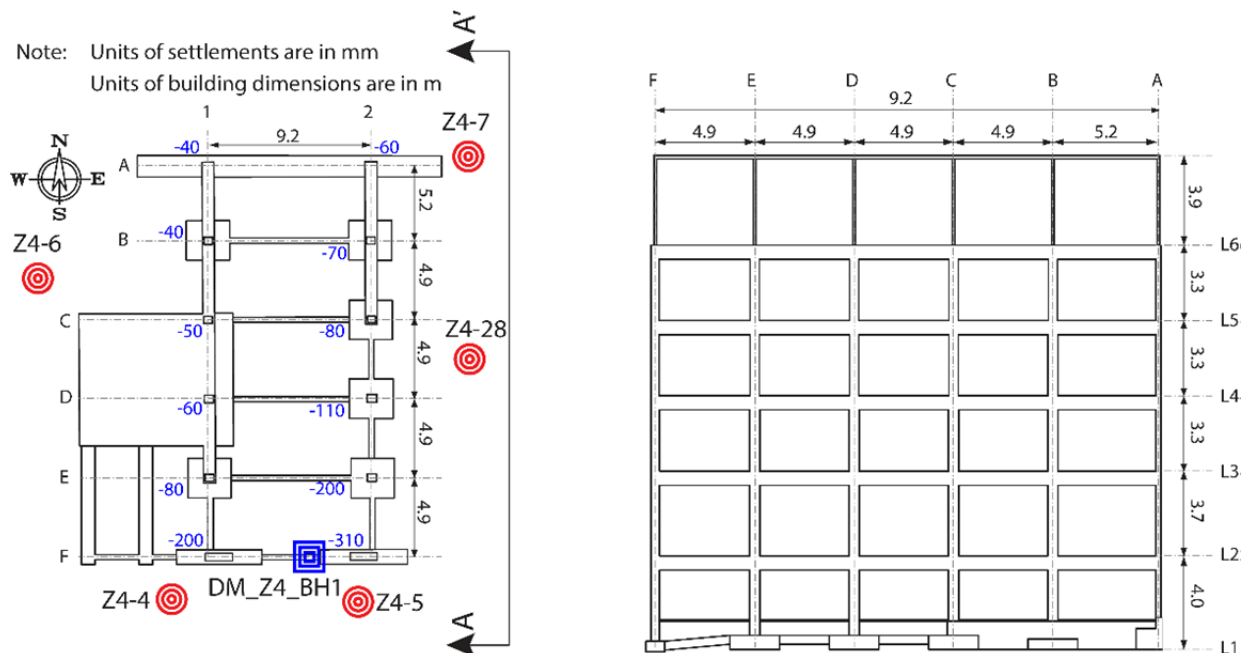


Figure 3.3. Foundation plan view of the CTUC building and elevation view of its eastern NS-oriented frame.

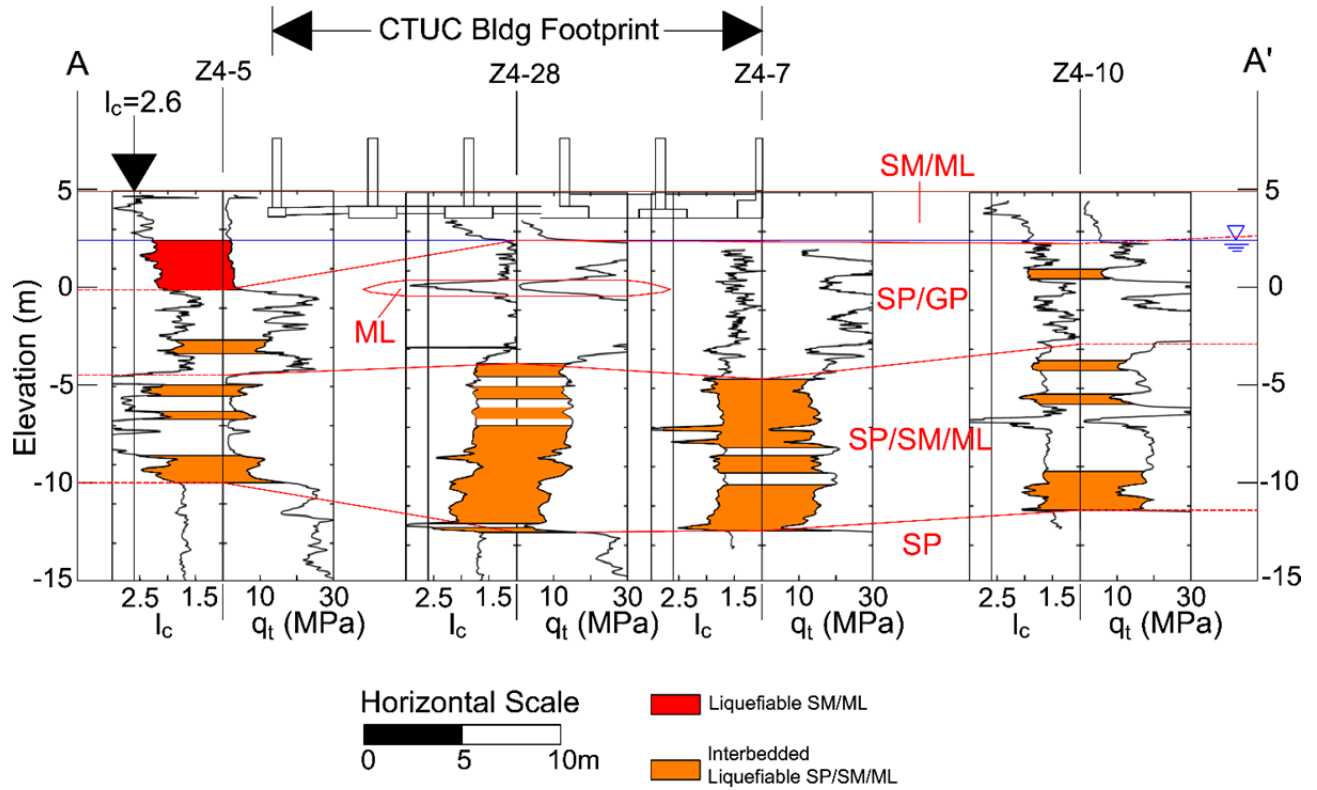


Figure 3.4. Subsurface conditions at the CTUC building site showing zones of materials with $FS_1 < 1.0$ based on the Robertson & Wride (1998) procedure using the median PGA from Bradley (2014) for the Christchurch earthquake (from Bray et al. 2014a).

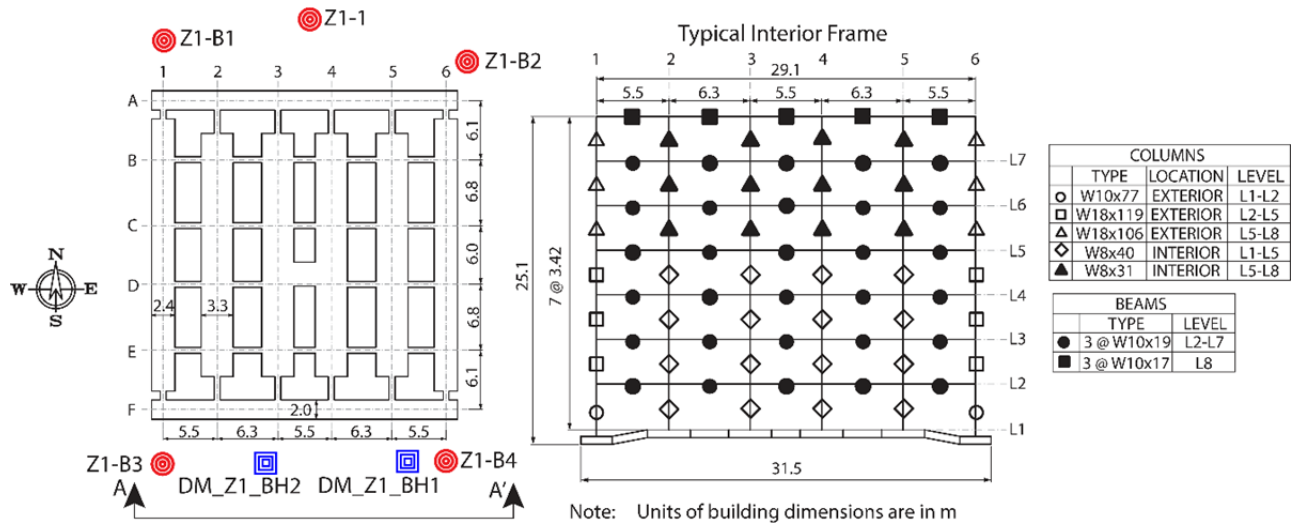


Figure 3.5. Foundation plan view of the FTG-7 building and elevation view of a typical interior frame in the EW direction.

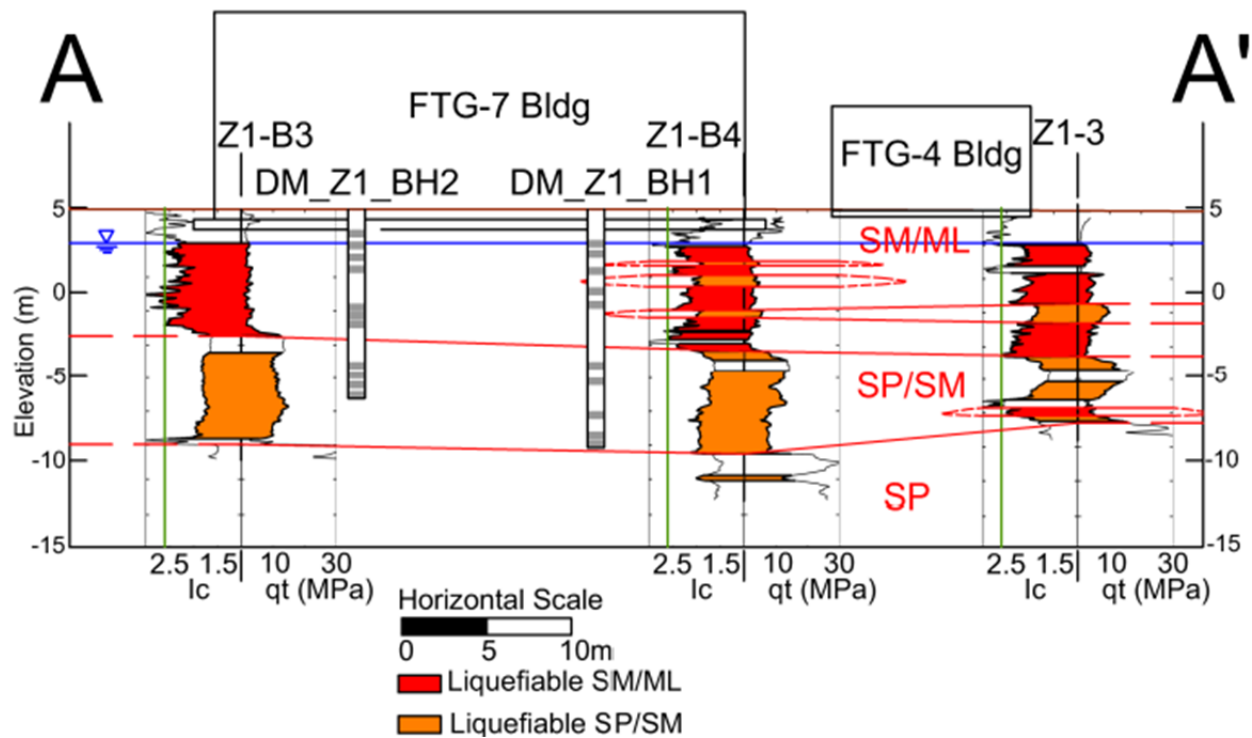


Figure 3.6. Subsurface conditions at the FTG-7 building site showing zones of materials with $FS_1 < 1.0$ based on the Robertson & Wride (1998) procedure using the median PGA from Bradley (2014) for the Christchurch earthquake (from Markham 2015).

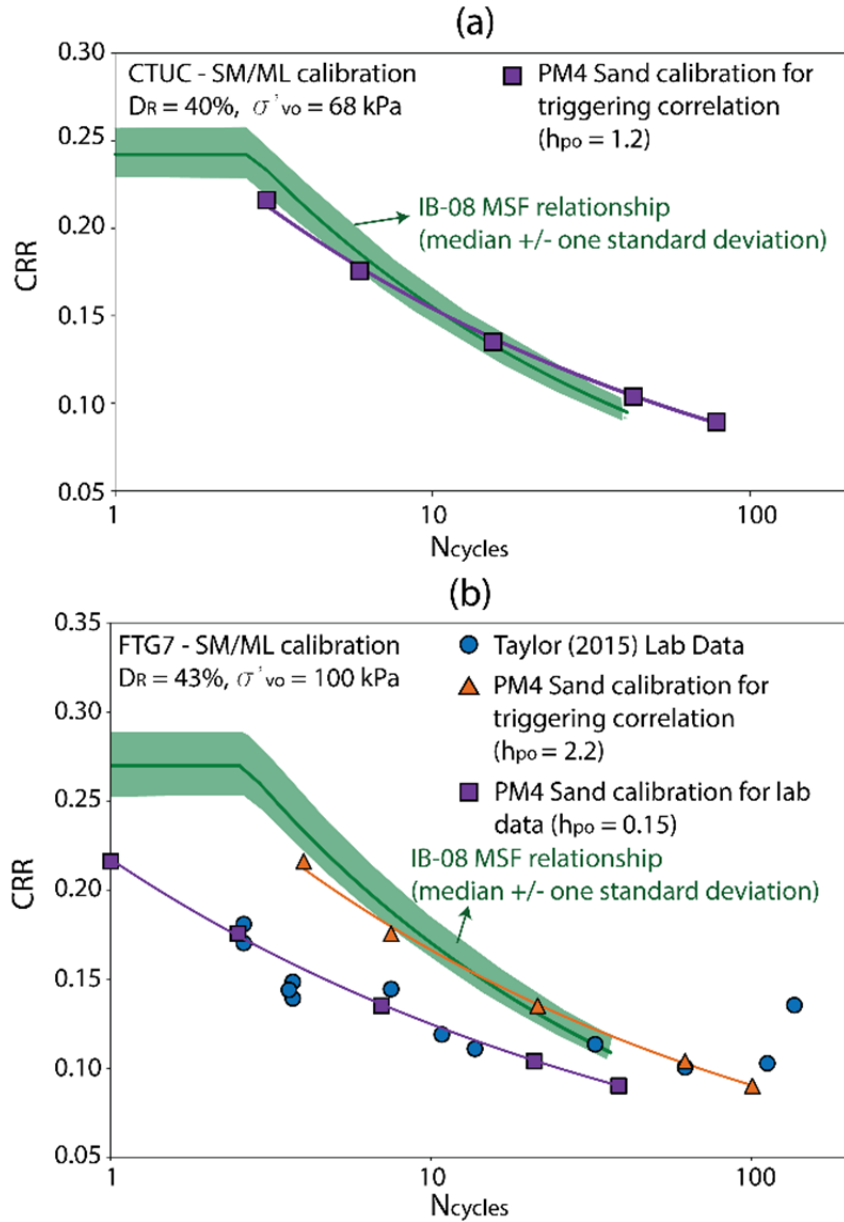


Figure 3.7. CRR- N_{cycles} curves for: (a) SM/ML soil at CTUC building and (b) SM/ML soil at FTG-7 building.

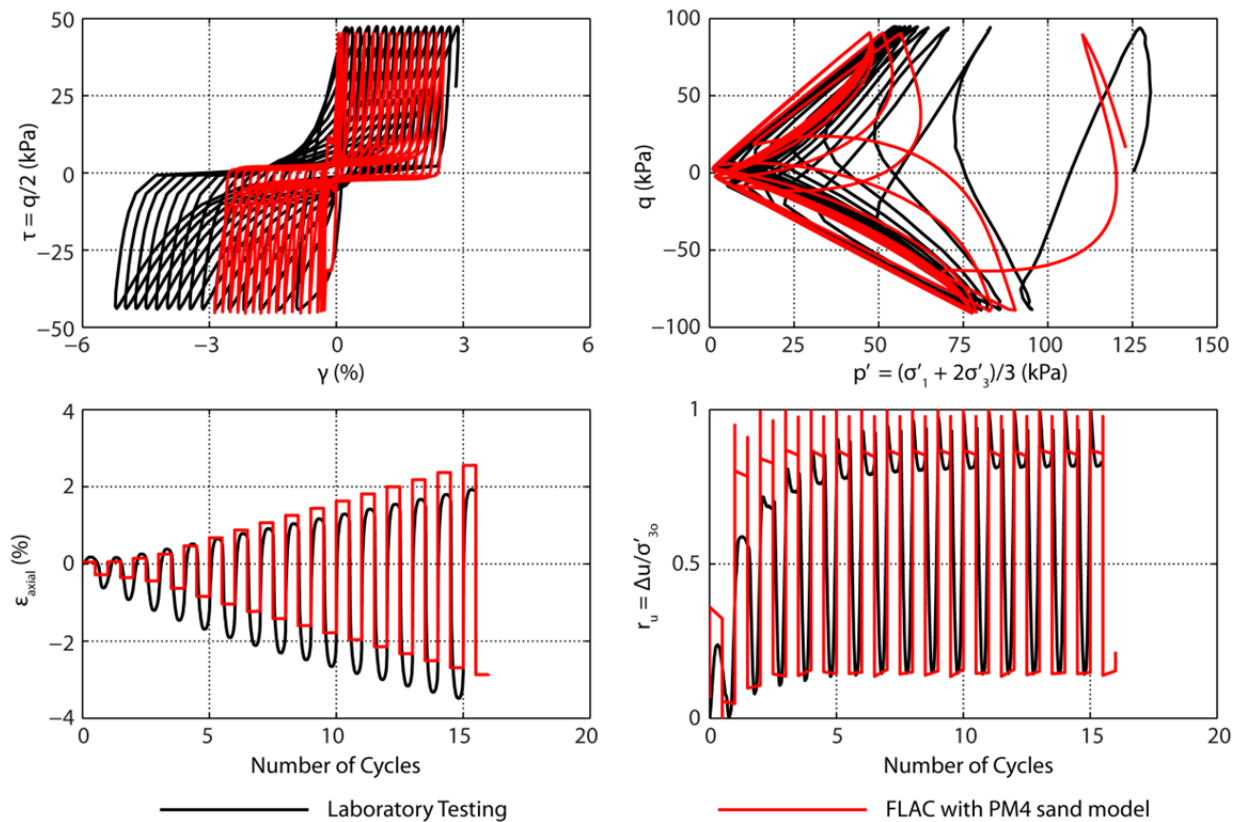


Figure 3.8. Comparison between laboratory cyclic triaxial test results (black) and FLAC simulated test (red) for a specimen from a depth of 10.97 m at the FTG-7 building site.

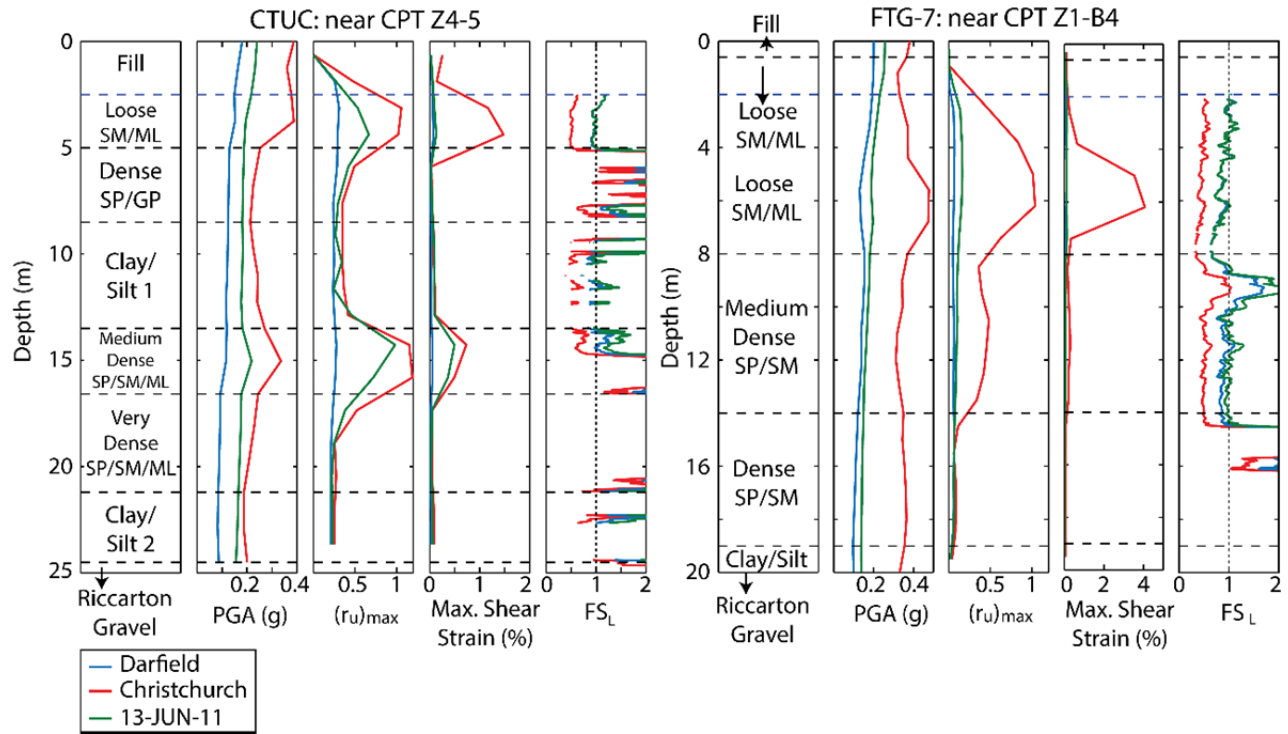


Figure 3.9. Seismic response of the free-field condition for the CTUC and FTG-7 building sites.

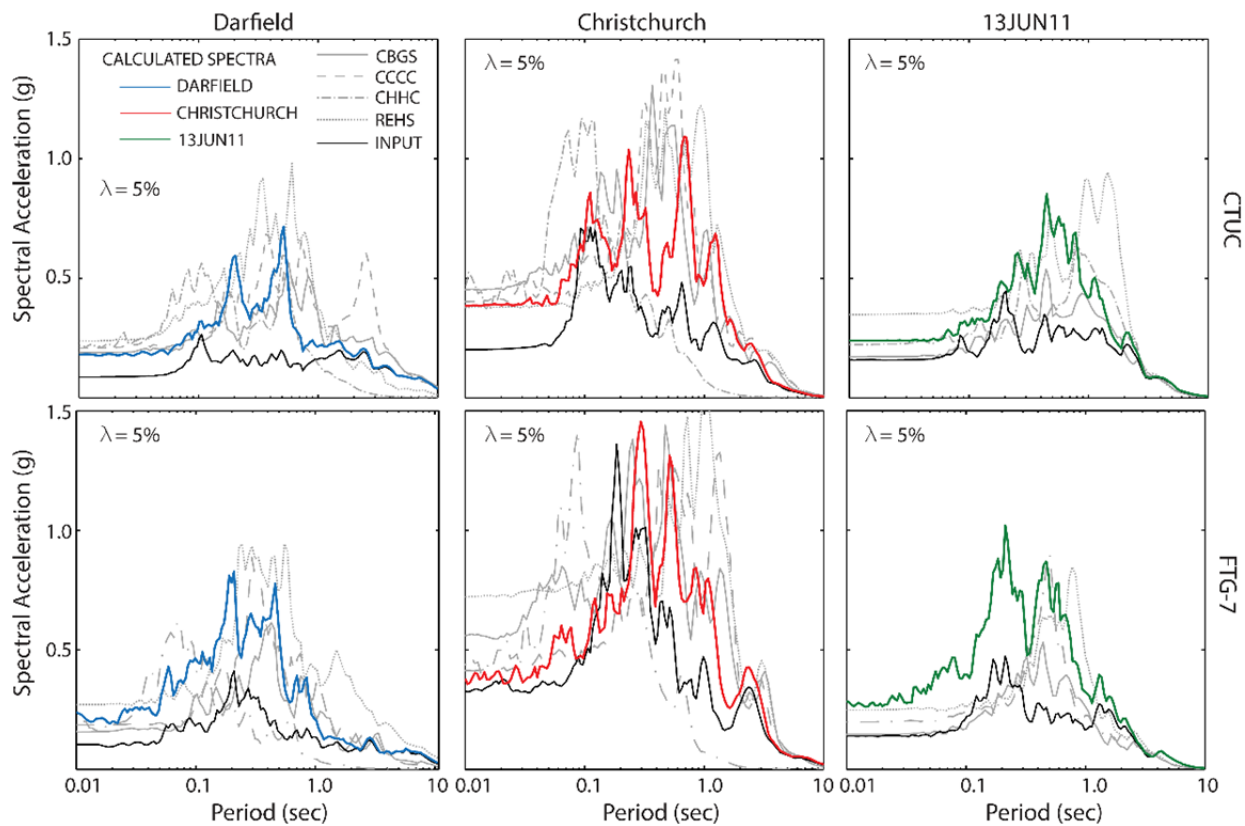


Figure 3.10. Acceleration response spectra (5% damped) calculated for the CTUC building site (top row) and FTG-7 building site (bottom row) compared to recorded response spectra at nearby recording stations.

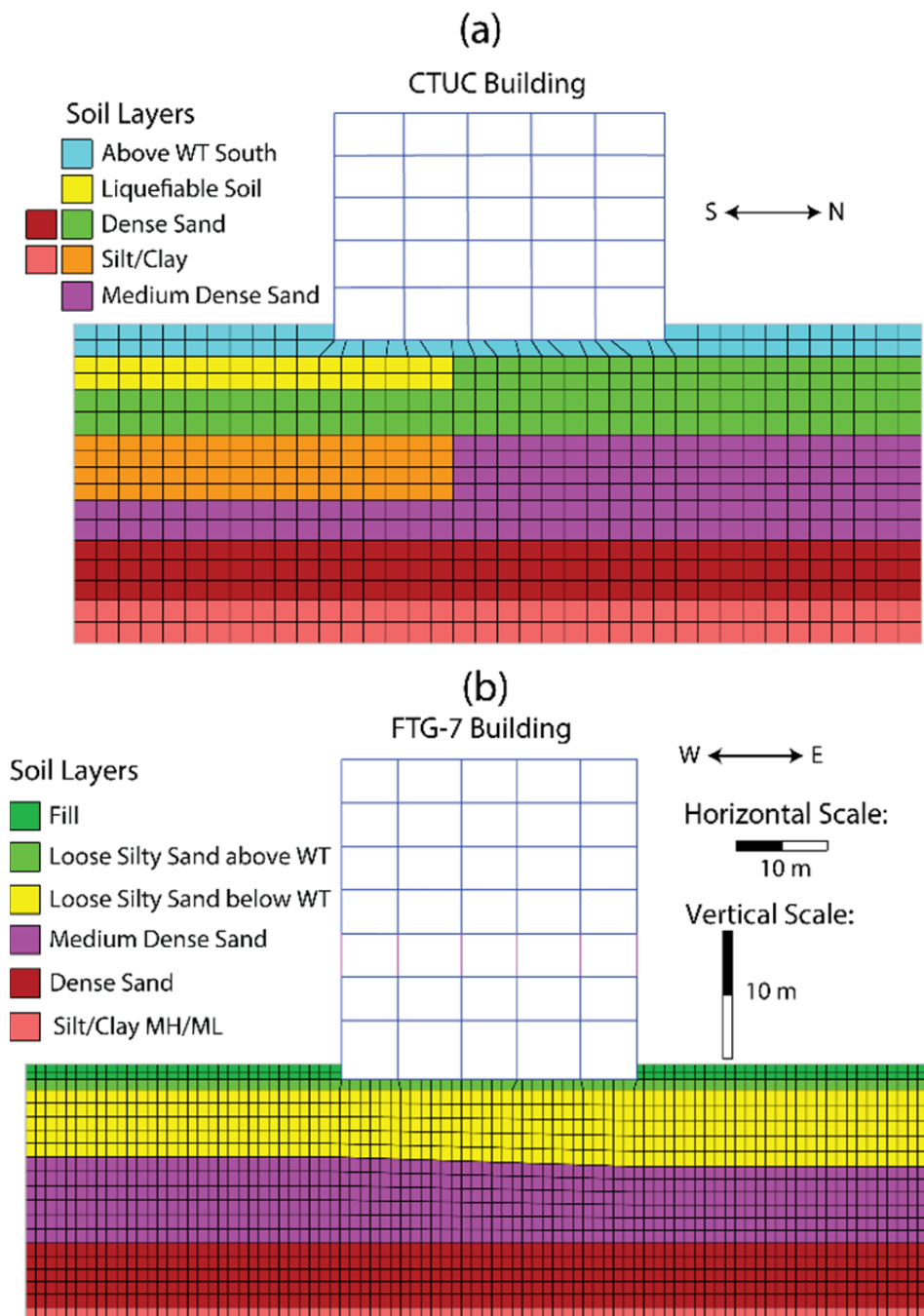


Figure 3.11. Geotechnical and structural model for the (a) CTUC and (b) FTG-7 buildings.

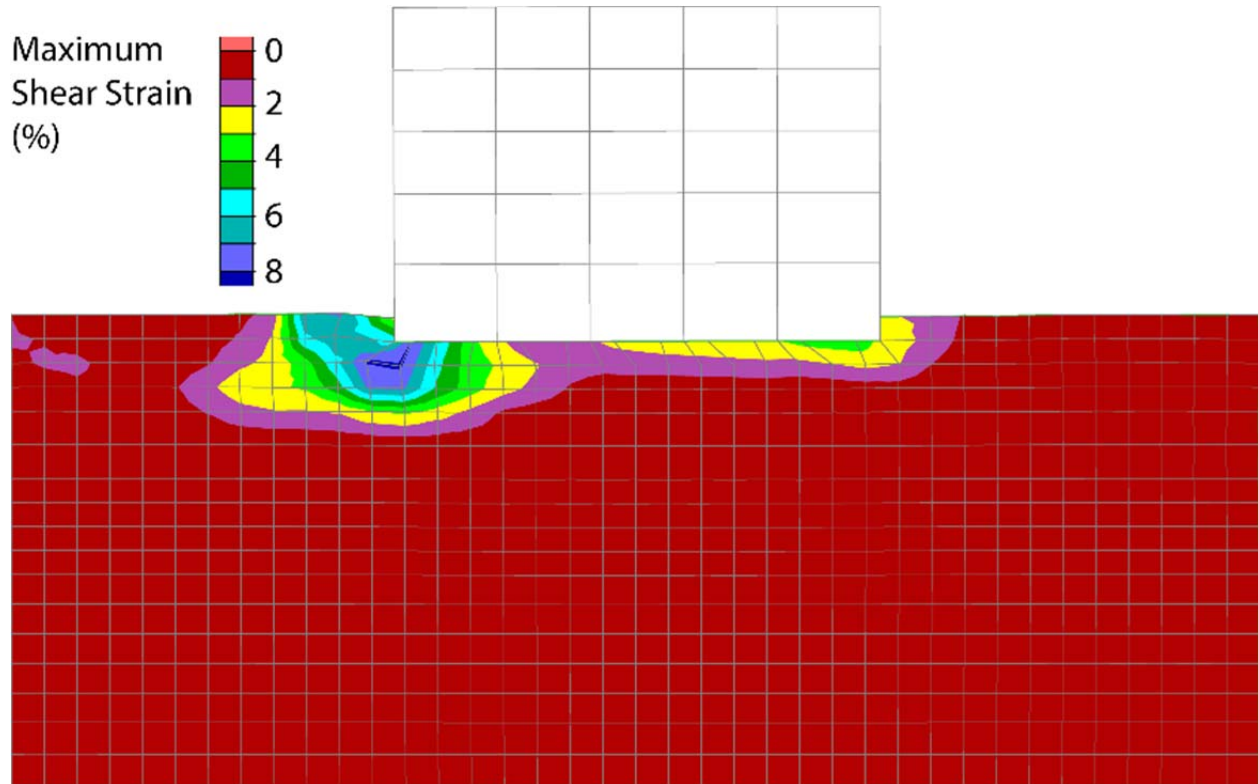


Figure 3.12. Shear strain contours for soils beneath the CTUC building at end of the Christchurch earthquake.

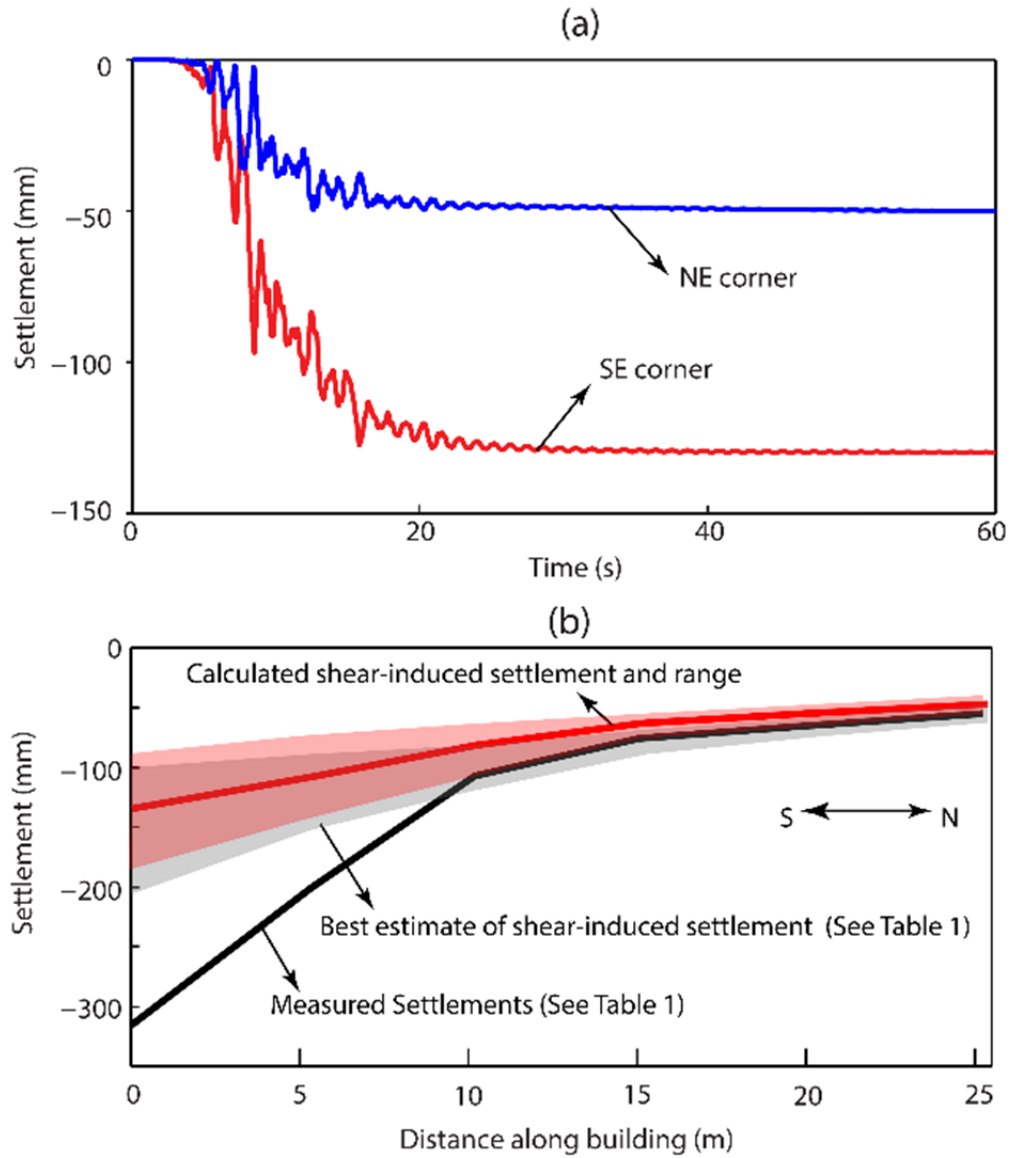


Figure 3.13. (a) Displacement time-history at the southern and northern columns of the CTUC building for the Christchurch earthquake, and (b) settlement profile along the building.

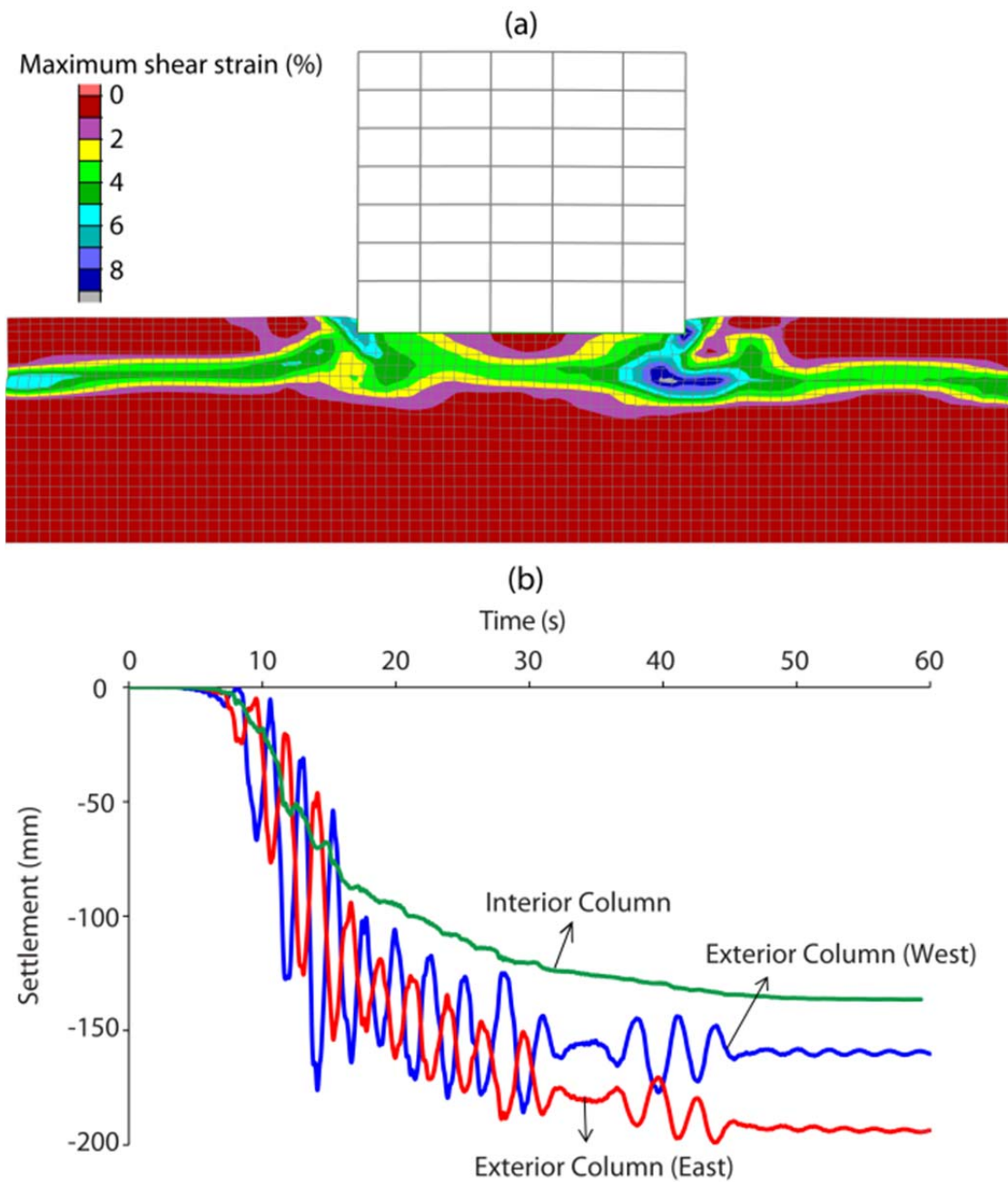


Figure 3.14. (a) Shear strain contours for soils beneath the FTG-7 building at the end of the Christchurch earthquake, and (b) displacement time-histories at western, eastern, and interior columns for the Christchurch earthquake.

CHAPTER 4: DYNAMIC SOIL-STRUCTURE INTERACTION ANALYSES OF TWO IMPORTANT STRUCTURES AFFECTED BY LIQUEFACTION DURING THE CANTERBURY EARTHQUAKE SEQUENCE

4.1. INTRODUCTION

Damaging liquefaction-induced building settlement has been observed in several earthquakes, including the classic bearing capacity failure of apartment buildings in the 1964 Niigata, Japan earthquake and in more recent earthquakes such as in the 2010 Maule, Chile, 2011 Tohoku, Japan, and 2010 Christchurch, New Zealand earthquakes. Researchers have studied the effects of liquefied ground on the response of shallow-founded buildings largely through physical tests (primarily centrifuge experiments) or numerical modeling of the tests or more general conditions (Popescu and Prevost 1995, Liu and Dobry 1997, Elgamal et al. 2005, Lopez-Caballero and Farahmand-Razavi 2008, Adrianopoulos et al. 2010, Shakir and Pak 2010, Dashti et al. 2010 a,b, Karamitros et al. 2013a, Dashti and Bray 2013, Bertalot et al. 2013, Bray and Dashti 2014, Bertalot and Brennan 2015, Karimi and Dashti 2016 a,b).

Bray et al. (2014a) identified the primary mechanisms controlling liquefaction-induced movements of shallow foundations as shear-induced, volumetric-induced, and ejecta-induced mechanisms. Shear-induced mechanisms can be further classified as bearing capacity and soil-structure-interaction (SSI) ratcheting settlements (Dashti et al. 2010a,b). Volumetric-induced mechanisms can be further classified as consolidation, sedimentation, and partial drainage mechanisms (Dashti et al. 2010a,b). One mechanism that has not been captured well by centrifuge experiments or continuum-based numerical simulations but has been observed to be important in several earthquake reconnaissance efforts is the loss of ground beneath the structure due to sediment ejecta to the ground surface (Bray et al., 2014a). Additionally, the presence of a free-face near the building may induce lateral displacement of the soil and building towards the free-face and produce an associated vertical movement of the ground and building. Numerical analyses of centrifuge experiments involving structures over liquefiable ground have been employed to validate numerical simulations and to gain insight into the mechanisms controlling the response of those systems (Popescu and Prevost 1995, Elgamal et al. 2005, Lopez-Caballero and Farahmand-Razavi 2008, Adrianopoulos et al. 2010, Shakir and Pak 2010, Karamitros et al. 2013a, Dashti and Bray 2013, Bray and Dashti 2014, Karimi and Dashti 2016 a,b). However, until recently, relatively few back-analyses of well-documented case histories have been performed (Luque and Bray 2015). Although there are uncertainties in the input motions and the structural and geotechnical response of the system in field case histories, there is much insight that can be gained through back-analyses. Moreover, numerical simulations should be shown to capture key trends in the field observations if they are to be used by practicing engineers with confidence.

The back analyses of two well documented landmark buildings in the Central Business District (CBD) of Christchurch, New Zealand, which are close to the Avon River (< 50 m), are presented. The 21-story PWC building was the third tallest building in Christchurch when the Canterbury earthquake sequence initiated. The CTH auditorium is an architectural landmark in Christchurch. Both buildings were subjected to a series of major earthquakes in the 2010-2011 Canterbury earthquake sequence. Minor to severe liquefaction manifestation (e.g. sediment

ejecta and lateral spreading) were observed at the building sites. Ground and building settlement measurements were taken after the most important earthquakes using several techniques, such as conventional measurements, topographical level and tilting surveys and LiDAR point-cloud analysis data. These data are interpreted to develop fully the field case histories, so the building performances can be compared with analytical results. Salient insights are shared and recommendations are made for performing non-linear dynamic soil-structure-interaction (SSI) effective stress analyses of structures founded on liquefied soils.

4.2. CANTERBURY EARTHQUAKE SEQUENCE

4.2.1. Earthquake ground shaking in Christchurch

The 2010-2011 Canterbury earthquake sequence includes seven earthquakes with $M_w \geq 5.5$, three of which had $M_w \geq 6.0$. Four strong ground motion stations recorded the ground shaking in the CBD. The study focuses on the three events that produced most damage in the CBD, which in chronological order are: the M_w 7.1 4-SEP-2010 Darfield event, the M_w 6.2 22-FEB-2011 Christchurch event, and the M_w 6.0 13-JUN-2011 event. The Darfield earthquake was located at source-to-site distances (R_{rup}) of about 14 to 16 km west from the CBD and recorded geo-mean peak ground accelerations (PGA) that ranged from 0.16 to 0.25 g . The Christchurch earthquake was located only 3 to 6 km south from the CBD, with the recorded geo-mean PGA between 0.37 and 0.52 g in the CBD. It produced widespread damage of infrastructure, the collapse of one building, and 185 casualties. The 13-JUN-11 event was located around 6 to 8 km southeast of the CBD, with recorded geo-mean PGAs ranging from 0.16 to 0.26 g . Several other earthquakes occurred in the period of September 2010 and December 2011 without producing significant damage in the CBD.

Bradley (2014) provides maps of median PGA and its variability (σ) making use of ground motion prediction equations (GMPE) and its within-event spatial correlation. These estimates are useful for simplified liquefaction triggering assessment and for comparison with the results of free-field numerical analyses of the sites of study. For the PWC and the CTH building sites estimates of 16th, 50th and 84th percentiles PGA values are provided in Table 4.1, which also lists the recorded geo-mean horizontal PGAs at the four strong motions stations in the CBD (Bradley 2014).

4.2.3. Input ground motions

There was a dense array of strong motion stations in the Canterbury plains at the time of the 2010-2011 Canterbury earthquake sequence. Unfortunately, none of the stations (except for one station that was located well south of the city on the other side of the Port Hills) are located on competent rock. Instead, they are located atop alluvial deposits in a deep basin. Without an “outcropping rock” site recording near the Christchurch CBD, recordings at stiff soil sites that displayed negligible nonlinearity were used to deconvolved “within motions” at the top of the pervasive, dense Riccarton Gravel layer. Even if an “outcropping rock” recording was available, there would be a high degree of uncertainty in performing seismic site response analyses, because bedrock is at a depth of over a kilometer in the CBD and the deeper soil deposits are not well characterized.

Markham et al. (2016a) performed deconvolution analyses using the Silva (1988) procedure at two seismic stations with stiff soil conditions. The deconvolution was completed to the depth of the dense Riccarton Gravel layer, which provides a significant impedance contrast with the overlying alluvial deposits. Markham et al. (2016a) 0 showed that using the deconvolved ground motions from one of the stiff soil sites as input in a site response analysis of the other stiff soil site computed motions similar to the recorded motions, which validated their approach.

The Markham et al. (2016a) deconvolved motions are modified before using them in dynamic analyses of a specific structure, because the deconvolved motions represent the shaking at the top of the Riccarton Gravel at the site of the deconvolution with the stiffness of the Riccarton Gravel at that site. The building sites analyzed in this study have different source-to-site distance (R_{rup}) and different depths and stiffness of the Riccarton Gravel. To account for these differences, the deconvolved motion was modified by applying an amplitude scaling factor, which was estimated based on the Bradley (2013) New Zealand-specific GMPE by estimating the 5% damped response spectra for the building site and deconvolution site, each with its corresponding R_{rup} and estimated or measured V_{S30} value of the Riccarton Gravel. Median scaling factors across the period range of interest of the sites and structures were used. Sensitivity analyses were performed to evaluate the influence of varying the scaling factor. Figure 4.1 shows the top of Riccarton Gravel acceleration time-histories for the CTH site from the scaled deconvolved “within motions” for the NS component from the CACS station for the three earthquakes analyzed herein. The Christchurch earthquake is most intense followed by the 13-JUN-11 and Darfield events. The Darfield event has longer significant duration, because of its larger magnitude and distance. The Christchurch and 13-JUN-11 motions have similar durations and frequency content.

4.3. STRUCTURE & SITE DESCRIPTIONS AND PERFORMANCE OBSERVATIONS

4.3.1. PWC building

4.3.1.1. Building description

The PWC building was a 21-story structure (composed of reinforced-concrete (RC) except for its smaller, top floor of steel) with a one-story basement (Holmes Consulting Group (HCG), 1988). It was demolished due to damage from the Christchurch earthquake. The plan view and cross section of the PWC Building are shown in Figures 4.2 and 4.3 respectively. The basement footprint was 55 m in the EW direction and approximately 60 m in the NS direction. The first three floors of the tower, which served as parking space, were 55 m by 38 m in the EW and NS directions, respectively. The tall tower (Floors 4 – 20) was 35 m by 25 m in the EW and NS directions, respectively, and its southern perimeter was located at about 5.3 m from the southern wall. The northern zone of the basement (without a structure on top) had an irregular shape in plan view (see Figure 4.2). The basement foundation consisted of a RC mat with variable thickness as follows: 0.4-m thick section around the edges of the basement (including the northern zone), 1.8- m thick section supporting the perimeter columns of the tower with a width of 7 m and 5 m in the EW and NS directions, respectively, and 0.9-m thick section in the

interior of the 1.8-m thick ring section in the interior of the tower. The elevator shaft in the center of the tower was supported on a 0.9-m thick mat that was about 3.1 m below the basement level. The embedment depth of the mat foundation varied in the same way as the mat foundation's thickness (i.e., 3.1 m, 3.6 m, and 4.5 m for the 0.4-m, 0.9-m and 1.8-m thick mats, respectively, and up to 7.6-m deep in the center of the building at the elevator shaft pit).

The RC basement walls were 0.3-m thick. At the ground floor level, pre-cast beams of varying size tied the columns together and the ground level floor consisted of a combination of a pre-cast 0.2-m thick double tee with 0.125-m thick RC topping. The tower structure consisted of stiff perimeter frames composed of five lines of columns in the NS direction (with spacing between 6.1 m and 6.3 m) and 4 lines of columns in the EW direction (with spacing of about 7 m). These perimeter columns varied in dimension as follows: 1.1 m square columns for the corner columns and 1.1 m by 0.8 m for the perimeter columns, with their long side oriented in the direction of the frame (e.g., the long side of the columns was oriented in the EW direction along the southern perimeter). The columns were connected to each other by pre-cast concrete beams of varying dimensions depending on the floor level. In the interior of the building there were eight smaller columns that were aligned with the southern and northern perimeter columns in the EW direction. In the NS direction, instead of three columns as in the eastern and western perimeters, only two lines of columns existed with spacing of about 8.3 m. These interior columns were rectangular initially with dimensions 0.9 m by 0.7 m with their longer side oriented in the NS direction with their dimensions decreased for the upper floors. The interior columns were generally interconnected in the NS direction by pre-cast concrete beams of varying dimensions. The floor consisted generally of 0.2-m thick double tee with 0.065-m thick concrete. The orientation of the double tee's web was usually in the EW direction.

4.3.1.2. Site conditions

The PWC site is characterized through 11 cone penetration tests (CPTs) and 2 soil exploratory boreholes with sampling and laboratory testing (Figure 4.2). An idealized geotechnical profile along Section A-A' of Figure 4.2 is depicted in Figure 4.3. From the ground surface to a depth of about 2 to 4 m, there is a silty sand and sandy silt (SM/ML) with a "sand-equivalent" relative density (D_R) of 40-50%, soil behavior type index (I_c) between 2.0 and 2.6, which is called Unit 1. This layer is in contact with the basement walls, but it is not below the mat foundation. Following this layer is Unit 2, which is a very dense ($D_r \approx 90\%$) sandy gravel and gravelly sand ($I_c < 1.2$, SP/GP) with thickness of around 7 m and 4 m at the south and north sides of the building, respectively. It is in direct contact with the basement foundation. A medium dense 1-m thick sandy layer with D_r of 50-60% (Unit 3) is located within the southern part of Unit 2 approximately 3 m below the mat foundation. Considering the lateral variability of Christchurch soil deposits, Unit 3 is likely a medium-dense sand pocket within dense gravel layer. Unit 4 underlies Unit 2. Unit 4 is a medium dense ($D_r \approx 60-70\%$) sandy soil (SP/SM), with I_c usually between 1.6 and 1.8. Cyclic triaxial (CTX) testing of this soil was performed by Markham (2015) and his results were to calibrate the constitutive model in the analyses. Two loose sandy silty, silty sand (SM/ML) pockets (Units 5 and 6) are present within Unit 4 towards the north side of the building. Units 5 and 6 are at depths of 8 m and 15 m, respectively, and about 1 m thick. There are also several thin clay layers (< 0.2 m thick) within Unit 4 under the southern part of the building, which are not modeled. Unit 7 underlies Unit 4. Unit 7 is a 1 to 1.5-m thick clayey silt, silty clay material with $I_c \approx 3$ and undrained shear strength (s_u) of about 130

to 170 kPa. Unit 8 underlies part of Unit 7. Unit 8 is a medium dense sand ($D_r \approx 65-75\%$) layer with $I_c \approx 2.3$. The Riccarton Gravel layer is at the base of the soil profile at a depth of 21 m.

Figure 4.3 also shows the Avon River, which southern free-face is located approximately 40 m away from the northern basement wall of the PWC building. The ground surface slopes gently down toward the river. These topographical features are important as they impose a static shear stresses in the ground, which may produce lateral spreading that could affect the building's vertical movement. The ground water table was located at depth of 1.5-2 m during the Canterbury earthquake sequence. The depositional environment of the soils at the PWC site is influenced by its proximity to the river. The 1850 "Black Maps" (NZGD, 2016), which show the surficial ground conditions in Christchurch at that time, indicate there was a stream located near the southern part of the PWC site. Zones where buried streams are present have higher liquefaction damage vulnerability (Bray et al. 2014a).

4.3.1.3. Seismic performance

Several research teams evaluated the seismic performance of the PWC building during the Canterbury earthquake sequence (Giorgini et al. 2011, Zupan 2014, Giorgini 2015), and their information is summarized herein with additional information taken from the NZGD (2016). LiDAR data analyzed and interpreted by M. Jacka (personal communication, 2016) provided important insights on the settlement of the PWC building. Reliable LiDAR data are available only for the Christchurch and 13-JUN-11 events.

Field surveys after the Christchurch earthquake found soil ejecta in Armagh Street and Oxford Terrace (south and north of the PWC building, respectively). Measured ground settlements in localized zones were up to 100-150 mm and 300 mm south and north side of the building, respectively. LiDAR data indicate average ground settlement for the Christchurch earthquake of 50-100 mm and 100-180 mm south and north of the building, respectively. A large crack in Oxford Terrace, which was oriented parallel to the Avon River, indicates lateral movement toward to river. Several other minor cracks were observed north and south of the building, and they were typically oriented parallel to the Avon River. After the PWC tower was demolished, water accumulated in the southern part of the basement, which indicates differential settlement of the originally level mat foundation. The differential settlement towards the south was confirmed by tilt measurements taken at 24 columns between the first and second floors as well as tilt measurements of the basement walls. There was also slight tilting towards the west. In addition to these field observations, the LiDAR data (M. Jacka, personal communication, 2016) and NZGD (2016) information were used to assess the seismic performance of the building.

Table 4.2 provides the author's best interpretation of the vertical movements that occurred during the Canterbury Earthquake Sequence. Vertical settlements are provided for the three primary events. The data interpretation, which relied heavily on the LiDAR data, indicate that shear-induced liquefaction building settlements were approximately 80-170 mm and 30-100 mm for the south and north sides of the building, respectively. Shear-induced differential settlement averaged 60 mm. Patches of the LiDAR data in the surrounding streets provided estimates of free-field ground settlement, which resulted from volumetric-induced, ejecta-induced, and lateral spreading-induced ground deformations.

4.3.2. CTH auditorium

4.3.2.1. Building description

The CTH facility is composed of several structurally independent buildings. The seismic performance of the CTH auditorium, which is located at the west end of the facility, is investigated. Figure 4.4 shows the plan view of the auditorium and the nearby site investigations. Figure 4.5 shows section A-A' of the CTH auditorium. The original structural design plans (Holmes Consulting Group (HCG), 1968) and the post-earthquake seismic rehabilitation report by HCG (2011) provided much of the building information.

The auditorium consists of a basement, ground floor, gallery, mezzanine, and roof. The auditorium structure is composed of two separate quasi-concentric "rings." The outer ring is an irregular octagon that is longer in the EW (63 m) direction than in the NS direction (47 m). The inner ring has an ellipsoidal shape with its longest side of 48 m oriented in the EW direction and its short side of 35 m oriented in the NS direction. The outer ring has fourteen rectangular shallow RC footings with thickness of 0.46 m and horizontal dimensions of either 2.2 m by 3.2 m or 3.2 m by 3.2 m. Each of these footings receives two columns, and the footings are connected to each other by 0.46-m square RC tie beams. The embedment depths of the outer footings are 3.6 m, 2.7 m, or 1.9 m, depending on the location of the footings. The columns in the outer ring are 10 m high. The inner ring has a continuous 0.66-m deep footing that generally has a width of 1.8 m and an embedment depth of either 3.8 m or 2.9 m. This long footing becomes a 3.65-m-square footing at the 14 footing locations in the inner ring. The combined system (1.8-m wide strip footing and 3.65-m square pads) support 0.25-m thick RC shear walls that are shaped as an irregular long "U" in plan view (Figure 4.4). The extremes of the U-shaped shear walls are located in the square footing where they meet the adjacent U-shaped shear wall, and they are attached together by a 0.2-m thick RC wall that is not-continuous along its height due to openings that serve as entrances to the auditorium.

The height of the inner ring shear walls varies along the footprint with a maximum height of 25 m. The roof that covers the inner ring is composed of NS-oriented 2.5-m deep steel struts spaced at about 4.4 m in the EW direction. The roof over the struts is composed of 0.05-m thick lightweight concrete on 0.1-m thick precast concrete slabs. The roof between the inner and outer circle is composed of a timber rafter, which is supported on struts that rest over a RC beam supported by the inner ring's shear walls. In the space between the outer and inner rings there is a mezzanine, which is located at a height of about 4 m over the ground floor. The floor of the mezzanine is composed of 0.46-m high precast tee units that are 3 m, 4.3 m, or 4.9 m wide with five webs and 0.05-m thick cast in-situ topping. These floor units rest over two 0.38 m by 1.06 m beams that connect a perimeter beam along the outer ring of the auditorium to the U-shaped shear walls. The perimeter precast RC 0.2-m by 0.6-m wide beam connects the columns of the exterior ring. At the mezzanine level the gallery of the auditorium is composed of one horizontal and one diagonal RC cantilever beams with a length of approximately 5 m to 7 m that are supported by the inner shear walls. Two bridges connect the auditorium with adjacent structures at its north and west ends.

Bearing pressures were estimated to be about 80-120 kPa for the outer ring footing and 150-200 kPa for the inner ring footing. The strength of the concrete was specified to be 18 MPa for the foundations and 21 MPa for the rest of the concrete members. HCG (2011) estimated the natural fixed-based period of the structure to be about 0.5 s in the NS and EW direction.

4.3.2.2. Site conditions

Site investigations for the CTH auditorium included 5 CPTs, 6 conventional exploratory soil boreholes with Standard Penetration Tests (SPT), and 2 boreholes where sampling for laboratory testing was performed (Figure 4.4). Additional site investigations were performed for the other structures at the facility. Section A-A' in Figure 4.5 shows the generalized subsurface conditions at the site. Unit 1 extends from the ground surface to a depth of about 4 m to 6 m. It is a loose silty sand and sandy silt with “sand-equivalent” relative density (D_r) of 40-50% and I_c values between 1.8 and 2.6, with I_c generally decreasing with depth. This soil unit underlies directly the shallow footings supporting the structure and is likely to liquefy during strong ground shaking. Unit 2, which like Unit 1 is part of the Springston formation, can be classified in two different units. Unit 2a is a very dense sandy gravel and gravelly sand ($D_r = 85-95\%$) with I_c generally below 1.8 and a thickness of about 4 m to 6 m. It is located primarily south of the auditorium (Figure 4.5). This very dense layer is not observed in the CPTs located north of the auditorium (CPTs Z2-8 and Z2-6). Unit 2b is a dense sand ($D_r = 70-80\%$) with higher fines content and higher I_c than Unit 2a. It is located below Unit 2a in the south with a thickness of about 2 m and below Unit 1 in the north with a thickness of about 8 m. Unit 3, which is part of the Christchurch formation, underlies Unit 2b. Unit 3 is also subdivide into two layers with different densities. Unit 3a is a medium dense sand with relative densities of 50-60% and I_c values between 1.8 and 2.2. It is located predominantly south of the auditorium, without any evidence of it north of the auditorium. Unit 3b is denser ($D_r = 75-85\%$) than Unit 3a with lower values of I_c (between 1.5 and 1.9) and is present across the entire site but with variable thickness of around 6-7 m to the north and about 2-3 m to the south. Between units 2a and 2b and units 3a and 3b, some thin (1-1.5-m thick) clayey layers exist that are not modeled. Unit 4 is a 1-2-m thick medium-stiff clay present throughout the site that overlies the dense Riccarton Gravel.

The groundwater table was 1.5 m below the ground surface for the Christchurch earthquake (NZGD, 2016). The free-face of the Avon River is located about 40 to 50 m south of the auditorium (Figure 4.5). The southern part of the site slopes downward towards the river. These topographical features are important as they impose static shear stresses in the ground, which may produce lateral spreading that could affect the building's vertical movement. The interpreted soil profile shown in Figure 4.5 is geologically consistent with the fluvial environment of the zone with horizontal variations in soil properties over short distances. There are streams, which are now buried, near the CTH Building depicted on the Black Maps (NZGD, 2016).

4.3.2.3. Seismic performance

The performance of the CTH complex, including the auditorium, was evaluated by several groups after the major earthquakes (Giorgini et al. 2011, Cubrinovski et al. 2011a, Bray et al. 2014a, Zupan 2014, Giorgini 2015, HCG 2011, T+T 2013). The information described in this section is a summary, and it provides the basis for comparison of the results of numerical analyses and settlement observations.

The entire facility moved laterally towards the Avon River with decreasing severity of lateral movements with increasing distance from the river. T+T (2013) summed the widths of mapped cracks to estimate lateral movements of approximately 350 mm within 20 m of the Avon

River bank, 100 mm at the south side of the auditorium, and about 50 mm at the north side of the auditorium for a total lateral ground stretch of 500 mm across the site. Their estimates are lower bound estimates, as some lateral deformation may occur without producing visible cracks. Other manifestations of liquefaction included soil ejecta, which was largely observed south of the auditorium (river side), at the north side of the building although in less amount than the south side, and within the auditorium basement, where about 70 m³ of soil ejecta were removed after the earthquakes (T+T, 2013). Dividing the volume of soil ejecta (70 m³) by the area of the auditorium's footprint (≈ 2500 m²) results in an average estimate of soil ejecta related settlement of about 30 mm. Additional significant ejecta occurred just south of the auditorium, so ejecta-related settlements should be higher at the south side relative to the north of the auditorium. A survey performed in April 2011 (HCG 2001, T+T 2013) indicated settlements of the structures in the CTH facility of approximately 240-630 mm, but typically between 300 and 500 mm. It is not clear which benchmark was used to estimate these settlements. The ground floor levels of that survey were analyzed, and it appears the inner footings in the southern part of the CTH auditorium settled about 40-80 mm more than the outer footings. The inner footings in the northern part of the auditorium settled likely about 20-40 mm more than the outer footings. The southern outer and inner footings settled about 150-230 mm more than the northern footings. There was obvious punching of the inner and outer ring footings into the surrounding ground. The inner columns settled more than the outer columns, but the outer columns also settled between 30 and 140 mm with respect to the surrounding ground and with respect to the ground slab between the two rings which produced a crack oriented in the EW direction. The significant settlement of the auditorium's inner columns produced a "domed" shape after the earthquake (Cubrinovski et al., 2011a). Structural distortions up to 1/70 (differential settlement of 80 mm) were measured between the outer and inner ring resulting in structural damage of the coupling beam. Additionally, tilt measurements indicated tilting of the columns toward the SE.

Table 3 presents the author's best interpretation of the vertical movements that occurred during the major events in the Canterbury earthquake sequence with the settlements classified by their likely mechanisms (volumetric-induced, lateral-spreading-induced, sediment-ejecta-induced, and shear-induced settlements). Settlements shown in Table 3 are also separated into "measured" or "estimated," with the "measured" values being obtained primarily from LiDAR data available in the NGZD (2016). Estimated values were obtained from calculations of post-liquefaction settlements based on the Boulanger and Idriss (2016) method for liquefaction triggering and Zhang et al. (2002) for the settlements estimation. Shear-induced settlements were estimated to be the difference between the total liquefaction-induced settlements and the other mechanisms. The southern side of the auditorium clearly settled more than its northern side, and the Christchurch earthquake was responsible for about 80% of the observed settlements. The primary sources of differential settlements were shear-induced settlements which likely produced significant excess pore pressure within the shallow loose silty sand/sandy silt of Unit 1, ejecta-induced settlements from Unit 1, and volumetric-induced settlements as the result of looser sand layers being present at the south side of the auditorium.

4.4. NUMERICAL ANALYSES OF THE PWC AND CTH BUILDINGS

4.4.1. General considerations

Nonlinear dynamic SSI effective stress analyses of the two buildings are performed using FLAC 7.0 (Itasca, 2009). This computer codes uses the finite difference method to solve the equation of motion and uses an explicit Lagrangian solution scheme, which allows large deformations problems to be solved.

The finite difference meshes shown in Figure 4.6 are based on the geotechnical profiles described in sections 4.3.1.2 and 4.3.2.2 for the PWC and CTH buildings, respectively. The sizes of the elements are less than one tenth of the wavelength associated to the maximum frequency of the input motion. The maximum frequency of the motion is controlled by the processing of the record performed for the deconvolution process (15 Hz). Maximum element sizes are about 1 m to 1.25 m. The ground motion is input in the base of the model, which is the dense Riccarton gravel layer, as a “within” acceleration time-history on a rigid base based on recommendations by Mejia and Dawson (2006). The lateral boundaries were modeled with FLAC’s “free-field” boundaries. The Mohr-Coulomb model is used in the elements adjacent to the free-field boundaries with representative properties, because the PM4Sand model (Boulangier and Ziotopoulou, 2015) cannot currently be used adjacent to a free-field boundary. Locating the lateral boundary one to two times the width of the building away from the edges resulted in minimal influence of the boundary on the response of the structure or the ground adjacent to the structure. Additionally, an elastic “wrap” in the face of the river is used to prevent flow failure and the consequent numerical instability and excessive deformation of the elements adjacent to the river. The constitutive model provides hysteretic damping. An additional 0.5% Rayleigh damping is used centered at an average frequency between the natural frequency of the structure and the mean frequency of the input motion (i.e., the inverse of its mean period, T_m).

The NS oriented frames shown in Figures 3 and 5 for the PWC and CTH buildings, respectively, are modeled. Both buildings are RC structures, for which the weight of the concrete is assumed to be 24 kN/m^3 and the elastic Young’s modulus (E) is calculated to be $2.0 \times 10^7 \text{ kPa}$. The structural elements are modeled as beam elements with area and second moment of inertia estimated from the building plans. The flexural cracking of the structural elements was considered by applying a factor of 0.35 and 0.7 to the EI of beams and columns, respectively, where I is the moment of inertia (ACI 318-14, 2014). Beams oriented in the direction of the analysis are modeled considering the contribution to the stiffness of the floor slab by using an effective width following recommendations of the ACI 318-14 (2014). The vertical load is due to the weight of the building and 20% of the design live load, which is estimated to be 3 kPa. Reasonable fixed-base natural periods of 1.9 s and 0.6 s were calculated for the PWC and CTH structures, respectively. The structural models of the two buildings are shown in Figure 4.6.

Based on numerical analysis of rigid structures, some researches (Adrianopoulos 2010, Popescu and Prevost 1993b) recommended lower estimates of bearing pressures be used to simulate a 3D structure in 2D plane-strain analyses. However, it is more important to capture the dynamic response of the structure by capturing the actual masses and stiffness of the structural elements and hence its natural period. In addition to the building’s weight, the structural response of the building plays an important role in the building’s movements when founded over liquefiable soils. In some cases, it may control the response because the inertial response of the building will induce higher stresses and strains to the underlying weakened soil compared to those experienced in the free-field, resulting in more settlements. The out-of-plane volumetric settlement that results from drainage in the out-of-plane direction is a limitation of 2D analysis as described by Popescu (2005). However, this mechanism is likely to play a less important role in the presence of a structure where shear-induced mechanisms control the response and the

settlements, as was the case for 2D analyses of 3D building models performed by Dashti and Bray (2013). Additionally, the uncertainty in estimating the hydraulic conductivities of the units underlying the building and their geometry prohibits performing detailed 3D analyses at these sites. Thus, 2D analyses were performed, as would typically be performed in engineering practice.

4.4.2. Calibration of the constitutive model

The PM4Sand Version 3 model developed by Boulanger and Ziotopoulou (2015) is a critical-state, bounding surface model that was adapted from the constitutive model developed by Dafalias and Manzari (2004). PM4Sand captures key aspects of the cyclic response of sands and has been calibrated extensively. The cyclic resistance of the constitutive model is calibrated in this study against site and layer-specific data when available. The laboratory test results on the soils at these sites and similar sites in the CBD are provided by Markham (2015) and Markham et al. (2016b). When site-specific data are not available, the basis for calibrating the cyclic resistance curves is the liquefaction resistance curves implied by the well-established simplified liquefaction triggering evaluation procedures of Idriss and Boulanger (2008) – herein called IB08 – and of the update by Boulanger and Idriss (2016) – herein called BI16.

PM4Sand model parameters are developed using best-estimated median values of unit weights (γ), relative densities (D_r), and shear wave velocities (V_s). The use of median values of relative density is consistent with the recommendations of Montgomery and Boulanger (2017) [42] who found characteristic values for models with uniform soil properties to be within the 30th and 70th percentiles when estimating liquefaction-induced displacements, which was judged to be more important than capturing pore water pressures, which was the focus of Popescu (1997) who recommended 20th percentile of density as a characteristic value to model a layer with variable densities as a uniform layer. Median values of unit weight are obtained through conventional correlations with the CPT (Robertson 2010). Three correlations are used to estimate D_r as a function of the CPT tip resistance (i.e., Kulhawy and Mayne, 1990, Jamiolkowski, 2001 and Idriss and Boulanger, 2008 with weights of 0.3, 0.3 and 0.4 respectively). The McGann et al. (2015) Christchurch-specific correlation for V_s , which is used as the basis to estimate (G_o), which is a dimensionless model constant controlling the small strain shear modulus (G_{max}). Other secondary model parameters that are available for Christchurch soils are used, such as the critical-state friction angle (ϕ_{cv}), maximum and minimum void ratios (e_{max} and e_{min}), which were generally found from Taylor (2015) as a function of fines content (FC) and geologic formation and the parameters Q and R, which define the critical state line in the D_R - p' space, were obtained from Markham (2015) and Markham et al. (2016b).

Once these parameters are selected for each soil unit (i.e., γ , D_r , G_o , ϕ_{cv} , e_{max} , e_{min} , Q, R), a target cyclic resistance ratio (CRR) vs. number of load cycles curve is established for each soil unit. The target CRR curves are estimated on the basis of CTX testing performed by Markham (2015) for Unit 4 for the PWC site and units 1 and 3a for the CTH site. The CTX testing was performed on high-quality specimens obtained using the Dames & Moore (DM) Osterberg-type hydraulic piston sampler, which has been successful in retrieving high quality samples in silty and some sandy soils (Bray and Sancio 2006 and Markham et al. 2016b). A single amplitude axial strain of 3% is the criterion for liquefaction triggering in the CTX tests. The CTX-based CRR curve is then corrected to field conditions by multiplying the CSR values by $C_r = (1+2 K_o)/3$ and an additional 0.9 multiplier to adjust for bi-directional loading conditions. The

resulting multipliers ($C_r' = 0.9 C_r$) are within the range of 0.57 to 0.66 depending on the fines content. When no laboratory testing is available, the target CRR curves are obtained from the CRR curves implied by simplified liquefaction triggering procedures cited previously. Once the target CRR curve for a unit is developed, the model parameters h_{po} (contraction-rate parameter) and n_b are changed to obtain the target CRR curve while keeping the other parameters fixed.

Examples of the target CRR curves and the numerical-based CRR curves are shown in Figure 4.7. Figure 4.7(a) shows the target and numerical CRR curves for soil Unit 1 (from the simplified procedure) and soil Unit 4 (from CTX testing) for the PWC site. Figure 4.7(b) shows the same two curves for soil units 1 (from CTX testing) and 2b (from the simplified procedure) for the CTH site. Tables 4.4 and 4.5 provide the values of the parameters calibrated for the PM4Sand model for the PWC and CTH buildings, respectively. Additionally, Tables 4 and 5 provide the values of the parameters used for the cohesive soil overlying the Riccarton Gravel, which is present in both sites. This layer is modeled as Mohr-Coulomb material and it has little influence on the building response.

The free-field seismic response of the site is also evaluated to ensure the seismic response calculated with the dynamic SSI analyses is reasonable. A direct comparison of recorded and calculated ground motions is not possible, because these sites are not instrumented. However, four strong motion stations are close to these sites in the CBD of Christchurch. Hence, the calculated response is compared to the recorded responses at the nearby strong motion stations. Figure 8 shows the comparison of the calculated and recorded 5%-damped acceleration response spectra for the PWC and CTH sites for the Christchurch earthquake. The comparisons of calculated and recorded ground motions for this event and the other events in the Canterbury earthquake sequence are reasonable.

Additionally, the free-field liquefaction response of the numerical model is evaluated. The calculated shear strain and maximum pore pressure ratio profiles are compared with the factor of safety against liquefaction estimated from established simplified procedures (e.g., Boulanger and Idriss 2016) [30]. Calculated zones of high pore pressure ratios and shear strains also had low factors of safety against liquefaction triggering using the simplified procedures. The level of liquefaction calculated with the dynamic analyses was more severe for the Christchurch event than for the 13-JUN-11 event, and the level of liquefaction of the 13-JUN-11 event was more severe than that for the Darfield event, which is consistent with field observations. Simplified procedures provided consistent results, except the 13-JUN-11 event was estimated by them to be slightly less damaging than the Darfield event. The slightly more intense shaking for the 13-JUN-11 earthquake relative to the Darfield earthquake is one reason the dynamic analyses calculated slightly more liquefaction. Conversely, the simplified procedures estimated slightly higher demand for the Darfield event.

4.4.3. Building response

The nonlinear dynamic SSI effective stress analysis calculates shear-induced liquefaction building settlement. The building settlement that occurs during earthquake strong shaking is primarily due to the shear-induced mechanism. The calculated building settlement during strong ground shaking also includes some volumetric settlement as the result of partial drainage. The latest version of the PM4Sand model includes a phenomenological method of accounting for the liquefaction-induced sedimentation and post-liquefaction reconsolidation (volumetric) mechanisms after strong shaking that consists of reducing the elastic modulus once the strong

shaking part of the motion is over. The method was validated against laboratory-based volumetric settlements as well as case histories (e.g., Port Island, Kobe) by Ziotopoulou and Boulanger (2013). This method was not used in this study because: 1) The method was calibrated against laboratory data that was also used to develop the available simplified procedures so consistent results could be obtained using the liquefaction-induced settlement procedures (e.g., Zhang et al. 2002); 2) The time required to run the complete analyses with post-liquefaction reconsolidation increases significantly; and 3) The shear-induced building settlement is significantly larger than the volumetric-induced building settlement during strong shaking (Bray et al. 2017). Sediment ejecta, which may be an important mechanism, is not captured in a continuum-based model. This is one of the limitations of this and most numerical studies of liquefaction-induced building settlements.

4.4.3.1. PWC building

The PWC building settled differential downward on its south side. Preliminary dynamic SSI analyses with a more simplified characterization of the subsurface conditions than shown in Figure 6(a) calculated more settlement on its north side. Once the subsurface model included units 3, 5 and 6 (Figure 4.6a), which better reflects the actual ground conditions, the direction of the differential settlements reversed to match the observed building tilt. The two factors contributing primarily to the greater settlement of the building's southern side are the extension of the basement beyond the north edge of the tower which acts as an inverse cantilever to resist settlement and the presence of Unit 3, a medium dense sand located within the dense Unit 2, which cyclic softens significantly in the Christchurch earthquake. Sensitivity analyses found that increasing the density of Unit 3 and decreasing the length of the basement extension on the north side resulted in less tilt towards the south and eventually tilt towards the north.

Figure 4.9 shows the vertical settlement-time histories of the nodes located at the intersection of the perimeter columns of the tower and the basement mat for the Christchurch earthquake. It shows the additional settlement that accumulates at the southern edge of the building. Figure 4.9 also shows the range of shear-induced displacements estimated using the LiDAR measurements, which were presented previously in Table 4.2. There is good agreement between the calculated and estimated shear-induced building settlements. Similar analyses for the Darfield and 13-Jun-11 events calculated significantly smaller building settlements for both sides of the building; however, the calculated settlements exceeded the values listed for shear-induced building settlement in Table 4.2. For example, the southern edge of the building calculated settlement was 10-25 mm compared to the observed settlement of 0-10 mm for the Darfield event (Table 4.2), and it was calculated to be 40-70 mm compared to the observed settlement of 0-20 mm for the 13-JUN-11 event (Table 4.2). The overestimation of building settlement for the Darfield event is relatively minor and judged to be acceptable given that simplified liquefaction procedures also over-estimated the level of liquefaction at this site for this event. The overestimation of building settlement for the 13-JUN-11 is greater most likely due to the overestimation of the input rock motion for this event, as the calculated surface motions exceeded those recorded in the CBD. Additionally, the overestimation of the settlements for the lower intensity motions has also been observed in several numerical analyses of centrifuge experiments (e.g., Dashti and Bray 2013). It results when the numerical analyses calculate higher excess pore water pressures under the building than measured in the experiments, and hence, slightly greater building settlement.

The distribution of the earthquake-induced shear strains in the soil layers helps to identify the soil units that played an important role in the seismic performance of the building. Figure 4.10 shows the earthquake-induced shear strains contours, which depicts the relative importance of the different soil units. Unit 1, develops significant shear strains. Although this unit is above the base of the foundation, its movement laterally towards the river affects building performance. Unit 3 develops up to 2.5 % shear strain, and its location under the southern side of the building produces more settlement at the southern edge of the building. Units 4, 5, and 6, develop shear strains of 1-3% under the building, with significant shearing of the foundation soils shown near the bottom of Unit 4.

4.4.3.2. CTH auditorium

The CTH auditorium settled differentially with larger building settlements along its southern side. There was also differential settlement between the less heavily loaded outer ring of columns and the more heavily loaded inner ring of columns, with the differential settlement between the inner and outer rings being more severe at the southern side. Dynamic SSI analyses were able to capture many of these field observations.

Figure 4.11 shows the vertical settlement-time history of the northern columns and southern columns calculated for the Christchurch earthquake. Figure 4.11 also depicts the amount of the shear-induced column settlements for the Christchurch earthquake (Table 4.3). As observed in the field, the calculated settlements of the southern columns are larger than those for the northern columns, and the inner columns settle more than the outer columns. The differential settlement calculated in the dynamic SSI analyses due to the shear-induced mechanism in this building is about 70 mm across the entire building in the NS direction, and the differential settlement between inner and outer columns, which are separated 6 m, is 15-30 mm for both sides, resulting in calculated angular distortions of 1/200 to 1/400. Measured angular distortions between inner and outer columns in the south side were on average 1/200, with the most severe case having an angular distortion of 1/70. In the northern side, the average angular distortion was 1/1500 with the most severe case of 1/180. If the contribution of ejecta-induced settlement is considered, which was more severe within the southern part of the auditorium, then the calculated angular distortions at the southern side are consistent with those observed. As mentioned previously, 70 m³ of soil was removed from inside the auditorium and significant soil ejecta was observed along the southern side of the auditorium. The differential settlement between north and south sides for the shear-induced mechanism was well captured by the numerical analyses with the calculated response being in the upper range of the estimated settlements shown in Table 4.3. However, the shear-induced liquefaction building settlement mechanism contributed only in part to the observed differential settlement of the auditorium. The ejecta-induced mechanism, volumetric-induced mechanism, and lateral spread movements also contributed to increased settlement of the southern side of the auditorium relative to its northern side.

Figure 4.12 shows the earthquake-induced shear strain contours calculated for the CTH auditorium for the Christchurch earthquake. Shear strains of up to 15% were calculated in the loose silty sand material directly beneath the foundation. The analysis shows the formation of a high shear zone starting near the most southern column and going through the liquefied material in the direction towards the river as expected because of the ground sloping toward the free-face of the Avon river channel. Unit 3a also develops relatively high shear strains of 1.5 to 2.5 %, and Unit 4 develops shear strains of 1-3% under the building, with significant shearing of the foundation soils shown near the bottom of Unit 4.

which helps produce greater building settlements along the south side of the building. There are also high liquefaction-induced shear strains concentrated within that part of Unit 1 below the water table. No one shear-induced mechanism controlled the performance of the auditorium. It is likely that a combination of both SSI ratcheting and bearing-capacity type of failure took place at this site, which helped generate the response shown in Figure 4.12. As mentioned previously, the other liquefaction-induced building settlement mechanisms (e.g., ejecta, volumetric, and lateral spreading) also contributed to the response shown in Figure 4.12. Details in the model of the subsurface conditions at the site (e.g., separating units 2 and 3 in two distinct layers and separating unit 3a from unit 3b) played important roles in capturing the observed performance of the CTH auditorium. This highlights the importance of defining well the soil stratigraphy, especially in cases where lateral spreading is involved and topography and ground conditions vary systematically around and under a structure.

4.5. CONCLUSIONS

Simplified procedures, such as 1D post-liquefaction reconsolidation settlement procedures, do not capture the complex shear strain response of liquefiable soils under significant structures. The presence of a free-face or sloping ground furthers complicates the challenge of estimating liquefaction-induced building settlements. Nonlinear dynamic SSI effective stress analyses can provide important insights into the governing mechanisms of liquefaction-induced building settlement.

Calibrated dynamic SSI effective stress analyses are shown to calculate settlement values that are in agreement with the observed field performance of two landmark structures in Christchurch. The analytical results compare most favorably for the more intense Christchurch earthquake, which in turn produced larger building settlements. For the less intense 13-JUN-11 and Darfield earthquakes, the dynamic analyses tended to overestimate building settlements. The over-estimations are most likely due to the overestimation of the intensity of the 13-JUN-11 earthquake shaking, the inherent conservatism of liquefaction triggering assessments which were used for the calibration of the model (e.g. the deterministic cyclic resistance curve has a probability of liquefaction of 15%), and the numerical analyses calculated excess pore water pressures higher than those likely experienced during the earthquakes. However, the expected trends of the observed building movements were captured well for all events. Importantly, the seismic performances of the buildings during the more severe Christchurch earthquake were captured well. The good comparison between calculated and observed response was obtained after carefully calibrating each soil unit against high-quality laboratory-based cyclic resistance curves (CRR), when available. When they were not available, well-established CPT-based simplified liquefaction triggering procedures were used as the basis for model calibration. Lastly, comparisons of the calculated free-field ground responses at the sites with the nearby recorded ground motions and with the results of simplified liquefaction triggering evaluations for each earthquake event were critical to developing confidence in the dynamic SSI analyses.

For the two buildings analyzed in this study, it is difficult to associate the calculated response to a single shear-induced mechanism (i.e., either bearing capacity or SSI ratcheting). A combination of the two mentioned mechanisms in addition to the ground adjacent to the buildings sloping toward the free-face of the Avon river channel influenced the seismic performance of the buildings. Volumetric-induced mechanism also played an important role,

especially at the CTH Auditorium site where there was significant difference in the soil stratigraphy between the north and south sides. The soil ejecta-induced building settlement mechanism is not captured by these continuum-based analyses. Capturing this mechanism remains an important topic in soil liquefaction research.

For both field case histories, details in the soil stratigraphy made important differences in the response of the building. The overall magnitude of liquefaction-induced building settlement was not greatly affected by these details, but the direction of building tilt was affected. For the PWC building site, the addition of units 3, 5, and 6 influenced the direction of tilting of the building. The separation of units 2 and 3 into units 2a, 2b, 3a, and 3b at the CTH building site also resulted in achieving a calculated response closer to the observed response. Lastly, the two buildings were located in a fluvial environment close the Avon river. The depositional environment implies that there is high likelihood of shallow buried streams. Indeed, some streams were shown on the 1850s Black Maps near these sites. The presence of buried streams at the sites increases greatly the likelihood of liquefaction-induced damage and its consequences. Thus, geologic details need to be considered when developing the numerical model.

Table 4.1. Seismic demand at the PWC and CTH sites and recorded PGAs in the CBD

Event	Estimated PGA ^a (g)						Recorded geo-mean PGA ^a (g)			
	PWC Site			CTH Site			CBGS	CCCC	CHHC	REHS
	16 th	50 th	84 th	16 th	50 th	84 th				
Darfield	0.16	0.21	0.27	0.17	0.22	0.28	0.16	0.22	0.17	0.25
Christchurch	0.34	0.45	0.59	0.35	0.45	0.58	0.50	0.43	0.37	0.52
13-Jun-11	0.18	0.24	0.28	0.18	0.24	0.32	0.16	N/A	0.22	0.26

^a Obtained from Bradley (2014)

Table 4.2. Settlement of the PWC tower (mm)

Type of Settlement	Event	South		North	
		Measured (mm)	Estimated (mm)	Measured (mm)	Estimated (mm)
Total Liquefaction-Induced Settlement ^a	Darfield		0 – 30		0 – 30
	Christchurch	190 – 250	160 – 280	140 – 200	120 – 220
	13 June 2011	10 – 30	0 – 40	20 – 40	10 – 50
	Total		160 – 350		130 – 300
Volumetric-Induced+ Sediment Ejecta + Lateral Spreading- Induced Settlement ^b	Darfield		0 – 20		0 – 20
	Christchurch	80 – 140	80 – 140	90 – 150	90 – 150
	13 June 2011	0 – 20	0 – 20	10 – 30	10 – 30
	Total		80 – 180		100 – 200
Shear-Induced Settlement ^c	Darfield		0 – 10		0 – 10
	Christchurch		80 – 140		30 – 70
	13 June 2011		0 – 20		0 – 20
	Total		80 – 170		30 – 100

^a Measurements obtained from LiDAR data for Christchurch and 13 June 11 events provided M. Jacka (personal communication, 2016) by tracking changes in elevation of the PWC tower roof. For Darfield event, no measurements were taken, and a value of settlement of less than 20 mm is assumed due to volumetric densification of the soils beneath the building and less than 10 mm for shear-induced settlements. Similar values were observed in lighter buildings over similar soil conditions in Christchurch (See Appendix A).

^b Measurements obtained from LiDAR data for Christchurch and 13 June 11 events provided M. Jacka (personal communication, 2016) by tracking changes in elevation of streets south and north of the PWC building (i.e., Armagh St. and Oxford Terrace, respectively).

^c Shear-induced deformations were estimated as the total measured settlement minus the estimated settlement from other mechanisms. A broader range was used, because of the uncertainty of the estimated values.

Table 4.3. Settlement of the CTH Auditorium building (mm)

Type of Settlement	Event	North		South	
		Measured	Estimated	Measured	Estimated
Total Settlement ^a (without considering tectonic settlement)			40 – 80		30 – 80
	Total	300 – 500	250 – 550	400 – 750	350 – 800
Volumetric-Induced Settlement ^b	Darfield		40 – 60		30 – 60
	Christchurch		80 – 120		120 – 190
	13-JUN-11		50 – 70		40 – 70
	Total		170 – 250		190 – 320
Lateral Spreading-Induced Settlement ^c	Darfield		0		0
	Christchurch		10 – 40		50 – 100
	13-JUN-11		0 – 10		0 – 20
	Total		10 – 50		50 – 120
Sediment ejecta Settlement ^d	Darfield		0		0
	Christchurch		10 – 50		50 – 100
	13-JUN-11		0		0
	Total		10 – 50		50 – 100
Shear-Induced Settlement ^e	Darfield		0 – 20		0 – 20
	Christchurch		40 – 140		50 – 210
	13-JUN-11		20 – 40		10 – 30
	Total		60 – 200		60 – 260

^a Values obtained from surface elevation changes in LiDAR (NGZD 2015), which were adjusted slightly using the results of building level surveys to capture measured differential settlements.

^b Obtained by estimating ranges of settlements using Zhang et al. (2002) procedure and Boulanger & Idriss (2016) and Robertson (2015) liquefaction methods. These estimates were reduced by approximately half for the Darfield earthquake to be consistent with observations from buildings at similar sites in Christchurch (See Appendix A).

^c Vertical settlements estimated as 0.5 to 1 times the lateral displacements obtained from T+T (2013) by adding crack widths parallel to the river.

^d Minor ejecta observed north of building and more ejecta observed south of it (Zupan 2014 and T+T 2013).

^e Difference between total settlements and settlement from other mechanisms, allowing for some uncertainty.

Table 4.4. Parameters used in the numerical analyses of the PWC building

Parameter	Unit 1	Unit 2	Unit 3	Unit 4	Unit 5	Unit 6	Unit 7
D_r (%)	50	90	55	65	45	50	$G = 75 \text{ MPa}$ $K = 225 \text{ MPa}$ $c = 150 \text{ kPa}$ $\phi = 0$
G_o	500	1400	750	950	500	700	
h_{po}	2	20	0.75	0.20	1.2	0.75	
n_b	0.5	2	0.5	0.2	0.15	0.2	
Q	8	8	8	8	8	8	
R	1	1	1	1	1	1	
e_{max}	1.3	1.1	1.3	1	1	1	
e_{min}	0.6	0.6	0.6	0.6	0.6	0.6	
ϕ_{cv}	35°	35°	35°	35°	35°	35°	
γ (kN/m ³)	17.0	20.5	19.5	19.0	18.0	17.0	18.0
k (m/s)	5.0E-5	4.0E-3	3.0E-4	1.5E-4	1.0E-6	1.0E-6	1.0E-9

Table 4.5. Parameters used in the numerical analyses of the CTH building

Parameter	Unit 1	Unit 2a	Unit 2b	Unit 3a	Unit 3b	Unit 4
D_r (%)	0.45	0.95	0.75	0.50	0.8	$G = 75 \text{ MPa}$ $K = 225 \text{ MPa}$ $c = 150 \text{ kPa}$ $\phi = 0$
G_o	460	1650	1000	850	1400	
h_{po}	1.5	20	1.3	1.2	2.0	
n_b	0.4	1.5	0.5	0.4	0.5	
Q	8	8	8	8	8	
R	1	1	1	1	1	
e_{max}	1.5	1.1	1.1	1.3	1.1	
e_{min}	0.6	0.6	0.6	0.6	0.6	
ϕ_{cv}	35°	35°	35°	35°	35°	
γ (kN/m ³)	16.0	20.0	19.5	19.5	19.5	18.0
k (m/s)	4.0E-5	3.0E-3	4.4E-4	6.7E-6	8.0E-5	1.0E-9

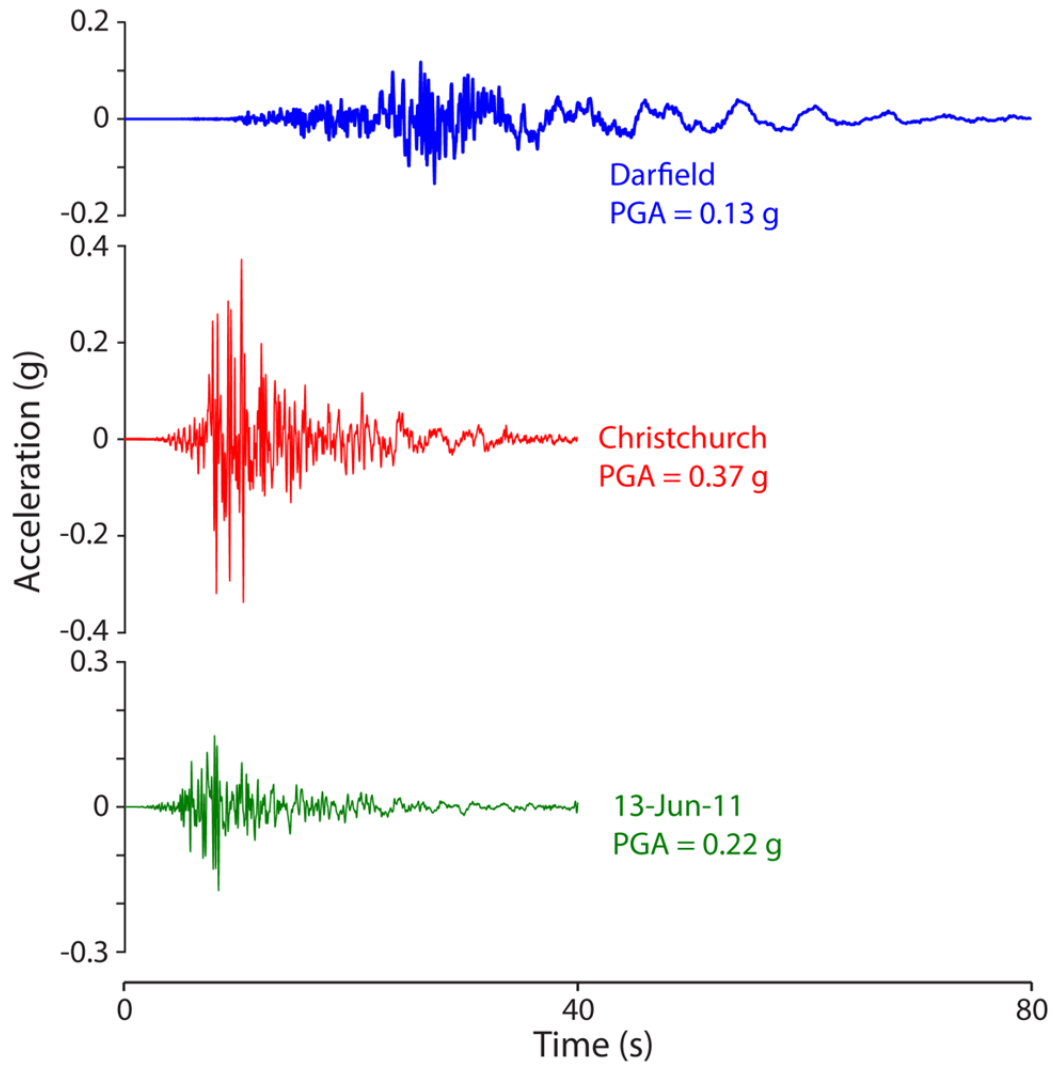


Figure 4.1. Input deconvolved “within” ground motions from the CACS station for the NS component for the three primary earthquakes of the Canterbury earthquake sequence scaled for the CTH site.

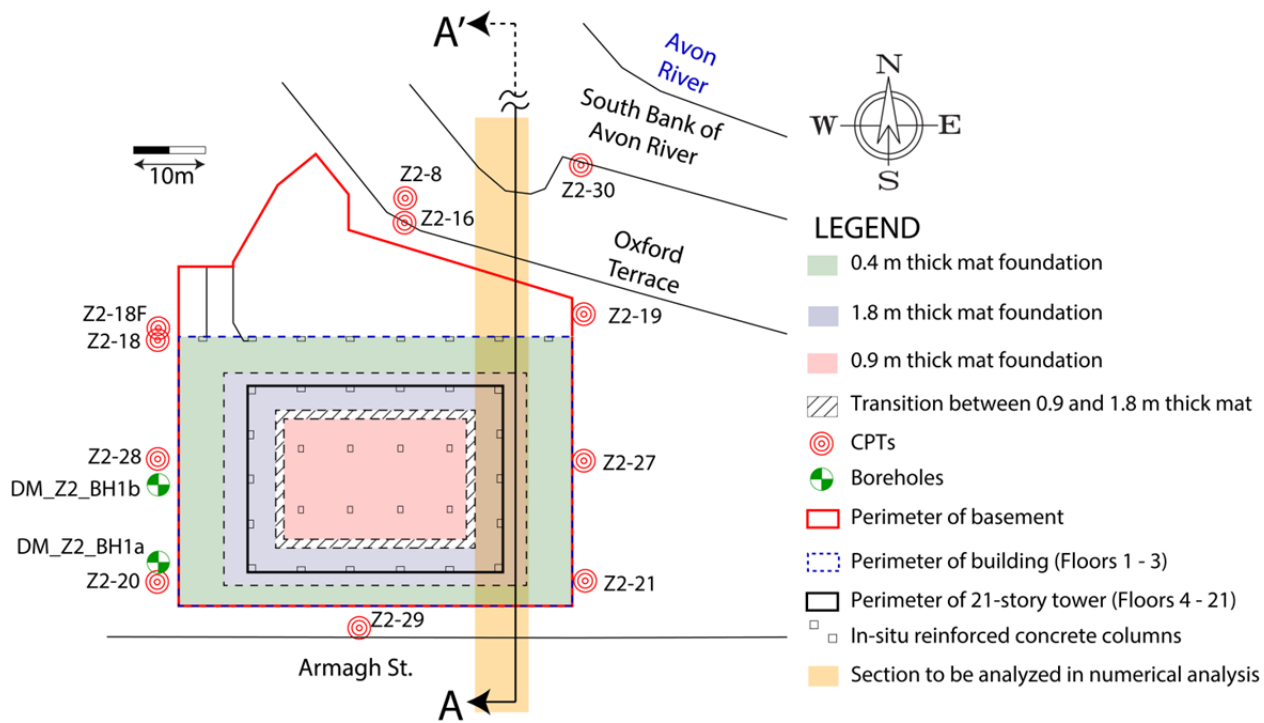


Figure 4.2. Footprint of PWC building, including location of columns, perimeter of basement and buildings; also showing the site investigation.

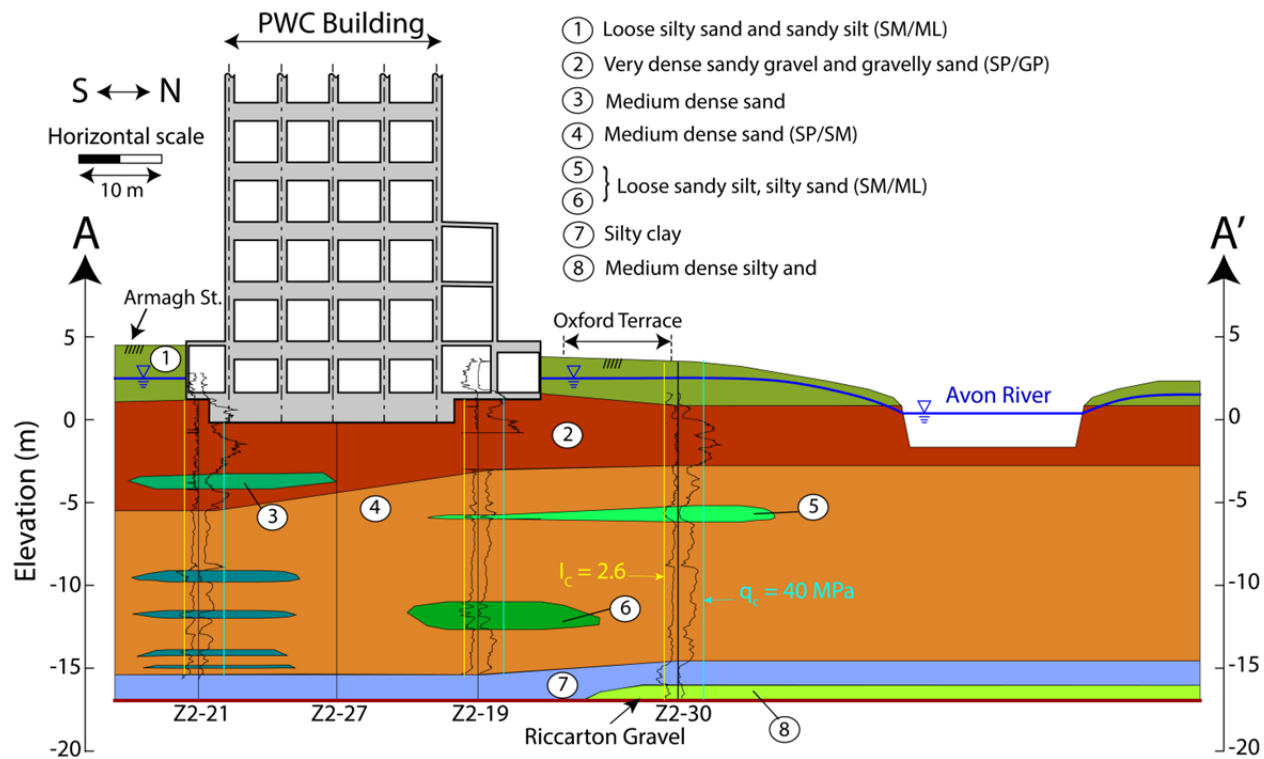


Figure 4.3. N-S cross section A-A' with the geotechnical profile of the PWC building including the building.

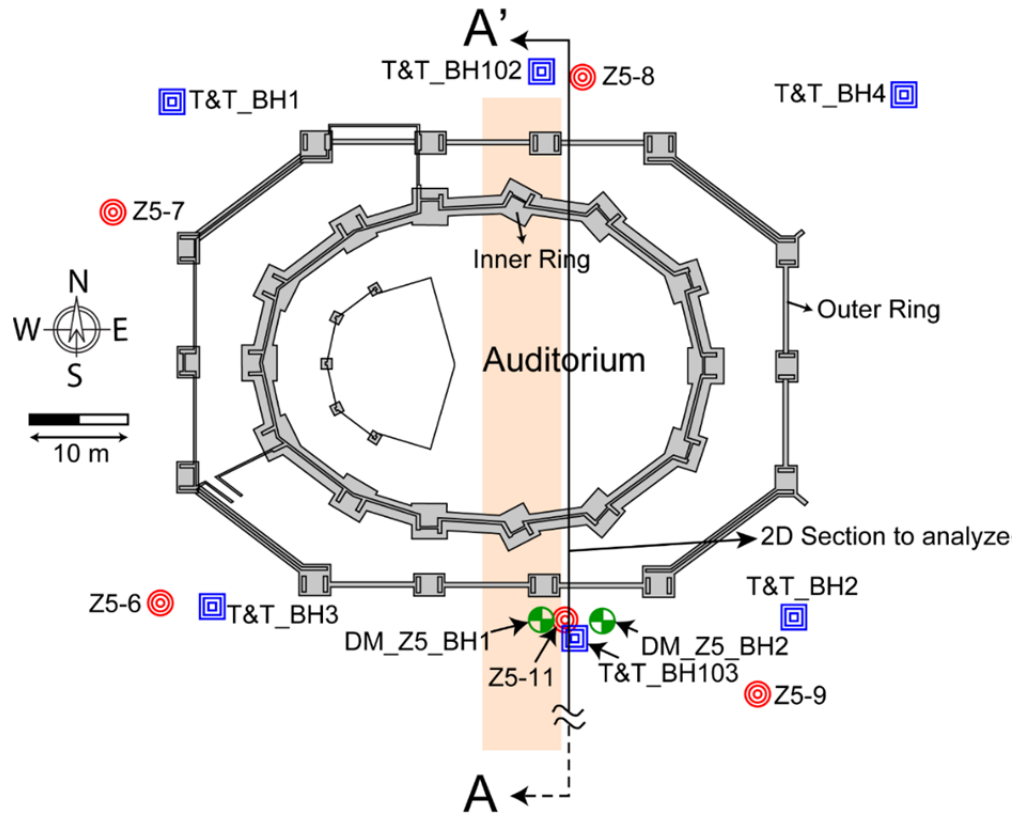


Figure 4.4. Plan view of the CTH Auditorium structure showing also the site investigation performed in the site.

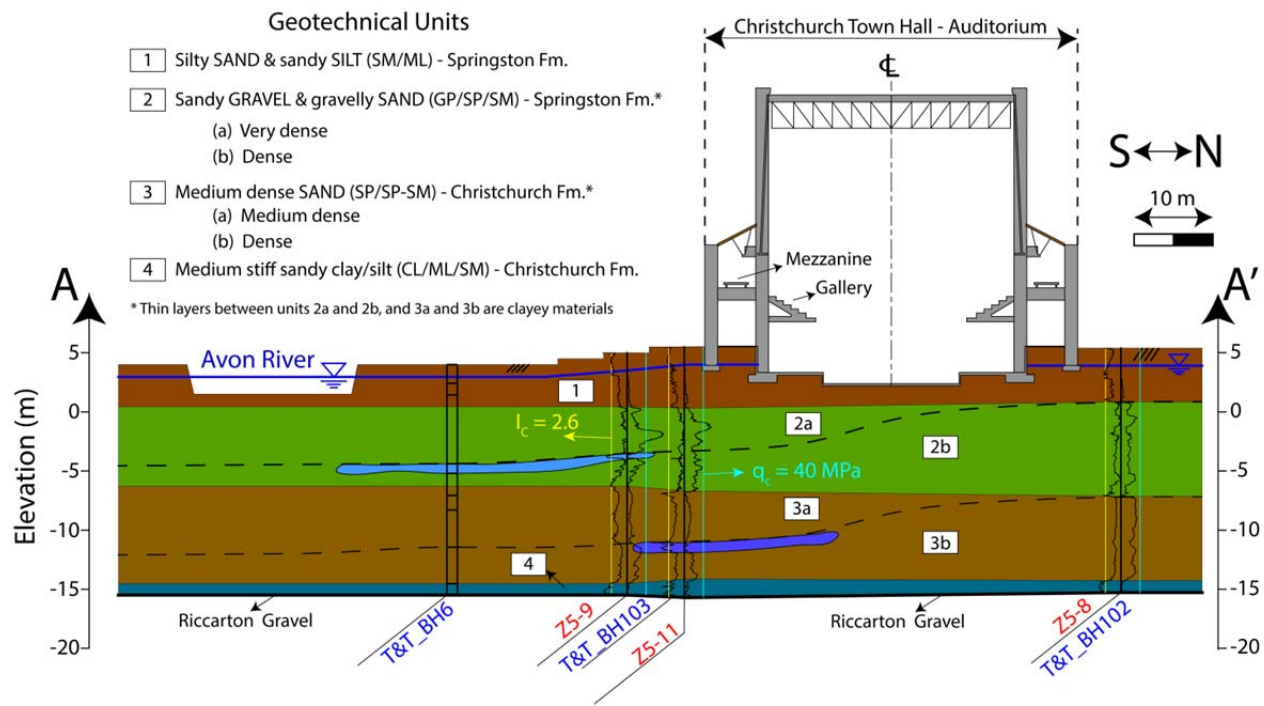
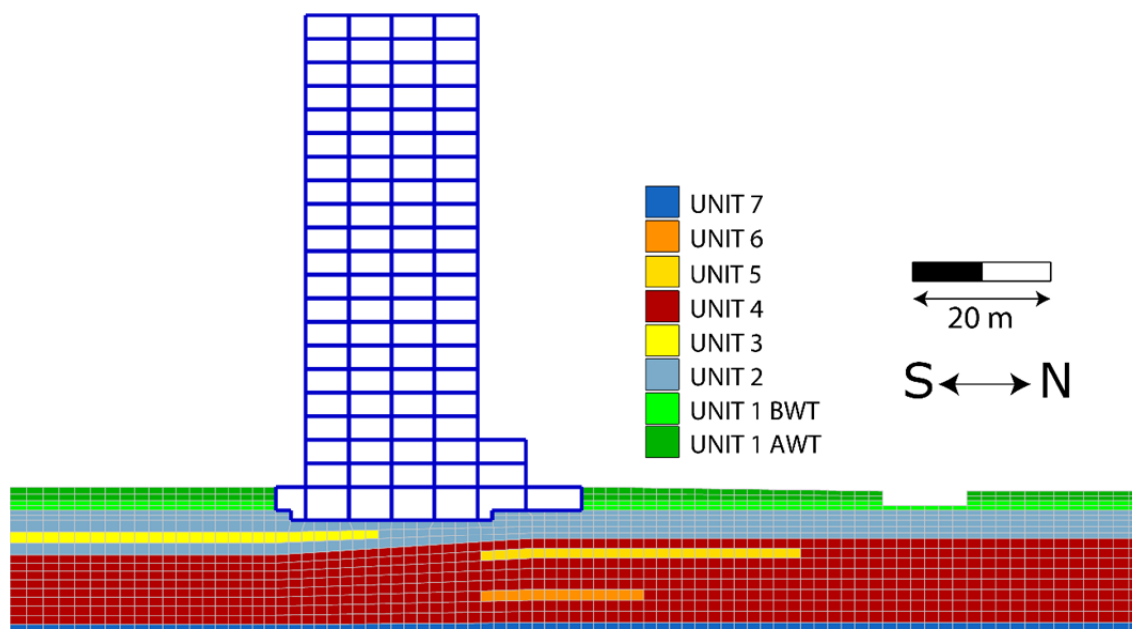


Figure 4.5. Cross section A-A' of the CTH site including the structure.

(a) PWC Building



(b) CTH Building

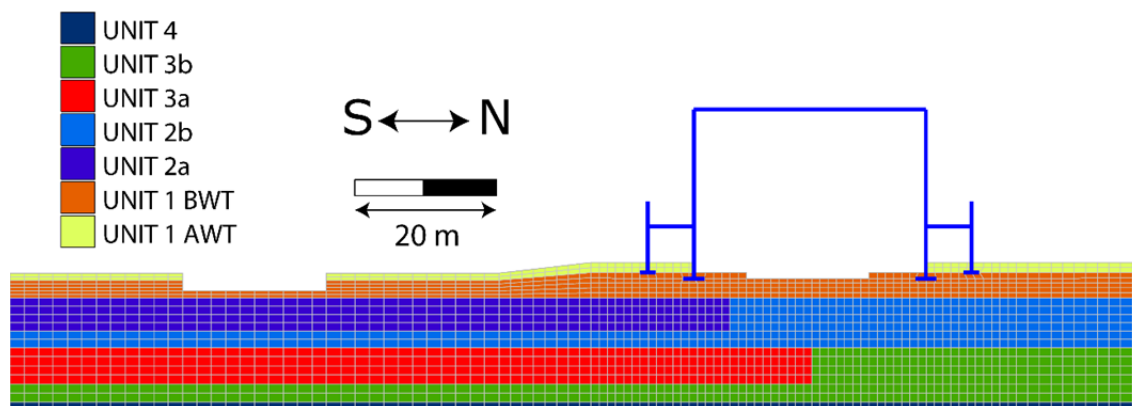


Figure 4.6. Numerical models of the (a) PWC building and (b) CTH building.

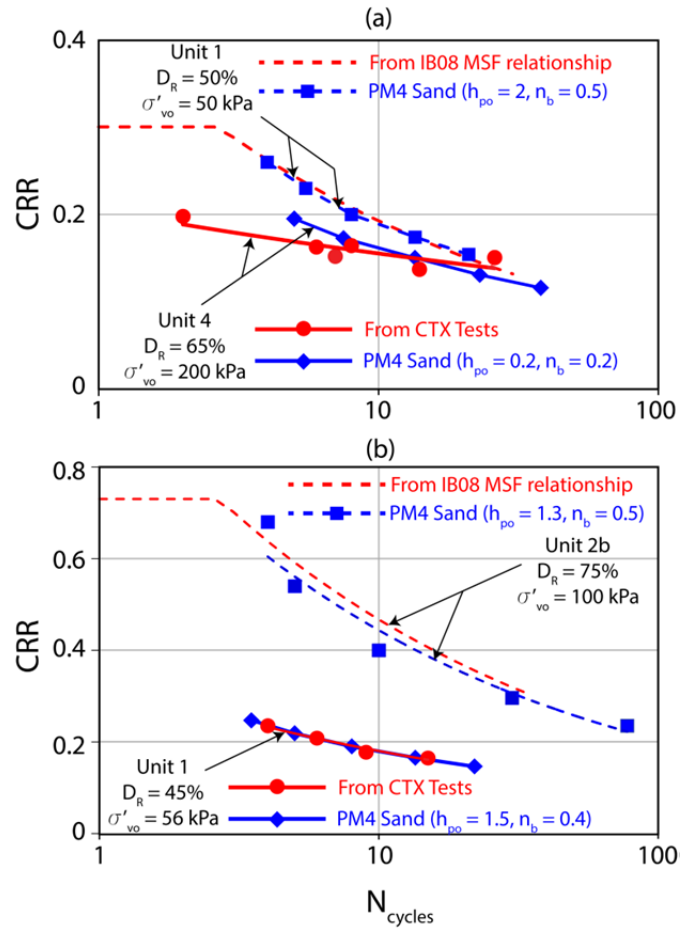


Figure 4.7. CRR vs. N_{cycles} curves for (a) PWC building: units 1 and 4, and (b) CTH building: units 1 and 2b. (CTX test results from Markham (2015) and Markham et al. (2016b)).

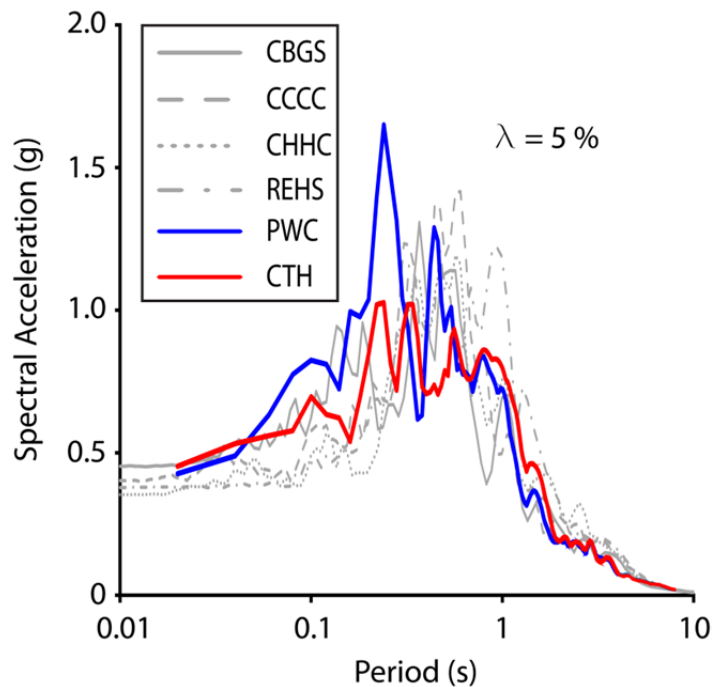


Figure 4.8. Calculated 5%-damped acceleration response spectra for free-field ground surface at the PWC and CTH sites compared to recorded NS recorded acceleration response spectra in the CBD for the Christchurch earthquake.

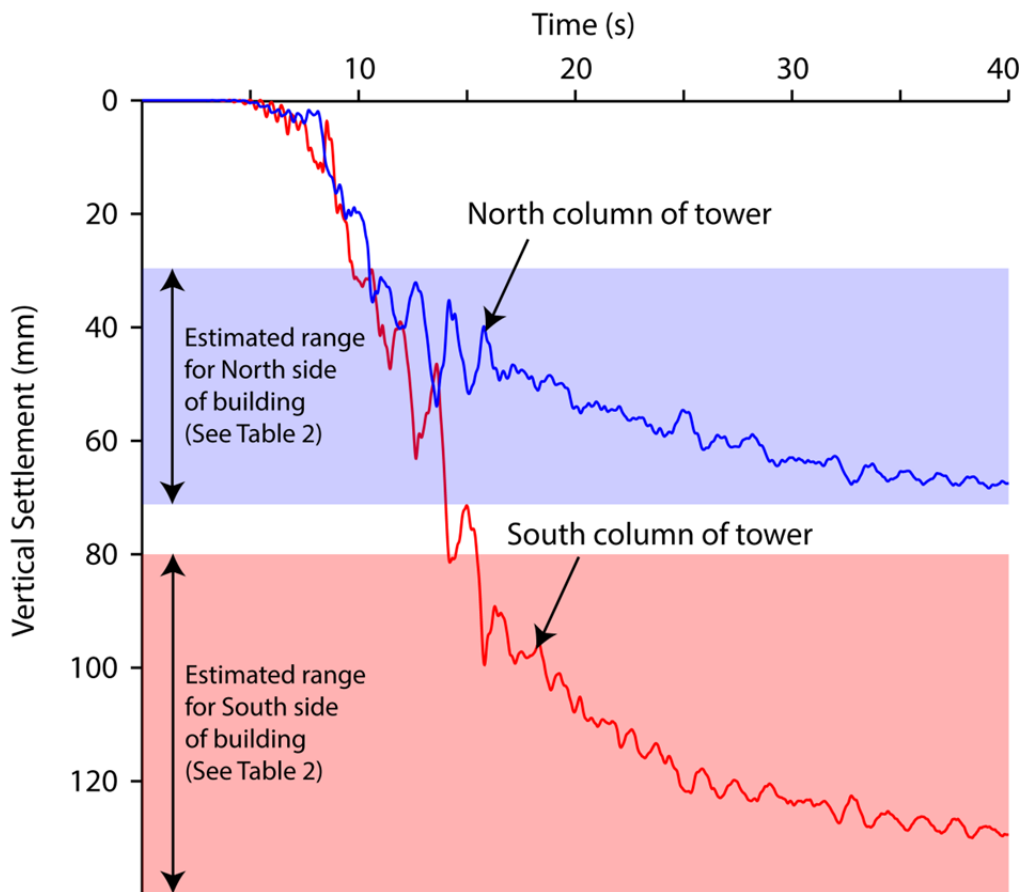


Figure 4.9. Shear-induced vertical settlement-time histories at the northern and southern column of the tower for the Christchurch earthquake compared to estimated settlements (Table 2).

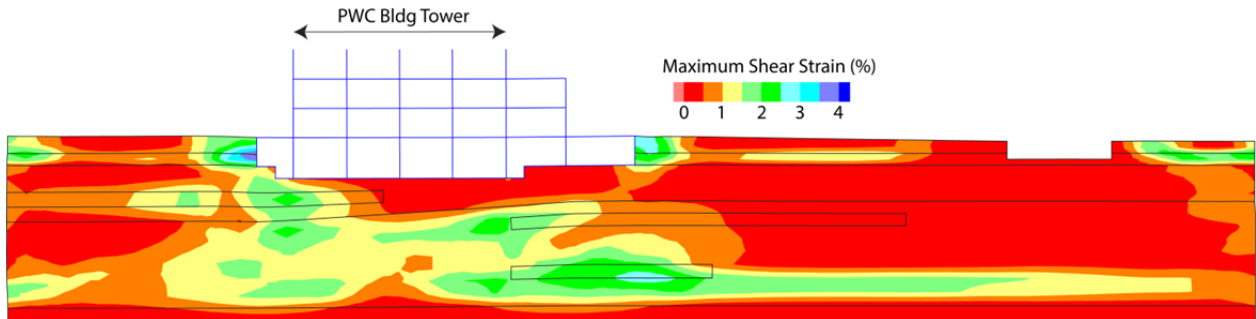


Figure 4.10. Shear strain contours for the PWC building for the Christchurch earthquake.

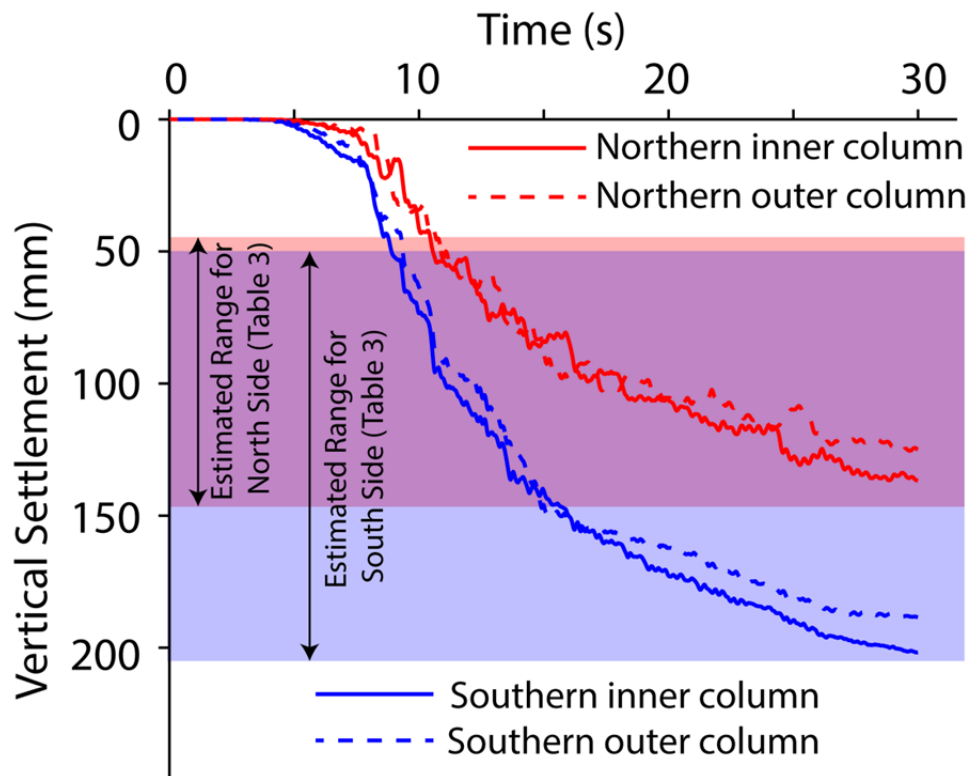


Figure 4.11. Shear-induced vertical settlement-time histories for northern and southern columns for the Christchurch event compared to estimated settlements (See Table 4.3)

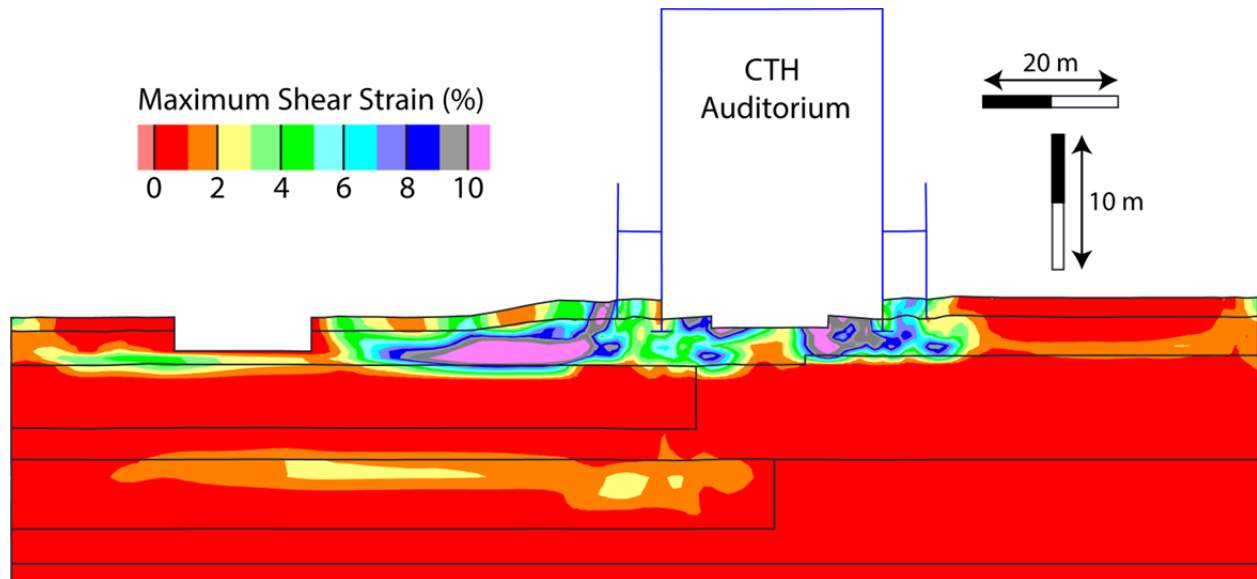


Figure 4.12. Shear strain contours for the CTH Auditorium for the Christchurch event.

CHAPTER 5: SEISMIC PERFORMANCE OF A BUILDING AFFECTED BY MODERATE LIQUEFACTION DURING THE CHRISTCHURCH EARTHQUAKE

The contents of this chapter are primarily from a journal article submitted to the Journal of Soil Dynamics and Earthquake Engineering by Bray, J.D. and Luque, R., entitled: “Seismic Performance of a Building Affected by Moderate Liquefaction during the Christchurch Earthquake”, submitted in October 2016 and which is under review.

5.1. INTRODUCTION

Significant liquefaction-induced ground movements and building deformations were observed in several areas in the Central Business District (CBD) of Christchurch, New Zealand (Cubrinovski et al., 2011a and Bray et al., 2014a). The comprehensive documentation of the seismic performance of an important building located in the CBD (herein referred to as Building C) during the 2010-2011 Canterbury earthquake sequence affords the opportunity to evaluate state-of-the-art nonlinear dynamic soil-structure-interaction (SSI) analytical procedures. The potential for liquefaction-induced ground movements to affect its performance is investigated.

After discussing liquefaction-induced building movements, the Building C case history is described in detail, which includes discussion of pre-seismic static settlement and earthquake-induced building movements. A recently recommended approach for evaluating liquefaction-induced building settlements is used and critiqued. Simplified liquefaction triggering and effects procedures are employed initially to gain insight. These analyses are followed by nonlinear dynamic SSI effective stress analyses. Analytical results are compared with field observations, and salient findings are presented.

5.2. LIQUEFACTION-INDUCED BUILDING MOVEMENTS

Liquefaction-induced building movements result from volumetric-induced deformation, shear-induced deformation, and loss of supporting ground due to the formation of sediment ejecta. Several publications discuss these phenomena (Dashti et al. 2010 a,b; Dashti and Bray, 2013 and Bray and Dashti, 2014). Some of these mechanisms are shown in Figure 5.1, which include: (a) ground loss due to soil ejecta; (b) shear-induced partial bearing capacity failure due to cyclic softening; (c) SSI shear-induced building ratcheting during earthquake loading; (d) volumetric strains due to sedimentation of the soil structure after liquefaction; and (e) post-liquefaction reconsolidation settlement. All of these mechanisms can contribute to the movement of a structure as a result of liquefaction in the soils beneath its foundation.

Post-liquefaction volumetric reconsolidation ground settlement calculations, such as those calculated using the Zhang et al. (2002) procedure, only capture some of these mechanisms. Liquefaction shear-induced displacements are not captured by simplified procedures that estimate only one-dimensional (1D), level ground, free-field, post-liquefaction volumetric settlements. Shear-induced building movements can be captured using advanced SSI numerical

simulations with a soil constitutive model that can capture the cyclic response of liquefied soil as shown by Dashti and Bray (2013), Luque and Bray (2015), Bray et al. (2017), Karimi and Dashti (2016a,b), among others. Cetin et al. (2012) and Unutmaz and Cetin (2012) proposed a method to estimate the cyclic stress ratio (CSR) that included the inertial effects of the structure; settlement is calculated by integrating the estimated volumetric and shear strains. Karamitros et al. (2013a,b,c) proposed a relationship for estimating liquefaction-induced building settlement as a function of the maximum ground surface acceleration, period of the ground motion, number of cycles, thickness of liquefiable layer, width of the building, and a degraded factor of safety. Bertalot et al. (2013, 2015) concluded that high bearing pressures and high initial static shear stresses prevent stress reversal, which limits pore water pressure generation and building settlement. There are not quantitative methods for evaluating the potential effects of sediment ejecta at a building site, so engineering judgment must be exercised when considering this mechanism.

5.3. BUILDING C CASE HISTORY DESCRIPTION

5.3.1. Structural Configuration

Building C is a 2-story structure built partially atop a one-level basement parking structure that occupies a site in Central Christchurch. The basement measures 69 m in the EW direction and 82 m in the NS direction (Figure 5.2). The 0.4-m thick perimeter basement wall is built of reinforced concrete (RC). The basement foundation is a combination of a 0.5-m thick RC mat in the SW corner and 0.4-m thick RC mat in the remainder of the basement. RC spread footings of varying dimensions directly underlie the mat below interior columns that support the ground floor. Irregularities exist in the North side of the basement where stairs and elevators are located. The design elevation of the basement floor is variable with the SW corner being around 0.6 m lower than the remainder of the basement. Anchor piles (0.3 m in diameter) are installed in the SW area of the basement to prevent uplift of the building due to a high water table. Anchor piles are also installed in some of the foundation pads located in its NE corner to resist uplift forces during earthquake shaking. Aurecon (2012) reports that the as-built anchor piles had significant differences with the designed piles; which included an increase in number of anchors and significant increase in the volume of grout required to fill the boreholes, indicating infiltration of grout in permeable layers, reducing their liquefaction hazard. The ground floor is a combination of a 0.4-m thick “unispans/concrete” slab and a 0.6-m thick in-situ concrete slab. The basement columns are connected with beams of variable sizes at the ground floor level in the NS direction.

Two almost separate structures, herein called C-N (North) and C-S (South) buildings, are supported on the east side of the basement (Figures 5.2 and 5.3). The C-S building is 30 m by 38 m in the NS and EW directions, respectively, and 14.2 m high above the ground level. The C-N building is 48 m by 31.5 m in the NS and EW directions, respectively, and 15.7 m high above the ground level. The C-S building’s eastern perimeter extends 6.5 m beyond the basement wall. The two buildings are connected along their eastern sides. Both structures consist of precast RC shear walls in the perimeters and interior RC columns and beams. The floors of both buildings consists of combinations of precast RC floors; either 0.6 m-thick precast pre-stressed RC double tees with 0.1-m thick concrete topping or 0.2-m thick hollow core floor units with 0.075 m topping.

5.3.2. Subsurface Conditions

The subsurface conditions at Building C have been characterized by several entities at different times using in-situ tests that include soil exploratory boreholes with the Standard Penetration Test (SPT), cone penetration testing (CPT), and Multi-Channel Analysis of Surface Waves (MASW) as shown in Figure 5.2. The groundwater surface is at a depth of about 3.0 m according to the NZGD (2016). Cross section C-C' of the structure and the underlying E-W subsurface profile are shown in Figure 5.3. The subsurface conditions at Building C site is summarized as:

- A very dense gravel with sand or very dense sand layer (Unit 1) exists between 0 and 8 m.
- Within this dense layer, there is a 0.5-0.8-m thick layer of medium dense sand (Unit 2) immediately underlying the basement foundation at some locations.
- A 1.5-2-m thick medium dense sandy gravel layer (Unit 3) underlies the uppermost very dense layer at some locations towards the western side of the basement.
- A medium dense to dense sand layer of variable thickness between 1 and 2 m (Unit 4) is found next; towards the east, some silty clay/clayey silt pockets are found within this layer.
- A 2-3-m thick very dense sand layer (Unit 5) is found consistently throughout the site.
- Below this layer, interbedded layers of stiff clayey type of materials and medium dense sands, each one with a thickness of about 1 to 1.5 m are found to a depth of 22 m (Units 6-11), where the dense Riccarton Gravel layer is found (Unit 12).

The “Black Maps,” which depict the surficial ground conditions in Christchurch as of March 1850 (Black Map 273, 1850) (NZGD, 2016), provide important information regarding streams of potentially liquefiable material that are now buried by earth fill. The effects of soil liquefaction on the infrastructure of Christchurch were typically more severe in areas shown as streams on the “Black Maps” (Cubrinovski et al., 2011a). The “Black Maps” indicate that a stream passed through the building site as late as March 1850. Therefore, the site is an area within the Christchurch CBD where the effects of shallow liquefaction may be more prominent. The thin layer of medium dense sand (Unit 2) is especially a concern, because it directly underlies the basement mat that supports the structure.

5.3.3. Canterbury Earthquake Sequence and Ground Shaking

The Canterbury earthquake sequence included seven events with $M_w \geq 5.5$, three of which had $M_w \geq 6.0$. Ground shaking was recorded at four strong motion stations within the CBD. Building C is located about 1 km to the east of the CBGS station, about 0.7 km NE of the CHHC station, and about 1 km SW of the REHS station. Recorded geo-mean peak ground accelerations (PGAs) at these strong motion stations are provided in Table 5.1, with the Bradley (2014)-estimated PGAs, which were used for the simplified liquefaction evaluation. Liquefaction was not observed at these stations for the 4 SEP 10 Darfield M_w 7.1 and 13 JUN 11 M_w 6.0 events, but it was observed at some of the stations for the 22 FEB 11 Christchurch M_w 6.2 event. However, in the latter case, the PGA values occurred before liquefaction effects are observed in the records. Thus, the estimated PGA values are not likely influenced by liquefaction.

Figure 5.4 shows acceleration–time histories for three earthquakes in the CBGS station (N89W component) showing the difference in the characteristics of the ground motion in terms of the intensity, duration, and frequency content. The M_w 6.2 Christchurch earthquake produced

the most intense ground shaking in the CBD, because the source-to-site distances (R) were only 3-6 km. Its PGA values were twice those recorded during the larger, but more distant ($R = 18-20$ km) M_w 7.1 Darfield event. The PGAs recorded in the CBD during the Darfield event are similar to those recorded during the 13 JUN 11 M_w 6.0 ($R = 5-7$ km) and 23 DEC 11 M_w 5.9 events. However, the Darfield records have a longer duration motion. The PGA values of the dozens of other M_w 5+ events are lower than those recorded during these events. Source-to-site distances (R_{RUP}) for Building C were 15.3, 4.3 and 6.8 for the Christchurch, Darfield and 13 JUN 11 events respectively.

5.3.4. Post-Canterbury Earthquake Sequence Condition

The post-Canterbury earthquake sequence condition of Building C was documented by several entities using different approaches, such as level surveys, crack mapping, LiDAR surveys, verticality surveys, and photographs. All measurements agree Building C underwent significant differential movement with the maximum settlement being in the SE area of the building. The post-earthquakes measured differential movement across the basement mat foundation is 135-150 mm. One of the provided differential settlement contour maps is presented in Figure 5.5 (PCR, 2013). Analysis of the airborne LiDAR survey captures the building's global movement (Tonkin & Taylor, 2015). It indicates that the western side of the basement uplifted slightly as a result of the Christchurch earthquake. Thus, the differential movement that was measured across the basement is likely a result of uplift in its western side and downward settlement in its eastern side.

Damage as the result of the 4 SEP 2010 Darfield earthquake was relatively minor. Photographs taken after the Darfield earthquake show some fresh minor cracks in the basement walls at entering staircases and in the structure's walls and roof. Photographs taken after the 22 FEB 2011 Christchurch earthquake show more extensive, significant cracking within the basement and overlying structures of Building C. A few photographs are shown in Figure 5.6. While there is no clear surficial evidence of sediment ejecta in the city block in which Building C is sited, there are indications of cyclic softening (e.g., rolled curb shown in Figure 5.6). The liquefaction of soils underlying a competent crust of non-liquefiable soil is often not expressed at the ground surface (Ishihara, 1985). The post-Christchurch earthquake aerial photography show significant sediment ejecta in the city blocks near Building C (NZGD, 2016). There is no evidence of lateral spreading at the site.

Aurecon (2013) produced crack maps of Building C. Detail documentation of existing cracks wider than 0.2 mm in the basement floor, basement walls, ground floor, and upper levels after the Canterbury earthquake sequence indicates distress in structural and non-structural elements. In particular, the basement floor had cracks up to 81 m long which were more intense towards the south side of the building. Cracks were also observed in the ground floor slab, which were detected from the bottom and top of the slab. Some of the cracks could possibly go completely through the slab. Several cracks occurred in the area that connects the buildings C-N and C-S. Minor cracking was generally observed in the walls, columns, and slabs in the upper floors.

As there is no survey of Building C before the Canterbury earthquake sequence, the post-event surveys reflect the total amount of foundation movement over the lifetime of the structure. It is clear from the photographic evidence before and after the Christchurch earthquake and from the mapping of cracks that would have been noticed if they occurred before the Christchurch

earthquake during the post-Darfield earthquake building inspection that a majority of the measured differential movement of the foundation resulted from the Christchurch earthquake. However, it is expected that the building was not perfectly level before the start of the earthquake sequence. Thus, some amount of the post-event surveys' measurement of differential foundation movement is likely due to static settlement that occurred before the earthquake sequence started.

5.3.5. Pre-Canterbury Earthquake Sequence Ground Movements

There is no evidence of building distress before the Canterbury earthquake sequence. However, minor static (pre-seismic) settlement of Building C likely occurred. Static settlements of Building C were estimated using the Schmertmann et al. (1978) CPT-based procedure for sand and gravel materials. Contributions from clayey soils were assessed using the Duncan and Buchignani (1976) undrained Young's modulus (E_u) correlation to estimate immediate settlement and the Robertson (2012) CPT-based 1D drained constrained modulus correlation to estimate consolidation settlement. Analyses were performed for the different sections of Building C, because its east side is significantly more loaded by the presence of the 2-story C-N and C-S buildings.

Static settlement was estimated using the entire width of the mat foundation, because this case is more reasonable given the integrated nature of the mat and spread footing foundation of the building, and this case led to greater settlement due to its deeper zone of influence. The static settlement of the structure is determined largely by the response of the upper 20 m of the soil profile, because the deeper Riccarton gravel layer is stiff. The east section of the building is estimated to settle, but the west section is not, because the foundation contact stress is less than the original vertical effective stress at this depth. Hence, anchor piles were installed in this area.

The minimum total static settlement of Building C is estimated to be approximately 0 mm (i.e., most likely within a range of -5 mm uplift to 5 mm settlement), which occurs near the western edge of the building. Its maximum total static settlement is estimated to be approximately 10 mm (i.e., most likely within a range of 5 mm to 15 mm), which occurs near the eastern edge of the basement. Thus, the pre-seismic maximum differential settlement across the west-to-east profile shown in Figure 5.3 is approximately 10 mm. This amount of movement is consistent with the lack of observed distress of the building and its foundation before the Canterbury earthquake sequence.

5.4. EVALUATION OF LIQUEFACTION-INDUCED BUILDING MOVEMENTS

5.4.1. Recommended Approach

General recommendations for evaluating the seismic performance of shallow-founded structures at liquefiable soil sites are presented by Bray et al. (2017). The potential effects of shear-induced deformations and sediment ejecta should be considered. They recommend that the engineer gain insight through a series of analyses and considerations as follows:

1. Perform liquefaction triggering assessment and calculate 1D post-liquefaction reconsolidation settlements.
2. Estimate the likelihood of sediment ejecta developing at the site by using ground

- failure indices such as the Ishihara (1985) ground failure design chart or Liquefaction Severity Number (LSN) (van Ballegoy et al. 2014). Estimate the amount of foundation settlement as a direct result of loss of ground due to the formation of sediment ejecta. Use relevant case histories to estimate the amount of ejecta, and assume the ejecta have been removed below the building foundation.
3. Perform bearing capacity analyses using post-liquefaction strengths of liquefied soils. If the post-liquefaction bearing capacity factor of safety (FS) is less than about 1.5 for light to medium size buildings or the post-liquefaction bearing capacity FS is less than about 2 for heavy or tall buildings, large movements are possible, and the potential seismic building performance is likely unsatisfactory.
 4. Perform nonlinear effective stress analyses to estimate building movements that includes shear-induced deformation.
 5. Use engineering judgment. Through identification of the key mechanisms of liquefaction-induced building movement, simplified and advanced analyses can be used to provide valid insights. However, case histories and judgment are equally important to consider.

These recommendations were followed in the seismic performance assessment of Building C.

5.4.2. Liquefaction Triggering Assessment

Liquefaction triggering was evaluated using the Boulanger and Idriss (2015) CPT-based procedure, herein called BI-15, using the 50% probability of liquefaction cyclic resistance ratio (CRR) curve and median PGA values (Table 5.1). The corresponding SPT-based procedure was also used, but it was given significantly less weight due to the large uncertainty in SPT blow count values (e.g., there were no energy measurements and often inadequate documentation of the SPT).

The CPT-based liquefaction triggering assessments of Building C site for the Darfield and Christchurch earthquakes are summarized in Figure 5.7. There are only a few deeper layers in which liquefaction triggering is indicated for the Darfield earthquake (Figure 5.7.a). Significantly more liquefaction is estimated for the more intense Christchurch earthquake shaking (Figure 5.7.b). These calculations are consistent with the area being classified as an area of “Minor Observed Liquefaction” for the Christchurch earthquake. Liquefaction triggering is expected throughout the shallow 0.5-0.8-m thick medium dense sand layer directly below much of Building C. This layer was identified by the CPTs that were advanced through the shallow dense gravel layer that overlies it. This layer of liquefiable layer directly below the Building C foundation is an important consideration when evaluating post-liquefaction stability of the spread footing elements as well shear-induced ground movements. Additionally, a medium dense sandy gravel that underlies the very dense shallow gravel at some locations is expected to develop significant excess pore water pressures (u_e) during strong shaking. Due to the difficulty of advancing CPTs through gravelly soils, insufficient data are often obtained to characterize them and their liquefaction potential may be underestimated. The borings with SPTs did help define the medium dense gravelly sand below the dense gravel as well as the thin shallow liquefiable layer towards the west section of the building. However, SPT-based analyses are less reliable than the CPT-based analyses as discussed previously.

The simplified liquefaction triggering assessment does not consider the potentially important role that installation of the anchor piles may have had on dramatically reducing the liquefaction susceptibility of sands penetrated by the grouting process utilized to install the anchor piles. The anchor piles were installed primarily under the west side of the basement at section C-C' (see Figures 5.2 and 5.3). The sensitivity of the liquefaction-induced building settlement estimates due to the improvement of the sands affected by the grouting is evaluated in this study.

5.4.3. Liquefaction-Induced Reconsolidation Volumetric Settlements

Post-liquefaction 1D reconsolidation volumetric settlements were estimated using the Zhang et al. (2002) procedure, herein called Z-02, for soil layers expected to liquefy based on the BI-15 CPT-based liquefaction triggering procedure. As noted previously, the Z-02 procedure only captures some of the principal mechanisms of liquefaction-induced ground movements under the multi-dimensional loading of a building. These analyses were performed to gain insight regarding the minimum amount of expected liquefaction-induced ground movement at the C building site as well as to estimate the post-liquefaction volumetric component of liquefaction-induced ground movement.

Representative calculations of post-liquefaction volumetric settlements are shown in Figure 5.8 for CPT-R7B, which is at west side of the building, and CPT-R5, which is at its east side. The extent of liquefaction triggering throughout the depth of the soil profile and the resulting post-liquefaction volumetric settlement are significantly greater for the Christchurch event than for the Darfield and 13JUN11 events. The estimated volumetric-induced component of ground movement for the Christchurch event was 60-85 mm (Table 5.2). If the grouting process to install the anchor piles is assumed to prevent liquefaction triggering in the upper 15 m of the soil profile on the western side of the building, these estimates are reduced to 30-50 mm. The estimated volumetric-induced ground movements for the Darfield event were generally less than half of the amount estimated for the Christchurch earthquake, and the volumetric-induced ground movements estimated for the 13JUN11 event were generally about a third of the amount estimated for the Christchurch earthquake. Therefore, although some minor amount of liquefaction induced ground movement likely occurred during the Darfield earthquake and the 13JUN11 event, the most severe liquefaction-induced ground movements occurred as a result of the Christchurch earthquake. This is consistent with the amount of mat deformation and damage observed in the basement of Building C following the Christchurch earthquake.

5.4.4. Sediment Ejecta-Induced Settlements

Sediment ejecta are not likely at this site based on the Ishihara (1985) ground failure design chart. Additionally, LSN values (van Ballegooy, 2014) are only 5-10, which is below the threshold value for moderate to severe liquefaction effects of 16 (Russell and van Ballegooy, 2015). The non-liquefiable surface layer thickness is at least 4 m for the Christchurch earthquake, and the shallowest liquefied sand layer is only 0.5-0.8 m thick. The next liquefiable layer is 1 to 2 m thick, but it is at a depth of 8 m. Thus, it is reasonable to neglect any contribution of sediment ejecta to the estimated liquefaction-induced ground movement. This assessment is consistent with observations, as sediment ejecta were not observed at this site following any of the earthquakes.

5.4.5. Shear-Induced Settlements

Shear-induced ground movements need to be added to the previously calculated volumetric-induced ground movements. A simplified evaluation of post-liquefaction bearing capacity provides insights on the possibility of shear-induced settlements (Bray et al. 2014a). The static bearing capacity of the square footing can be estimated using procedures developed for a two-layer cohesive deposit (NAVFAC, 1986) by using the residual undrained shear strength of the liquefiable layer and equivalent undrained shear strength of the gravel below the liquefiable layer.

A representative 3-m deep 5 x 5 m spread footing located along Section C-C' has a bearing pressure of around 130 kPa. The post-liquefaction residual undrained shear strength of the 0.5-0.8-m thick liquefied soil layer directly under the footing is estimated to be 13-16 kPa using an average of the procedures described by Idriss and Boulanger (2008) and Olson and Stark (2002). The post-liquefaction static FS against bearing capacity failure is only slightly greater than unity (i.e., FS = 1.05-1.20). The bearing capacity FS would be lower if the seismic demand of inertial loading of the building due to shaking and rocking were included. However, this simplified analysis assumes that the 5 x 5 m footing carries the entire column load without any contribution of the mat foundation. Punching bearing failures of shallow footings were observed in Christchurch when low bearing capacity FS were calculated even for relatively thin layers of liquefied soil. Thus, shear-induced settlement where this shallow liquefied soil deposit exists could induce settlement under the heavily loaded east side of the basement mat. Additional shear-induced settlement components would be expected for deeper medium-dense sands and gravels layers as well.

5.4.6. Simplified Liquefaction-Induced Building Settlement Assessment Summary

The first three steps of the recommended approach to evaluating liquefaction-induced building settlement employ simplified analyses (i.e., liquefaction triggering, volumetric-induced movements, sediment ejecta assessment, and bearing capacity analysis). Based on results of these analyses, Building C is expected to undergo at least 60-70 mm due to volumetric-induced settlement mechanisms. This downward foundation movement likely occurred near its eastern end where the shallow liquefiable soils are present, and less movement likely occurred near its western end where the anchor piles have improved the ground and provided vertical support. Sediment ejecta are not expected to be significant. The bearing capacity analysis using the residual strength of the liquefied shallow medium dense sand layer indicates that considerable shear-induced settlements may take place. Additionally, shear-induced deformations in the deeper medium dense sand and gravels are possible. There is not a reliable simplified method to estimate liquefaction shear-induced building settlements. A rough preliminary estimate is made using relevant case histories (e.g., Bray and Sancio 2009). The shear-induced settlement mechanisms are expected to produce an additional 100-200 mm of building settlement. Thus, the maximum total settlement of Building C is expected to be 160-270 mm. The differential settlement across the mat is expected to be on the order of the maximum total settlement given that the building's west side is buoyant. Thus, the differential settlement of Building C is judged to be 160-270 mm. The estimates based on simplified methods are uncertain, so dynamic soil

structure interaction analyses are performed (i.e., Step 4 of the recommended approach presented in Section 5.4.1).

5.5. DYNAMIC SOIL-STRUCTURE-INTERACTION (SSI) ANALYSIS

5.5.1. Numerical Model

Nonlinear dynamic SSI effective stress analyses are performed to estimate building movements that includes shear-induced deformation. *FLAC2D V7.0* (Itasca, 2009) with the *PM4Sand V3.0* constitutive model, developed by Boulanger and Ziotopoulou (2015) were used. *PM4Sand* is a stress-ratio controlled, critical state compatible, bounding surface plasticity model for sands that has been shown to produce results consistent with commonly observed soil responses.

The development of realistic earthquake ground motions is a critical component of the SSI analyses. Earthquake ground motions are input at the top of the dense Riccarton Gravel unit that pervasively underlies the shallow soils in the Christchurch CBD, because the depth to bedrock is large and unknown. Moreover, there are no nearby outcropping rock sites with recorded ground motions. The input base motions are developed from recorded surface motions that are not significantly affected by soil nonlinearity. Deconvolved “within” input earthquake motions at the top of the Riccarton Gravel unit were developed previously for the Canterbury earthquake sequence by Markham et al. (2016a). These earthquake motions were deconvolved at strong ground motion stations (CACS and RHSC) where the surficial earth materials were sufficiently stiff and strong. The ground motions were rotated to EW and NS directions, because the principal directions of Building C are coincident with those directions. Furthermore, a scale factor was applied to account for the differences in source-to-site distance (R_{RUP}) and site conditions (V_S of the Riccarton Gravel) between the stations where the deconvolution was performed and the Building C site. The scaling factor was obtained by dividing at each period the response spectra at the site of interest by the response spectra at the site seismic station (CACS or RHSC) obtained from the ground motion prediction equation (GMPE) presented in Bradley (2013). Then, an average across all periods was selected as the scaling factor. These scaling factors were calculated for each earthquake event. The input earthquake motions were applied as “within” motions to a rigid base. Using the approach described in Luque and Bray (2015), the free-field surface motions at Site C calculated with *FLAC* using the *PM4Sand* model compared well to the ground motions recorded at the nearby strong motion stations as part of the calibration process.

Cross section C-C' of the structure, which is shown in Figure 5.3, was developed from the original design plans by the Holmes Consulting Group (1999). This cross section was selected to be analyzed, because it is a heavily loaded frame, and it is located within the zone of the building where most of the differential deformation was observed.

The geotechnical model shown in Figure 5.9 is an idealization of the soil profile shown in Figure 5.3. The geotechnical units described previously in Section 3 as well as calculation points that will be discussed later are shown in Figure 5.9. The *PM4Sand* model was used to capture the cyclic response of sandy and gravelly materials, and clayey materials were assigned a Mohr-Coulomb model with properties obtained from the CPT data. Most of the geotechnical properties were obtained from the in-situ data identified in Figure 5.2. More weight was given to the data obtained from the CPT than the SPT for the reasons stated previously. The correlations used for

estimating relative density (D_r) using the CPT were from a combination of three correlations presented in Idriss and Boulanger (2008), Kulhawy and Mayne (1990) and Jamilkowski et al. (2001) with 0.4, 0.3 and 0.3 weights, respectively. The SPT- D_r correlation used was that by and Boulanger (2008). Field shear wave velocity (V_s) measurements were used in conjunction with the Christchurch specific CPT- V_s correlation by McGann et al. (2014) to obtain the small-strain shear modulus (G_o). More weight was given to the V_s measurements for surficial and gravelly soils. For other soil units equal weights were used. The mass density of the soils was obtained using the Robertson (2010) CPT correlation. The contraction parameter, h_{po} , which controls the triggering of liquefaction, was calibrated to obtain similar CRR as the BI-15 simplified liquefaction triggering curve for probability of liquefaction (P_L) of 50%. Other parameters for the *PM4Sand* constitutive model used default values (Boulanger and Ziotopoulou, 2015) or values of the critical state friction angle (ϕ_{cv}) = 35° and of the parameters that defined the relative density at critical state for the current mean effective stress: $Q = 8.0$ and $R = 1.0$. These latter values are Christchurch-specific and were obtained from laboratory testing performed on Christchurch soils by Markham (2015) and Taylor (2015). Table 5.3 shows the key parameter values used for the *PM4Sand* model.

The undrained strength (s_u) of the clayey soils was obtained from the CPT, with an N_{kt} value of 14, using the relationship of $s_u = (q_t - \sigma_v)/N_{kt}$, where q_t is the corrected CPT tip resistance and σ_v is the total vertical stress. These materials generally have low to moderate plasticity and undrained shear strength of 100 to 200 kPa. In some zones, these materials have organic content. Table 5.4 provides the key parameter values used for the clayey materials.

Structural elements were modeled as linear beam elements. The elastic Young's modulus was estimated based on a concrete compressive strength of 35 MPa. The second moment of inertia was estimated for each element considering the contribution of the slabs when the connection was monolithic. The flexural cracking of the structural elements was considered by applying a factor of 0.35 and 0.7 to the inertia of beams and columns, respectively (ACI 318-14, 2014). The loading conditions were due to the self-weights of all structural elements within the tributary length of the structural frame at cross section C-C' (i.e., 5.2 m to the south and 3.9 m to the north), an additional 1 kPa of dead load for services and finishes, and 25% of live load that was considered to be 5 kPa. A superimposed load of 3 kPa was used in the plant room area. A spacing of 9.1 m was specified for all structural elements simulating the effect of a structural frame with a constant spacing in the out-of-plane direction.

Anchor pile elements were modeled using two approaches: i) applying a downward load equal to the estimated shaft resistance of the anchor pile at their location in the raft and modeling the piles as soil with elastic properties, and ii) through modeling explicitly the anchor piles in the analyses. The results using the two approaches were similar. The results shown in the next section are based on the analyses that modeled the anchor piles explicitly as structural elements.

5.5.2. Results

The results of the SSI analyses show about 60 to 70 mm differential settlements induced by the Christchurch earthquake. As shown on Figure 5.11, this differential settlement in the basement slab results due to about 25 mm heave on the west end of the building (Point 1 in Figures 5.9 and 5.10) and 40 mm settlement on the east end of the basement (Point 2 in Figures 5.9 and 5.10). Figure 5.10 also shows the excess pore water pressure generation in the medium dense sandy gravel, with values of excess pore water ratio ($r_u = u_e/\sigma'_{vo}$) larger than 0.9,

indicating cyclic softening of this material. The primary contributors to shear-induced building settlement are the shallow thin liquefiable layer and the medium dense sandy gravel as shown by the larger shear strains in Figure 5.11. The large shear strains calculated in the medium dense sand that directly overlies the Riccarton Gravel are discounted somewhat, because excessively large shear strains are often calculated near the rigid base of nonlinear effective stress simulation. Figure 5.12 shows the results of the SSI analysis for the Christchurch earthquake in terms of vertical displacements contours. The differential settlement that occurs is a result of downward settlement on the order of 40 to 50 mm at the east edge of the building and upward movements (uplift) on the order of 20 to 30 mm near the west edge of the building. These results are in agreement with the analysis of the airborne LiDAR data by Tonkin and Taylor (2015), which was discussed previously, that suggested uplift of Building C's basement on its west side and downward settlement of its east side as a result of the Christchurch earthquake.

SSI analyses of Building C were also performed for the Darfield and 13JUN11 earthquakes. The results for the Darfield earthquake are presented in Figure 5.13 in terms of vertical displacement contours and vertical displacement-time histories at Points 1 and 2 shown in the same figure. A similar mode of response as that observed for the Christchurch earthquake is observed for the Darfield earthquake (i.e., slight uplift on the west side and downward settlement on the east side) but the settlements are only about 20 to 25% of the estimated values for the Christchurch event. The 13JUN11 event produced displacements that were on the order of only 10% of the Christchurch event.

5.6. OVERALL ASSESSMENT OF LIQUEFACTION-INDUCED BUILDING SETTLEMENT

Through examination of the key liquefaction-induced building movement mechanisms, simplified analyses of Section 4 and the advanced analyses of Section 5.5 provide important insights. However, case histories and engineering judgment are equally important. Thus, the final step in the recommended approach to evaluating liquefaction-induced building settlement is to utilize engineering judgment as one interprets the results of the analyses and considers the insights offered by previous field case histories (Step 5 in Section 5.4.1). The primary advantage of the dynamic SSI analysis relative to the simplified assessment is that it can capture explicitly shear-induced ground deformation and the dynamic interaction of the structure and the ground. Therefore, the dynamic SSI analyses provide the primary basis of this assessment. However, these results are interpreted while also considering the results of the liquefaction triggering and liquefaction reconsolidation analyses, as well as observations from field case histories.

The results of the dynamic SSI analyses of Building C during the primary events of the Canterbury earthquake sequence and the static (pre-seismic) settlement analyses are summarized in Table and Figure 5.14. . The differential movement of the building's foundation is estimated to be approximately 145 mm (with a range of 90 mm to 200 mm). This is close to the measured range of differential foundation movement of 135 mm to 150 mm. The preliminary estimate of differential building settlement based on the simplified assessments presented in Section 5.4 was 160-270 mm, which is conservative in this case. The preliminary settlement estimate is uncertain and may be unconservative at times. Thus, there is merit to performing fully nonlinear dynamic SSI effective stress analyses to gain greater insight and confidence.

A majority of the differential movement is due to the Christchurch earthquake (i.e., approximately 95 mm). A lesser amount is due to the Darfield earthquake (i.e., approximately 40

mm). On average, 10 mm of the differential foundation movement is due to static settlement that occurred before the Canterbury earthquake sequence commenced. Thus, slightly more than 90% of the measured differential ground movement was due to earthquake-induced ground deformation during the Canterbury earthquake sequence. This analytically based assessment is consistent with observations before and after the Christchurch earthquake that indicated that a large majority of the building and foundation cracking and damage was a result of the Christchurch earthquake.

5.7. CONCLUSIONS

Building C was damaged significantly primarily by the 22 FEB 2011 Christchurch earthquake. Liquefaction of several layers of loose to medium dense granular materials underneath its foundation induced permanent ground movements that distorted its foundation, which led to the observed cracking and damage of its basement and overlying structure following the Christchurch earthquake. Additionally, some minor distortion of the building's foundation likely resulted from the 4 SEP 2010 Darfield earthquake. Any distortion that may have occurred as a result of the 13 JUN 2011 earthquake or later earthquakes was likely negligible. Before the Canterbury earthquake sequence began, Building C's foundation was likely already distorted slightly due to static settlement as would be expected for any structure that non-uniformly loaded the ground beneath its foundation.

Important shear-induced settlement mechanisms are not captured well by available simplified procedures. The dynamic SSI analyses provide good insights if the constitutive model captures the liquefaction response of the loose and medium-dense soils. The results of the analyses indicate that a relative thin liquefiable layer is of great importance, because it directly underlies the building's foundation, and this soil layer can undergo significant shear-induced deformation. Volumetric-induced mechanisms are important, but procedures intended to capture them do not place sufficient weight on the importance of relatively thin layers.

Engineers often underestimate the liquefaction potential of gravelly soils. The limited capacity of some CPT rigs lead to CPTs being performed only in non-gravelly soils. In this case history, CPTs advanced through the shallow gravel, in conjunction with soil borings, identified and characterized a critical medium-dense gravel layer with high sand content. The CPT results were essential in developing the model parameters for this layer which captured the cyclic induced shear strains due to increased pore water pressure. High capacity or modified CPT equipment can be used to characterize sites with gravelly soils effectively (e.g., Bray et al. 2014b).

Lastly, it should not be surprising for significant liquefaction-induced ground movements to occur in the medium dense sand layers underlying Building C under the intense earthquake shaking of the Christchurch earthquake, especially in an area mapped as having a stream present in the 1850 "Black Maps." Historic maps are invaluable for understanding fully the site geology.

Table 5.1. Recorded geometric mean PGAs at three Strong Ground Motion Stations near Building C and median PGAs estimated by Bradley (2014)

EARTHQUAKE	STRONG GROUND MOTION STATION			Bradley (2014) (g)
	CBGS (g)	CHHC (g)	REHS (g)	
DARFIELD	0.15	0.17	0.25	0.20
CHRISTCHURCH	0.50	0.37	0.52	0.43
13 JUN 2011	0.16	0.22	0.26	0.22

Table 5.2. Post-liquefaction volumetric settlements calculated using Z-02 procedure with BI-15 median triggering estimates based on median Bradley (2014) PGA estimates.

CPT ID	Post-Liquefaction Volumetric Reconsolidation Settlement (mm)		
	DARFIELD	CHRISTCHURCH	13 JUN 2011
CPT – 2 ^a	35	85	16
CPT – 3 ^a	30	60	14
CPT – R7B	30	82	14
CPT – R5	26	62	24
CPT – R2B	40	70	29

^aThese CPTs were not advanced throughout the entire soil profile shown in Figure 5.3. CPT–R6 was not included as it only penetrated the top few meters of the soil profile.

Table 5.3. Soil properties and model parameters for cohesionless soils modeled with *PM4Sand*

Soil Unit	Unit Weight, γ (kN/m ³)	Relative Density, D_R (%)	Norm. Shear Modulus, G_o	Contraction parameter, h_{po}	Permeability, k (m/s)
1	19.7	88	1150	20	1.0e-3
2	17.0	50	400	0.38	3.0e-5
3	19.2	56	500	0.29	4.0e-6
4	19.3	71	750	0.62	3.0e-5
5	20.2	84	1100	20	5.0e-5
7	19.4	69	925	0.50	2.0e-5
9	18.8	57	1000	0.28	2.0e-6
11	18.6	54	900	0.32	5.0e-5

Note: Values of Q , R and ϕ_{cv} were set to 8.0, 1.0, and 35, respectively.

Table 5.4. Soil properties and model parameters for cohesive soils modeled with Mohr-Coulomb

Soil Unit	Unit Weight, γ (kN/m³)	Cohesion, c (kPa)	Shear Modulus, G (kPa)	Bulk Modulus, K (kPa)	Permeability, k (m/s)
6	18.1	130	47000	87000	9.5e-9
8	16.7	100	46000	85000	2.5e-9
10	17.3	160	70000	132000	5.0e-9

Note: Friction angle, tension, and dilation angle were set to zero.

Table 5.5. Average vertical movements (mm) in Building C's foundation (+ heave / - settlement; ranges of movement given in brackets)

Type of Settlement	West Side of Basement	East Side of Basement
Static (Pre-Seismic)	0 [+5 to -5]	-10 [-5 to -15] ^a
Shear-Induced for Darfield EQ	+10 [+15 to +5]	-10 [-5 to -15]
Volumetric for Darfield EQ	-10 [-10 to -20]	-30 [-25 to -35]
Shear-Induced for Christchurch EQ	+25 [+30 to +20]	-40 [-35 to -45]
Volumetric for Christchurch EQ	-40 [-30 to -50] ^b	-70 [-60 to -85] ^c
TOTAL	-15 [+10 to -40]	-160 [-130 to -190]

^aBased on CPT-R5

^bThis correspond to volumetric settlements from all CPTs from a depth of around 15 m (i.e., where the anchor piles tip extends) to the Riccarton Gravels

^cThis correspond to volumetric settlements from all CPTs for the entire soil column

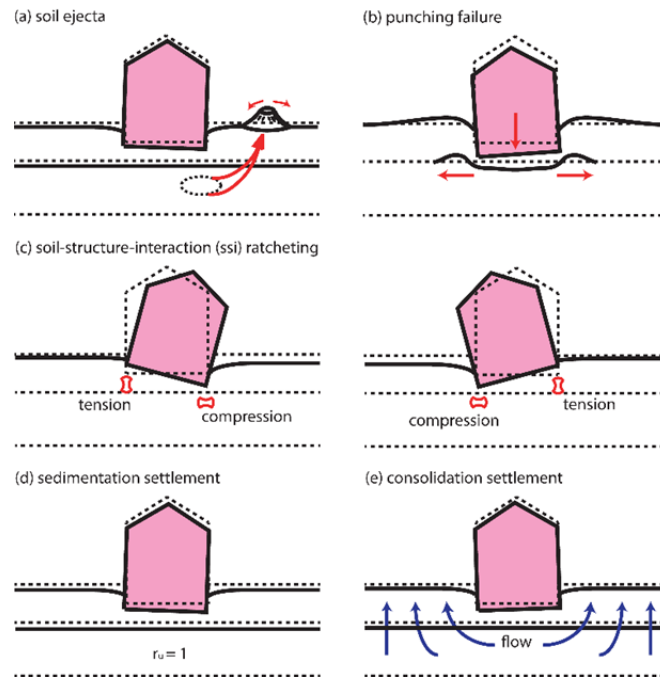


Figure 5.1. Liquefaction-induced displacement mechanisms: (a) soil ejecta; (b) punching failure, (c) soil-structure-interaction (SSI) shear-induced ratcheting; (d) sedimentation and (e) consolidation (modified from Bray and Dashti 2014).

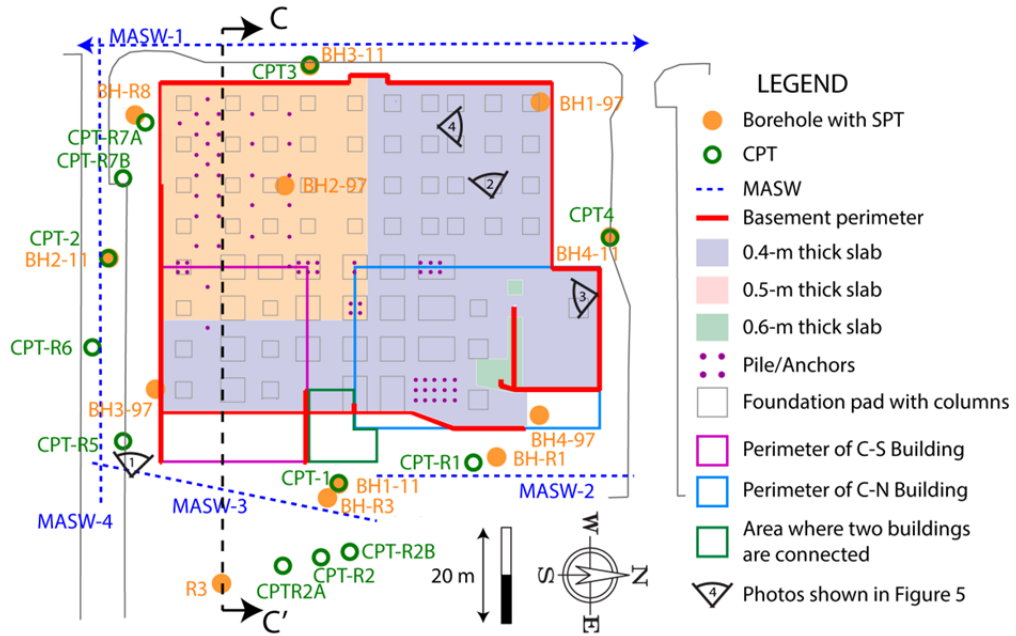


Figure 5.2. Building C basement and structure plan areas with geotechnical data.

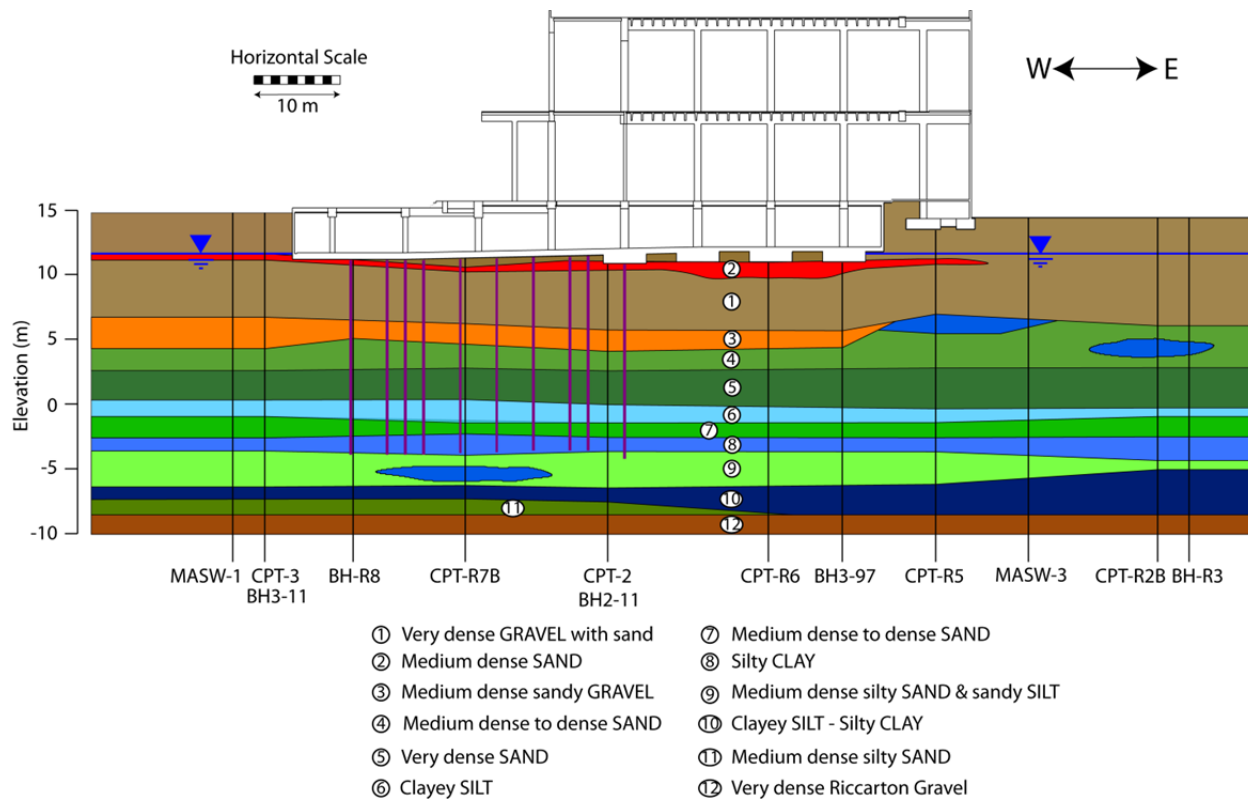


Figure 5.3. Subsurface conditions at Building C showing different geotechnical units and structural frame at cross section C-C'.

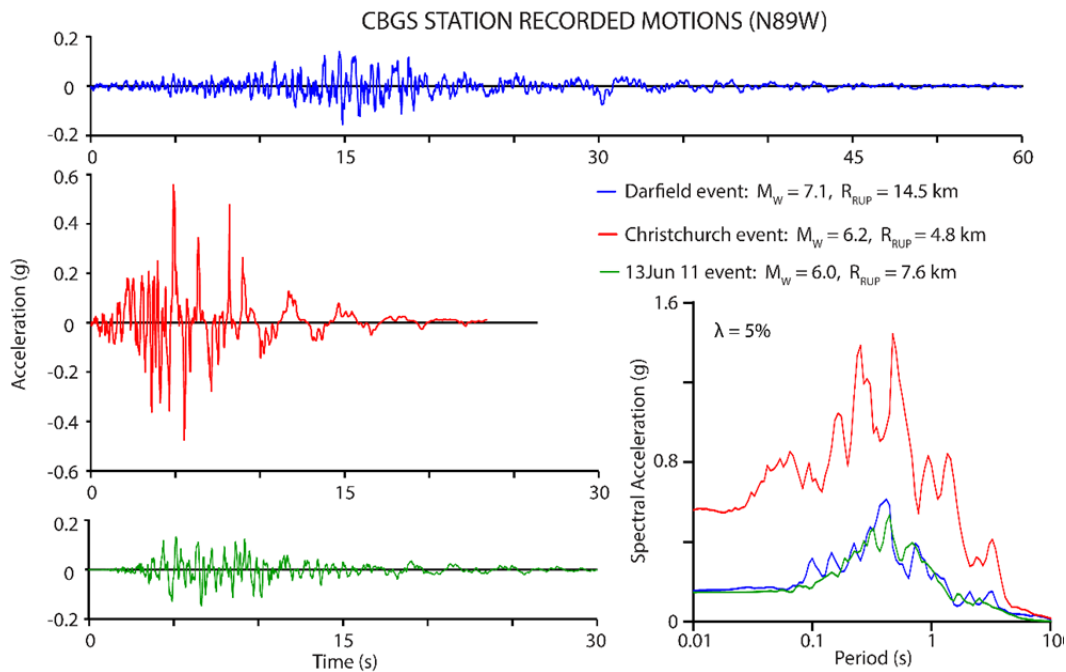


Figure 5.4. Recorded acceleration-time histories at the CBGS strong motion station for the three Canterbury earthquakes: Darfield, Christchurch, and 13JUN11

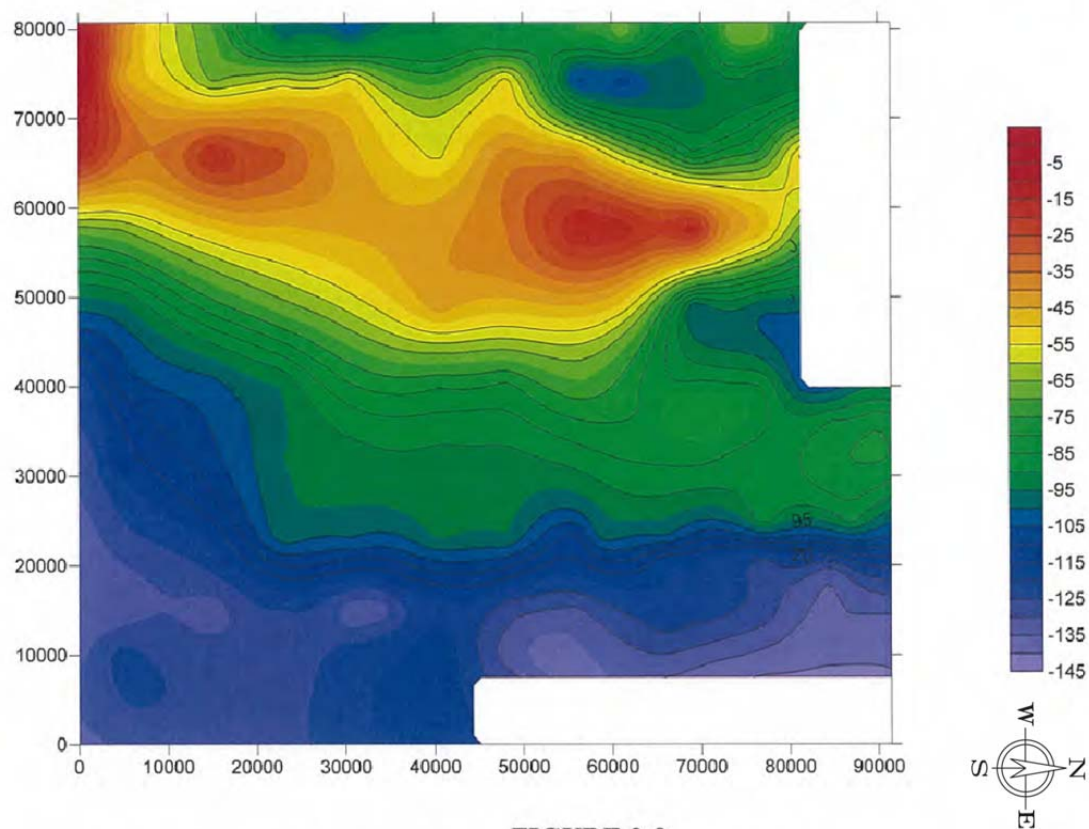


FIGURE 3-9
MEASURED RELATIVE POST-EARTHQUAKE SETTLEMENT CONTOUR PLOTS (MM)
Figure 5.5. Post-Canterbury earthquake sequence relative settlement contours on the foundation slab of the Building C from PCR (2013).



Figure 5.6. Post-Christchurch earthquake photographs of Building C: (upper-left) rolling of curb outside of building indicated area of cyclic softening-induced ground movement; (upper-right) deformation in tiled walkway and planter walls on west side of building above basement; (lower-left) cracking of wall in north corner stairway to car park; and (lower-right) cracking of garage basement RC mat (from CCC)

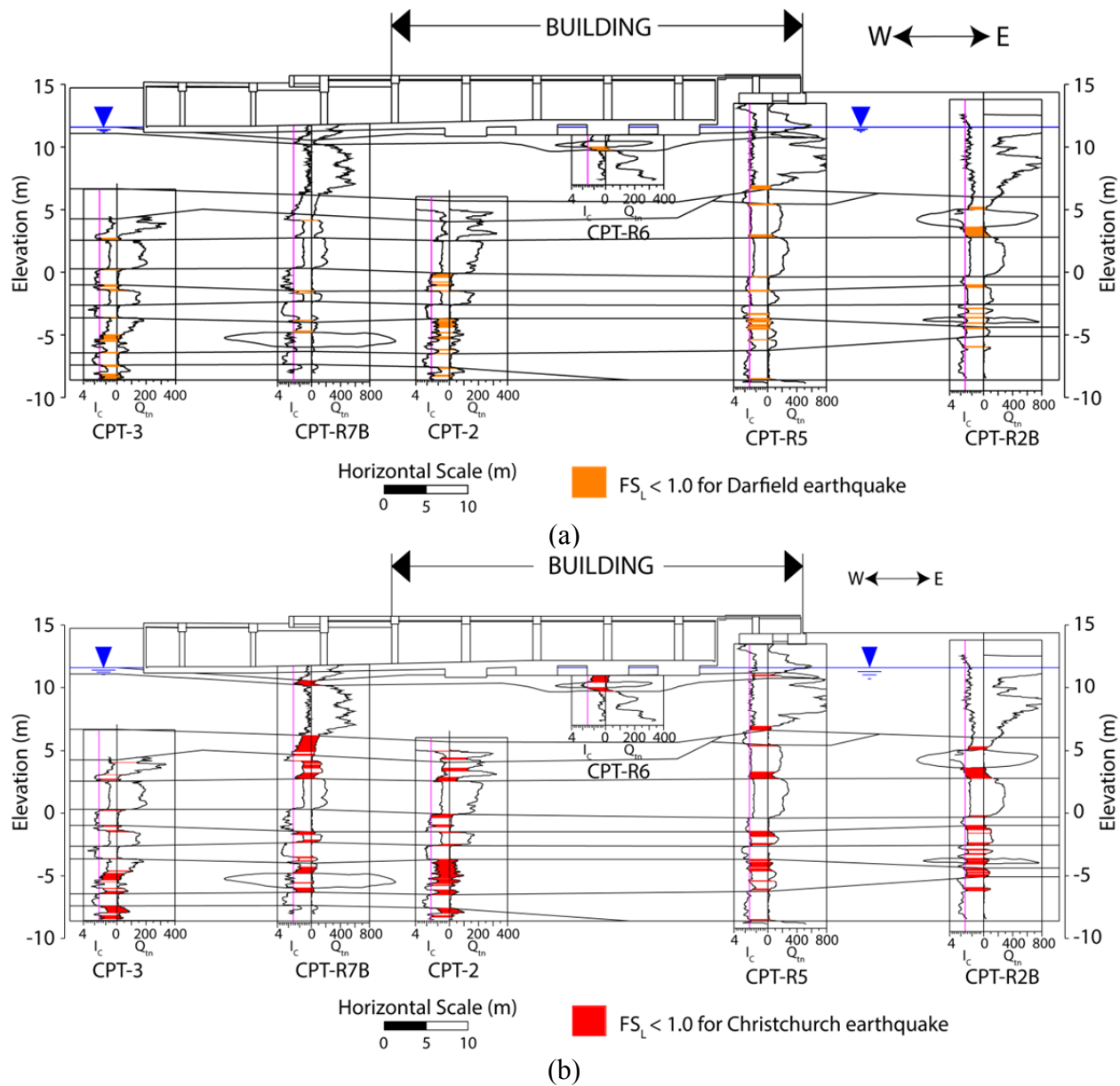


Figure 5.7. Subsurface conditions at Building C showing zones of materials with $FS_L < 1.0$ based on the median probability of liquefaction triggering using the BI-15 CPT-based procedure with the median PGAs from Bradley (2014) for the: (a) Darfield and (b) Christchurch earthquakes.

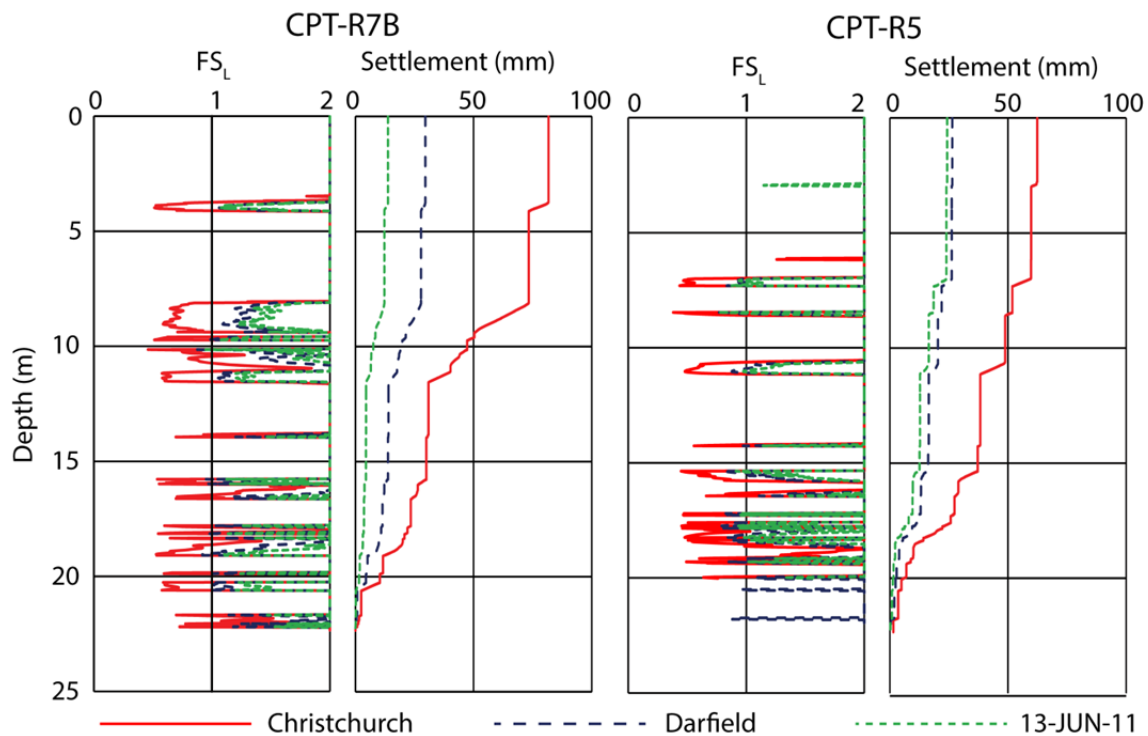


Figure 5.8. FS_L and settlement due to post-liquefaction volumetric strain profiles at CPT R7B and CPT R5 using Z-02 procedure for settlements and median BI-15 liquefaction triggering estimate at the Bradley (2014) median PGA

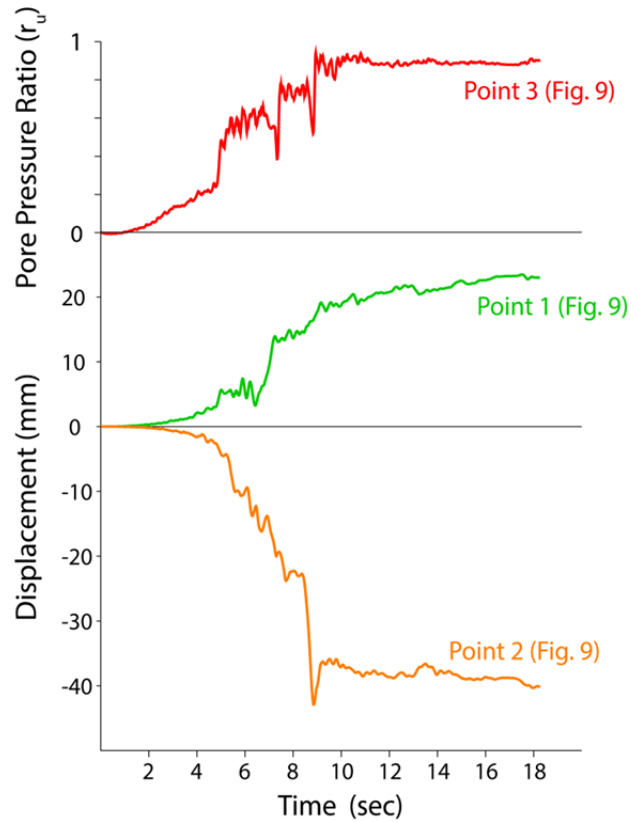


Figure 5.10. Shear-induced displacements-time histories at the west edge of the building (Point 1) and at the east edge of the basement (Point 2) and pore water pressure ratio-time history at the medium dense sandy gravel (Point 3) for the Christchurch earthquake (see Figure 5.9 for locations).

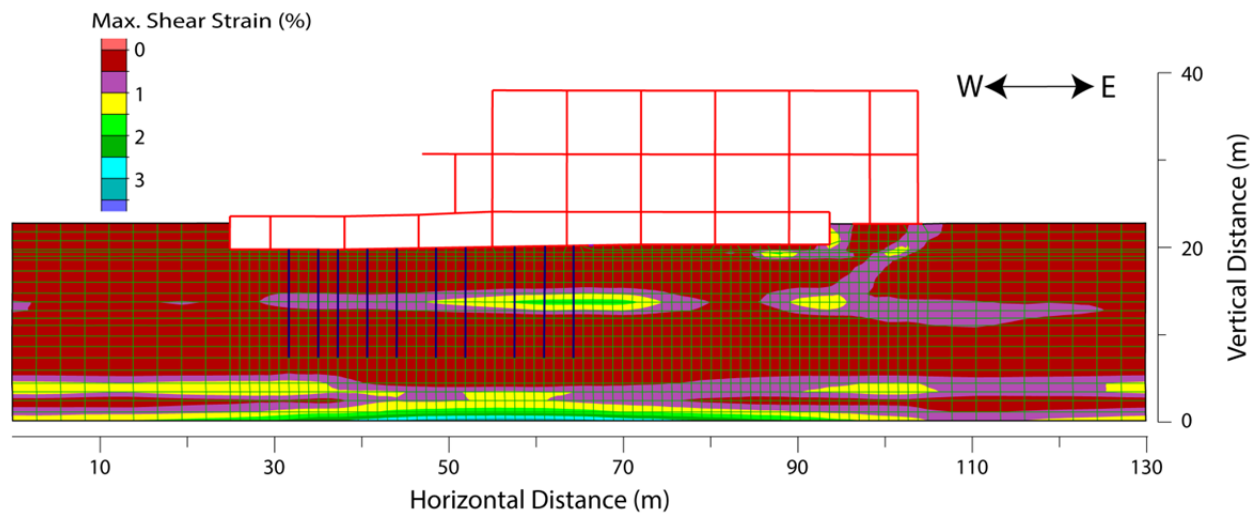


Figure 5.11. Contours of maximum shear strain increments developed from the Christchurch earthquake for the analysis of section C-C.

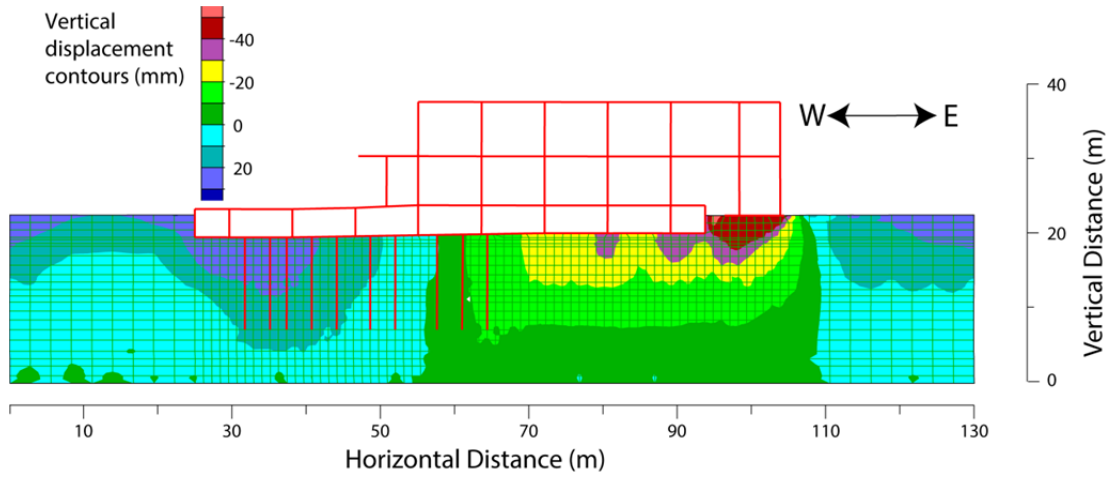


Figure 5.12. Contours of vertical displacement developed from the Christchurch earthquake for the analysis of section C-C'.

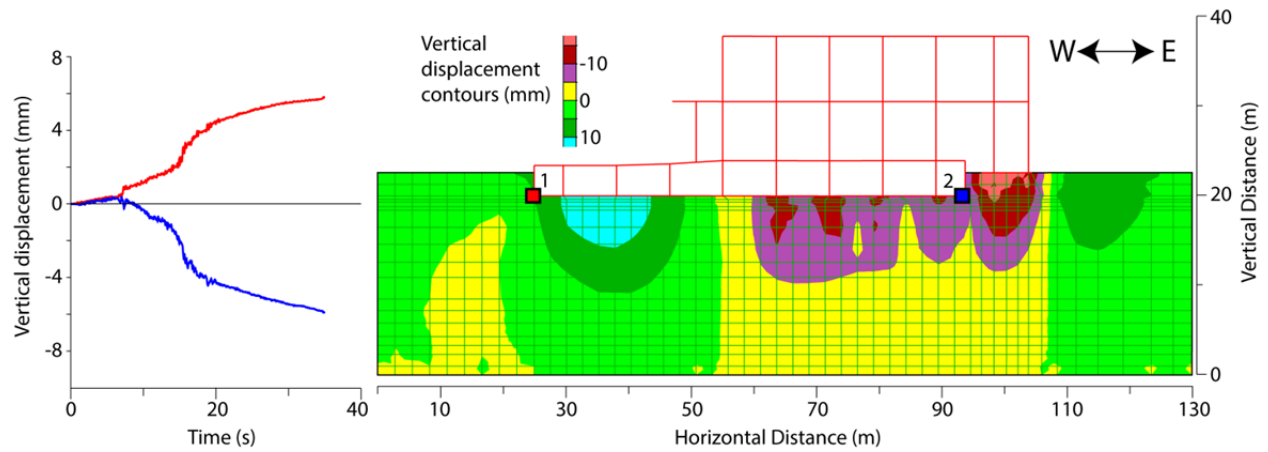


Figure 5.13. Contours of vertical displacement developed from the Darfield earthquake for the analysis of section C-C'.

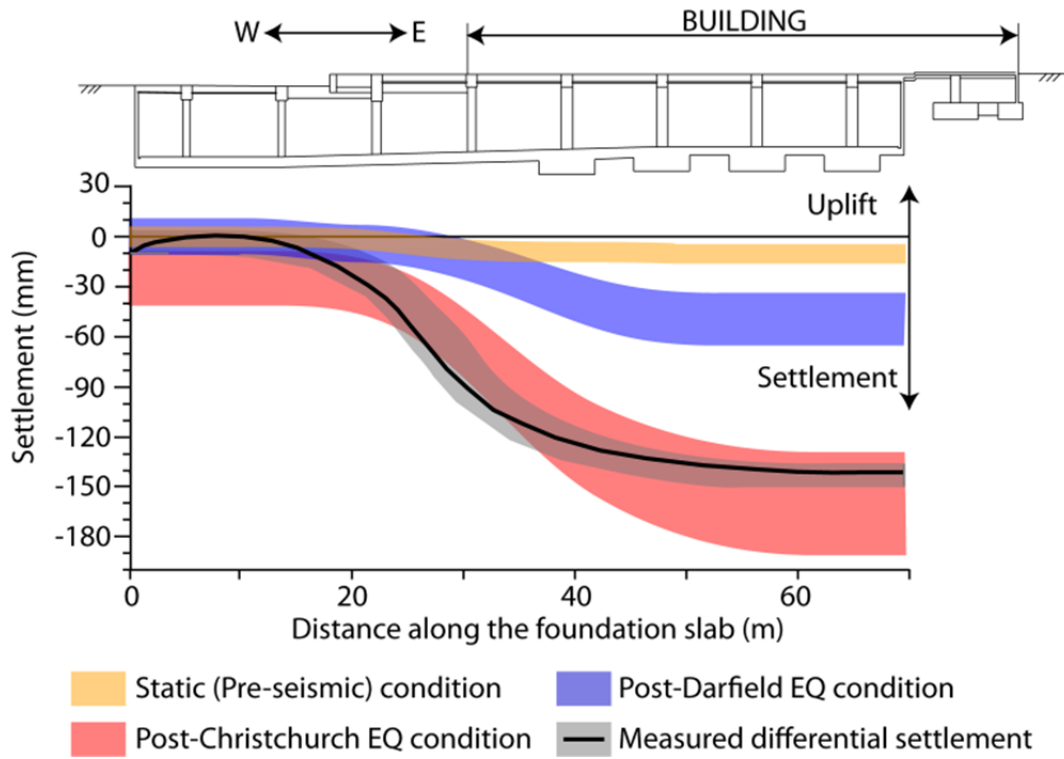


Figure 5.14. Vertical movement of Building C before and during the CES.

CHAPTER 6: CONCLUSIONS

6.1. SUMMARY

Engineers often estimate liquefaction-induced settlement of shallow-founded buildings using simplified procedures that only capture volumetric-induced settlement due to re-consolidation and sedimentation mechanisms (e.g., use of Zhang et al. 2002). These simplified procedures do not capture the important effects of shear-induced strains, which have been shown to play an important role in liquefaction-induced building settlement (e.g., Dashti et al. 2010a,b). For performance-based design, engineers need to be able to estimate the amount of building settlement under different levels of demand to evaluate building performance. A simplified procedure that estimates shear-induced liquefaction building settlement using readily available seismic demand parameters, key building properties, and important site characteristics, such as the liquefiable soil characteristics, would be helpful to engineers. Unfortunately, a robust, widely accepted simplified procedure is not available yet. However, personal computers are capable of performing large calculations in relatively short times. Thus, employing advanced numerical analytical procedures is a viable option, especially for important projects that have a sufficient budget to support advanced analyses.

In this thesis, nonlinear dynamic soil-structure-interaction (SSI) effective stress analyses were employed to evaluate shear-induced liquefaction building settlement. The software FLAC 2D was selected, because it is powerful, established, and widely used in practice. Therefore, the procedures used in this thesis may be used by practicing engineers to perform analyses that will enable robust estimation of liquefaction-induced building settlement. The soil constitutive model selected was PM4Sand (Boulangier and Ziotopoulou, 2015), which is a stress-ratio based, critical-state compatible model that has been shown to capture key response characteristics of liquefiable soil. The model accurately reproduced liquefaction response at the element level and field conditions under several loading paths.

After calibrating the numerical model at the element level and for free-field conditions, it was used to back-analyze 36 cases of liquefaction-induced building settlement from several geotechnical centrifuge experiments. Several single-degree-of-freedom model structures placed on top of layered soil deposits in which one layer was likely to liquefy when strong shaken were analyzed. There was generally good agreement between the results of the carefully performed centrifuge tests and the results of the numerical analyses performed as part of this study.

The primary goal of this program of research, however, was to evaluate the capabilities of nonlinear dynamic SSI effective stress analyses to capture the seismic performance of multi-story buildings damaged by liquefaction in Christchurch, New Zealand during the 2010-2011 Canterbury earthquake sequence. The seismic performance of five buildings undergoing three major earthquakes were characterized, back-analyzed, and evaluated. The numerical analyses provided important insights regarding the dominant mechanisms controlling liquefaction-induced building settlement. The numerical model, once calibrated against available laboratory test results of Christchurch soils, simplified CPT-based liquefaction triggering procedures, and free-field seismic site response, were able to capture the key aspects of building performance. The estimated levels of building settlement compared favorably with the observed performance in the field for these well-documented case histories. Thus, nonlinear dynamic SSI effective stress analysis provides a reliable approach for estimating liquefaction-induced building settlement.

6.2. FINDINGS

In this thesis, several centrifuge and field cases of building performance at sites that liquefied were analyzed with nonlinear dynamic SSI effective stress analyses to evaluate its capabilities, to provide insights regarding the governing mechanisms of liquefaction-induced building settlement, and to provide guidance for engineers to perform such analyses. As a result of this study, these key findings were developed:

- Calibration of the constitutive model is a key aspect of performing reliable numerical analyses. There were significant data for the Nevada Sand material used in the centrifuge experiments. However, the properties of Nevada Sand can change significantly from batch to batch, because it is an unprocessed, mined sand. Thus, the results are not always consistent among different researchers or the several types of tests used to characterize it. Capturing reasonable trends in the soil's cyclic response as key parameters varied (e.g., relative density, effective confining stress, and a non-zero initial static horizontal shear stress) is most important.
- The free-field responses measured in the centrifuge experiments were captured well in the numerical analyses, especially in terms of acceleration-time histories and pore water pressure generation during strong shaking. However, free-field liquefaction-induced ground settlement was underestimated significantly by the numerical analyses, largely because of the lack of a yield cap in the constitutive model. Constitutive models that include a cap in its yield surface should be able to produce plastic deformations at constant stress ratio, and hence capture better free-field settlement.
- The numerical analyses captured liquefaction-induced building settlement in the centrifuge experiments reasonably well, although there was a tendency for it to over-estimate the amount of measured building settlement. The tendency for and amount of over-estimation were greater for cases in which the ground motions induced relatively small settlements (< 200 mm) and for cases with rocking structures. The over-estimation of the settlement of rocking structures is explained by the observation in centrifuge testing of migration of soil from the sides of the foundation (adjacent to the footing) to the zone below the footing. The over-estimation of building settlement due to low-intensity motions is explained by the numerical model over-estimating when liquefaction was triggered by calculating pore water pressure ratios of close to one for these cases when the centrifuge experiment measurements indicated the pore water ratios were lower than one. Thus, numerical analyses resulted in higher settlements for these cases. The over-estimation of liquefaction-induced building settlement for these cases is consistent with the findings of Dashti and Bray (2013), who used a different soil constitutive model (e.g., UBCSAND).
- Site-specific CPT and laboratory test data, especially for loose-to-medium dense soil units that control the seismic response of the ground and building, were essential in refining the calibration of the effective stress model for the field case histories. For other geotechnical units, where unit-specific data were not available, the use of CRR-

N_{cycles} curves based on established magnitude scaling factors (MSF) and CPT-based simplified liquefaction procedures for estimating the cyclic resistance ratio (CRR), was satisfactory. The values of important parameters such as relative density and small strain shear modulus can be obtained reliably from correlations with the CPT measurements and from measurements of shear wave velocities, respectively.

- The free-field ground response should be evaluated by comparing the results of the numerical analyses with observations and the results of trusted simplified procedures in terms of pore water pressure ratios, shear strains, and factors of safety against liquefaction. The 5%-damped acceleration response spectra for the motions calculated at the ground surface should also be compared with recorded free-field motions when available or evaluated against the results of empirically based methods when nearby recorded ground motions are not available.
- Building performance was evaluated primarily in terms of building settlement. The displacement-time histories calculated at different points of the structure and the vertical displacement and shear strain contours calculated with the nonlinear dynamic SSI effective stress analyses provided useful information when assessing the governing mechanisms of liquefaction-induced building settlement.
- The large building settlement observed at the SE corner of the CTUC building resulted from a bearing-capacity type of failure that occurred for the footing located in that corner of the building as well as due to sediment ejecta. The continuum-based dynamic SSI effective stress analyses captured the former mechanism (i.e., shear-induced settlement), but it could not capture the latter mechanism (i.e., ejecta-induced settlement). The dynamic SSI effective stress analyses calculated a high concentration of shear strains in the loose silty sand/sandy silty layer found just below the SE corner footing, which was not present below the other footings. Shear strain-induced settlements for the CTUC building compared well to best-estimated values of the observed shear-induced settlement mechanism.
- The results of the nonlinear dynamic SSI effective stress analyses of the FTG-7 building, which had a robust foundation consisting of intersecting strip footings, identified the governing building settlement mechanism to be SSI-ratcheting as well as due to ejecta formation. The SSI-ratcheting mechanism is best reflected in the vertical settlement-time histories in the building's exterior columns. At a point during each cycle of loading, when the exterior columns on one side of the building are moving upward, the exterior columns at the other side of the building are moving downward. This rocking of the building translates to high shear stresses and high shear strains near the edges of the building. Significant shear strains were also induced below the center of the building but to a lesser degree. The calculated differential settlement across the building foundation compared favorably to that measured in post-earthquake surveys.
- The PWC building settled differentially in the Canterbury earthquake sequence. It was found that relatively thin, medium dense silty sand soil layers located within

more pervasive uniform soil layers had a significant effect on the direction of tilting. The response of the PWC building was influenced by several factors including the shape of the basement, a medium dense sandy soil layer located close to the base of the foundation, lateral movements towards the river, etc. Thus, a single controlling mechanism was not clearly defined, and it was likely that the observed movements were a combination of the previously cited factors.

- The CTH auditorium building was founded on a loose silty sand material. The inner columns, which were more heavily loaded, settled more relative to the outer columns, which were more lightly loaded. In addition to shear-induced settlements, soil ejecta-induced and volumetric-induced building settlements were important contributors to the seismic performance of the CTH auditorium. The volume of soil removed from inside the building after the earthquake was about 70 m³. The soil deposit beneath the building was also heterogeneous with more loose soil present south of the building, which resulted in more building settlement of its southern side. Lastly, lateral spreading toward the Avon river, which is south of the building, produced additional differential settlement across the building from its southern side to its northern side.
- The difference in weight and bearing pressures of each side of the “C” building in the west and east direction and the unintended consequence of soil improvement due to installing tie-downs to resist static buoyant water pressures under the western part of the facility that did not have a structure atop of the basement caused differential settlement that induced structural cracking of some elements. The nonlinear dynamic SSI effective stress analyses were able to capture the tendencies of the basement mat to uplift on its western end and to settle on its eastern end. The analyses highlighted the important roles played by a thin layer of loose sand directly beneath the foundation and by a gravelly sand/sandy gravel layer of medium density.
- Good agreement between the calculated and measured building settlements was obtained for these buildings for the Christchurch earthquake, which shook them most intensely. The analyses over-estimated building settlements for the lower intensity Darfield and 13-Jun-11 earthquakes. The over-estimation of building settlements for the Darfield earthquake was relatively minor and judged to be acceptable. The over-estimation of building settlements for the 13-Jun-11 event was more significant, and it was judged to occur because the analyses over-estimated the free-field response recorded at nearby strong motion stations for this event. Additionally, as observed in the centrifuge experiments, the numerical analyses may predict triggering of liquefaction in zones when it is close to triggering but it does not actually trigger, which in turn leads to over-estimating liquefaction-induced building settlement. The inherent conservatism of liquefaction evaluation procedures, and hence the soil models developed to capture the expected liquefaction behavior, is a likely reason for the over-estimation of building settlement for the low intensity ground motions.
- Understanding site geology is critically important when developing analytical models. The “Black Maps” (NZGD, 2016) prepared in the 1850’s identified small

streams in the vicinity of several of the buildings studied in this research. The CPT investigations confirmed that shallowly buried streams were beneath parts of some of the buildings. Thus, the buried stream channels had to be included in the heterogeneous soil profiles modelled with the numerical simulations. The analyses identified zones of localized high shear strains in those areas for the CTUC, PWC and C buildings.

- Soil ejecta were observed to be of primary importance in the settlement of some of the buildings. One of the shortcomings of the presented analyses is from the continuum model not reproducing the removal of soil beneath building foundations due to the formation of soil ejecta. Liquefaction ground failure indexes, such as LPI, LSN, or the Ishihara (1985) chart, remain useful tools to estimate the amount of ejecta-induced building settlement. However, more research is needed to quantify better building settlement caused by soil ejecta.

6.3. FUTURE RESEARCH

The numerical analyses presented in this thesis provide useful insights into the seismic response of shallow-founded buildings situated atop liquefiable soils. As a result of this work, research opportunities related to the problem of liquefaction-induced building settlement have been identified, including:

- Centrifuge experiments provide great model case histories to back-analyze and to understand. More centrifuge experiments involving structures on liquefiable deposits should be performed. Additionally, large-scale shaking table experiments that investigate the issue of sediment ejecta would provide important data and insights.
- This thesis relied heavily on well-documented field case histories. The collection of detailed measurements, photos, LiDAR data, tilting measurements, ground motion data, in-situ testing, laboratory testing, etc. after an earthquake produces well-documented case histories that provide invaluable opportunities to gain insight and to identify key deformation mechanisms through back-analysis. Therefore, continued and improved efforts to capture systematically perishable data after major earthquakes are highly encouraged.
- The same type of analyses performed in this thesis should also be performed by different researchers using different numerical methods and different constitutive models. Comparison of the results of different nonlinear dynamic SSI effective stress analyses will provide important insights, develop confidence in the methods examined, and encourage practicing engineers to perform these types of analyses more routinely.
- The potential for important 3D effects of building response should be investigated. In this research, critical sections of buildings and soil profiles were analyzed in a

2D plane strain analyses. Simplifying assumptions were required, which resulted in limitations of the analyses reported in this thesis. The potential benefits of 3D analyses need to be weighed against the limitations of knowledge of the true variability of ground and whether important aspects of the 3D system can be captured reasonably well.

- The effects that soil ejecta have on building settlement and seismic performance has been observed to be important in some of these cases. The occurrence of soil ejecta depends on many factors such as geologic environment, characteristics of the crust layer, and the depth and thickness of the liquefiable layer, among others, which are often difficult to characterize. Research in this area is highly encouraged to advance the profession.
- The profession would benefit from the development of simplified procedures that estimate liquefaction-induced building settlement based on key properties that describe the geometry and the density of the liquefiable soil, the geometry, weight, and properties of the structural system, and ground parameters that define the seismic demand of the earthquake.

REFERENCES

- Adrianopoulos, K.I., Papadimitriou, A.G., and Bouckovalas, G.D. (2010). "Bounding Surface Plasticity Model for the Seismic Liquefaction Analysis of Geostuctures." *Soil Dynamics and Earthquake Engineering* 30 (2010) 895-911.
- Allmond, J., Kutter, B.L. (2012). Centrifuge testing of rocking foundations on saturated and submerged sand: Centrifuge Data Report for JDA01, UCD/CGMDR-12/01, Univ. of Calif., Davis, CA.
- Allmond, J., Kutter, B.L. (2013). Centrifuge testing of rocking foundations on saturated and submerged sand: Centrifuge Data Report for JDA02, UCD/CGMDR-13/01, Univ. of Calif., Davis, CA.
- Allmond, J., Kutter, B.L., Bray, J.D., Hayden, C.P. (2014). FLIQ: Foundation and ground performance in liquefaction experiments, Network for Earthquake Engineering Simulation (NEES distributor). DOI: 10.4231/D3M61BQ73
- Allmond, J., Kutter, B.L., Bray, J.D., Hayden, C.P. (2015). New Database for Foundation and Ground Performance in Liquefaction Experiments. *Earthquake Spectra*: November 2015, Vol. 31, No.4, pp. 2485-2509.
- American Concrete Institute (2014). "Building Code Requirements for Structural Concrete. (ACI 318-14) and Commentary (ACI 318R-14).
- American Concrete Institute (2014). "Building Code Requirements for Structural Concrete. (ACI 318-14) and Commentary (ACI 318R-14).
- American Institute of Steel Construction (2014). "Steel Construction Manual Shapes Database". From: <http://www.aisc.org/WorkArea/showcontent.aspx?id=34922>, Last accessed: May 16th 2015.
- Armstrong, R. J. (2010). "Evaluation of the Performance of Piled Bridge Abutments Affected by Liquefaction-Induced Ground Deformations through Centrifuge Tests and Numerical Analysis Tools". Ph.D. dissertation, University of California, Davis, CA.
- Arulmoli, K., Muraleetharan, K.K., Hossain, M.M. and Fruth, L.S. (1992). "VELACS Verification of Liquefaction Analyses by Centrifuge Studies Laboratory Testing Program Soil Data Report". Earth Technology Corporation, March 1992, Irvine, CA, USA.
- Arulnathan, R., Boulanger, R.W., Kutter, B.L., Sluis, W.K. (2000). "New Tool for Shear Wave Velocity Measurements in Model Tests". *Geotechnical Testing Journal*, Vol. 23, No.4, 2000, pp.444-453, <https://doi.org/10.1520/GTJ11065J>. ISSN 0149-6115
- Aurecon (2012) Geotechnical Report - Christchurch [...] Repair and Reinstatement Project, Revision 2, 20-Apr-2012.
- Aurecon (2013) Structural Crack Mapping – Christchurch [...] Repair & Reinstatement Project, Revision 0, 10-Apr-2013.
- Beca Carter Hollings & Ferner Ltd. (2011a). Earthquake Damage Assessment – 151 Kilmore Street. Technical report prepared for Westpark Estates 151 Ltd.
- Bertalot, D., Brennan, A.J. and Avillalobos, F.A. (2013). "Influence of Bearing Pressure on Liquefaction-Induced Settlement of Shallow Foundations". *Geotechnique* 63, No. 5, 391-399.
- Bertalot, D. and Brennan, A.J. (2015). "Influence of Initial Stress Distribution on Liquefaction-Induced Settlements of Shallow Foundations". *Geotechnique* 65, No. 5, 418-428.
- Bolton, M.D. (1986). "The Strength and Dilatancy of Sands". *Geotechnique* 36, No.1, 65-78.
- Boulanger, R.W. and Ziotopoulou, K. "PM4Sand (Version 3): A Sand Plasticity Model for Earthquake Engineering Applications." Report No. UCD/CGM-15/01, Center for

- Geotechnical Modeling, Department of Civil and Environmental Engineering, Univ. of California, Davis, CA; 2015, 108 pp.
- Boulanger, R.W. and Idriss, I.M. (2014). "CPT and SPT Based Liquefaction Triggering Procedures." Report No. UCD/CGM-14/01. Center for Geotechnical Modeling, Dept. of Civil and Environmental Engineering, University of California, Davis.
- Boulanger, R.W. and Idriss, I.M. (2016). "CPT- Based Liquefaction Triggering Procedures." *Journal of Geotechnical and Geoenvironmental Engineering*, 142(2), 04015065.
- Bradley, B.A. (2013). "A New Zealand-Specific Pseudospectral Acceleration Ground-Motion Prediction Equation for Active Shallow Crustal Earthquakes Based on Foreign Models." *Bulletin of the Seismological Society of America*. Vol. 103, No. 3, pp. 1801-1822, June 2013.
- Bradley, B.A., and Hughes, M. (2012). "Conditional Peak Ground Accelerations in the Canterbury Earthquakes for Conventional Liquefaction Assessment." Tech. Report for the Depart. of Building & Housing, 22 pp.
- Bradley, B.A. (2014). "Site-specific and Spatially-distributed Ground-motion Intensity Estimation in the 2010-2011 Canterbury Earthquakes." *Journal of Soil Dynamics and Earthquake Engineering* 61-62 (2014) 83–91
- Bray, J.D. and Sancio, R.B. (2006). "Assessment of the Liquefaction Susceptibility of Fine-Grained Soils". *Journal of Geotechnical and Geoenvironmental Engineering*, ASCE, Vol. 132, No. 9, pp.1165-1177.
- Bray, J.D. and Sancio, R. (2009). "Performance of buildings in Adapazari during the 1999 Kocaeli, Turkey Earthquake". *Earthquake Geotechnical Case Histories for Performance-Based Design*, pp. 325-340.
- Bray, J.D., and Dashti, S. (2014). "Liquefaction-Induced Building Movements". *Bulletin of Earthquake Engineering*, Springer, Vol. 12(3), 2014, pp. 1129-1156.
- Bray, J.D., Cubrinovski, M., Zupan, J., and Taylor, M. (2014a). "Liquefaction Effects on Buildings in the Central Business District of Christchurch". *Earthquake Spectra J., Earthquake Engineering Research Institute*, Vol. 30(S1).
- Bray, J.D., Cubrinovski, M., Zupan, J., and Taylor, M. (2014b). "CPT-Based Liquefaction Assessments in Christchurch, New Zealand". *CPT'14: Third International Symposium on Cone Penetration Testing*, Las Vegas, NV, May 13-14.
- Bray, J.D., Markham, C.S., and Cubrinovski, M. (2015). "Liquefaction assessments in the Central Business District of Christchurch, New Zealand". Invited Keynote Paper. Proc. of the 6th Inter. Conf. on Earthquake Geotechnical Engineering, 6ICEGE, 1-4 November, Christchurch, New Zealand.
- Bray, J.D., Markham, C.S., Cubrinovski, M. (2017). "Liquefaction assessment at shallow foundation building sites in the Central Business District of Christchurch, New Zealand". *Soil Dynamics and Earthquake Engineering Journal*, Vol. 92, pp 153 – 164, <http://dx.doi.org/10.1016/j.soildyn.2016.09.049>.
- Chen, Y. (1995). "Behavior of a Fine Sand in Triaxial, Torsional and Rotational Shear Tests". Ph.D. Dissertation, University of California, Davis, CA, USA.
- Cetin, K.O., Unutmaz, B., Jeremic, B. (2012). "Assessment of seismic soil liquefaction triggering beneath building foundation systems". *Soil Dynamics and Earthquake Engineering* 43 (2012) 160–173.

- Cubrinovski, M., Bray, J.D., Taylor, M., Giorgini, S., Bradley, B., Wotherspoon, L., and Zupan, J. (2011a). "Soil Liquefaction Effects in the Central Business District during the February 2011 Christchurch Earthquake." *Seismological Research Letters*, 82(6), 893-904.
- Cubrinovski, M., Bradley, B., Wotherspoon, L., Green, R., Bray, J., Wood, C., Pender, M., Allen, J., Bradshaw, A., Rix, G., Taylor, M., Robinson, K., Henderson, D., Giorgini, S., Ma, K., Winkley, A., Zupan, J., O'Rourke, T., DePascale, G. and Wells, D. (2011b) "Geotechnical Aspects of the 22 February 2011 Christchurch Earthquake." *Bulletin of the New Zealand Society of Earthquake Engineering*, 44(4): 205-226.
- Cubrinovski, M., Green, R.A., and Wotherspoon, L. [Eds] (2011c). "Geotechnical Reconnaissance of the 2011 Christchurch Earthquake." Technical Report. Retrieved from http://geerassociation.org/GEER_Post%20EQ%20Reports/Christchurch_2011/Index_Christchurch_2011.html.
- Dafalias and Manzari (2004). "Simple plasticity and sand model accounting for fabric change effects." *Journal of Engineering Mechanics*, ASCE, 130(6), 622-634.
- Darendeli, M. (2001). "Development of a new family of normalized modulus reduction and material damping curves". Ph.D. Thesis, Dept. of Civil Eng., Univ. of Texas, Austin.
- Dashti, S. (2009). "Toward evaluating building performance on softened ground" Ph.D. Dissertation, Univ. of California, Berkeley, CA.
- Dashti, S., Bray, J.D., Pestana, J.M., Riemer, M.R., and Wilson, D. (2010a). "Mechanisms of Seismically-Induced Settlement of Buildings with Shallow Foundations on Liquefiable Soil." *Journal of Geotechnical and Geoenvironmental Engineering*, 136(1), 151-164.
- Dashti, S., Bray, J.D., Pestana, J.M., Riemer, M.R., and Wilson, D. (2010b). "Centrifuge Testing to Evaluate and Mitigate Liquefaction-Induced Building Settlement Mechanisms." *Journal of Geotechnical and Geoenvironmental Engineering*, 136(7), 918-929.
- Dashti, S. and Bray, J.D. (2013). "Numerical Simulation of Building Response on Liquefiable Sand" *Journal of Geotechnical and Geoenvironmental Engineering*, 139(8), 1235-1249.
- Doygun, O. (2009). "Monotonic and Cyclic Undrained Loading Behavior of Intermediate Soils" M.Sc. Dissertation, Technische Universitat Darmstadt, Germany.
- Duncan, J.M. and Buchignani, A.L. (1976). *An Engineering Manual for Settlement Studies*, Depart. Of Civil Engineering, Univ. of California, Berkeley.
- Elgamal, A., Lu, J., and Yang, Z. (2005). "Liquefaction-Induced Settlement of Shallow Foundations and Remediation: 3D Numerical Simulation." *Journal of Earthquake Engineering*, V 9, Special Issue, 17-45.
- Eliot Sinclair & Partners Limited (2011). "Ground Floor Levels – 4 March 2011."
- Giorgini, S., Taylor, M., Cubrinovski, M., and Pampanin, S. (2011). "Preliminary Observations of Multistorey RC Building Foundation Performance in Christchurch Following the 22nd February 2011 Earthquake." *New Zealand Concrete Industry Conference*, Energy Events Centre, Rotorua, New Zealand, August 2011.
- Giorgini (2015). "Towards Performance-Based Seismic Design and Assessment of Integrated Foundation-Structure Systems". Ph.D. dissertation, Department of Civil and Natural Resources Engineering, University of Canterbury, Christchurch, New Zealand.
- Hayden, C.P., Allmond, J.D., Rawlings, I.A., Kutter, B.L., Bray, J.D., Hutchinson, T.C., Fiegel, Zupan, J.D., Whittaker, A.S. (2014). *Seismic performance assessment in dense urban environments: Centrifuge Data Report for Test-6*, Univ. of California, Davis, CA.
- Hayden, C.P., Zupan, J.D., Bray, J.D., Allmond, J.D., and Kutter, B.L. (2015) "Centrifuge Tests of Adjacent Mat-Supported Buildings Affected by Liquefaction," *J. of Geotechnical and*

- Geoenvironmental Engineering, ASCE, V. 141(3), Paper 04014118, [http://dx.doi.org/10.1061/\(ASCE\)GT.1943-5606.0001253](http://dx.doi.org/10.1061/(ASCE)GT.1943-5606.0001253).
- Holmes Consulting Group (1968). "Christchurch Town Hall Structural Drawings."
- Holmes Consulting Group (1999). "Christchurch [...] Project – Structural Drawings"
- Holmes Consulting Group (2011). "Detailed Structural Engineering Evaluation of the Christchurch Town Hall For Performing Arts." Technical Report prepared for Vbase Limited, 8 August 2011.
- Hsu, C. and Vucetic, M. (2002). "Dynamic and Cyclic Behavior of Soils Over a Wide Range of Shear Strains in NGI-type Simple Shear Testing Device", UCLA Research Report No. ENG-02-228, Civil and Environmental Engineering Department, University of California, Los Angeles, January, CA, 267 pp.
- Idriss, I.M, and Boulanger R, W. "Soil Liquefaction during Earthquakes." Earthquake Engineering Research Institute (EERI), MNO-12; 2008.
- Idriss, I.M. and Akky, M.R. (1979). "Primary Variables Influencing Generation of Earthquake Ground Motions by a Deconvolution Process." Paper K 1/3. Proceedings of the 5th Annual SMiRT Conference, August 1979.
- Ishi, Y. and Tokimatsu, K. (1988). "Simplified Procedures for the Evaluation of Settlements of Structures during Earthquakes" Proceedings of Ninth World Conference on Earthquake Engineering, Tokio-Kyoto, Japan, August 1988.
- Ishihara, K., and Yoshimine, M. (1992). "Evaluation of settlements in sand deposits following liquefaction during earthquakes". Soils and Foundations, 32(1): 173–188.
- Ishihara, K. (1985). "Stability of natural deposits during earthquakes," Proc. 11th International Conf. on Soil Mechanics and Foundation Engineering, Vol. 1., pp. 321-376.
- Itasca (2009). "Flac – Fast Lagrangian Analysis of Continua, Version 6.0." Itasca Consulting Group, Inc., Minneapolis, Minnesota.
- Jacka, M. (2016), Personal Communication.
- Jamiolkowski, M., LoPresti, D.C.F., and Manassero, M. (2001). "Evaluation of Relative Density and Shear Strength of Sands from Cone Penetration Test and Flat Dilatometer Test." Soil Behavior and Soft Ground Construction (GSP 119), American Society of Civil Engineers, Reston, Virginia, 201 – 238.
- Kammerer, A.M., Wu, J., Pestana, J.M., Riemer, M., Seed, R.B. (2000). "Cyclic Simple Shear Testing of Nevada Sand for PEER Center Project 205199". Geotechnical Engineering Report No. UCB/GT/00-01, Civil and Environmental Engineering Department, University of California, Berkeley, CA.
- Kammerer, A., Wu, J., Riemer, M., Pestana, J., and Seed, R. (2004). "A new multi-directional simple shear testing database." Proc., 13th World Conf. on Earthquake Engineering, Canadian Association for Earthquake Engineering, Ottawa.
- Kamai, R. and Boulanger, R.W. (2013). "Simulations of a Centrifuge Test with Lateral Spreading and Void Redistribution Effects". Journal of Geotechnical and Geoenvironmental Engineering, 139(8), 1250-1261.
- Kano, S. (2008). "Torsional Hollow Cylinder Tests on Nevada Sand." Hiroshima, Japan.
- Karimtros, D.K., Bouckovalas, G.D. and Chaloulos, Y.K. (2013a) "Seismic Settlements of Shallow Foundations on Liquefiable Soil with a Clay Crust". Soil Dynamics and Earthquake Engineering, 46 (2013) 64-76.
- Karamitros, D.K., Bouckovalas, G.D., Chaloulos, Y.K., Andrianopoulos, K.I. (2013b). "Numerical analysis of liquefaction-induced bearing capacity degradation of shallow

- foundations on a two-layered soil profile” *Soil Dynamics and Earthquake Engineering* 44 (2013) 90–101.
- Karamitros, D.K., Bouckovalas, G.D., Chaloulos. (2013c). “Insight into the Seismic Liquefaction Performance of Shallow Foundations”. *Journal of Geotechnical and Geoenvironmental Engineering*, 139(4), 599-607
- Karimi, Z., and Dashti, S. (2016a). “Numerical and Centrifuge Modeling of Seismic Soil-Foundation-Structure Interaction on Liquefiable Ground.” *Journal of Geotechnical and Geoenvironmental Engineering*, Vol. 142, No.1.
- Karimi, Z., and Dashti, S. (2016b). “Seismic Performance of Shallow-Founded Structures on Liquefiable Ground: Validation of Numerical Simulations Using Centrifuge Experiments.” *Journal of Geotechnical and Geoenvironmental Engineering*, Vol. 142, No.6.
- Kulhawy, F.H. and Mayne, P.H. (1990). “Manual on estimating soil properties for foundation design” Electric Power Research Institute, August 1990.
- Liu, H. (1995). “An Empirical Formula for Evaluation of Buildings Settlements Due to Earthquake Liquefaction” *Proceedings of the 3rd International Conference on Recent Advances in Geotechnical Earthquake Engineering and Soil Dynamics*, 2-7 April, St. Louis, Missouri, USA.
- Liu, H. and Dobry, R. (1997). “Seismic Response of Shallow Foundation on Liquefiable Sand”. *Journal of Geotech. Geoenviron. Eng.*, ASCE, 123(6): 557–567.
- Lopez-Caballero, F., and Farahmand-Razavi A.M. (2008). “Numerical Simulation of Liquefaction Effects on Seismic SSI.” *Soil Dynamics and Earthquake Engineering*, 49 (2013) 2-38.
- Luque, R., and Bray, J.D. (2015). “Dynamic analysis of a shallow-founded building in Christchurch during the Canterbury Earthquake Sequence”. *Proc. 6th Inter. Conf. on Earthquake Geotechnical Engineering*, 6ICEGE, 1-4 November, Christchurch, New Zealand.
- Manzari, M.T., Arulanandan, K. (1992). “Numerical Predictions for Model No.1”. K. Arulanandan, R.F. Scott (Eds.), *Verification of Numerical Procedures for the Analysis of Soil Liquefaction Problems*, A.A. Balkema, Rotterdam (1993), pp. 179-185
- Markham, C., Macedo, J., and Bray, J. D. (2014). “Evaluating Fully Nonlinear Effective Stress Site Response Analyses using Records from the Canterbury Earthquake Sequence.” U.S.G.S. Award No.: G13AP00029. August 29, 2014. Final Technical Report. Downloaded from: <http://earthquake.usgs.gov/research/external/reports/G13AP00029.pdf>
- Markham, C. (2015). “Response of Liquefiable Sites in the Central Business District of Christchurch, New Zealand.” Ph.D. Dissertation, University of California, Berkeley, CA.
- Markham, C., Bray, J.D., Macedo, J., Luque, R. (2016a). “Evaluating Nonlinear Effective Stress Site Response Analyses using Records from the Canterbury Earthquake Sequence.” *Soil Dynamics and Earthquake Engineering*, 82, 84-98.
- Markham, C. S., Bray, J. D., Riemer, M. F., and Cubrinovski, M. (2016b). “Characterization of Shallow Soils in the Central Business District of Christchurch, New Zealand,” *Geotechnical Testing Journal*, 39(6), 1–16.
- McGann, C., Bradley, B., Taylor, M., Wotherspoon, L., and Cubrinovski, M. (2015). “Development of an Empirical Correlation for Predicting Shear Wave Velocity of Christchurch Soils from Cone Penetration Test Data.” *Soil Dynamics and Earthquake Engineering*, Volume 75, 66-75.

- Mejia, L. H., and E. M. Dawson. (2006). "Earthquake Deconvolution for FLAC." In *FLAC and Numerical Modeling in Geomechanics*. Proceedings of the 4th International FLAC Symposium, Madrid, Spain.
- Menq, F.Y. (2003). "Dynamic Properties of Sandy and Gravelly Soils". Ph.D. Dissertation, University of Texas, Austin, TX, USA.
- Montgomery, J. and Boulanger, R.W. (2017). "Effects of spatial variability on liquefaction-induced settlement and lateral spreading." *J. Geotech. Geoenviron. Eng.*, 10.1061/(ASCE)GT.1943-5606.0001584
- NAVFAC (1986). DM-7.02, Foundations and Earth Structures. Alexandria, VA: U.S. Department of Navy, Naval Facilities Engineering Command.
- New Zealand Geotechnical Database (2016). Funded by the Ministry of Business, Innovation and Employment and the Earthquake Commission, New Zealand. <
<https://www.nzgd.org.nz>> (Aug. 08, 2016)
- Olson, S.M. and Stark, T. D. (2002). Liquefied strength ratio from liquefaction flow failure case histories. *Canadian Geotechnical Journal*, Vol. 39: 629-647.
- PCR (2013) Seismic Structural Analysis – Christchurch [...], Paul C. Rizzo Associates, Inc. report Revision 0, 08-Jul-2013.
- Popescu, R. and Prevost, J.H. (1993a). "Centrifuge Validation of a Numerical Model for Dynamic Soil Liquefaction". *Soil Dynamics and Earthquake Engineering* 12 (1993) 73-90.
- Popescu and Prevost (1993b). "Numerical class A predictions for Model Nos. 1, 2, 3, 4a, 4b, 6, 7, 11 & 12." *Proceedings of the International Conference on Verification of Numerical Procedures for the Analysis of Soil Liquefaction Problems*, Davis, Ca, 17-20 October, 1994, 2: 1105-1207.
- Popescu, R., Prevost, J.H., Deodatis, G. (1997). "Effects of Spatial Variability on Soil Liquefaction: Some Design Recommendations." *Geotechnique* 47, No. 5, 1019-1036.
- Popescu, R., Prevost, J.H., Deodatis, G. (2005). "3D effects in Seismic Liquefaction of Stochastically Variable Soil Deposits." *Geotechnique* 55, No. 1, 21-31.
- Popescu, R., Prevost, J.H., Deodatis, G., and Chakraborty, P. (2006). "Dynamics of Nonlinear Porous Media with Applications to Soil Liquefaction." *Soil Dynamics and Earthquake Engineering*, 26, 648-655.
- Robertson, P.K., and Wride, C.E. (1998). "Evaluating Cyclic Liquefaction Potential using the Cone Penetration Test." *Canadian Geotechnical Journal*, Ottawa, 35(3), 442-459.
- Robertson, P.K. (2010). "Soil behavior type from the CPT: an update." 2nd International Symposium on Cone Penetration Testing, CPT'10, Huntington Beach, CA, USA.
- Robertson P.K. (2012). Interpretation of In-situ Tests – some insights. Kames K. Mitchell Lecture, Proc. 4th International Conference on Geotechnical and Geophysical Site Characterization (ISC'4), Porto de Galinhas, Pernambuco – Brazil, September 18-21, 2012.
- Robertson, P.K., and Kabal, K.L. (2015). "Guide to Cone Penetration Testing for Geotechnical Engineering, 6th Edition." Gregg Drilling & Testing, Inc.
- Robinson, K., Cubrinovski, M., Bradley, B.A. (2013). "Sensitivity of Predicted Liquefaction-Induced Lateral Displacements from the 2010 Darfield and 2011 Christchurch Earthquakes" Proc. 2013 New Zealand Society of Earthquake Engineering Conference, (NZSEE 2013), 26-28 April, Wellington, New Zealand.
- Rollins, K. and Seed, H.B. (1990). "Influence of Buildings on Potential Liquefaction Damage". *Journal of Geotechnical and Geoenvironmental Engineering*, 116(2), 165-185.

- Russell, J. and van Ballegooy, S. (2015). "Canterbury Earthquake Sequence: Increased Liquefaction Vulnerability Assessment Methodology". Technical Report prepared by Tonkin + Taylor, Ltd. for Chapman Tripp acting on behalf of the NZ Earthquake Commission.
- Schmertmann, J.H., Hartmann, J.P. and Brown, P.R. (1978). "Improved Strain Influence Factor Diagrams". ASCE Journal of the Geotechnical Engineering Division, 104 (GT8), 1131-1135.
- Seed, H.B. (1979). "Soil Liquefaction and Cyclic Mobility Evaluation for Level Ground during Earthquakes." Journal of the Geotechnical Engineering Division, 105(GT2), 201-255.
- Silva, W. J., (1988). "Soil response to earthquake ground motion", EPRI Report NP-5747, Electric Power Research Institute, Palo Alto, California.
- Shakir, H. and Pak, A. (2010). "Estimating Liquefaction-Induced Settlement of Shallow Foundations by Numerical Approach." Computer and Geotechnics, 37(3), 267-279.
- Taylor, M. (2015). "The Geotechnical Characterization of Christchurch Sands for Advanced Soil Modelling." Ph.D. Dissertation, University of Canterbury, New Zealand.
- Tokimatsu, K., and Seed, H.B. (1987). "Evaluation of Settlement in Sands Due to Earthquake Shaking." Journal of Geotechnical Engineering, 113, 861-878.
- Tonkin & Taylor Limited. (2013) "Christchurch Town Hall for Performing Arts Post Earthquake and Foundation Repair Assessment." Technical report prepared for the Christchurch City Council, June 2013.
- Tonkin & Taylor, Limited (2015) "Evaluation of Building Settlements during the Canterbury Earthquake Sequence using LiDAR". Job # 53841, November.
- Travasarou, T., Bray, J.D., and Sancio, R.B. (2006). "Soil-structure-interaction analyses of building responses during the 1999 Kocaeli earthquake." Proc. 8th U.S. National Conf. Earthquake Eng., April 18-22, EERI, Oakland, California, USA.
- Unutmaz, B., Cetin, K.O. (2012). "Post-cyclic settlement and tilting potential of mat foundations". Soil Dynamics and Earthquake Engineering 43 (2012) 271-286.
- van Ballegooy, S., Malan, P., Lacrosse, V., Jacka, M.E., Cubrinovski, M., Bray, J.D., O'Rourke, T.D., Crawford, S.A., and Cowan, H. (2014). "Assessment of Liquefaction-Induced Land Damage for Residential Christchurch." Earthquake Spectra Journal, Earthquake Engineering Research Institute, 30(S1), 31-55.
- Whitman and Lambe (1982). "Liquefaction: Consequences for a Structure". Soil Dynamics and Earthquake Engineering Conference, Southampton, 1982.
- Yoshimi, Y. and Tokimatsu, K. (1977). "Settlement of Buildings of Saturated Sand during Earthquakes". Soil and Foundations, 17(1): 23-38.
- Zhang, G., Robertson, P.K. and Brachman, R.W.I. (2002). "Estimating Liquefaction Induced Ground Settlements from CPT for Level Ground." Canadian Geotechnical Journal, Ottawa, 39(5):1168-1180.
- Ziotopoulou, K., and Boulanger, R. W. (2013). "Numerical Modeling Issues in Predicting Post-Liquefaction Reconsolidation Strains and Settlements." Proc. 10th International Conference on Urban Geotechnical Engineering (CUEE), March 1-2, Tokyo, Japan.
- Zupan, J.D., Trombetta, N.W., Puangnak, H., Paez, D., Bray, J.D., Kutter, B.L., Hutchinson, T.C., Fiegel, G.L., Bolisetti, C., Whittaker, A.S. (2013). "Seismic performance assessment in dense urban environments: Centrifuge Data Report for Test-5". Univ. of Calif., Davis, CA.
- Zupan, J. (2014). "Seismic Performance of Buildings Subjected to Soil Liquefaction." Ph.D. dissertation, University of California, Berkeley, Berkeley, CA.

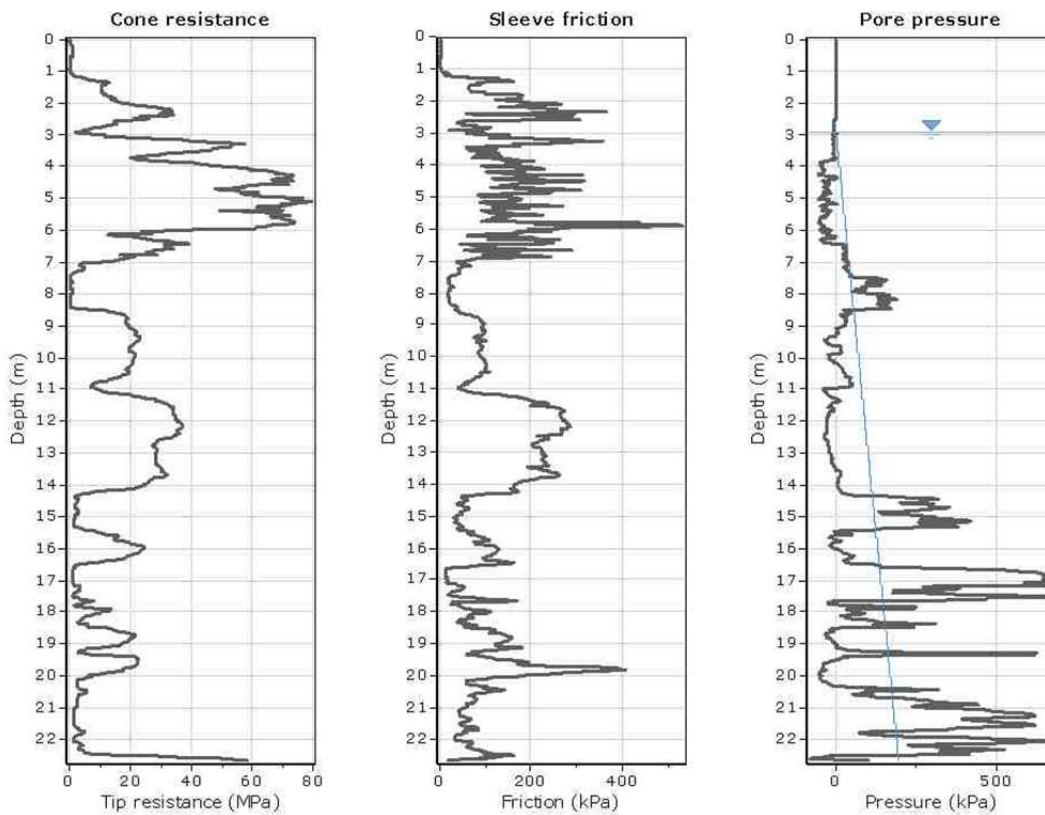
Appendix A - Building “C”: Supporting information

Appendix A.1 - Building “C”: Subsurface Characterization Data

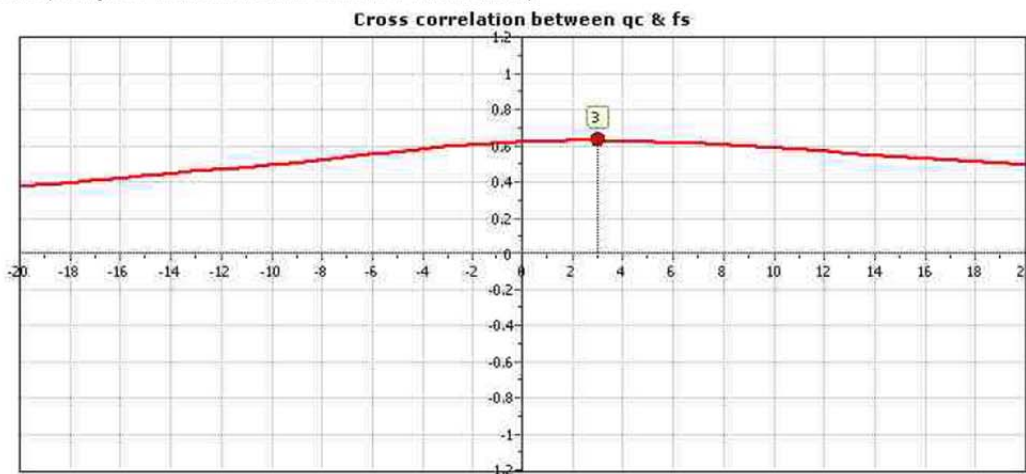
Roberto Luque
 University of California, Berkeley
 435 Davis Hall
 Berkeley, CA, 94720

Project: CBuilding
Location: Christchurch, NZ

CPT: CPT-R5
 Total depth: 22.66 m



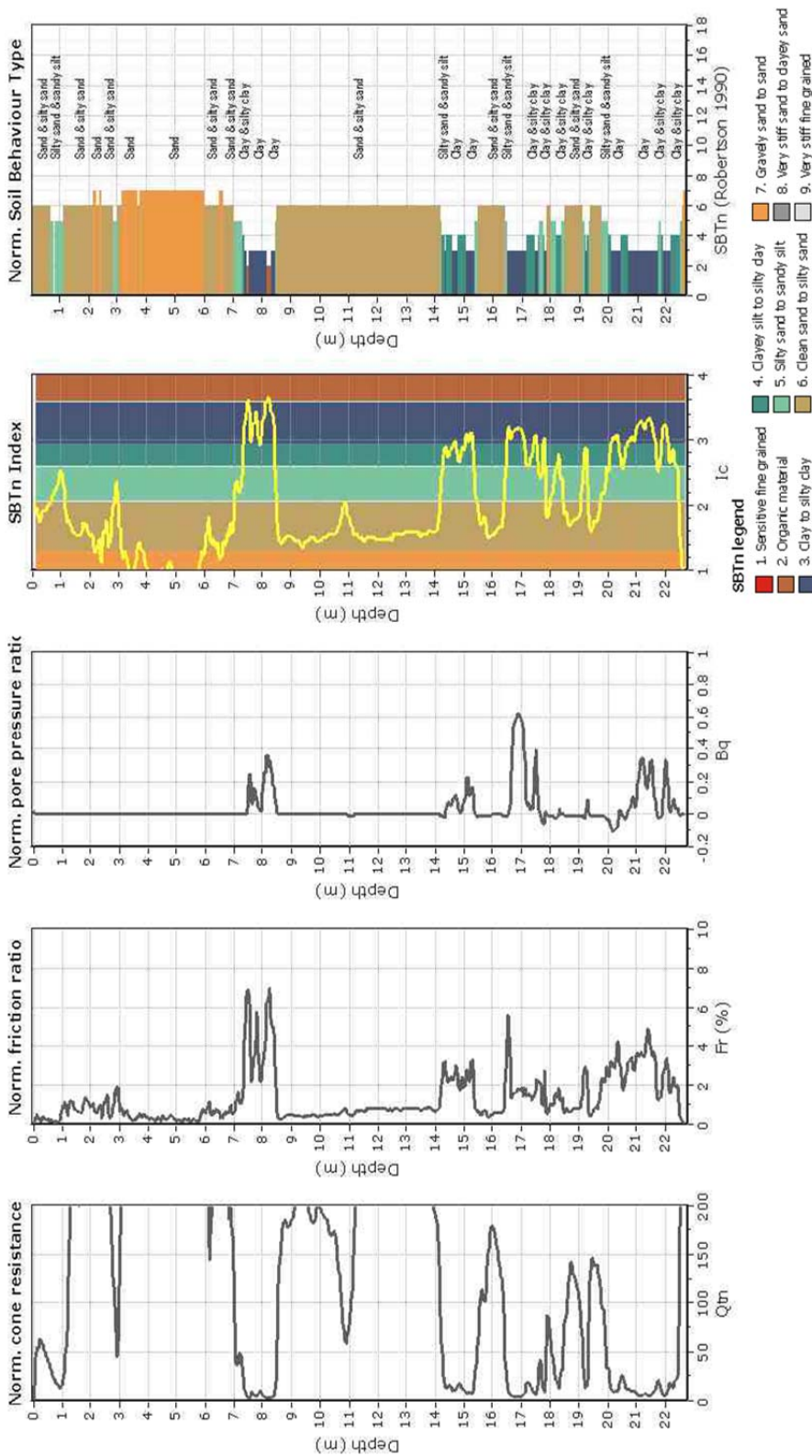
The plot below presents the cross correlation coefficient between the raw q_c and f_s values (as measured on the field). X axes presents the lag distance (one lag is the distance between two successive CPT measurements).



Roberto Luque
 University of California, Berkeley
 435 Davis Hall
 Berkeley, CA, 94720

Project: C Building
 Location: Christchurch, NZ

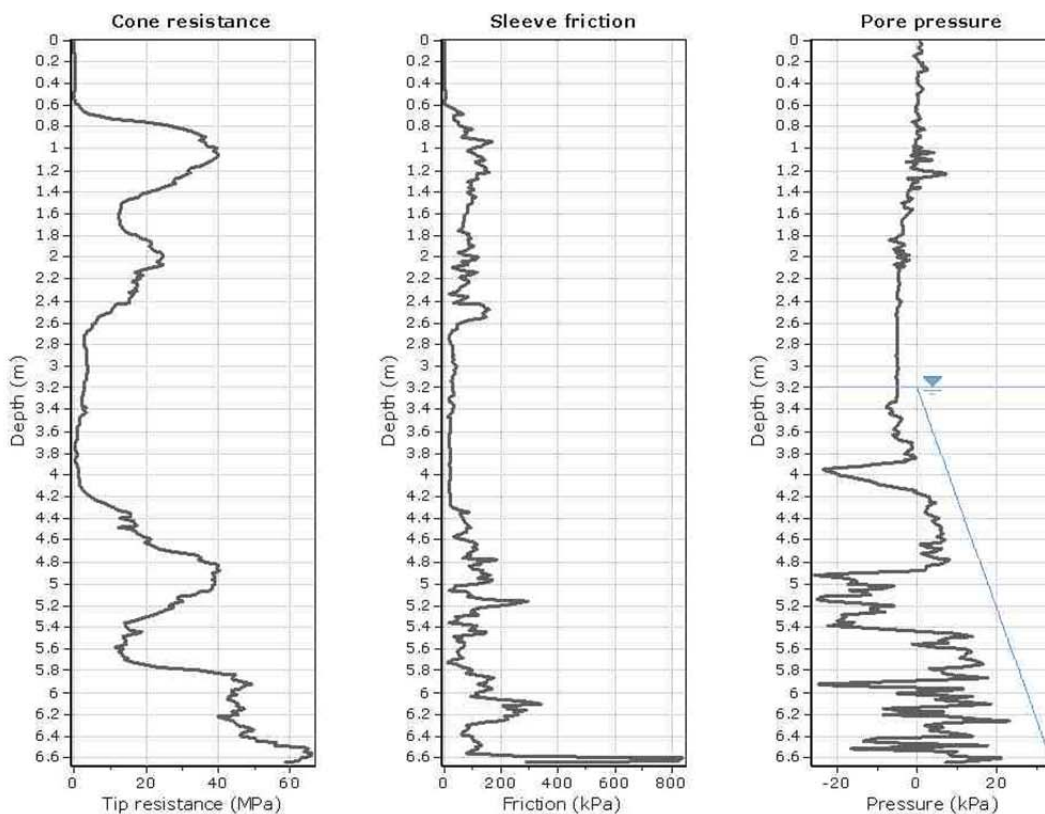
CPT: CPT-R5
 Total depth: 22.66 m



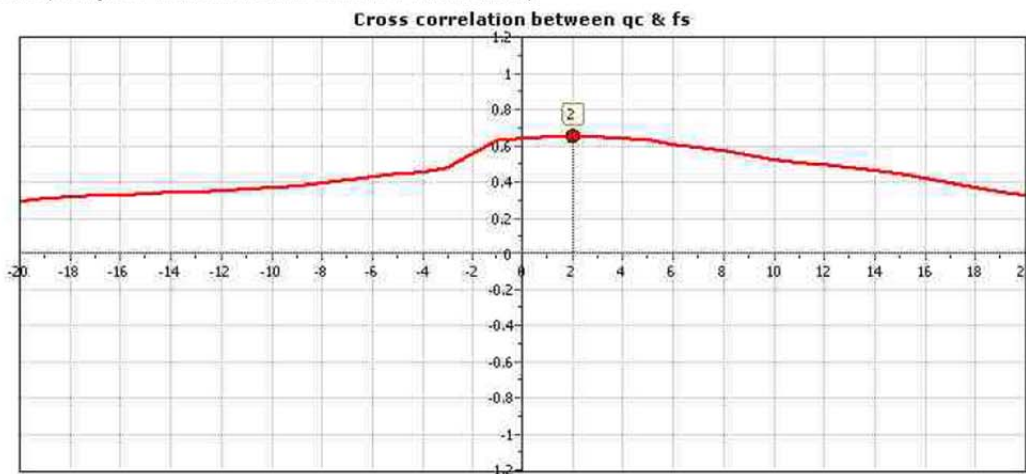
Roberto Luque
 University of California, Berkeley
 435 Davis Hall
 Berkeley, CA, 94720

Project: CBuilding
 Location: Christchurch, NZ

CPT: CPT-R6
 Total depth: 6.64 m



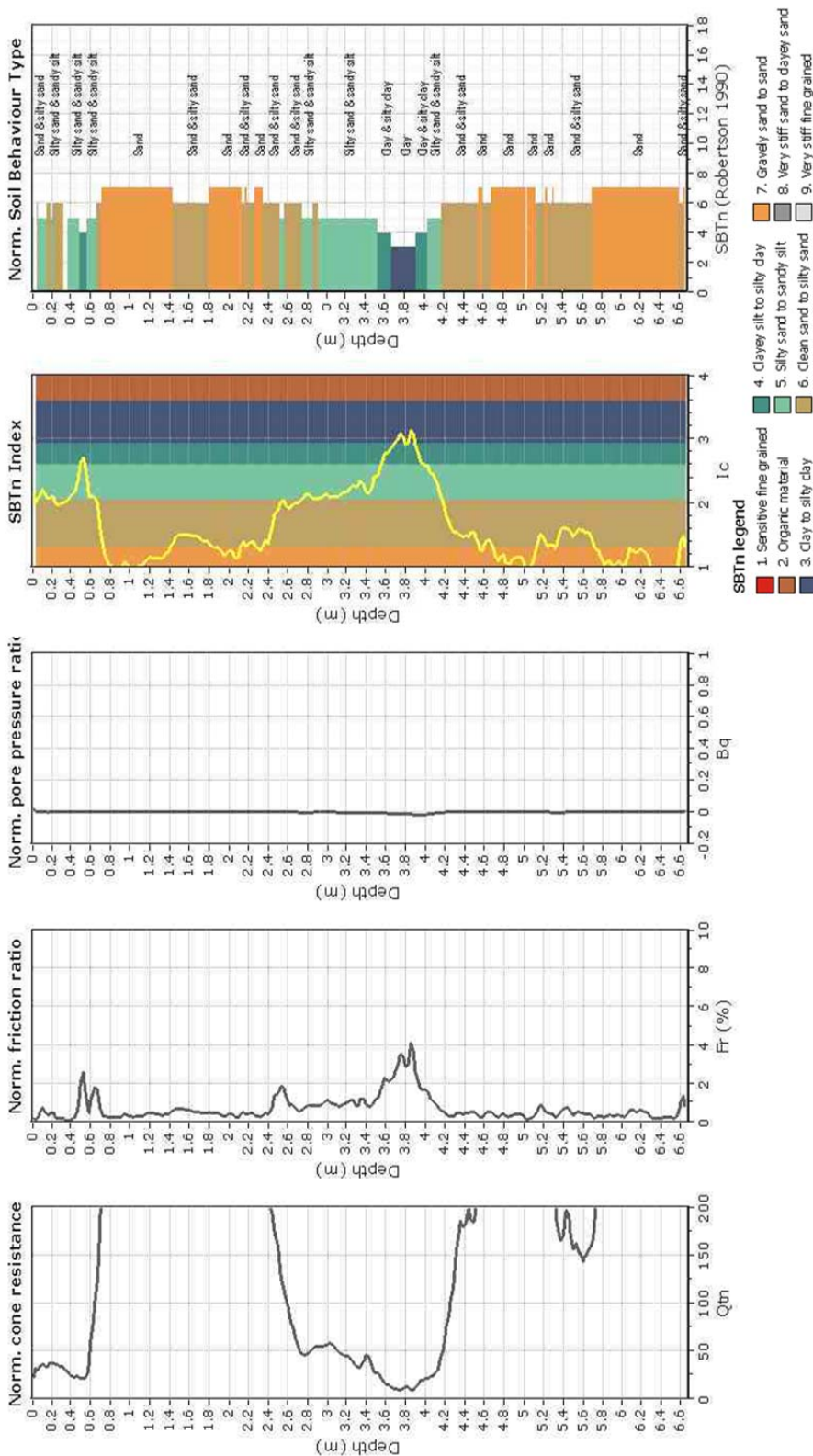
The plot below presents the cross correlation coefficient between the raw qc and fs values (as measured on the field). X axes presents the lag distance (one lag is the distance between two successive CPT measurements).



Roberto Luque
 University of California, Berkeley
 435 Davis Hall
 Berkeley, CA, 94720

Project: C Building
 Location: Christchurch, NZ

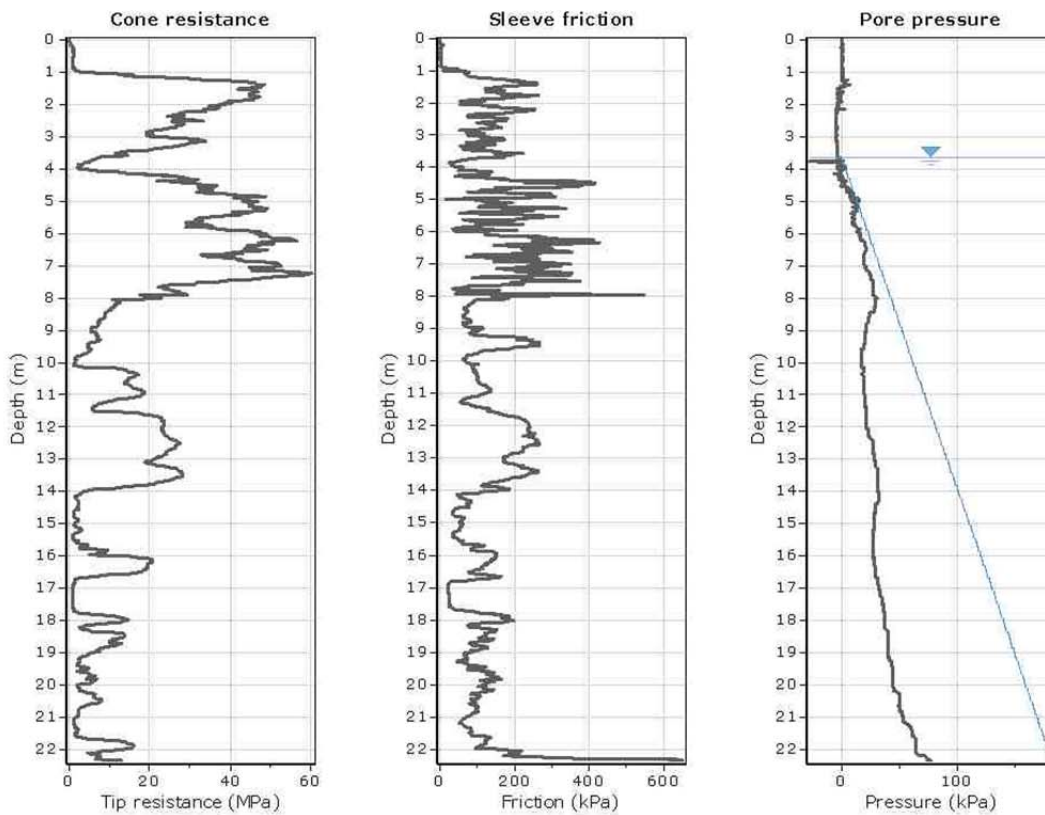
CPT: CPT-R6
 Total depth: 6.64 m



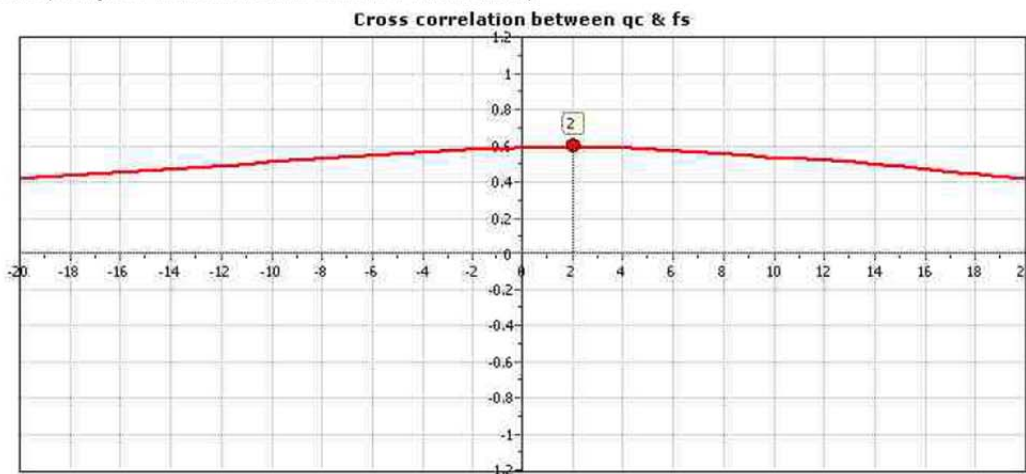
Roberto Luque
 University of California, Berkeley
 435 Davis Hall
 Berkeley, CA, 94720

Project: CBuilding
Location: Christchurch, NZ

CPT: CPT-R7B
 Total depth: 22.34 m



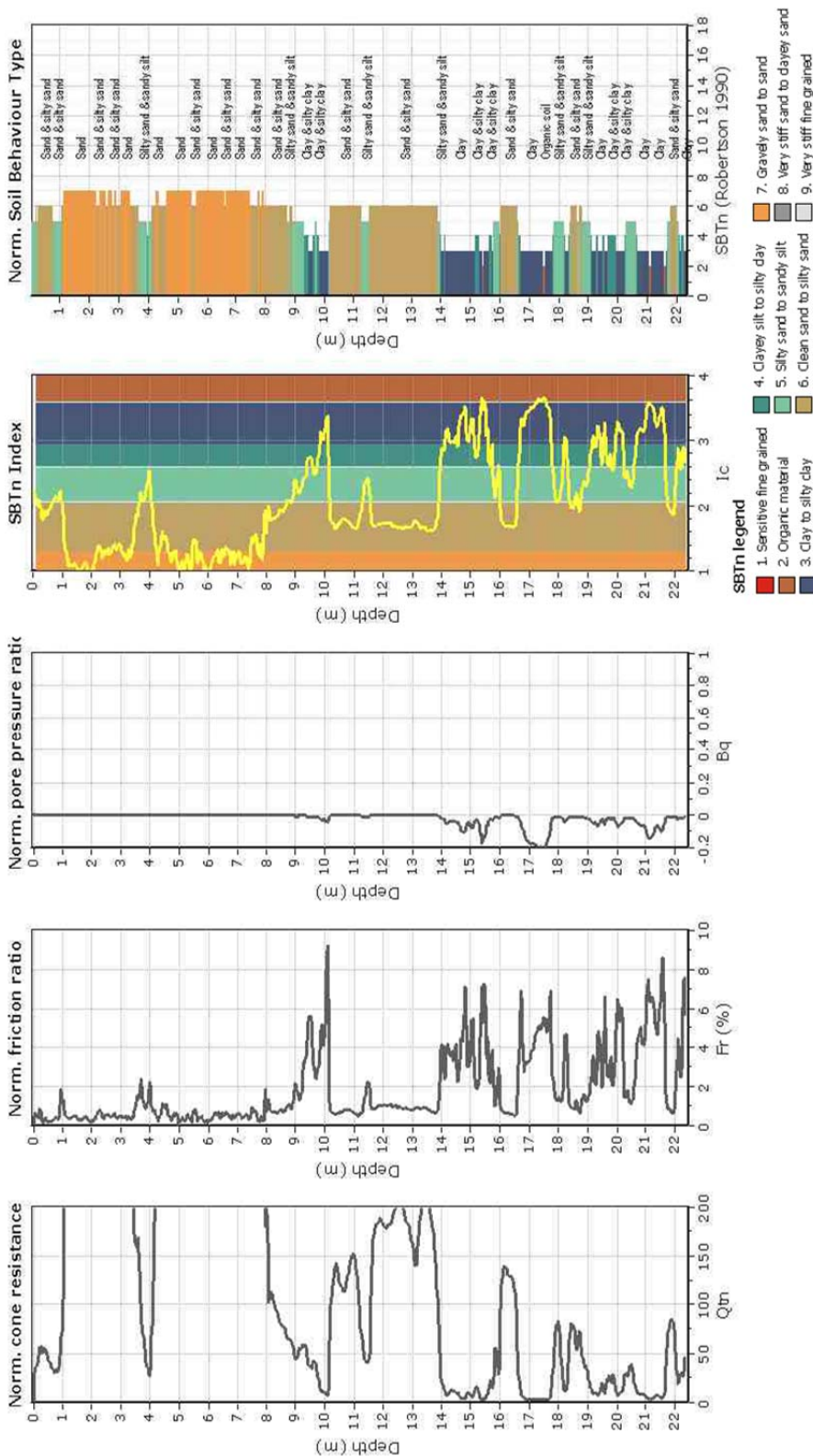
The plot below presents the cross correlation coefficient between the raw q_c and f_s values (as measured on the field). X axes presents the lag distance (one lag is the distance between two successive CPT measurements).



Roberto Luque
 University of California, Berkeley
 435 Davis Hall
 Berkeley, CA, 94720

Project: C Building
 Location: Christchurch, NZ

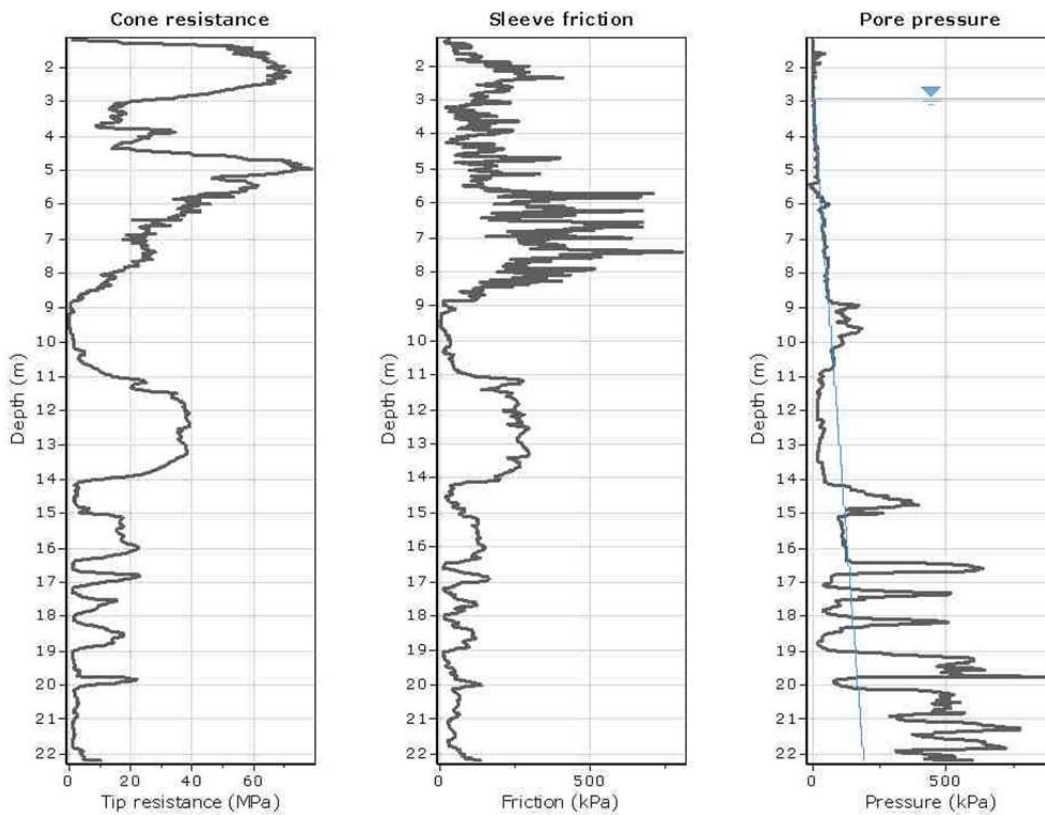
CPT: CPT-R/7B
 Total depth: 22.34 m



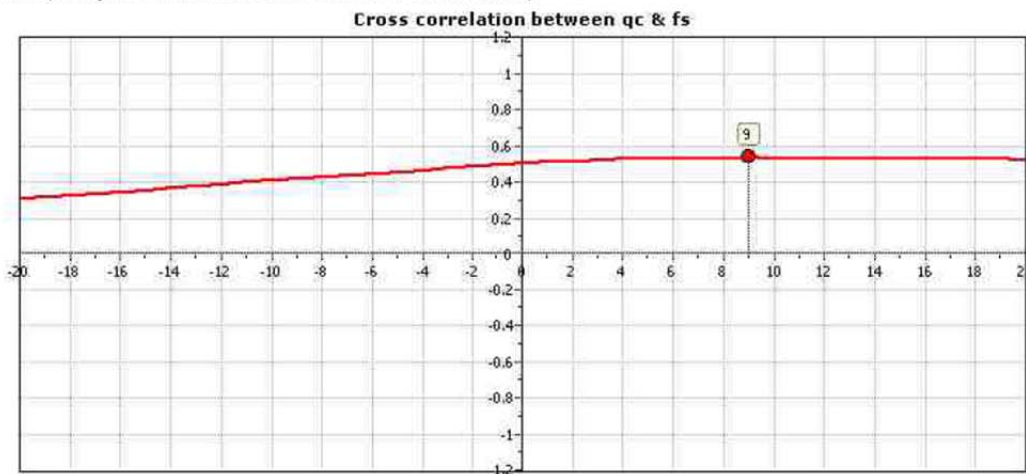
Roberto Luque
 University of California, Berkeley
 435 Davis Hall
 Berkeley, CA, 94720

Project: CBuilding
Location: Christchurch, NZ

CPT: CPT-R2B
 Total depth: 22.20 m



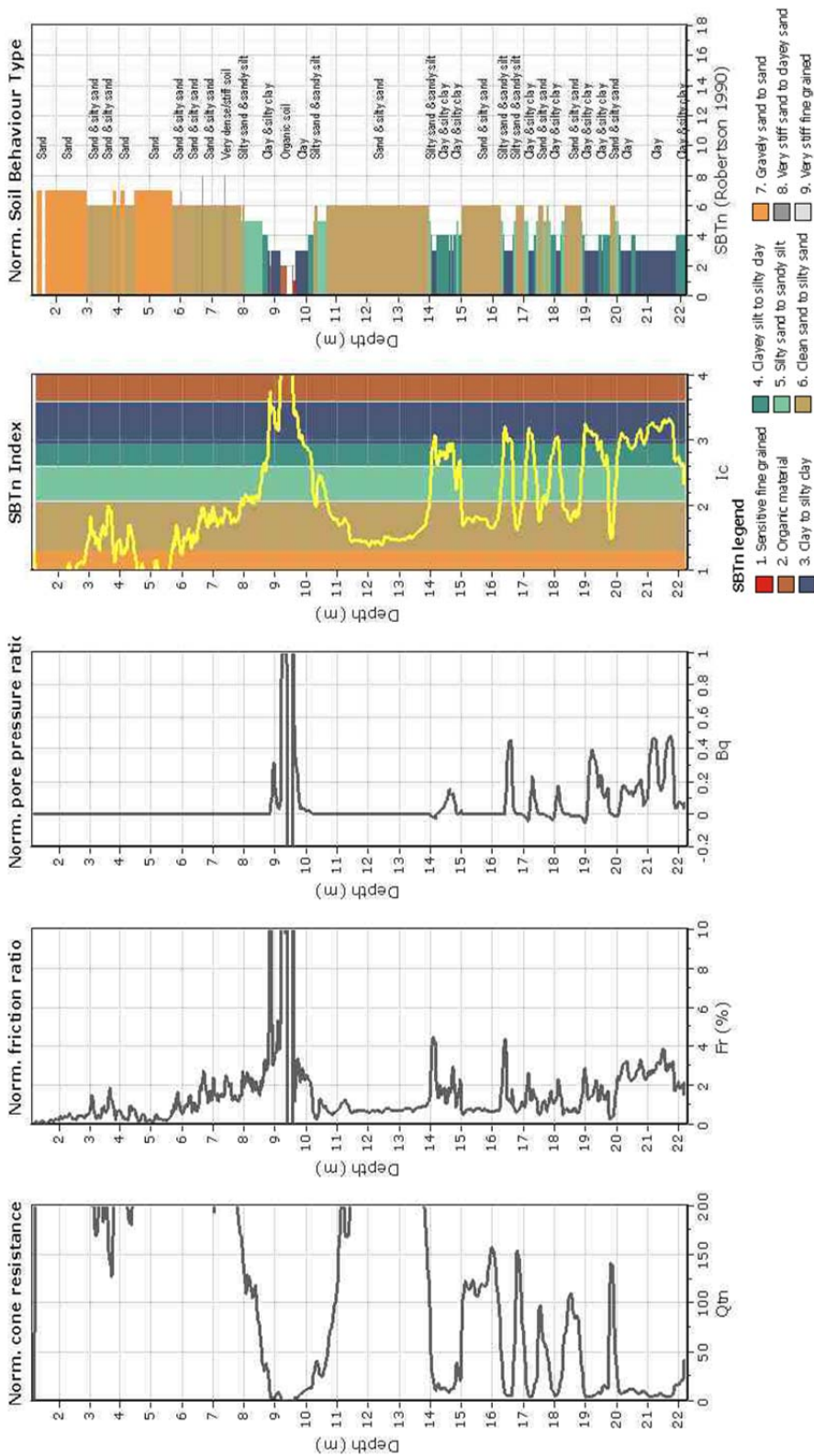
The plot below presents the cross correlation coefficient between the raw q_c and f_s values (as measured on the field). X axes presents the lag distance (one lag is the distance between two successive CPT measurements).



Roberto Luque
 University of California, Berkeley
 435 Davis Hall
 Berkeley, CA, 94720

Project: C Building
 Location: Christchurch, NZ

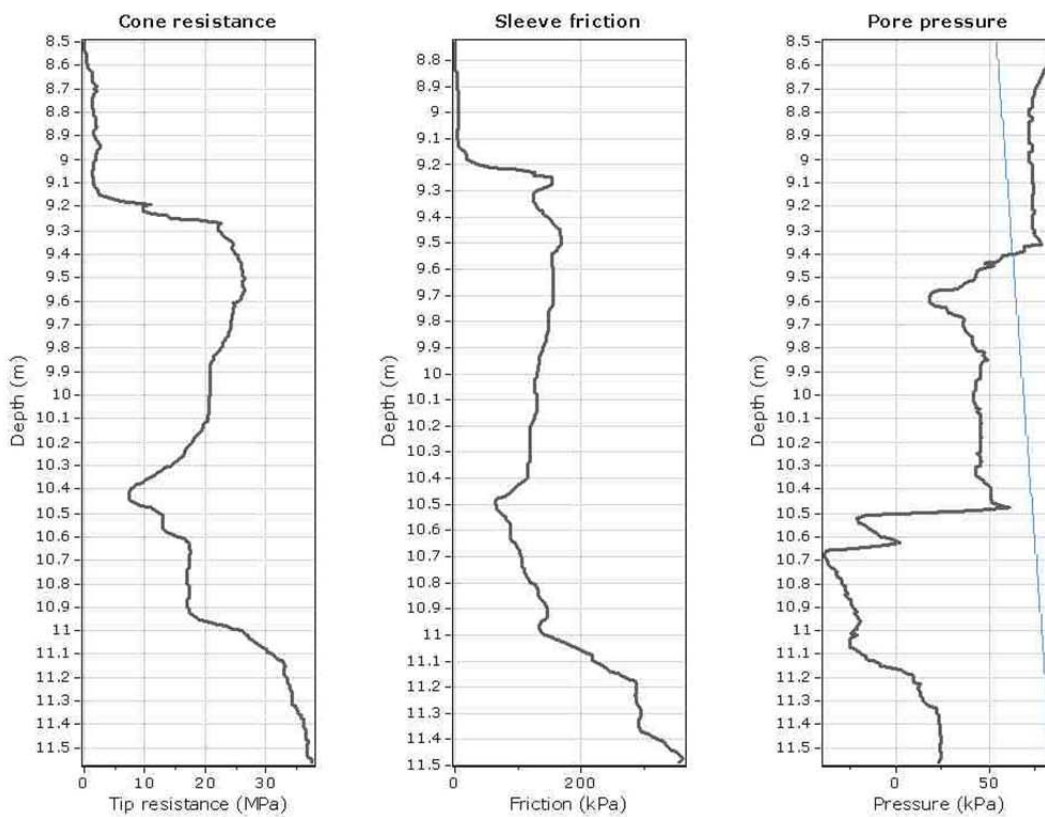
CPT: CPT-R2B
 Total depth: 22.20 m



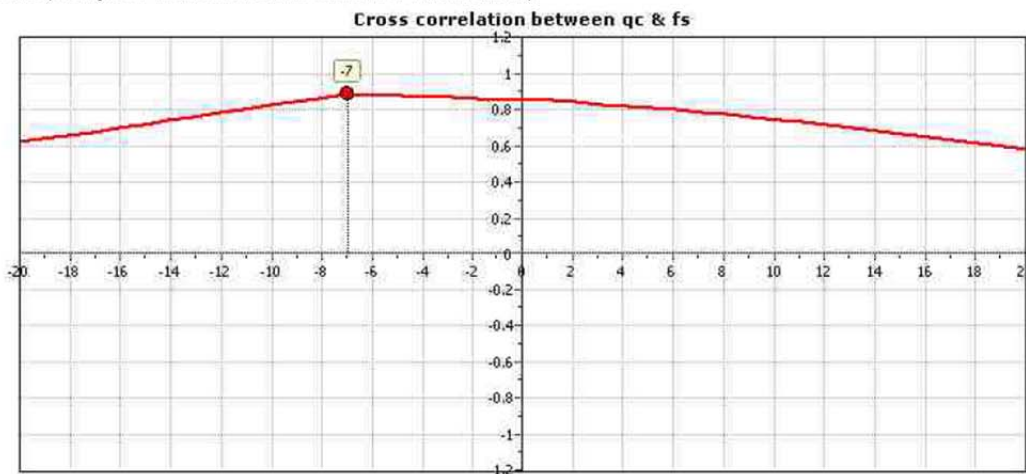
Roberto Luque
 University of California, Berkeley
 435 Davis Hall
 Berkeley, CA, 94720

Project: CBuilding
 Location: Christchurch, NZ

CPT: CPT-01
 Total depth: 11.56 m



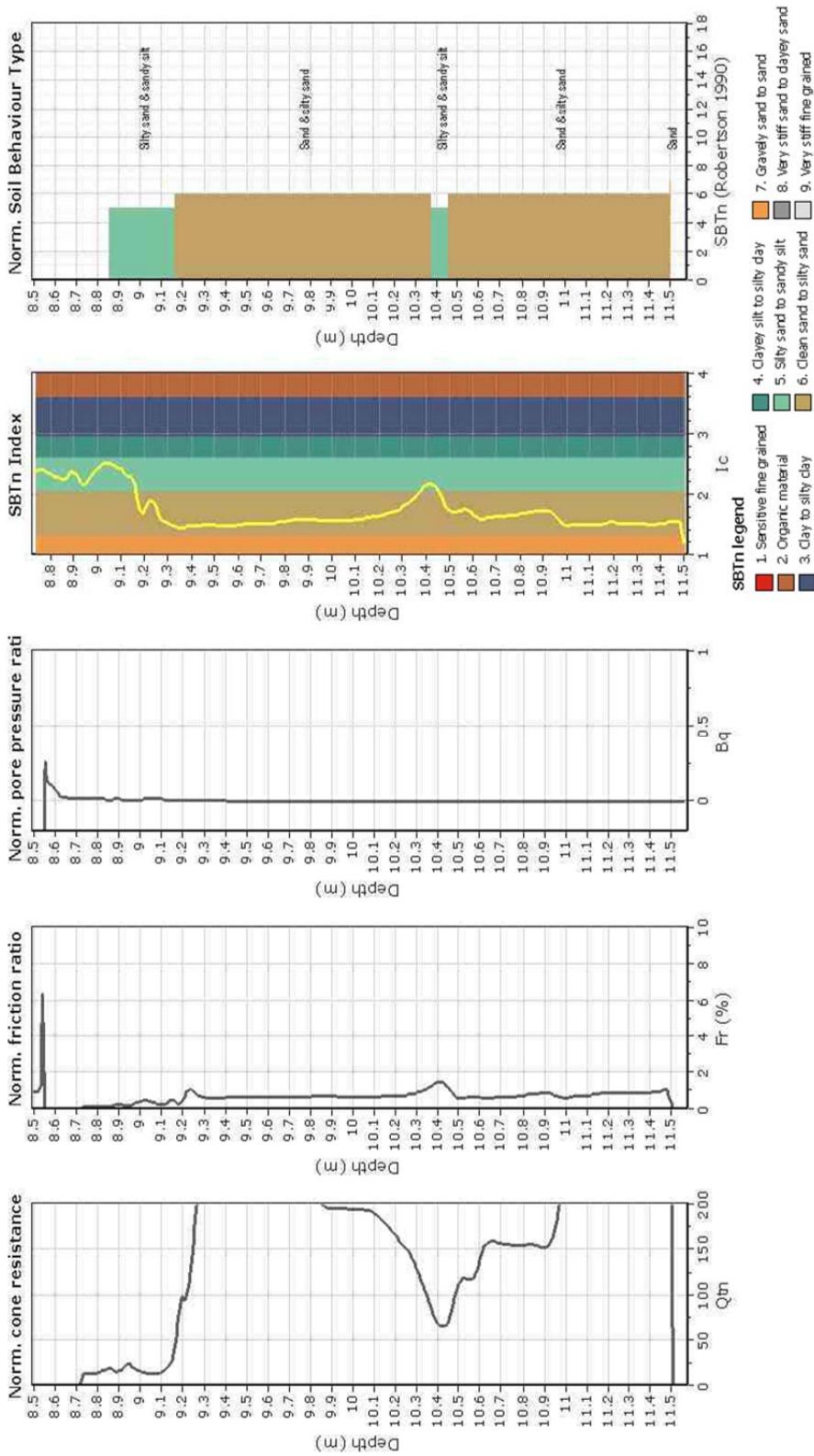
The plot below presents the cross correlation coefficient between the raw qc and fs values (as measured on the field). X axes presents the lag distance (one lag is the distance between two successive CPT measurements).



Roberto Luque
 University of California, Berkeley
 435 Davis Hall
 Berkeley, CA, 94720

Project: C Building
 Location: Christchurch, NZ

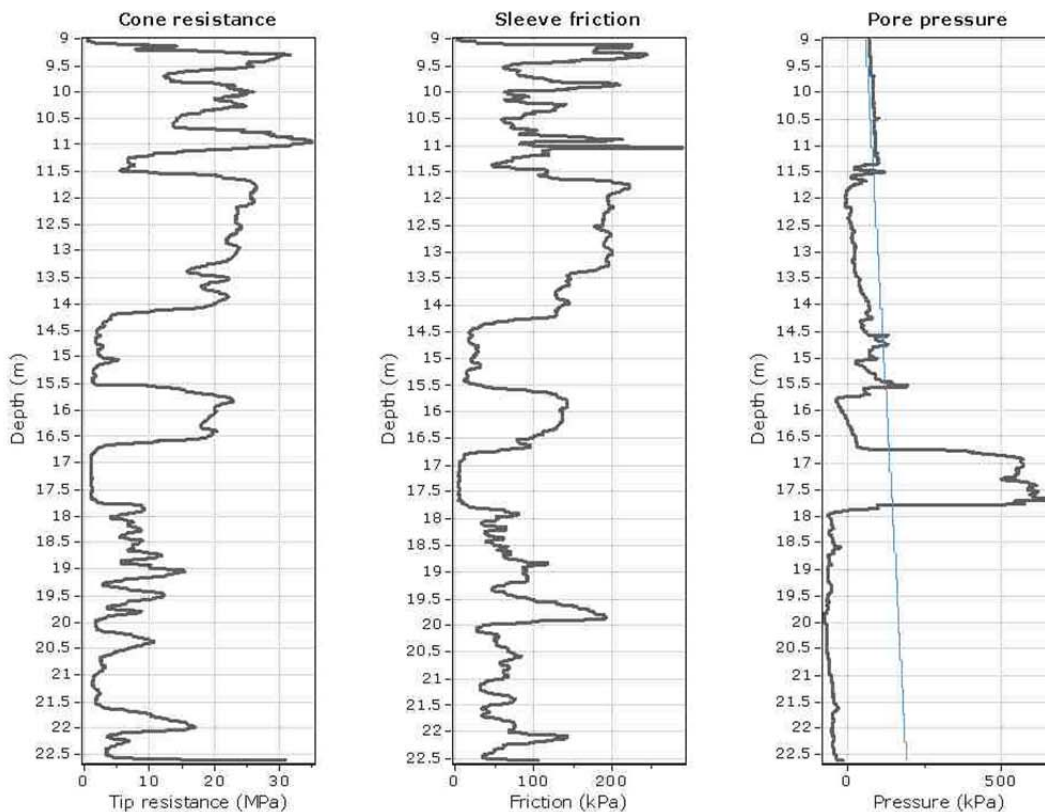
CPT: CPT-01
 Total depth: 11.56 m



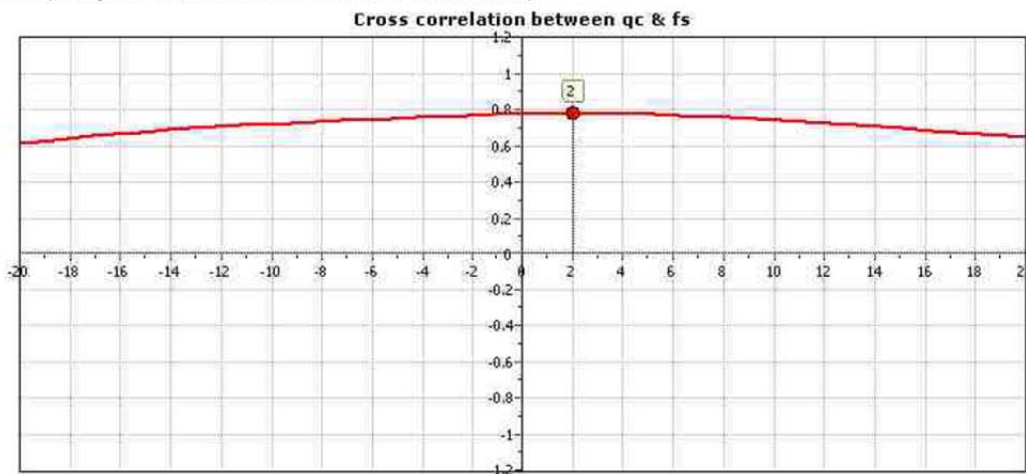
Roberto Luque
 University of California, Berkeley
 435 Davis Hall
 Berkeley, CA, 94720

Project: CBuilding
Location: Christchurch, NZ

CPT: CPT-02
 Total depth: 22.61 m



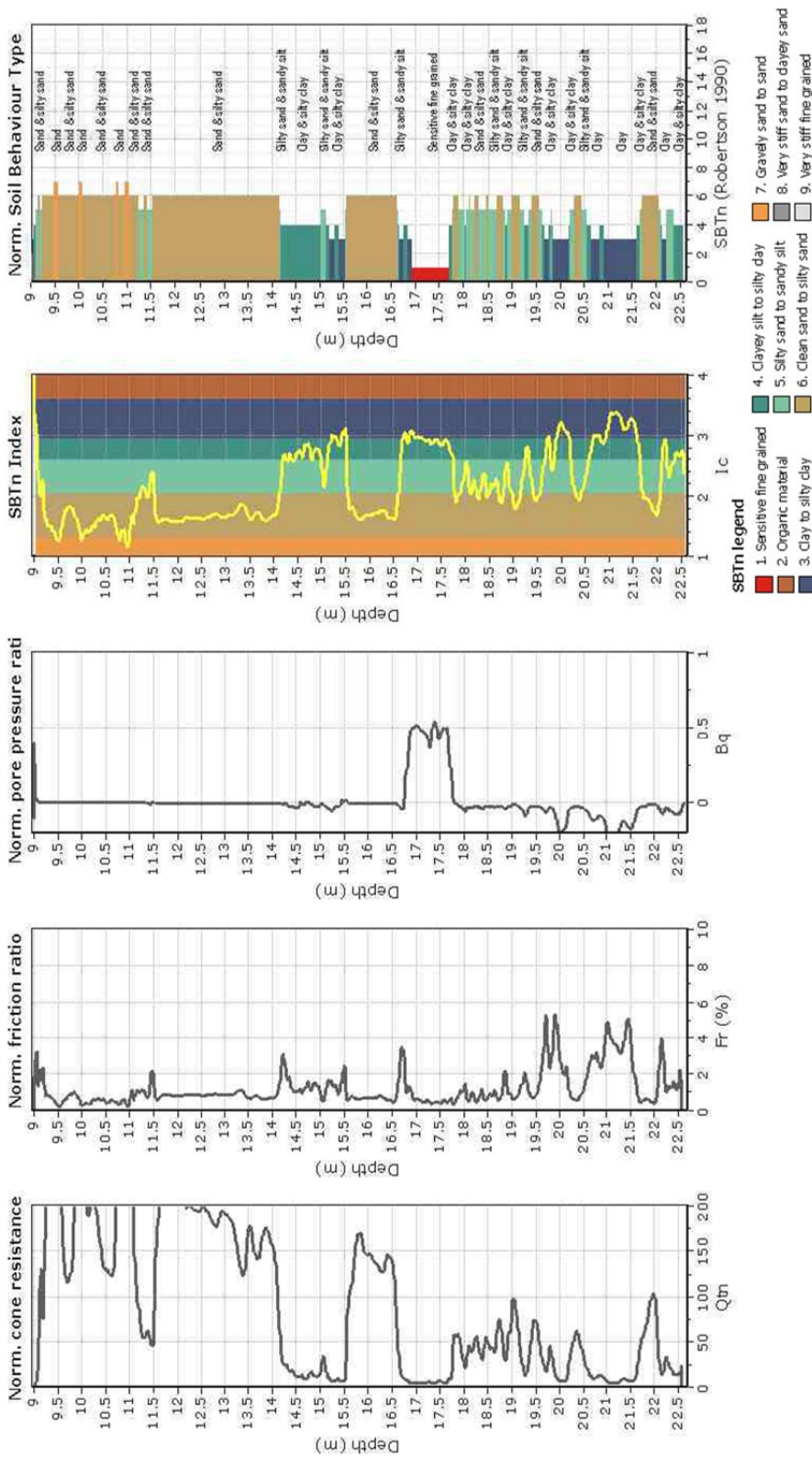
The plot below presents the cross correlation coefficient between the raw qc and fs values (as measured on the field). X axes presents the lag distance (one lag is the distance between two successive CPT measurements).



Roberto Luque
 University of California, Berkeley
 435 Davis Hall
 Berkeley, CA, 94720

Project: C Building
 Location: Christchurch, NZ

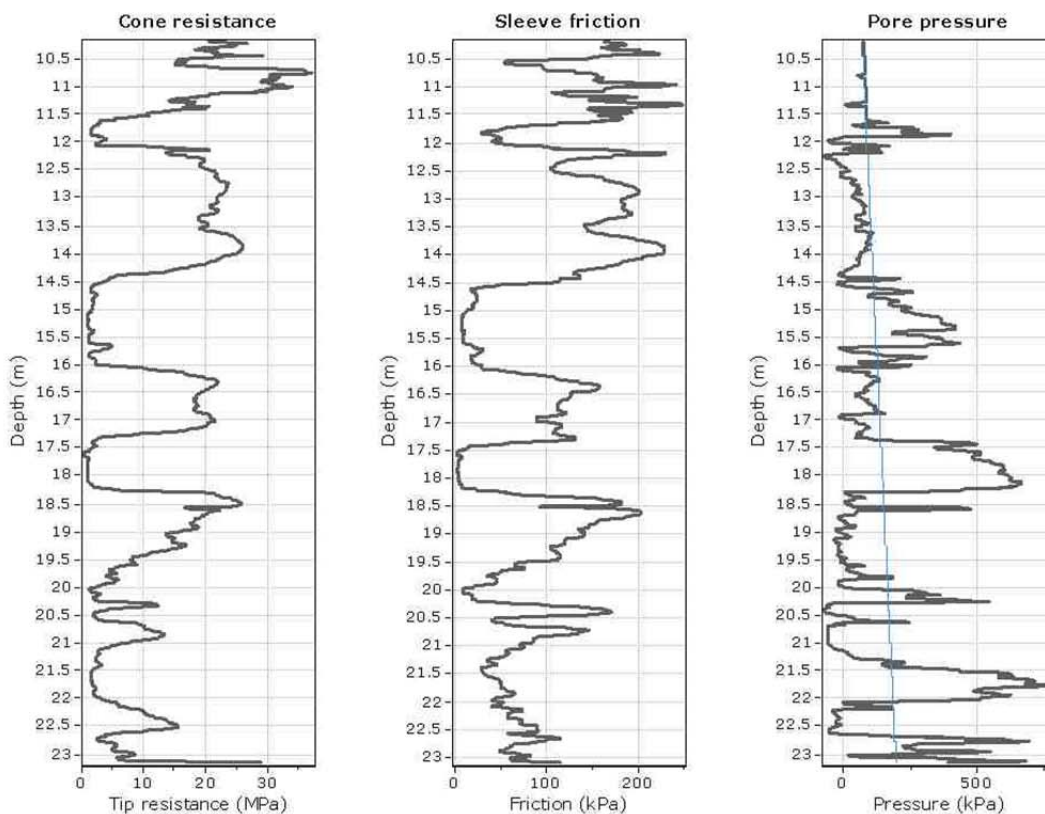
CPT: CPT-02
 Total depth: 22.61 m



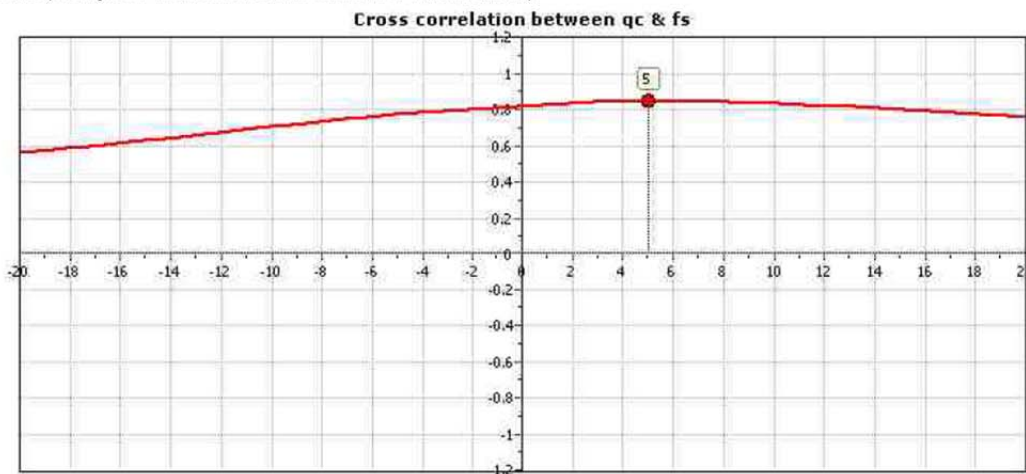
Roberto Luque
 University of California, Berkeley
 435 Davis Hall
 Berkeley, CA, 94720

Project: CBuilding
Location: Christchurch, NZ

CPT: CPT-03
 Total depth: 23.15 m



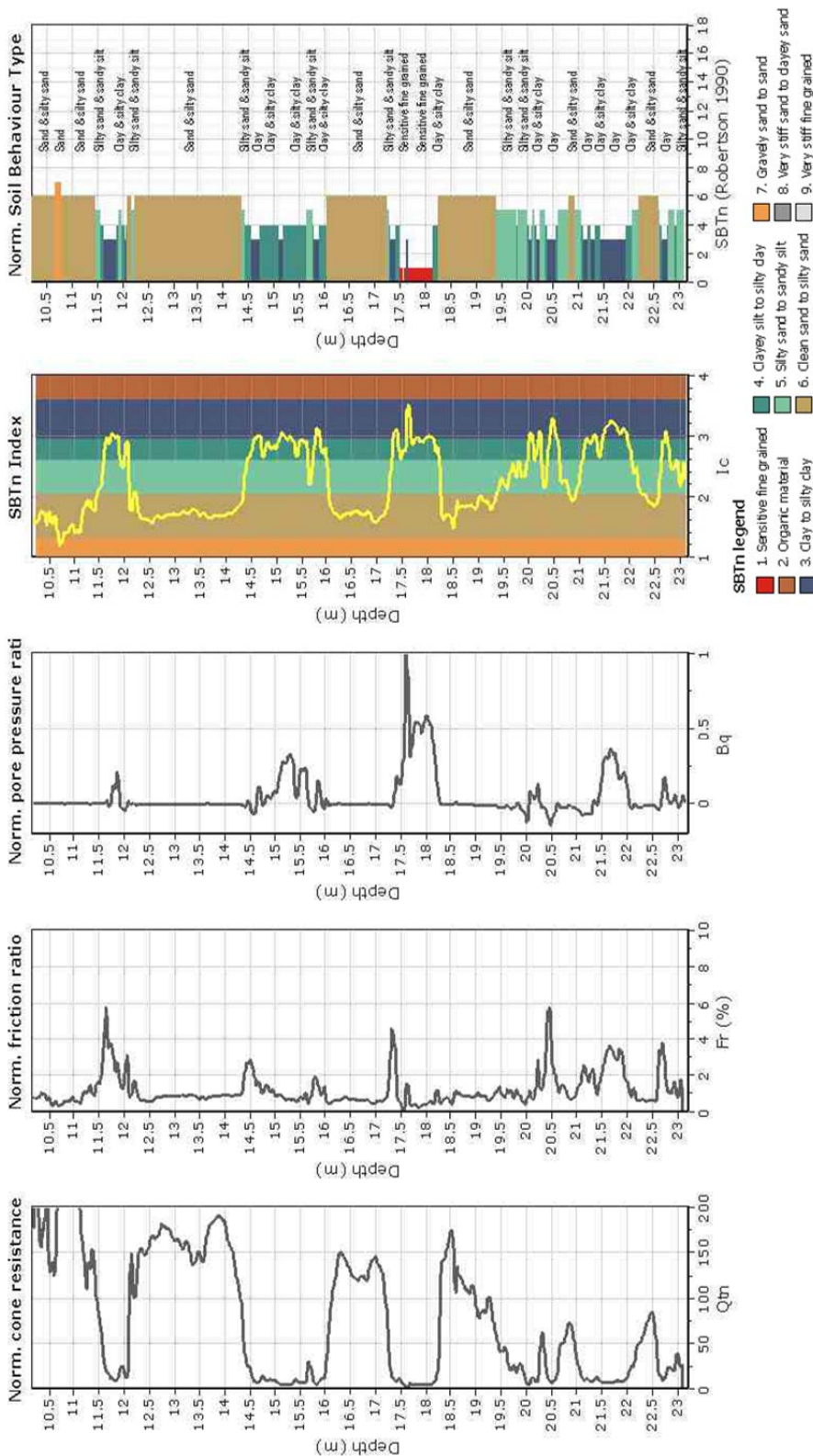
The plot below presents the cross correlation coefficient between the raw qc and fs values (as measured on the field). X axes presents the lag distance (one lag is the distance between two successive CPT measurements).



Roberto Luque
 University of California, Berkeley
 435 Davis Hall
 Berkeley, CA, 94720

Project: C Building
 Location: Christchurch, NZ

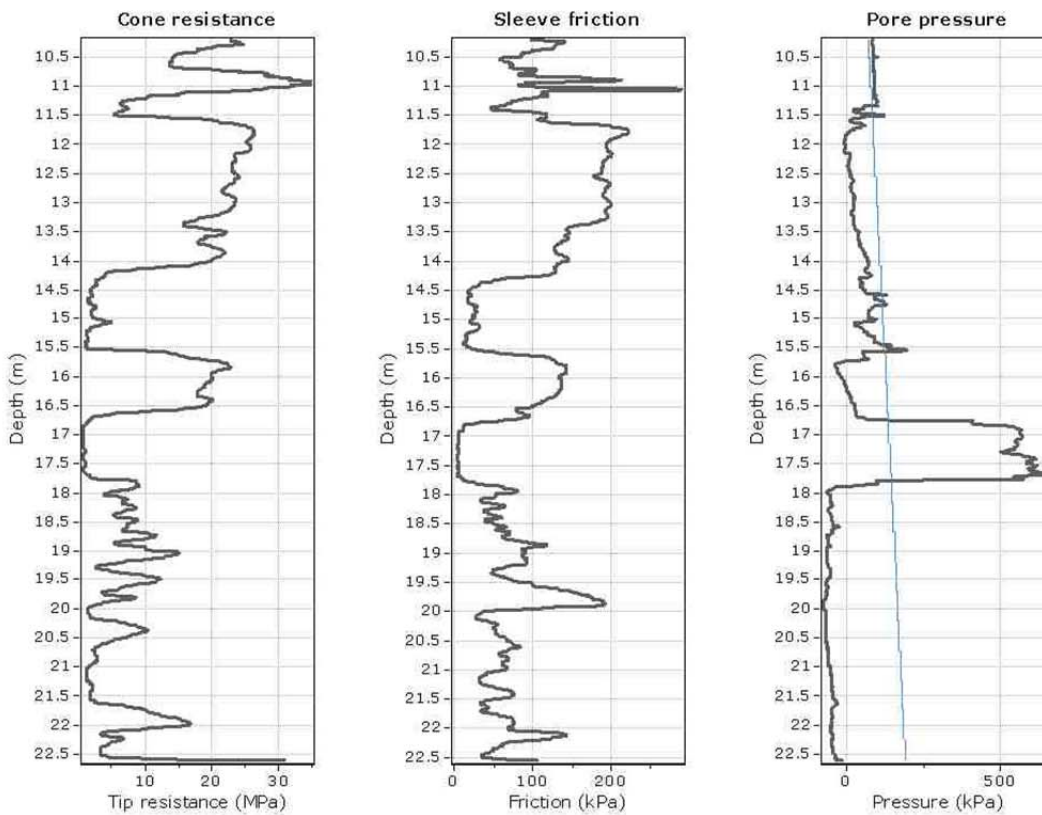
CPT: CPT-03
 Total depth: 23.15 m



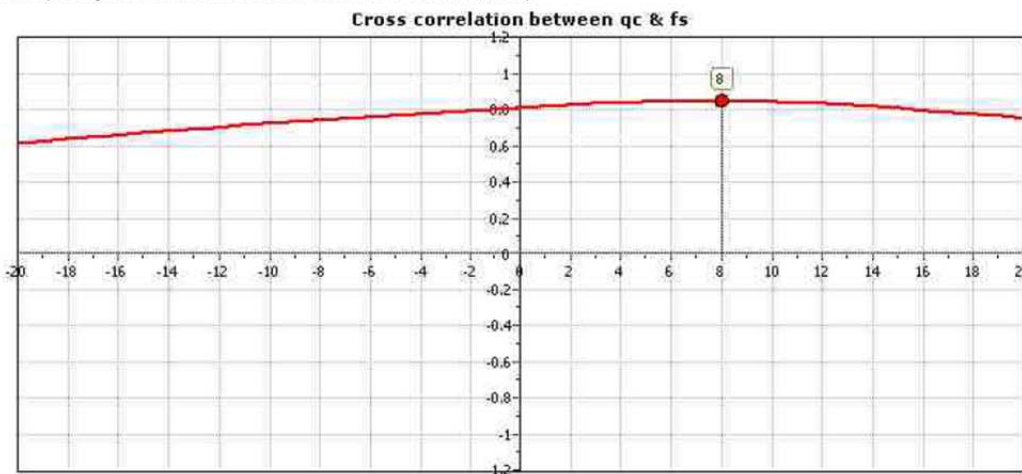
Roberto Luque
 University of California, Berkeley
 435 Davis Hall
 Berkeley, CA, 94720

Project: CBuilding
Location: Christchurch, NZ

CPT: CPT-04
 Total depth: 22.61 m



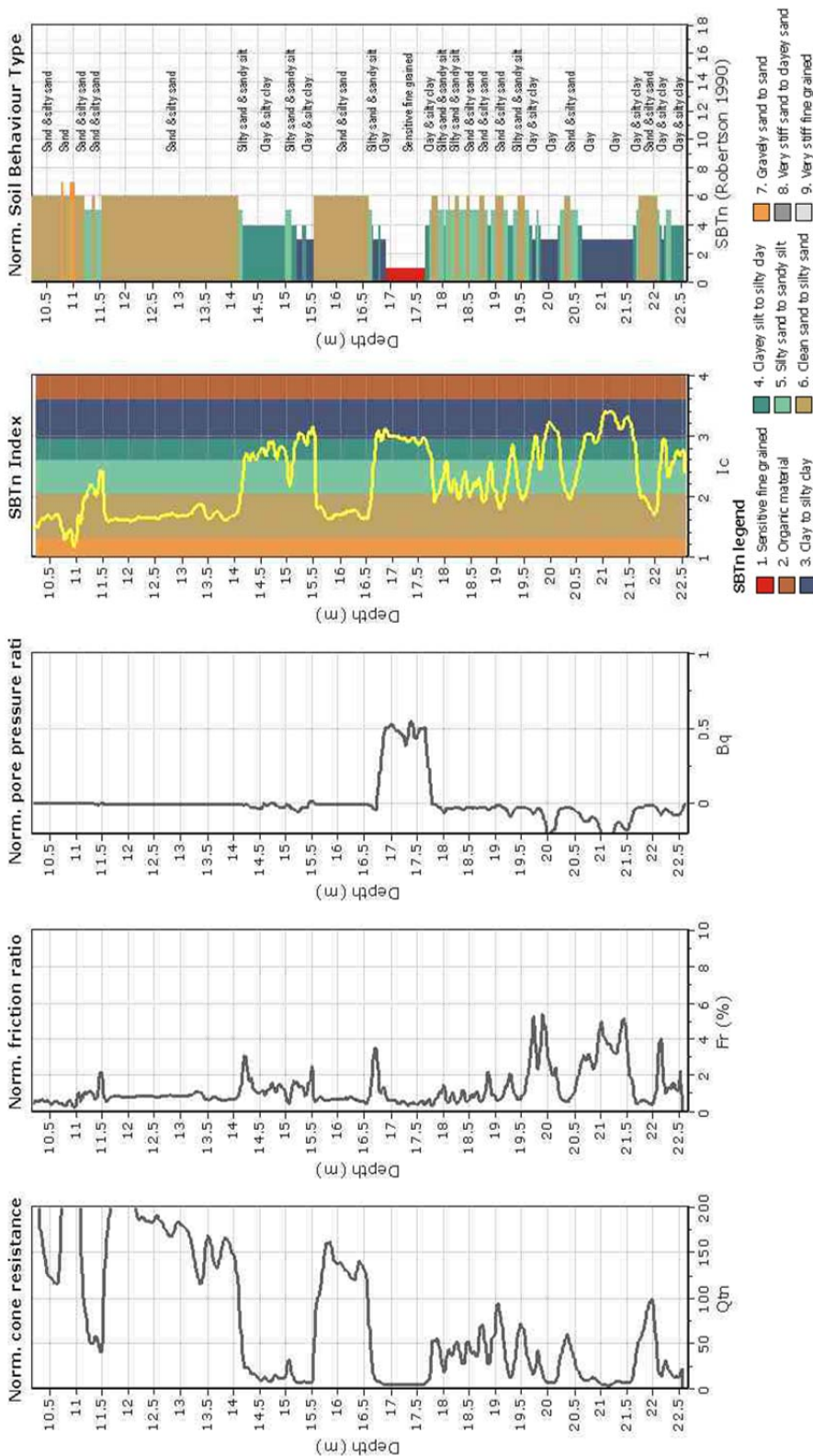
The plot below presents the cross correlation coefficient between the raw qc and fs values (as measured on the field). X axes presents the lag distance (one lag is the distance between two successive CPT measurements).









Roberto Luque
 University of California, Berkeley
 435 Davis Hall
 Berkeley, CA, 94720

Project: C Building
 Location: Christchurch, NZ

CPT: CPT-04
 Total depth: 22.61 m



Location/Position:													
Contractor: Canterbury Drilling			Start date: 30-9-97		Coords:		Diameter: 250 mm		Notes: BH1 M35/7771				
Drill rig: Cable Tool			Finish date: 30-9-97		Datum:		Depth: 25 m						
Driller: Canterbury Drilling			Ground R.L.(m): 15.530				Inclination: Vertical						
R.L./DEPTH SCALE 1: (m)	SOIL TYPE	U.S.C.S.	SOIL DESCRIPTION	GEOLOGIC DESCRIPTION	DATE/DEPTH	DRILL MTH	SAMPLES	% REC	PENETRATION (SPT) (Blows / 300 mm)	PIEZO & STANDPIPE	WATER CONTENT (%)	STRENGTH (kPa)	DEPTH (m)
									0 20 40 60 80		20 40 60 80		
15	SW		ASPHALT. basecourse										
14			Brown grey SAND. -fine to medium sand -moist	N=5									
13	GW		SANDY GRAVEL. -fine to medium sand -fine to medium rounded gravel	N=25									
12				N=27									
11				N=37									
10				N=31									
9			-fine rounded gravel -less sand with depth	N=32									
8				N=30									
7	GW		GRAVEL with minor sand. -fine to medium rounded gravel	N=62									
6				N=47									
5				N=45									
4	GW		SANDY GRAVEL. -fine to coarse rounded gravel -fine to medium sand	N=27									
3	SW		Blue grey SAND. -fine sand	N=27									
2				N=26									
1			-trace of timber material -clear sand	N=26									
0				N=26									
-1	SM		SILTY SAND. -fine to medium sand -trace of white shell material -increased shell material with depth	N=27									
-2				N=22									
-3	SW		Grey SAND. -fine sand -clean sand	N=38									
-4				N=38									
-5	SM		Grey SILTY SAND. -fine sand -trace of white shell material	N=57									
-6				N=57									
-7	MP		Grey SILT with trace of organics. -firm	N=74									
-8	CM		Grey SILTY GRAVEL. -fine to medium rounded gravel	N=74									

Location/Position:											
Contractor: Canterbury Drilling		Start date: 8-9-97		Coords:		Diameter: 250 mm		Notes: BH2 M35/7772			
Drill rig: Cable Tool		Finish date: 8-9-97		Datum:		Depth: 6 m					
Driller: Canterbury Drilling		Ground R.L.(m): 15.000				Inclination: Vertical					
R.L./DEPTH SCALE 1: (m)	GRAPHIC LOG	U.S.C.S.	SOIL DESCRIPTION	GEOLOGIC DESCRIPTION	DATE/DEPTH DRILL MTR	SAMPLES % REC	PENETRATION (SPT) (Blows / 300 mm)	PIEZO & STANDPIPE	WATER CONTENT (%)	STRENGTH (KPa)	DEPTH (m)
15			ASPHALT. -basecourse			0 50	20 40 60 80		20 40 60 80		
14		SW	Brown grey SAND. -fine to medium sand -moist	N=8			▽				1
13		SW	SILT SANDY GRAVEL. -fine to medium sand -fine to medium rounded gravel	N=13	CABLE		▽				2
12			-coarser gravel with depth	N=32	TOOL		▽				3
11				N=31			▽				4
10				N=42			▽				5

SOILS & FOUNDATIONS LTD

Job No:
95234/00

Logged: Cant Drill
Checked: Cant Drill
Date:

FIGURE 95234/00/BH2
BOREHOLE RECORD

Location/Position:										
Contractor: Canterbury Drilling		Start date: 13-9-97		Coords:		Diameter: 250 mm		Notes: BH3 M35/7773		
Drill rig: Cable Tool		Finish date: 18-9-97		Datum:		Depth: 25 m				
Driller: Canterbury Drilling		Ground R.L. (m): 14.340				Inclination: Vertical				
R.L./DEPTH SCALE 1: (m)	GRAPHIC LOG U.S.C.S.	SOIL DESCRIPTION	GEOLOGIC DESCRIPTION	DATE/DEPTH DRILL METERS	SAMPLES % REC	PENETRATION (SPT) (Blows / 300 mm)	PIEZO & STANDPIPE	WATER CONTENT (%)	STRENGTH (kPa)	DEPTH (m)
					0 50	20 40 60 80		20 40 60 80		
14		CONCRETE.								
		BRICK FILL.								
13	SW	Brown SAND. -fine to medium sand	N=14			▽	▽			
	GW	Brown SANDY GRAVEL. -fine to medium sand -fine to medium rounded gravel	N=13			▽				
12		Blue grey SANDY GRAVEL. -fine to medium sand -fine to medium rounded gravel -minor timber material -clean gravels	N=21			▽				
11			N=23			▽				
10			N=41			▽				
9			N=55			▽				
8			N=57			▽				
7			N=31			▽				
6			N=16			▽				
5	GW	GRAVEL with minor sand. -fine to medium rounded gravel	N=28			▽				
10	MP	Dark grey SILT with minor organic material. -some tree material with depth -minor sand with depth	N=59			▽				
11			N=44			▽				
12	SW	Grey SAND. -fine to medium sand -saturated	N=37			▽				
13		-trace of white shell material	N=22			▽				
14			N=33			▽				
15			N=73			▽				
16		-trace of white shell material	N=59			▽				
17			N=30			▽				
18			N=23			▽				
19	ML	Grey SILT with minor sand. -fine sand -firm -less sand with depth	N=66			▽				
20						▽				
21						▽				
22						▽				
23	GP	GRAVEL. -fine to medium rounded gravel				▽				
24						▽				
25						▽				

SOILS & FOUNDATIONS LTD

Job No:
95234/00

Logged: Cant Drill
Checked: G.Clark
Date:

FIGURE 95234/00/BH13
BOREHOLE RECORD

Location/Position:															
Contractor: Canterbury Drilling		Start date: 12-9-97		Coords:		Diameter: 250 mm		Notes: BH4 M35/7770							
Drill rig: Cable Tool		Finish date: 12-9-97		Datum:		Depth: 6 m									
Driller: Canterbury Drilling		Ground R.L.(m): 15.690				Inclination: Vertical									
R.L./DEPTH SCALE 1: (m)	GRAPHIC LOG U.S.C.S.	SOIL DESCRIPTION	GEOLOGIC DESCRIPTION	DATE/DEPTH DRILL MTH	SAMPLES % REC	PENETRATION (SPT) (Blows / 300 mm)				PIEZO & STANDPIPE	WATER CONTENT (%)			STRENGTH (KPa)	DEPTH (m)
						20	40	60	80		20	40	60	80	
15		CONCRETE SLAB. -reinforced													
		SANDY GRAVEL FILL. -fine to medium sand -fine to medium rounded gravel													
1		CONCRETE SLAB.													
14	SW	Brown SAND. -fine to medium sand -dry													
2															
13	SW	Brown SANDY GRAVEL. -fine to medium sand -fine to medium rounded gravel								▽					
3			N=42												
12															
4			N=46												
11															
5			N=63												


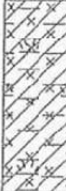


SOILS & FOUNDATIONS LTD

Job No:
95234/00


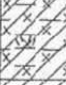



Logged: Cant Drill
Checked: Cant Drill
Date:

FIGURE 95234/00/BH4
BOREHOLE RECORD

SOILS & FOUNDATIONS LTD.

Project:		Project Number: 95234/00		Boring ID. HA1				
Client: DESIGN SERVICES UNIT				Sheet No.1 of 1				
Boring Depth (m.): 1.3		Elevation:	Engineer: G.Clark		Starting Date: 16/9/97			
Datum/Notes/				Ending Date: 16/9/97				
Elev. (m)	Depth (m)	Lithology	Material Description	Well Detail	Comments	Scala Penetration (mm/blow)		
						0	50	100
			Brown BARK.					
			Brown SILTY TOPSOIL. -dry					
			Brown SANDY SILT. -fine sand					
	1		Brown SAND. -fine to medium sand -moist -trace of rounded gravel NO FURTHER PROGRESS DUE TO GRAVELS.					
	2							

SOILS & FOUNDATIONS LTD.

Project:		Project Number: 95234/00		Boring ID. HA2				
Client: DESIGN SERVICES UNIT				Sheet No.1 of 1				
Boring Depth (m.): 1.8		Elevation:	Engineer: G.Clark		Starting Date: 16/9/97			
Datum/Notes/				Ending Date: 16/9/97				
Elev. (m)	Depth (m)	Lithology	Material Description	Well Detail	Comments	Scala Penetration (mm/blow)		
						0	50	100
(	Brown BARK.					
(	Brown SILTY TOPSOIL FILL. -dry					
(	Brown GRAVELLY SANDY FILL. -trace of red brick -trace of concrete					
(1		Brown SAND with minor silt. -fine to medium sand -moist					
(2		Brown GRAVELLY SAND. -fine to medium rounded gravel NO FURTHER PROGRESS DUE TO GRAVELS.					

<small>Aurcon (New Zealand) Limited Unit 1, 150 Cavendish Road PO BOX 1961 Christchurch 8140 New Zealand www.aurcongroup.com Email: christchurch@ap.aurcongroup.com</small>	Client: Chch City Council c/o RCP Ltd Project Name: Location: Project Reference: 226228	<h1 style="margin: 0;">BH 1</h1>	Sheet 1 of 3
---	--	----------------------------------	--------------

BOREHOLE INFORMATION Drilling Method: DT Diameter Core: Hq Contractor: Pro Drill	CO-ORDINATES N/A Easting: 2480249.22 m Northing: 5741823.02 m Ground Level: 4.61 m	Date Started: 12/20/2011 Date Completed: 12/20/2011 Inclination: Orientation:	Logged by: TJM Input by: TJM Checked by: DPM Verified by: JK
--	--	--	---

Method/Casing	Core Recovery (%)	Water Loss (%)	Groundwater Level (m)	R.L. (m)	Depth (m)	Graphic Log	Material Description	USC Description	Consistency/Density	Moisture	Sample	In-Situ Testing	Laboratory Testing	Notes	Backfill	Geological Unit
			▽	4.61	0	0	Asphalt.									
					1	1	Sandy fine to coarse GRAVEL with minor cobbles; light brownish grey. Well graded; subrounded to subangular; sand, medium to coarse.	D to M			D					
					3	3	...1.5 No cobbles; moist to wet.	M to W			D	SPT at 1.5m N ₆₀ = 17 2, 2/2, 5, 4, 5 450mm (SS)				
					2	2	Medium to coarse GRAVEL with minor cobbles; light brown with orangish brown staining. Poorly graded; subrounded to subangular.	MD			D					
					4	4	...3.5 Becoming sandy fine to coarse GRAVEL; dark brownish grey. Well graded; sand, fine to coarse.				D	SPT at 3.5m N ₆₀ = 44 11, 10/11, 11, 10, 12 450mm (SS)				
					4	4	Fine to coarse GRAVEL; light grey with orangish brown staining. Well graded; subrounded to subangular.	D			D					
					5	5	...5.0 Becoming sandy fine to medium GRAVEL; dark brownish grey. Well graded; sand, fine to coarse.				D	SPT at 5m N ₆₀ = 28 7, 9/11, 13, 15, 14 450mm (SS)				
					6	6	Fine to coarse GRAVEL; light grey stained orangish brown. Well graded; subrounded to subangular.				D					
					7	7	...6.5 Becoming sandy; dark brownish grey. Sand, fine to coarse.	VD			D	SPT at 6.5m N ₆₀ = 51 3, 7/9, 12, 14, 16 450mm (SS)				
					8	8	Fine to coarse GRAVEL; light grey iron stained orangish brown. Well graded; subrounded to subangular, some weathering and drilling induced fractures.				D					
					8	8	...7.7 Becoming clayey coarse GRAVEL; brownish grey. Clay, high plasticity.				D					
					9	9	Silty CLAY with some sand; brownish grey. Moderate plasticity; sand, fine to medium.	D			D	SPT at 8m N ₆₀ = 32 8, 9/11, 11, 11, 9 450mm (SS)				
					9	9	Sandy medium to coarse GRAVEL; brownish grey. Poorly graded; subrounded to subangular; sand, fine to medium.	D			D					
					10	10	Fine to medium SAND; dark grey. Poorly graded.	MD			D	SPT at 9.5m N ₆₀ = 28 3, 3/4, 6, 8, 8 450mm (SS)				

Method CC concrete core OB open barrel SSA solid stem auger HSA hollow stem auger WASH wash drill PQ Triple Tube HQ3 Triple Tube HQ Triple Tube NMLC NMLC Triple Tube DP Direct Push DT Dual Tube (70mm) Casing	USC Classification CH Inorganic CLAYS high plasticity CI Inorganic CLAYS medium plasticity CL Inorganic CLAYS low plasticity GC Clayey GRAVEL GM Silty GRAVEL GP Poorly Graded GRAVEL GW Well Graded GRAVEL MH Inorganic SILT high plasticity ML Inorganic SILT low plasticity OC ORGANIC CLAY medium to high plasticity OL ORGANIC SILT low plasticity PEAT peat and highly organic soils SC Clayey SAND SM Silty SAND SP Poorly graded SAND SW Well graded SAND	Consistency VS very soft S soft F firm S stiff VS very stiff H hard Density VL very loose L loose MD medium dense D dense VD very dense	Soil Samples B bulk U undisturbed D disturbed Water ∇ at end of excavation ∇ at time of excavation ∇ at time of closure Moisture D dry M moist W wet S saturated	In Situ Testing PP pen penetrometer VS vane shear SPT sid. pen. test SS split spoon SC solid core HB hammer bouncing SH sinks under own weight Backfill	Graphic Log
--	--	---	---	---	------------------------

Last Generated: 2/24/2012 2:29:17 PM

Library: SWS LIBRARY FEB 2012.GLB, Data template: CHCH DATA TEMPLATE NOV 2010.GDT, Last Generated: 2/24/2012. Database File: Springston Formisón

<p>aurecon Aurecon (New Zealand) Limited Unit 1, 150 Cavendish Road PO BOX 1081 Christchurch 8140 New Zealand www.aurecongroup.com Email: christchurch@nz.aurecongroup.com</p>		<p>Client: Chch City Council c/o RCP Ltd Project Name: Location: Project Reference: 226228</p>		<p>BH 1</p>													
<p>Sheet 2 of 3</p>		<p>CO-ORDINATES N/A Easting: 2480249.22 m Northing: 5741623.02 m Ground Level: 4.61 m</p>		<p>Date Started: 12/20/2011 Date Completed: 12/20/2011 Inclination: Orientation:</p>													
<p>BOREHOLE INFORMATION Drilling Method: DT Diameter Core: Hq Contractor: Pro-Drill</p>		<p>Logged by: TJM Input by: TJM Checked by: DPM Verified by: JK</p>															
Method/Casing	Core Recovery (%)	Water Loss (%)	Groundwater Level (m)	Depth (m)	Graphic Log	Material Description	USC Description	Consistency/Density	Moisture	Sample	In-Situ Testing	Laboratory Testing	Notes	Backfill	Geological Unit		
				90		...9.95 Becoming gravelly; Gravel, coarse, subrounded.				D							
				90		Fine to medium SAND; dark grey. Poorly graded. (Layer Continued from previous page)		MD		D							
				70		...10.5 No gravel				D							
				70						D	SPT at 11m N ₆₀ = 51 3, 4/7, 11, 15, 18 450mm (SS)						
				100		...11.45 Minor silt; Low plasticity.				D							
				100		Sandy fibrous PEAT; dark brown. Sand, fine to medium.		VD		D							
				100		Fine to medium SAND with minor silt; dark grey.				D	SPT at 12.5m N ₆₀ = 50+ 4, 8/14, 15, 21 375mm (SS)						
				100		...13.7 Peaty; dark brownish grey. Peat, fibrous.				D							
				100		SILT; light grey. Low plasticity.		S to F		D							
				100		...14.45 Trace clay; soft, moderate plasticity.				D							
				100		...14.5 No clay; soft; low plasticity.				D							
				100		Fine to medium SAND; dark grey.		W		D							
				100						D							
				50				MD		D	SPT at 15.5m N ₆₀ = 16 2, 2/3, 4, 5, 4 450mm (SS)						
				80		SILT with some fine sand; grey. Low plasticity.				D							
				80		Fine to medium SAND; dark grey.				D							
				80		Sandy SILT with trace of shell; grey. Low plasticity.		F		D							
				50		Fine to medium SAND with minor silt; dark grey.				D							
				50		Poorly graded.				D	SPT at 17m N ₆₀ = 21 2, 3/3, 5, 6, 7 450mm (SS)						
				80						D							
				65		...18.75 Fine with some silt.				D							
				50						D	SPT at 18.5m N ₆₀ = 19 7, 5/4, 3, 4, 8 450mm (SS)						
				100		SILT; bluish grey. Low plasticity.				D							
				100		Silty fine SAND; bluish grey.		S		D							
<p>Method CC concrete core OB open barrel SSA solid stem auger HSA hollow stem auger WASH wash drill PO3 PO Triple Tube HO3 HO Triple Tube NO3 NO Triple Tube NMLC NMLC Triple Tube DP Direct Push DT Dual Tube (70mm) Casing</p>		<p>USC Classification CH Inorganic CLAYS high plasticity CI Inorganic CLAYS medium plasticity CL Inorganic CLAYS low plasticity GC Clayey GRAVEL GM Silty GRAVEL GP Poorly Graded GRAVEL GW Well Graded GRAVEL MH Inorganic SILT high plasticity ML Inorganic SILT low plasticity OH ORGANIC CLAY medium to high plasticity OL ORGANIC SILT low plasticity PT PEAT and highly organic soils SC Clayey SAND SM Silty SAND SP Poorly graded SAND SV Well graded SAND</p>		<p>Consistency VS very soft S soft F firm S stiff VS very stiff H hard</p> <p>Density VL very loose L loose MD medium dense D dense VD very dense</p>		<p>Soil Samples B bulk U undisturbed D disturbed</p> <p>Water ∇ at end of excavation ∇ at time of excavation ∇ at time of closure</p>		<p>In Situ Testing PP pen penetrometer VS vane shear SPT sst. pen. test SS split spoon SC solid cone HB hammer bouncing SH sht. under own weight</p> <p>Moisture D dry M moist W wet S saturated</p>		<p>Graphic Log Asphlt SAND Sandy GRAVEL GRAVEL Silty CLAY SAND Sandy Organic CLAY SILT Sandy SILT Silty SAND Clayey SILT</p>		<p>Backfill</p>		<p>NO LABORATORY TESTING</p>		<p>Springbank Formation</p>	

Last Generated: 2/24/2012 2:29:17 PM

Library: SWS LIBRARY FEB 2012.GLB, Data template: CHCH DATA TEMPLATE NOV 2010.GDT, Last Generated: 2/24/2012.

Database File:

 Aurecon (New Zealand) Limited Unit 1 100 Caversham Road PO BOX 1061 Christchurch 8146 New Zealand www.aurecongroup.com Email: christchurch@ap.aurecongroup.com		Client: Chch City Council c/o RCP Ltd Project Name: Location: Project Reference: 226228		<h1 style="text-align: right;">BH 1A</h1>												
BOREHOLE INFORMATION Drilling Method: Sonic Diameter Core: Hq Contractor: Pro-Drill		CO-ORDINATES N/A Easting: 2480252.19 m Northing: 5741820.71 m Ground Level: 4.52 m		Date Started: 10/1/2012 Date Completed: 10/1/2012 Inclination: Orientation:												
				Logged by: TJM Input by: ATS Checked by: DPM Verified by: JK												
Method/Casting	Cone Recovery (%)	Water Loss (%)	Groundwater Level (m)	R.L. (m)	Depth (m)	Graphic Log	Material Description	USC Description	Consistency/Density	Moisture	Sample	In-Situ Testing	Laboratory Testing	Notes	Backfill	Geological Unit
100				4	0		Fine to coarse GRAVEL with some sand and minor cobbles; brownish grey. Well graded; subrounded to subangular; sand, fine to coarse.				M to W	D				Fill
100				3	1		Sandy fine to coarse GRAVEL; dark greyish brown. Well graded; subrounded to subangular; sand, fine to coarse.									
100				2	2		...1.3 minor cobbles Gravelly fine to coarse SAND with some silt; grey. Poorly graded; gravel, fine to medium, subrounded.				L	D	SPT at 1.5m N ₆₀ = 10 1, 1/1, 1, 3, 5 450mm (SS)			
50				2	3		Gravelly fine to medium SAND; dark brown. Poorly graded; gravel, fine to coarse, subrounded.									
100				1	4		Sandy fine to coarse GRAVEL with minor cobbles; dark grey. Well graded; subrounded to subangular; sand, fine to coarse.						SPT at 3m N ₆₀ = 43 15, 21/12, 10, 10, 11 450mm (SS)			
100				0	5						MD to D	D	SPT at 4.5m N ₆₀ = 29 7, 3/0, 6, 7, 6 450mm (SS)			
100				1	6						W to S	D	SPT at 6m N ₆₀ = 48 5, 12/13, 12, 13, 10 450mm (SS)			
100				2	7		Peat; Yellowish brown. Fibrous; wood.									
100				3	8		Fine to coarse GRAVEL with some cobbles; light bluish grey. Well graded; subrounded to subangular.						SPT at 7.5m N ₆₀ = 29 4, 3/1, 1, 11, 16 450mm (SS)			
80				4	9		...7.5 becoming Sandy with some silt Silty fine to coarse GRAVEL with some sand; dark greyish brown. Well graded; subrounded to subangular; silt, organic, moderately plastic.									
100				5	10		Fine to medium SAND; dark brown.						SPT at 9m N ₆₀ = 34 1, 3/4, 3, 1, 16 450mm (SS)			
80				5	11											

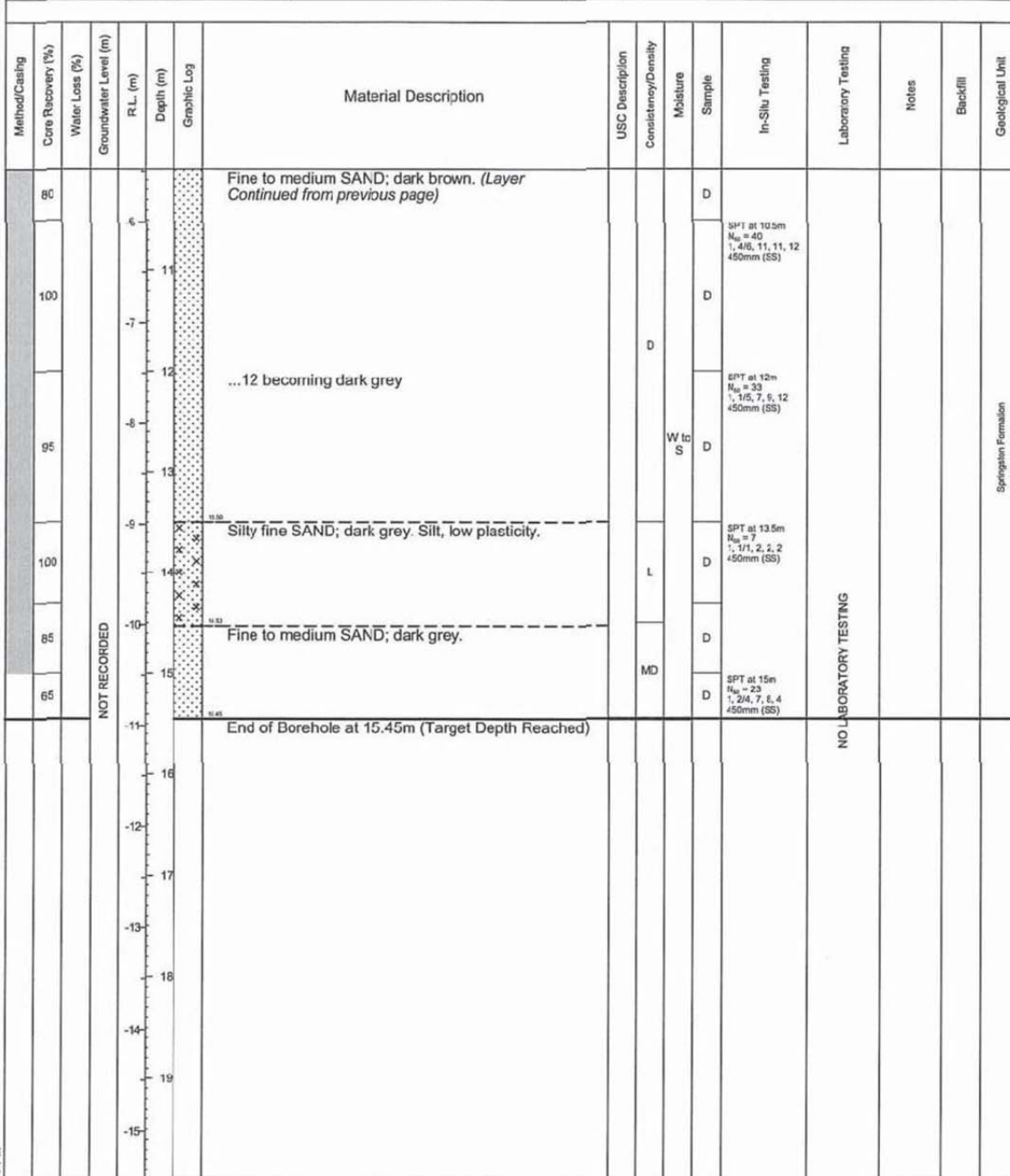
Library: SWS LIBRARY FEB 2012.GLB, Data template: CHCH DATA TEMPLATE NOV 2010.GDT, Last Generated: 2/24/2012.

Database File:

Method CC concrete core OB open barrel SSA solid stem auger HSA hollow stem auger WASH wash drill PO3 PO Triple Tube HO3 HO Triple Tube HQ3 HQ Triple Tube NMLC NMLC Triple Tube DP Direct Push DT Dual Tube (70mm) Casing	USC Classification CH Inorganic CLAYS high plasticity CI Inorganic CLAYS medium plasticity CL Inorganic CLAYS low plasticity GS Clayey GRAVEL GM Silty GRAVEL GP Poorly Graded GRAVEL GW Well Graded GRAVEL MH Inorganic SILT high plasticity ML Inorganic SILT low plasticity OH ORGANIC CLAY medium to high plasticity OL ORGANIC SILT low plasticity PT PEAT and highly organic soils SC Clayey SAND SM Silty SAND SP Poorly graded SAND SW Well graded SAND	Consistency VS very soft soft stiff VS very stiff H hard Density VL very loose L loose MD medium dense D dense VD very dense	Soil Samples B bulk U undisturbed D disturbed Water at time of excavation at time of closure	In Situ Testing PP psc penetrometer VS vane shear SPT std. pen. test SS split spoon SC solid cone SH hammer bouncing sinks under own weight Moisture D dry M moist W wet S saturated	Graphic Log
---	--	---	--	--	------------------------

aurecon <small>Aurecon (New Zealand) Limited Unit 1, 150 Cavendish Road PO BOX 1061 Christchurch 8140 New Zealand www.aurecongroup.com Email: christchurch@aurecongroup.com</small>	Client: Chch City Council c/o RCP Ltd Project Name: Location: Project Reference: 226228	<h1 style="margin: 0;">BH 1A</h1> Sheet 2 of 2
---	--	--


BOREHOLE INFORMATION Drilling Method: Sonic Diameter Core: Hq Contractor: Pro-Drill	CO-ORDINATES N/A Easting: 2480252.19 m Northing: 5741920.71 m Ground Level: 4.62 m	Date Started: 10/1/2012 Date Completed: 10/1/2012 Inclination: Orientation:	Logged by: TJM Input by: ATS Checked by: DPM Verified by: JK
---	--	--	---



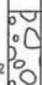





Last Generated: 2/24/2012 2:28:18 PM

Method CC concrete core OB open barrel SSA solid stem auger HSA hollow stem auger WASH wash drill PQ3 PQ Triple Tube HQ3 HQ Triple Tube NQ3 NQ Triple Tube NMILC NMILC Triple Tube DP Direct Push DT Dual Tube (70mm) Casing	USC Classification CH Inorganic CLAYS high plasticity CI Inorganic CLAYS medium plasticity CL Inorganic CLAYS low plasticity GC Clayey GRAVEL GM Silty GRAVEL GP Poorly Graded GRAVEL GW Well Graded GRAVEL MH Inorganic SILT high plasticity ML Inorganic SILT low plasticity OH ORGANIC CLAY medium to high plasticity OL ORGANIC SILT low plasticity PT PEAT and highly organic soils SC Clayey SAND SM Silty SAND SP Poorly graded SAND SW Well graded SAND	Consistency VS very soft S soft F firm S stiff VS very stiff H hard Density VL very loose L loose MD medium dense D dense VD very dense	Soil Samples B bulk U undisturbed D disturbed Water ∇ at end of excavation ∇ at time of excavation ∇ at time of closure	In Situ Testing PP pen penetrometer VS vane shear SPT std. pen. test SS split spoon SC solid cone HB hammer bouncing SH sinks under own weight Moisture D dry M moist W wet S saturated	Graphic Log <table style="width:100%;"> <tr> <td>[Symbol] GRAVEL</td> <td>[Symbol] Silty GRAVEL</td> </tr> <tr> <td>[Symbol] Sandy GRAVEL</td> <td>[Symbol] SAND</td> </tr> <tr> <td>[Symbol] Gravelly SAND</td> <td>[Symbol] Silty SAND</td> </tr> <tr> <td>[Symbol] Peat</td> <td></td> </tr> </table>	[Symbol] GRAVEL	[Symbol] Silty GRAVEL	[Symbol] Sandy GRAVEL	[Symbol] SAND	[Symbol] Gravelly SAND	[Symbol] Silty SAND	[Symbol] Peat	
[Symbol] GRAVEL	[Symbol] Silty GRAVEL												
[Symbol] Sandy GRAVEL	[Symbol] SAND												
[Symbol] Gravelly SAND	[Symbol] Silty SAND												
[Symbol] Peat													

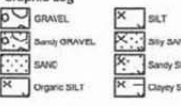
Library: SWS LIBRARY FEB 2012.GLB, Data template: CHCH DATA TEMPLATE NOV 2010.GDT, Last Generated: 2/24/2012. Database File:

 <p>aurecon Aurecon (New Zealand) Limited Unit 1, 150 Cavendish Road PO BOX 1961 Christchurch 8140 New Zealand www.aurecongroup.com Email: christchurch@aurecongroup.com</p>	<p>Client: Chch City Council c/o RCP Ltd Project Name: Location: Project Reference: 226228</p>	<h1 style="margin: 0;">BH 2</h1> <p>Sheet 1 of 3</p>
--	--	--


BOREHOLE INFORMATION Drilling Method: Sonic Diameter Core: Hq Contractor: Pro Drill	CO-ORDINATES N/A Easting: 2460200.26 m Northing: 5741772.98 m Ground Level: 6.04 m	Date Started: 11/1/2012 Date Completed: 11/1/2012 Inclination: Orientation:	Logged by: ATS Input by: ATS Checked by: DPM Verified by: JK
---	--	--	---

Method/Casing	Core Recovery (%)	Water Loss (%)	Groundwater Level (m)	R.L. (m)	Depth (m)	Graphic Log	Material Description	USC Description	Consistency/Density	Moisture	Sample	In-Situ Testing	Laboratory Testing	Notes	Backfill	Geological Unit
	0			4	1		No sample returned									
	60			3	2		Fine to coarse GRAVEL with some sand; dark brownish grey. Well Graded; sub-rounded to sub-angular; sand, fine to coarse.	MD			D	SPT at 1.5m N ₆₀ = 10 1, 7, 7, 5, 3, 4 450mm (SS)				
	65			2	3		Sandy fine to coarse GRAVEL with occasional cobbles; dark grey. Well Graded; sub-rounded to sub-angular; wood inclusions; sand, fine to coarse.	L			D	SPT at 3m N ₆₀ = 10 3, 3/3, 3, 1, 1 450mm (SS)				
	50			0	5		Fine to coarse GRAVEL with some sand; brownish grey. Well graded; angular to sub-rounded; sand, fine to coarse.				D	SPT at 4.5m N ₆₀ = 34 2, 0/0, 10, 0, 7 450mm (SS)				
	85			-1	6		...6.5 with occasional cobbles				D	SPT at 6m N ₆₀ = 34 1, 9/8, 8, 8, 10 450mm (SS)				
	75			-3	8		Sandy fine to coarse GRAVEL with minor cobbles; dark bluish grey. Well graded; sub-rounded to sub-angular; sand, medium to coarse.	S			D	SPT at 7.5m N ₆₀ = 30 10, 9/8, 8, 7, 7 450mm (SS)				
	75			-4	9		...9.8 150mm thick medium to coarse SAND lens; dark bluish grey.	L to MD			D	SPT at 9m N ₆₀ = 10 4, 6/3, 2, 2, 3 450mm (SS)				

Last Generated: 2/24/2012 2:29:19 PM

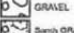
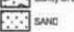






Method CC concrete core OB open barrel SSA solid stem auger HSA hollow stem auger WASH wash drill PQ3 PQ Triple Tube HQ3 HQ Triple Tube NQ3 NQ Triple Tube HMLC HMLC Triple Tube DP Direct Push DT Dual Tube (70mm) Casing	USC Classification CH Inorganic CLAYS high plasticity CI Inorganic CLAYS medium plasticity CL Inorganic CLAYS low plasticity GC Clayey GRAVEL GM Silty GRAVEL GP Poorly Graded GRAVEL GW Well Graded GRAVEL MH Inorganic SILT high plasticity ML Inorganic SILT low plasticity OH ORGANIC CLAY medium to high plasticity OL ORGANIC SILT low plasticity PT PEAT and highly organic soils SC Clayey SAND SM Silty SAND SP Poorly graded SAND SW Well graded SAND	Consistency VS very soft S soft F firm S stiff VS very stiff H hard Density VL very loose L loose MD medium dense D dense VD very dense	Soil Samples B bulk U undisturbed D disturbed Water at end of excavation at time of excavation at time of closure	In Situ Testing PP pen penetrometer VS vane shear SPT std. pen. test SS spill spoon SC solid cone HB hammer bouncing SH sinks under own weight Moisture D dry M moist W wet S saturated	Graphic Log  GRAVEL Silty GRAVEL SAND Organic SILT SILT Silty SAND Sandy SILT Clayey SILT
---	--	---	--	---	---

Library: SWS LIBRARY FEB 2012.GLB; Data template: CHCH DATA TEMPLATE NOV 2010.GDT; Last Generated: 2/24/2012
Springton Formation

 <p>aurecon Aurecon (New Zealand) Limited Unit 1, 150 Cleveland Road PO BOX 1061 Christchurch 8140 New Zealand www.aurecongroup.com Email: christchurch@ap.aurecongroup.com</p>	<p>Client: Chch City Council c/o RCP Ltd Project Name: Location: Project Reference: 226228</p>	<h1 style="font-size: 2em; margin: 0;">BH 2</h1> <p>Sheet 2 of 3</p>
---	--	--

BOREHOLE INFORMATION Drilling Method: Sonic Diameter Core: Hq Contractor: Pro Drill	CO-ORDINATES N/A Easting: 2480200.26 m Northing: 5741772.98 m Ground Level: 5.04 m	Date Started: 11/1/2012 Date Completed: 11/1/2012 Inclination: Orientation:	Logged by: ATS Input by: ATS Checked by: DPM Verified by: JK
---	--	--	---

Method/Casing	Core Recovery (%)	Water Loss (%)	Groundwater Level (m)	R.L. (m)	Depth (m)	Graphic Log	Material Description	USC Description	Consistency/Density	Moisture	Sample	In-Situ Testing	Laboratory Testing	Notes	Backfill	Geological Unit
	75						Medium to coarse SAND; dark bluish grey. Poorly graded.	L to MD			D					
							Sandy fine to coarse GRAVEL; dark bluish grey. Well graded; sub-rounded to sub-angular; sand, medium to coarse.	MD				SPT at 10.5m N ₆₀ = 13 1, 4/5, 4, 4, 5 450mm (SS)				
							Organic SILT with some clay; dark brown becoming grey. Low to moderately plastic; occasional wood inclusions and rootlets. Fine SAND; grey.				D					
							...13 becoming fine to medium SAND	MD		W	D	SPT at 12m N ₆₀ = 12 1, 1/1, 2, 4, 5 450mm (SS)				
							SILT with some sand; grey. Low plasticity; sand, fine; occasional shells				D	SPT at 13.5m N ₆₀ = 5 1, 1/1, 1, 1, 2 450mm (SS)				
							Fine to medium SAND; grey. Well graded; gradual increase in silt toward next layer.				D	SPT at 15m N ₆₀ = 12 1, 1/2, 2, 4, 5 450mm (SS)				
							SILT with some clay and minor fine sand; grey. Low to moderate plasticity; occasional shells.	VS			D					
							Silty fine SAND; grey.	F			S	SPT at 16.5m N ₆₀ = 9 1, 1/1, 2, 2, 4 450mm (SS)				
							Fine SAND with some silt; grey.	L			D					
											D	SPT at 18m N ₆₀ = 20 1, 4/5, 3, 3, 5 450mm (SS)				
							Sandy SILT; grey. Low plasticity; sand, fine Clayey SILT; bluish grey. Moderate to highly plastic; occasional rootlets.	F to St			S	D	SPT at 19.5m N ₆₀ = 12 1, 2/3, 4, 2, 3 450mm (SS)			

Method CC concrete core OB open barrel SSA solid stem auger HSA hollow stem auger WASH wash drill PQ3 PQ Triple Tube HQ3 HQ Triple Tube NQ3 NQ Triple Tube NMLC NMLC Triple Tube DP Direct Push DT Dual Tube (70mm) Casing	USC Classification CH Inorganic CLAYS high plasticity CI Inorganic CLAYS medium plasticity CL Inorganic CLAYS low plasticity GC Clayey GRAVEL GM Silty GRAVEL GP Poorly Graded GRAVEL GW Well Graded GRAVEL MH Inorganic SILT high plasticity ML Inorganic SILT low plasticity OH ORGANIC CLAY medium to high plasticity OL ORGANIC SILT low plasticity PT PEAT and highly organic soils SC Clayey SAND SM Silty SAND SP Poorly graded SAND SW Well graded SAND	Consistency VS very soft S soft F firm S stiff VS very stiff H hard Density VL very loose L loose MD medium dense D dense VD very dense	Soil Samples B bulk U undisturbed D disturbed Water at end of excavation at time of excavation at time of closure Moisture D dry M moist W wet S saturated	In Situ Testing PP pen penetrometer VS vane shear SPT est. pen. test SS split spoon SC solid cone HB hammer bouncing SH sinks under own weight Backfill	Graphic Log  GRAVEL  Sandy GRAVEL  SAND  Organic SILT  SILT  Silty SAND  Sandy SILT  Clayey SILT
---	--	---	---	---	---

Last Generated: 2/24/2012 2:29:19 PM


Library: SWS LIBRARY FEB 2012.GLB, Data template: CHCH DATA TEMPLATE NOV 2010.GDT, Last Generated: 2/24/2012. Database File:

		Client: Chch City Council c/o RCP Ltd Project Name: Location: Project Reference: 226228			BH 3											
BOREHOLE INFORMATION Drilling Method: Sonic Diameter Core: Hq Contractor: Pro-Drill		CO-ORDINATES N/A Easting: 2480157.97 m Northing: 5741816.31 m Ground Level: 5.76 m			Date Started: 12/1/2012 Date Completed: 12/1/2012 Inclination: Orientation:											
					Logged by: ATS/TJM Input by: ATS Checked by: DPM Verified by: JK											
					Sheet 1 of 3											
Method/Casing	Core Recovery (%)	Water Loss (%)	Groundwater Level (m)	R.L. (m)	Depth (m)	Graphic Log	Material Description	USC Description	Consistency/Density	Moisture	Sample	In-Situ Testing	Laboratory Testing	Notes	Backfill	Geological Unit
							No sample returned.				D					
	0			5	1											
					2		Sandy fine to coarse GRAVEL; dark brownish grey. Well graded; subrounded to subangular; sand is fine to coarse.					SPT at 1.5m N ₆₀ = 20 4, 5/7, 5, 4, 4 450mm (SS)				
	70				3		Fine to medium SAND with trace of gravel; dark greyish brown. Poorly graded; gravel is fine to medium.	MD			D					
					3		Sandy COBBLES; dark brownish grey. Poorly graded; subrounded; sand is fine to medium					SPT at 3m N ₆₀ = 7 2, 2/1, 2, 3, 1 450mm (SS)				
					4		Fine to medium SAND; greyish brown.									
	80			2	4		...3.7 becoming fine to coarse SAND; brownish grey. Well graded	L			D					
					0		Sandy fine to coarse GRAVEL; dark brownish grey. Well graded; subrounded to subangular; sand is fine to coarse					SPT at 4.5m N ₆₀ = 36 7, 11/10, 6, 9, 9 450mm (SS)				
	85				0		...5.5 some cobbles									
					6		Fine to medium SAND with occasional cobbles; dark grey.					SPT at 6m N ₆₀ = 23 5, 6/6, 6, 6, 5 450mm (SS)				
	65				7		...6.9 200mm thick Sandy fine to coarse GRAVEL lense, subrounded to subangular.	MD			D					
					-1		Fine to coarse GRAVEL with some sand; dark grey. Well graded; sand is fine to coarse.					SPT at 7.5m N ₆₀ = 23 5, 3/5, 4, 4, 6, 8 450mm (SS)				
	80				8											
					9											
	75				9							SPT at 9m N ₆₀ = 13 4, 3/3, 4, 4, 2 450mm (SS)				
					-3											
					-4											
Method CC concrete core OB open barrel SSA solid stem auger HSA hollow stem auger WASH wash drill HQ3 HQ Triple Tube HQ3 HQ Triple Tube NQ3 NQ Triple Tube NMLC NMLC Triple Tube DP Direct Push DT Dual Tube (70mm) Casing		USC Classification CH Inorganic CLAYS high plasticity CL Inorganic CLAYS medium plasticity CI Inorganic CLAYS low plasticity GC Clayey GRAVEL GM Silty GRAVEL GP Poorly Graded GRAVEL GW Well Graded GRAVEL MH Inorganic SILT high plasticity ML Inorganic SILT medium plasticity OL ORGANIC CLAY medium to high plasticity OLC ORGANIC SILT low plasticity PEAT sand highly organic soils. SC Clayey SAND SM Silty SAND SP Poorly graded SAND SW Well graded SAND		Consistency VS very soft S soft F firm S stiff VS very stiff H hard Densky VL very loose L loose MD medium dense D dense VD very dense		Soil Samples B bulk U undisturbed D disturbed Water at end of excavation at time of excavation at time of closure		In Situ Testing PP pen penetrometer VS vane shear SPT spt, pen, test SS split spoon SC solid cone HB hammer bouncing SH sinks under own weight Moisture D dry M moist W wet S saturated		Graphic Log 						

Last Generated: 2/24/2012 2:29:20 PM

Library: SWS LIBRARY FEB 2012.GLB, Data template: CHCH DATA TEMPLATE NOV 2010.GDT, Last Generated: 2/2/2012.

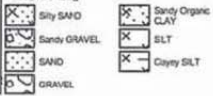
Database File:

 <p style="font-size: small;">Aurecon (New Zealand) Limited Unit 1, 150 Cowditch Road PO BOX 1061 Christchurch 8140 New Zealand www.aurecongroup.com Email: christchurch@nz.aurecongroup.com</p>	<p>Client: Chch City Council c/o RCP Ltd Project Name: Location: Project Reference: 226228</p>	<h1 style="margin: 0;">BH 4</h1> <p>Sheet 1 of 3</p>
---	--	--

BOREHOLE INFORMATION Drilling Method: Sonic Diameter Core: Hq Contractor: Pro-Drill	CO-ORDINATES N/A Easting: 2480195.09 m Northing: 5741881.48 m Ground Level: 6.23 m	Date Started: 1/13/2012 Date Completed: 1/13/2012 Inclination: Orientation:	Logged by: ATS/TJM Input by: ATS Checked by: DPM Verified by: JK
---	--	--	---

Method/Casing	Core Recovery (%)	Water Loss (%)	Groundwater Level (m)	R.L. (m)	Depth (m)	Graphic Log	Material Description	USC Description	Consistency/Density	Moisture	Sample	In-Situ Testing	Laboratory Testing	Notes	Backfill	Geological Unit
				6	0		No sample returned									
				5	1											
				4	2		Silty fine SAND with some gravel; greyish brown. Poorly graded; gravel is fine to coarse, angular.					SPT at 1.5m N ₆₀ = 8 2, 4, 2, 1, 1, 2 450mm (SS)				
				3	3		Silty fine to medium SAND; greyish brown.									
				2	4		... 2.35 becoming SAND, no silt.									
				1	3		Sandy fine to coarse GRAVEL; dark grey. Well graded; subrounded to subangular; sand is fine to coarse.					SPT at 3m N ₆₀ = 14 3, 2/3, 4, 3, 4 450mm (SS)				
				0	4		...4.3 ~50mm thick SILT lense; low plasticity.									
				1	5		...4.8 Large wood inclusion									
				0	6		Fine to medium SAND with some peat; grey, mottled dark brown. Peat is fibrous.					SPT at 4.5m N ₆₀ = 10 3, 3/5, 4, 5, 5 450mm (SS)				
				0	7		Fine to medium GRAVEL with some sand and some cobbles; dark grey. Well graded; fine to medium, subrounded to subangular; sand is medium to coarse.					SPT at 6m N ₆₀ = 29 4, 5/7, 7, 7, 8 450mm (SS)				
				0	8											
				0	9											
				0	10											
				0	11											
				0	12											
				0	13											
				0	14											
				0	15											
				0	16											
				0	17											
				0	18											
				0	19											
				0	20											
				0	21											
				0	22											
				0	23											
				0	24											
				0	25											
				0	26											
				0	27											
				0	28											
				0	29											
				0	30											
				0	31											
				0	32											
				0	33											
				0	34											
				0	35											
				0	36											
				0	37											
				0	38											
				0	39											
				0	40											
				0	41											
				0	42											
				0	43											
				0	44											
				0	45											
				0	46											
				0	47											
				0	48											
				0	49											
				0	50											
				0	51											
				0	52											
				0	53											
				0	54											
				0	55											
				0	56											
				0	57											
				0	58											
				0	59											
				0	60											
				0	61											
				0	62											
				0	63											
				0	64											
				0	65											
				0	66											
				0	67											
				0	68											
				0	69											
				0	70											
				0	71											
				0	72											
				0	73											
				0	74											
				0	75											
				0	76											
				0	77											
				0	78											
				0	79											
				0	80											
				0	81											
				0	82											
				0	83											
				0	84											
				0	85											
				0	86											
				0	87											
				0	88											
				0	89											
				0	90											
				0	91											
				0	92											
				0	93											
				0	94											
				0	95											
				0	96											
				0	97											
				0	98											
				0	99											
				0	100											

Last Generated: 2/24/2012 2:29:21 PM

Method CC concrete core OB open barrel SSA solid stem auger HSA hollow stem auger WASH wash drill PQ3 PO Triple Tube HQ3 HO Triple Tube NQ3 NO Triple Tube NMLC NMLC Triple Tube DP Direct Push DT Dual Tube (70mm) Casing	USC Classification CH Inorganic CLAYS high plasticity CI Inorganic CLAYS medium plasticity CL Inorganic CLAYS low plasticity CA Clayey GRAVEL GM Silty GRAVEL GP Poorly Graded GRAVEL GW Well Graded GRAVEL MH Inorganic SILT high plasticity ML Inorganic SILT low plasticity OH ORGANIC CLAY medium to high plasticity OL ORGANIC SILT low plasticity PT PEAT and highly organic soils SI Silty SAND SP Poorly graded SAND SW Well graded SAND	Consistency VS very soft S soft F firm S stiff VS very stiff H hard Density VL very loose L loose MD medium dense D dense VD very dense	Soil Samples B bulk U undisturbed D disturbed Water ▽ a: end of excavation ▽ a: time of excavation ▽ a: time of closure	In Situ Testing PP pen penetrometer VS vane shear SPT std. pen. test SS split spoon SC solid cone HB hammer bouncing SH sinks under own weight Moisture D dry M moist W wet S saturated	Graphic Log 
---	--	---	--	---	---

Library: SWS LIBRARY FEB 2012.GLB, Data template: CHCH DATA TEMPLATE NOV 2010.GDT, Last Generated: 2/24/2012. Database File:

Aurecon <small>Aurecon (New Zealand) Limited Unit 1, 150 Cavendish Road PO BOX 1961 Christchurch 8140 New Zealand www.aurecongroup.com Email: christchurch@ap.aurecongroup.com</small>	Client: Chch City Council c/o RCP Ltd Project Name: Location: Project Reference: 226228	<h1 style="margin: 0;">BH 4</h1> Sheet 2 of 3
--	--	---

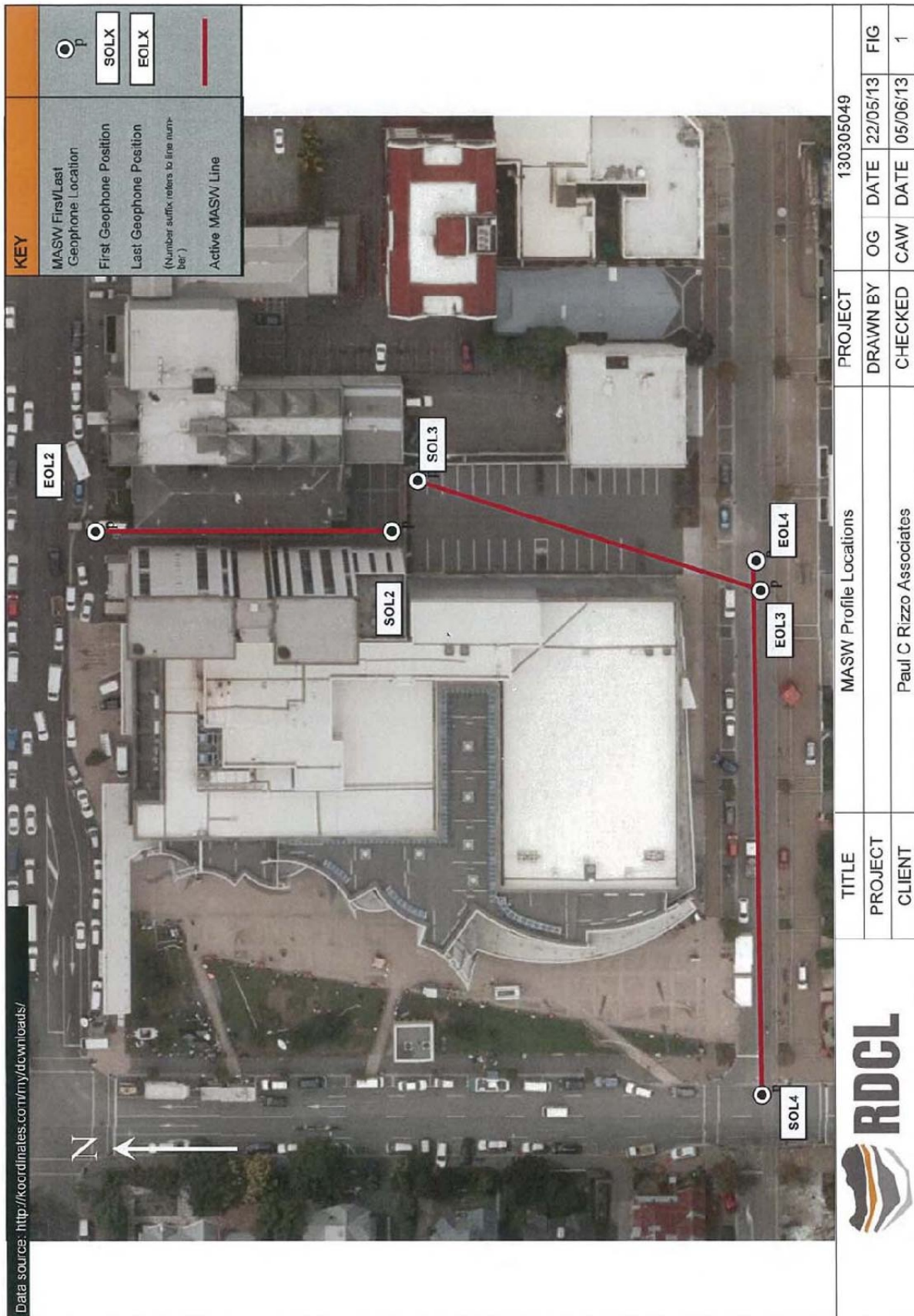
BOREHOLE INFORMATION Drilling Method: Sonic Diameter Core: Hq Contractor: Pro-Drill	COORDINATES N/A Easting: 2480195.09 m Northing: 5741881.48 m Ground Level: 6.23 m	Date Started: 1/13/2012 Date Completed: 1/13/2012 Inclination: Orientation:	Logged by: ATS/TJM Input by: ATS Checked by: DPM Verified by: JK
---	---	--	---

Method/Casing	Core Recovery (%)	Water Loss (%)	Groundwater Level (m)	R.L. (m)	Depth (m)	Graphic Log	Material Description	USC Description	Consistency/Density	Moisture	Sample	In-Situ Testing	Laboratory Testing	Notes	Backfill	Geological Unit	
	75			-4	0		Fine to medium GRAVEL with some sand and some cobbles; dark grey. Well graded; fine to medium, subrounded to subangular; sand is medium to coarse. <i>(Layer Continued from previous page)</i>	D			D	SPT at 10.5m N ₆₀ = 14 2, 2, 2, 3, 4, 5 450mm (SS)					
	75			-5	11		Sandy PEAT with some gravel; dark brown and grey. Low Plasticity; peat is amorphous, odourless; sand is fine to coarse; gravel is medium to coarse; large wood inclusions.	MD			D						
	85			-6	12		Sandy PEAT with some gravel; dark brown and grey. Low Plasticity; peat is amorphous, odourless; sand is fine to coarse; gravel is medium to coarse; large wood inclusions.	S			D	SPT at 12m N ₆₀ = 8 1, 2, 2, 1, 2, 3 450mm (SS)					
	85			-7	13		Fine to medium SAND; grey.				D	SPT at 13.5m N ₆₀ = 10 0, 0, 1, 1, 3, 5 450mm (SS)					
	85			-8	14		Fine to medium SAND; grey.	L			D	SPT at 15m N ₆₀ = 6 1, 1, 1, 1, 1, 1 450mm (SS)					
	80			-9	15		SILT with some sand; grey. Low plasticity; sand is fine.	S to F			D	SPT at 15.5m N ₆₀ = 4 1, 2, 2, 3, 3, 2 450mm (SS)					
	80			-10	16		Medium to coarse SAND; grey.				D	SPT at 16.5m N ₆₀ = 10 1, 2, 2, 3, 3, 2 450mm (SS)					
	70			-11	17		...17.8 Medium to coarse SAND; grey.	L			D	SPT at 18m N ₆₀ = 9 1, 1, 1, 3, 3, 2 450mm (SS)					
	80			-12	18		...17.8 Becoming fine to medium SAND with some silt. SILT; grey. Low plasticity.	S			D	SPT at 18m N ₆₀ = 9 1, 1, 1, 3, 3, 2 450mm (SS)					
	80			-13	19		...18.8 becoming sandy SILT; sand is fine.				D						
	75			-14	20		...19.5 -300mm lense of fine sand.	F			D	SPT at 19.5m N ₆₀ = 6 1, 0, 1, 2, 2, 1 450mm (SS)					

Method CC concrete core OB open barrel SSA solid stem auger BEA hollow stem auger WASH wash drill PO3 PO Triple Tube HQ3 HQ Triple Tube NQ3 NQ Triple Tube NMLC NMLC Triple Tube DP Direct Push DT Dual Tube (70mm) Casing	USC Classification CH Inorganic CLAYS high plasticity CI Inorganic CLAYS medium plasticity CL Inorganic CLAYS low plasticity GC Clayey GRAVEL GM Silty GRAVEL GP Poorly Graded GRAVEL GW Well Graded GRAVEL MH Inorganic SILT high plasticity ML Inorganic SILT low plasticity OH ORGANIC CLAY medium to high plasticity OL ORGANIC SILT low plasticity PT PEAT and highly organic soils SC Silty SAND SM Silty SAND SP Poorly graded SAND SW Well graded SAND	Consistency VS very soft S soft F firm S stiff VS very stiff H hard Density VL very loose MD medium dense D dense VD very dense	Soil Samples B bulk U undisturbed D disturbed Water at end of excavation at time of excavation Moisture D dry M moist W wet S saturated	In Situ Testing PP pen penetrometer VS vane shear SPT std. pen. test SS split spoon SC solid cone HB hammer bouncing SH sinks under own weight Backfill D dry M moist W wet S saturated	Graphic Log
---	---	--	---	---	------------------------

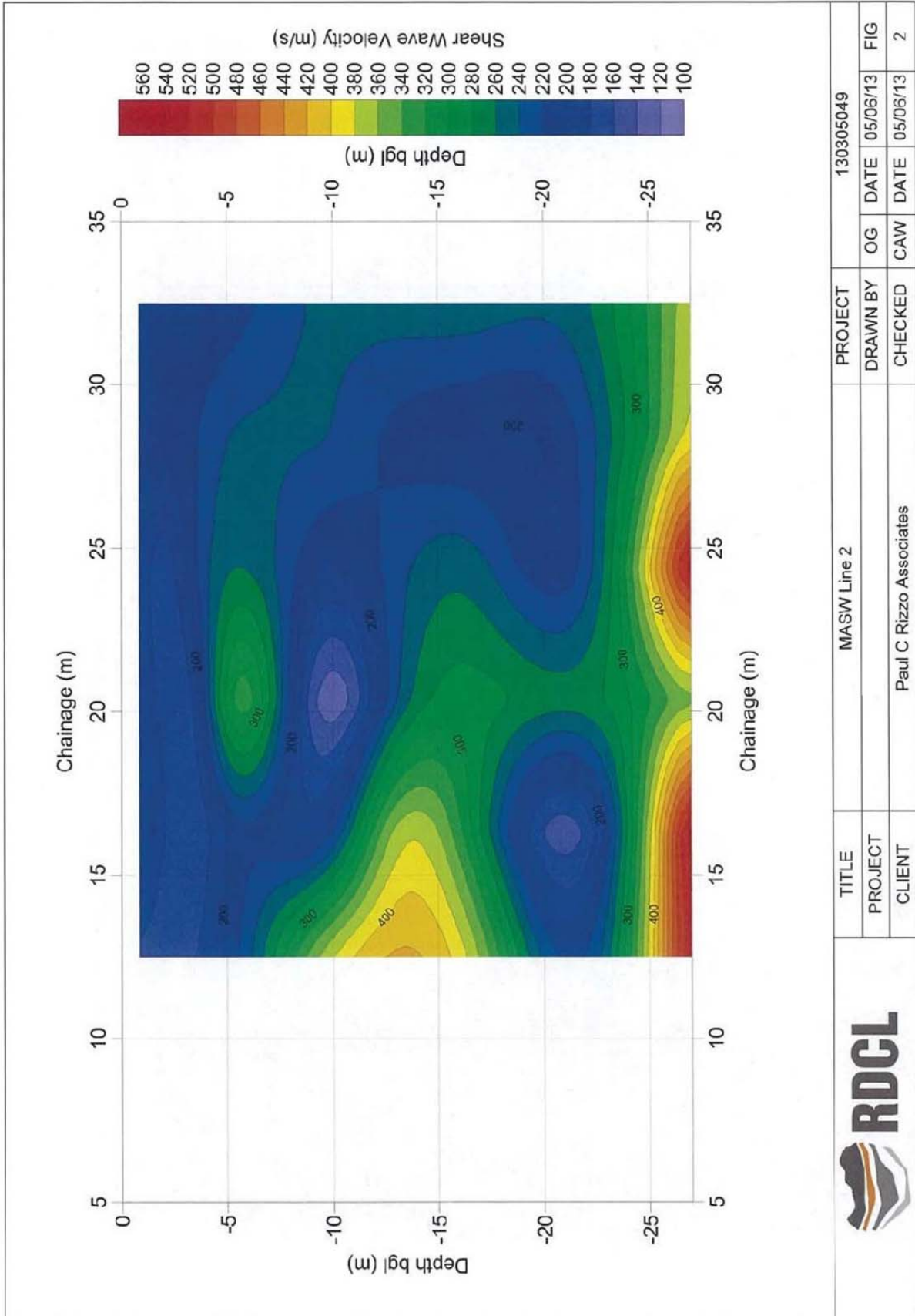
Last Generated: 22/01/2012 2:29:21 PM

Library: SWS LIBRARY FEB 2012.GLB, Data template: CHCH DATA TEMPLATE NOV 2010.GDT, Last Generated: 2/2/2012, Database File:

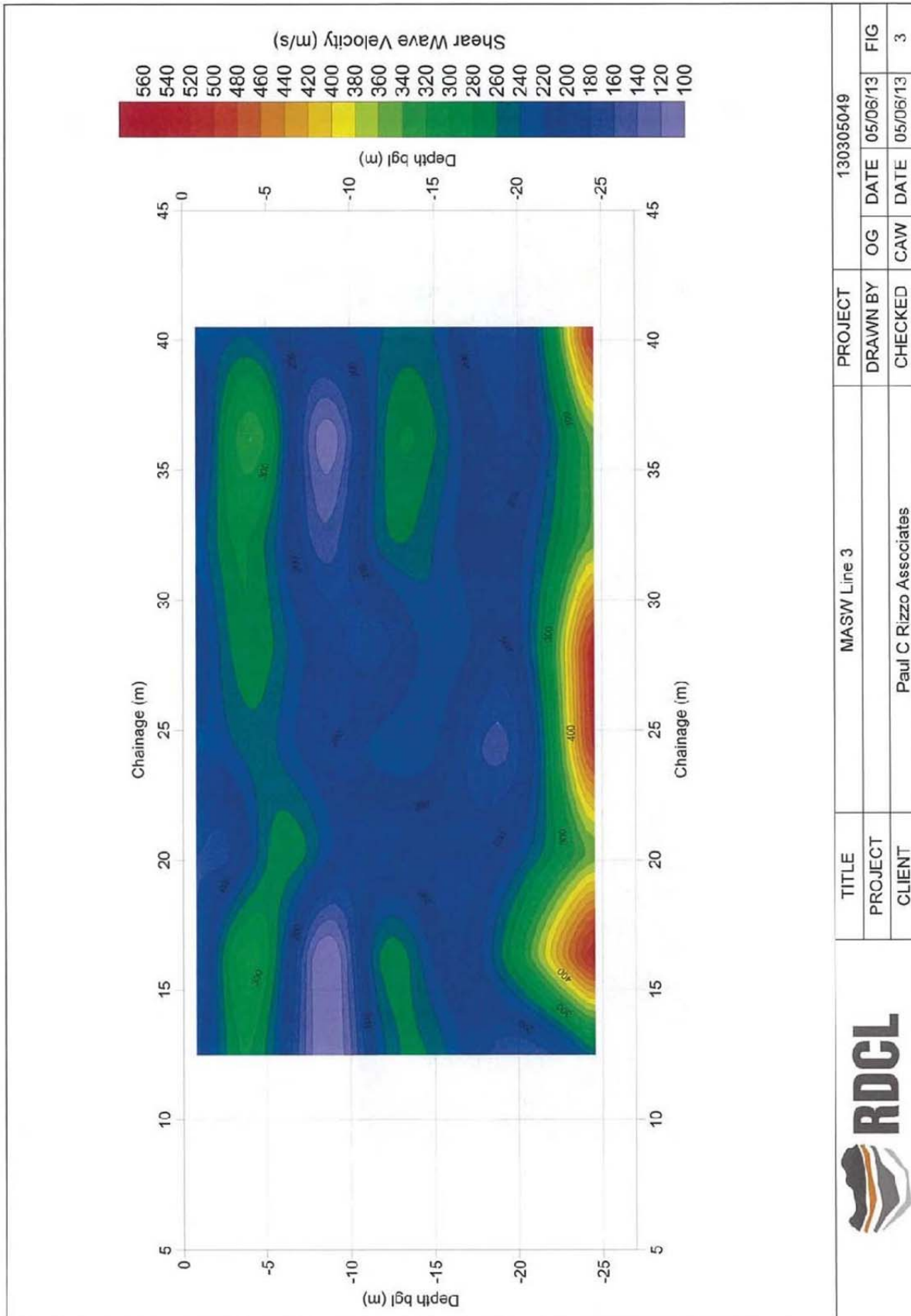


Data source: <http://kooordinates.com/my/downloads/>

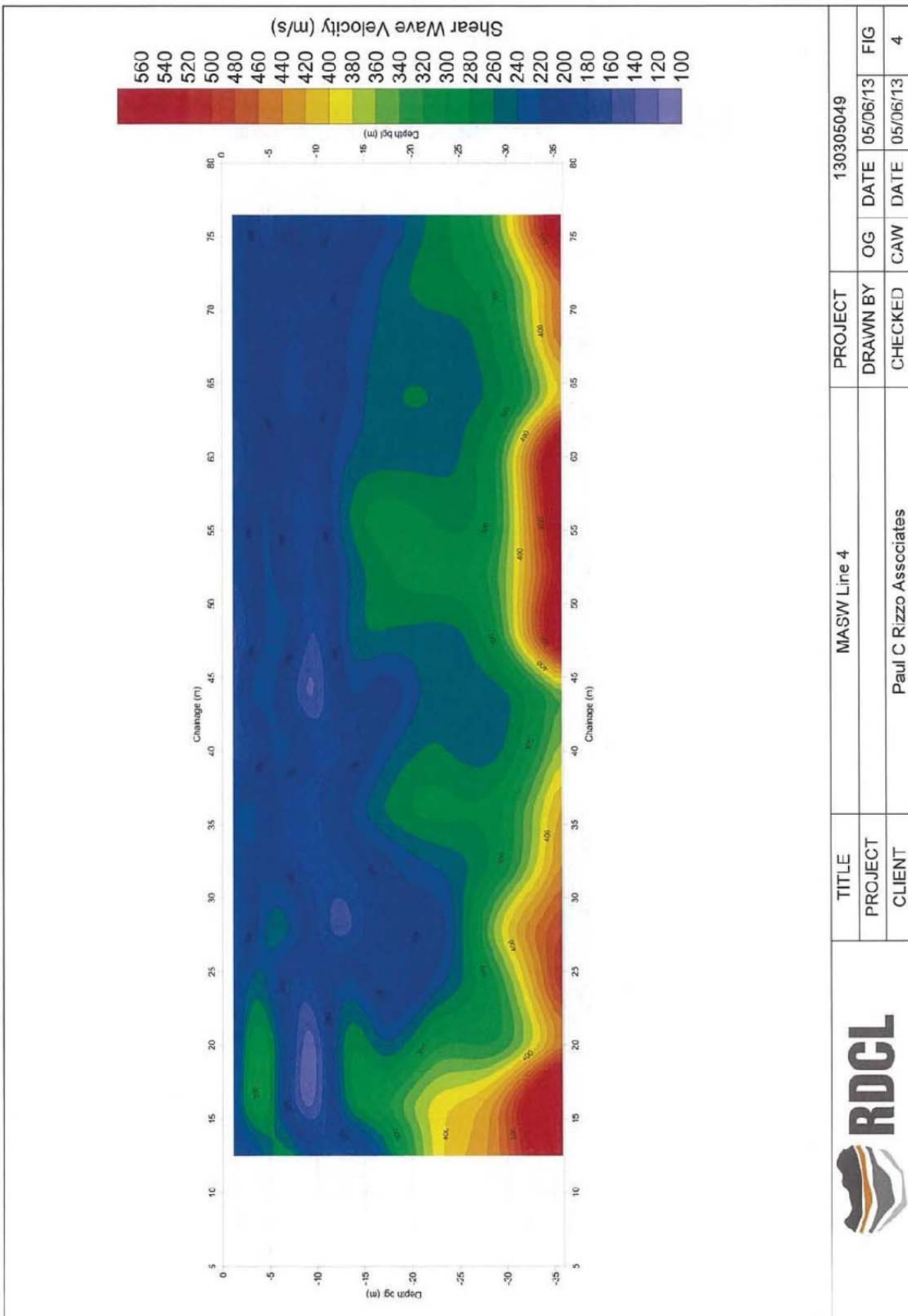




TITLE	MASW Line 2	PROJECT	130305049	
PROJECT		DRAWN BY	OG	DATE 05/06/13
CLIENT	Paul C Rizzo Associates	CHECKED	CAW	DATE 05/06/13
				FIG 2



TITLE	MASW Line 3	PROJECT	130305049	
PROJECT		DRAWN BY	OG	DATE 05/06/13
CLIENT	Paul C Rizzo Associates	CHECKED	CAW	DATE 05/06/13
				FIG 3



TITLE		MASW Line 4		PROJECT		130305049	
PROJECT				DRAWN BY		OG	
CLIENT		Paul C Rizzo Associates		CHECKED		CAW	
				DATE		05/06/13	
				DATE		05/06/13	
				FIG		4	

Appendix A.2 - Building “C”: Static Settlement Analyses

STATIC SETTLEMENT CALCULATION

PROJECT: EAST SECTION OF THE BUILDING
 FOR: CPT - R5
 USING: CPT - R5

INPUT DATA

B = 34 m Footing width
 L = 91 m Footing Length
 q_b = 42 MPa Bearing pressure -> Estimated in this Study
 z_b = 80.7 m Depth of influence: z_b = B * min(4, 2 + 0.22 * (L/B - 1))
 I_{bs} = 0.12 Influence Factor at footing elevation: I_{bs} = min(0.2, 0.1 + 0.011 * (L/B - 1))
 z_s = 20.2 m Depth of maximum influence factor: z_s = B * min(1, 0.5 + 0.055 * (L/B - 1))
 σ_{v,so} = 38 MPa Effective Stress at footing elevation
 σ_{v,ls} = 200 MPa Effective stress at depth of maximum influence factor
 I_{bs} = 0.51 Maximum Influence Factor: I_{bs} = 0.5 + 0.1 * sqrt((q_b - σ_{v,so}) / (σ_{v,so} - σ_{v,ls}))
 C₁ = 0.50 Embodiment factor: C₁ = max(0.5, 1 - 0.5 * (σ_{v,so} / (q_b - σ_{v,so})))
 t = 7 years Time of settlement calculation since construction
 t_r = 1 years Reference Time
 C₂ = 1.37 Time factor: C₂ = 1 + 0.2 * log₁₀(t / (0.1 * t<sub>r}))
 C₃ = 0.94971 Shape factor: C₃ = max(0.73, 1.03 - 0.03 * (L/B))</sub>

Layer	GENERAL PARAMETERS			GRAULAR MATERIAL SETTLEMENTS					IMMEDIATE SETTLEMENTS					COHESIVE MATERIAL SETTLEMENTS					SEC. COMPRESSION					SUMMARY				
	Type	Depth, z _r (m)		Δh (m)	q _s (MPa)	q _b (MPa)	E (MPa)	Δσ _r (kPa)	κ (%)	Δs (mm)	S _p (kPa)	OCR	K	E _s (Mpa)	Δσ _r (kPa)	κ (%)	Δs (mm)	M (Mpa)	ε _{sw} (%)	C _r (m ² /s)	T _{1,90}	t ₉₀ (days)	σ' _{vc} (kPa)	C _g	Δs (mm)	Δs (mm)	s (mm)	
1	granular	0.00	1.00	0.50	1.00	16	3.0	47	0.01	n/a	n/a	n/a	n/a	n/a	n/a	n/a	n/a	n/a	n/a	n/a	n/a	n/a	n/a	n/a	n/a	n/a	0.01	10.0
2	granular	1.00	1.50	1.45	0.90	39	3.0	118	0.00	n/a	n/a	n/a	n/a	n/a	n/a	n/a	n/a	n/a	n/a	n/a	n/a	n/a	n/a	n/a	n/a	n/a	0.00	10.0
3	granular	1.90	3.80	2.85	1.90	66	3.0	197	0.00	n/a	n/a	n/a	n/a	n/a	n/a	n/a	n/a	n/a	n/a	n/a	n/a	n/a	n/a	n/a	n/a	n/a	0.00	10.0
4	granular	3.80	5.10	4.45	1.30	116	3.0	47	0.01	n/a	n/a	n/a	n/a	n/a	n/a	n/a	n/a	n/a	n/a	n/a	n/a	n/a	n/a	n/a	n/a	n/a	0.01	10.0
5	cohesive	5.10	6.26	5.68	1.16	0.23	n/a	n/a	n/a	37.4	1.7	600	22	3.0	0.01	0.11	1.3	3	0.11	2.1E-07	1.781	33	85	0.003	3	4.43	10.0	
6	granular	6.26	8.40	7.33	2.14	0.26	19	3.0	58	n/a	n/a	n/a	n/a	n/a	n/a	n/a	n/a	n/a	n/a	n/a	n/a	n/a	n/a	n/a	n/a	n/a	0.02	5.5
7	granular	8.40	8.90	8.65	0.50	0.29	10	3.0	30	n/a	n/a	n/a	n/a	n/a	n/a	n/a	n/a	n/a	n/a	n/a	n/a	n/a	n/a	n/a	n/a	n/a	0.01	5.5
8	granular	8.90	12.02	10.46	3.12	0.32	29	3.0	87	n/a	n/a	n/a	n/a	n/a	n/a	n/a	n/a	n/a	n/a	n/a	n/a	n/a	n/a	n/a	n/a	n/a	0.03	5.5
9	cohesive	12.02	13.16	12.59	1.14	0.37	n/a	n/a	n/a	143.8	4.0	400	58	2.4	0.00	0.01	0.1	22	0.01	2.0E-05	1.781	0.3	137	0.001	1	0.75	5.5	
10	granular	13.16	14.24	13.70	1.08	0.39	15	3.0	46	n/a	n/a	n/a	n/a	n/a	n/a	n/a	n/a	n/a	n/a	n/a	n/a	n/a	n/a	n/a	n/a	n/a	0.02	4.7
11	cohesive	14.24	15.62	14.93	1.38	0.41	n/a	n/a	n/a	100.1	2.5	500	50	2.2	0.00	0.02	0.3	10	0.02	2.8E-06	1.781	4	155	0.002	2	2.15	4.7	
12	granular	15.62	16.94	16.28	1.32	0.44	12	3.0	37	n/a	n/a	n/a	n/a	n/a	n/a	n/a	n/a	n/a	n/a	n/a	n/a	n/a	n/a	n/a	n/a	n/a	0.04	2.6
13	granular	16.94	17.84	17.39	0.90	0.46	18	3.0	53	n/a	n/a	n/a	n/a	n/a	n/a	n/a	n/a	n/a	n/a	n/a	n/a	n/a	n/a	n/a	n/a	n/a	0.02	2.5
14	cohesive	17.84	20.22	19.03	2.38	0.49	n/a	n/a	n/a	152.4	3.2	500	76	2.0	0.00	0.01	0.2	19	0.01	5.8E-06	1.781	5	187	0.001	2	2.28	2.5	
15	granular	20.22	80.67	50.44	60.45	0.36	50	3	150	n/a	n/a	n/a	n/a	n/a	n/a	n/a	n/a	n/a	n/a	n/a	n/a	n/a	n/a	n/a	n/a	n/a	0.25	0.3
													0.2						1.9						7.4	10		

TOTAL SETTLEMENT = 10 mm

STATIC SETTLEMENT CALCULATION

PROJECT: EAST SECTION OF THE BUILDING
 FOR: CPT - R5
 USING: CPT - R5

INPUT DATA

B =	34	m	Footing width
L =	91	m	Footing Length
q _b =	56	kPa	Bearing pressure -> From PCR report
z _b =	80.7	m	Depth of influence: z _b = B * min(4, 2 + 0.22 * (L/B - 1))
I _{ps} =	0.12		Influence Factor at footing elevation: I _{ps} = min(0.2, 0.1 + 0.011 * (L/B - 1))
z ₀ =	20.2	m	Depth of maximum influence factor: z ₀ = B * min(1, 0.5 + 0.055 * (L/B - 1))
σ' _{vertical} =	38	kPa	Effective Stress at footing elevation
σ' _{vertical} =	173	kPa	Effective stress at depth of maximum influence factor
I _{ps} =	0.53		Maximum Influence Factor: I _{ps} = 0.5 + 0.1 * sqrt((q _b - σ' _{vertical}) / (q _b - σ' _{vertical}))
C ₁ =	0.50		Embedment factor: C ₁ = max(0.5, 1 - 0.5 * (σ' _{vertical} / (q _b - σ' _{vertical})))
t =	7	years	Time of settlement calculation since construction
t _r =	1	years	Reference Time
C ₂ =	1.37		Time factor: C ₂ = 1 + 0.2 * log ₁₀ (t / (0.1 * t _{r}))}
C ₃ =	0.94971		Shape factor: C ₃ = max(0.73, 1.03 - 0.03 * (L/B))

Layer	GENERAL PARAMETERS			GRAULAR MATERIAL SETTLEMENTS					COHESIVE MATERIAL SETTLEMENTS										SUMMARY							
	Type	Depth, z _r (m)		I _r	q _b (MPa)	q _e	E (MPa)	Δs (mm)	S _u (kPa)	OCR	K	E _y (MPa)	Δσ _r (kPa)	ε	Δs (mm)	ε _{sw} (%)	M (MPa)	C _v (m ² /s)	T _{1,90}	t ₉₀ (days)	σ' _{vd} (kPa)	C _α	Δs (mm)	Δs (mm)	s (mm)	
1	granular	0.00	1.00	0.50	1.00	0.13	16	3.0	47	0.03	n/a	n/a	n/a	n/a	n/a	n/a	n/a	n/a	n/a	n/a	59	n/a	n/a	n/a	0.03	20.7
2	granular	1.00	1.90	1.45	0.90	0.15	39	3.0	118	0.01	n/a	n/a	n/a	n/a	n/a	n/a	n/a	n/a	n/a	n/a	66	n/a	n/a	n/a	0.01	20.7
3	granular	1.90	3.80	2.85	1.90	0.18	66	3.0	197	0.02	n/a	n/a	n/a	n/a	n/a	n/a	n/a	n/a	n/a	n/a	76	n/a	n/a	n/a	0.02	20.7
4	granular	3.80	5.10	4.45	1.30	0.21	16	3.0	47	0.07	n/a	n/a	n/a	n/a	n/a	n/a	n/a	n/a	n/a	n/a	87	n/a	n/a	n/a	0.07	20.6
5	cohesive	5.10	6.26	5.68	1.16	0.24	n/a	n/a	n/a	37.4	1.7	600	22	14.5	0.05	0.6	3	2.1E-07	1.781	33	96	0.004	3	10.17	20.6	
6	granular	6.26	8.40	7.33	2.14	0.27	19	3.0	58	0.12	n/a	n/a	n/a	n/a	n/a	n/a	n/a	n/a	n/a	n/a	108	n/a	n/a	n/a	0.12	10.4
7	granular	8.40	8.90	8.65	0.50	0.30	30	3.0	30	0.06	n/a	n/a	n/a	n/a	n/a	n/a	n/a	n/a	n/a	n/a	118	n/a	n/a	n/a	0.06	10.3
8	granular	8.90	12.02	10.46	3.12	0.33	29	3.0	87	0.14	n/a	n/a	n/a	n/a	n/a	n/a	n/a	n/a	n/a	n/a	131	n/a	n/a	n/a	0.14	10.2
9	cohesive	12.02	13.16	12.59	1.14	0.38	n/a	n/a	n/a	143.8	4.0	400	58	11.5	0.02	0.2	22	2.0E-05	1.781	0.3	146	0.001	1	1.39	10.1	
10	granular	13.16	14.24	13.70	1.08	0.40	15	3.0	46	0.11	n/a	n/a	n/a	n/a	n/a	n/a	n/a	n/a	n/a	n/a	155	n/a	n/a	n/a	0.11	8.7
11	cohesive	14.24	15.62	14.93	1.38	0.42	n/a	n/a	n/a	100.1	2.5	500	50	10.7	0.02	0.2	10	2.6E-06	1.781	4	164	0.002	2	3.60	8.6	
12	granular	15.62	16.84	16.28	1.32	0.45	12	3.0	37	0.19	n/a	n/a	n/a	n/a	n/a	n/a	n/a	n/a	n/a	n/a	174	n/a	n/a	n/a	0.19	5.0
13	granular	16.84	17.84	17.39	0.90	0.48	18	3.0	53	0.09	n/a	n/a	n/a	n/a	n/a	n/a	n/a	n/a	n/a	n/a	182	n/a	n/a	n/a	0.09	4.8
14	cohesive	17.84	20.22	19.03	2.38	0.51	n/a	n/a	n/a	152.4	3.2	500	76	9.5	0.01	0.2	19	5.8E-06	1.781	5	194	0.001	2	3.45	4.7	
15	granular	20.22	80.67	50.44	60.45	0.27	50	3	150	1.25	n/a	n/a	n/a	n/a	n/a	n/a	n/a	n/a	n/a	n/a	431	n/a	n/a	n/a	1.25	1.3

TOTAL SETTLEMENT = 21 mm

Appendix A.3 - Building “C”: Simplified Liquefaction Triggering and Volumetric- Induced Deformation Analyses

Roberto Luque
 University of California, Berkeley
 435 Davis Hall
 Berkeley, CA, 94720

LIQUEFACTION ANALYSIS REPORT

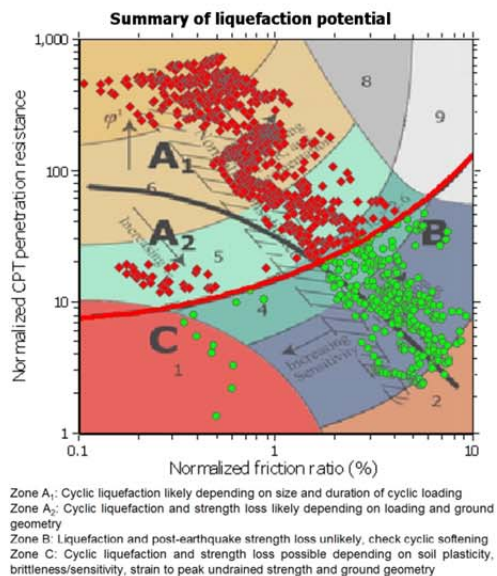
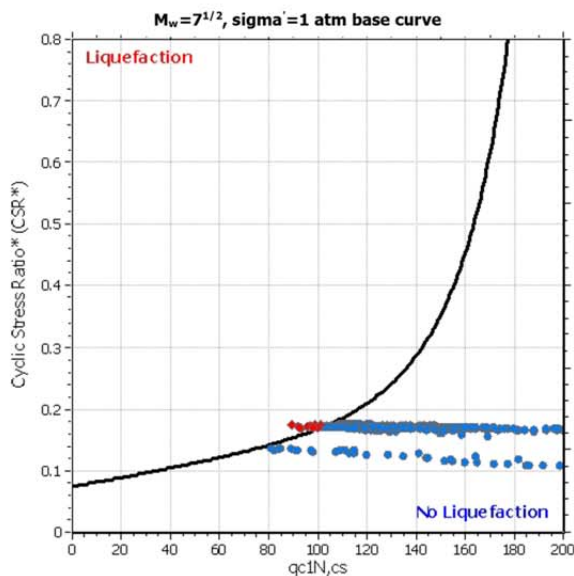
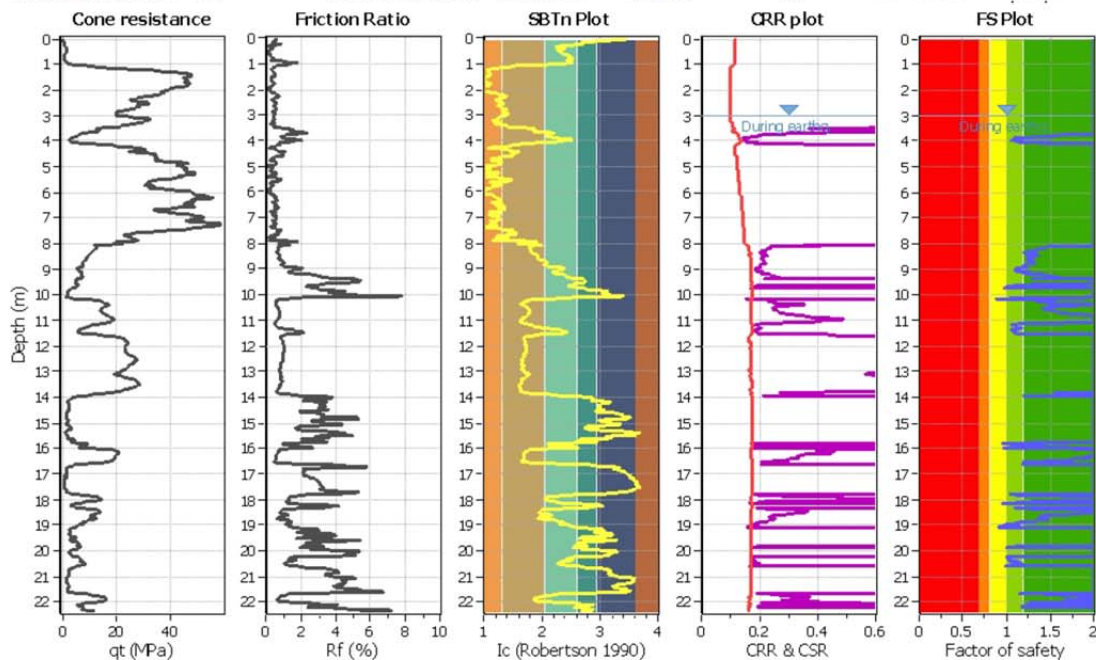
Project title : C Building Event: Darfield

Location : Christchurch, NZ

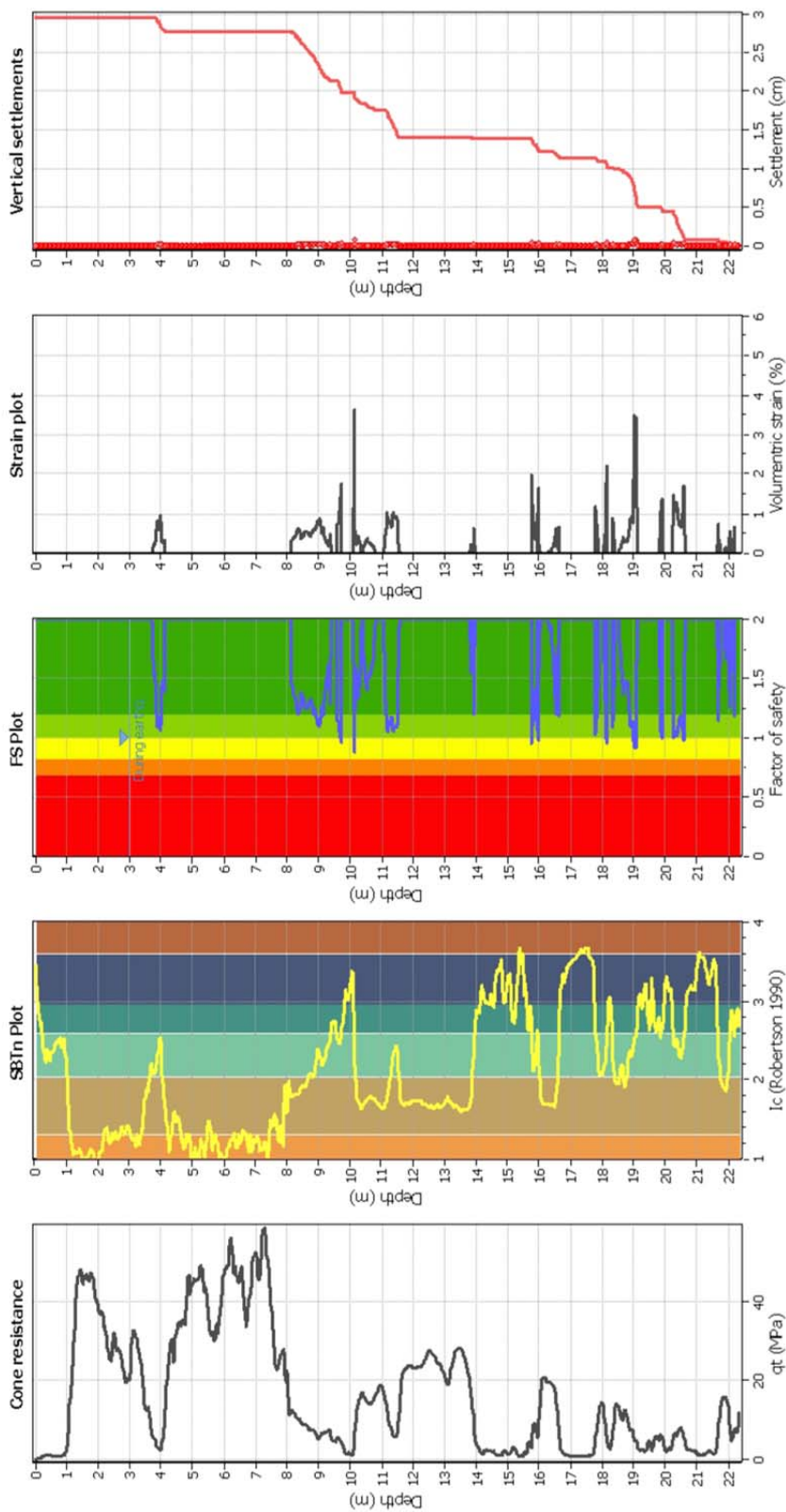
CPT file : R7B

Input parameters and analysis data

Analysis method:	B&I (2014)	G.W.T. (in-situ):	3.70 m	Use fill:	No	Clay like behavior applied:	Sands only
Fines correction method:	B&I (2014)	G.W.T. (earthq.):	3.00 m	Fill height:	N/A	Limit depth applied:	No
Points to test:	Based on Ic value	Average results interval:	3	Fill weight:	N/A	Limit depth:	N/A
Earthquake magnitude M_w :	7.10	Ic cut-off value:	2.60	Trans. detect. applied:	No	MSF method:	Method
Peak ground acceleration:	0.20	Unit weight calculation:	Based on SBT	K_u applied:	Yes		



Estimation of post-earthquake settlements



Abbreviations

- q_t : Total cone resistance (cone resistance q_c corrected for pore water effects)
- I_c : Soil Behaviour Type Index
- FS: Calculated Factor of Safety against liquefaction
- Volumetric strain: Post-liquefaction volumetric strain

Roberto Luque
 University of California, Berkeley
 435 Davis Hall
 Berkeley, CA, 94720

LIQUEFACTION ANALYSIS REPORT

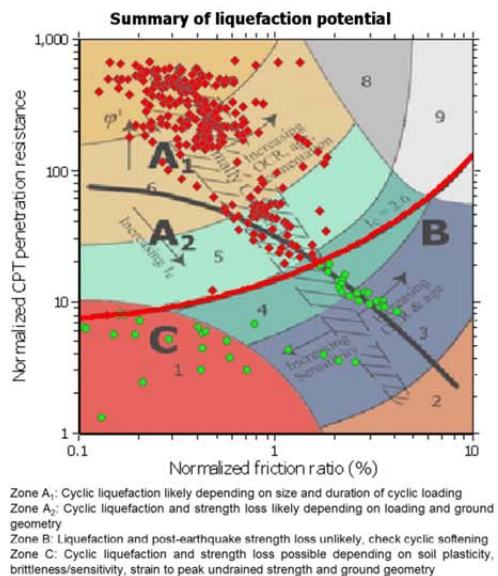
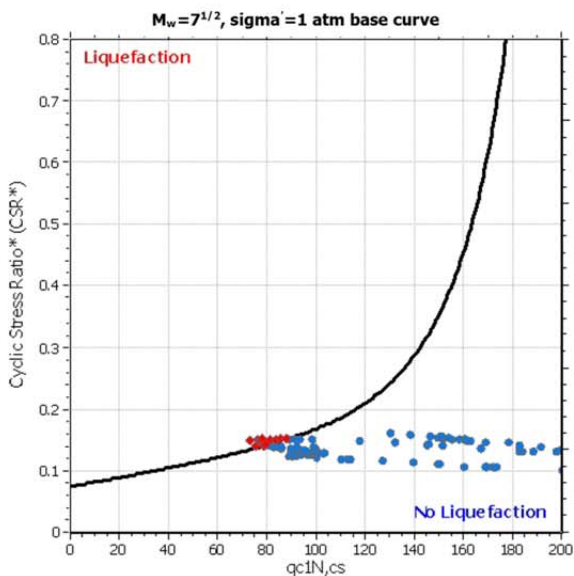
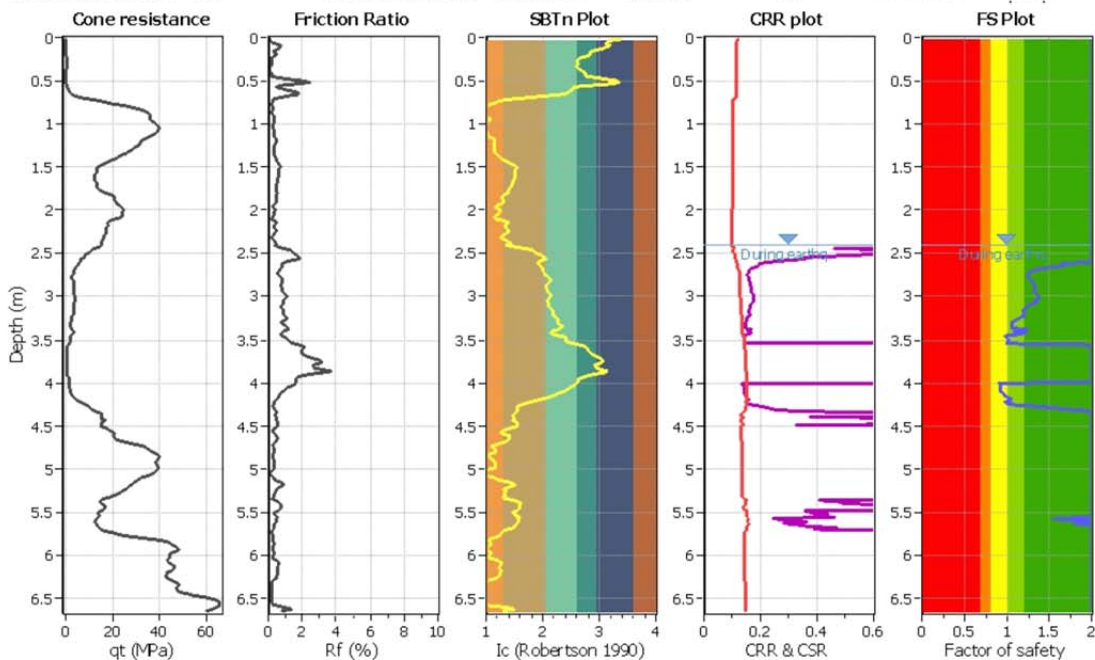
Project title : C Building Event: Darfield

Location : Christchurch, NZ

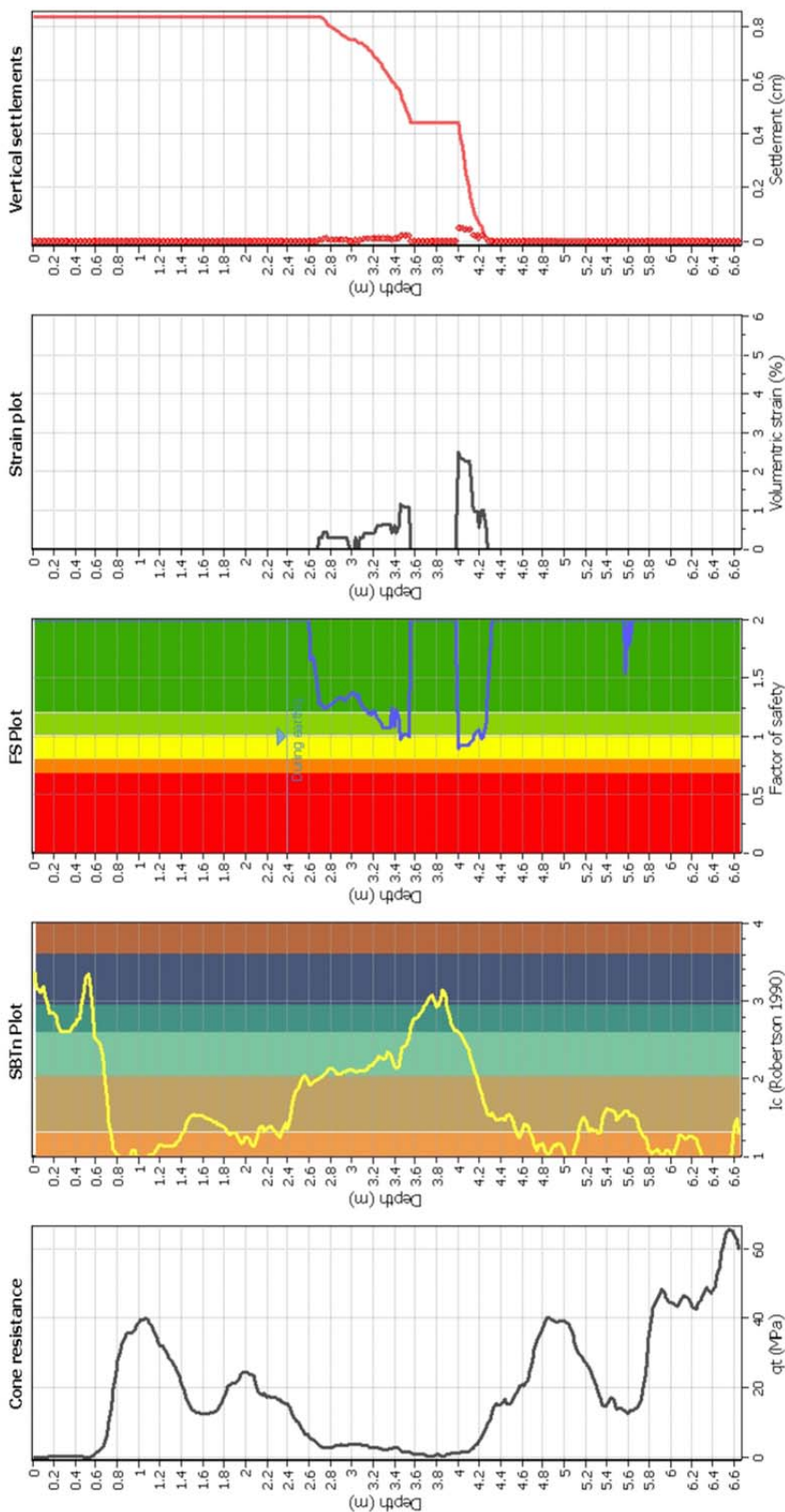
CPT file : R6

Input parameters and analysis data

Analysis method:	B&I (2014)	G.W.T. (in-situ):	3.20 m	Use fill:	No	Clay like behavior applied:	Sands only
Fines correction method:	B&I (2014)	G.W.T. (earthq.):	2.40 m	Fill height:	N/A	Limit depth applied:	No
Points to test:	Based on Ic value	Average results interval:	3	Fill weight:	N/A	Limit depth:	N/A
Earthquake magnitude M_w :	7.10	Ic cut-off value:	2.60	Trans. detect. applied:	No	Limit depth:	N/A
Peak ground acceleration:	0.20	Unit weight calculation:	Based on SBT	K_σ applied:	Yes	MSF method:	Method



Estimation of post-earthquake settlements



Abbreviations

- q_t: Total cone resistance (cone resistance q_c corrected for pore water effects)
- I_c: Soil Behaviour Type Index
- FS: Calculated Factor of Safety against liquefaction
- Volumetric strain: Post-liquefaction volumetric strain

Roberto Luque
 University of California, Berkeley
 435 Davis Hall
 Berkeley, CA, 94720

LIQUEFACTION ANALYSIS REPORT

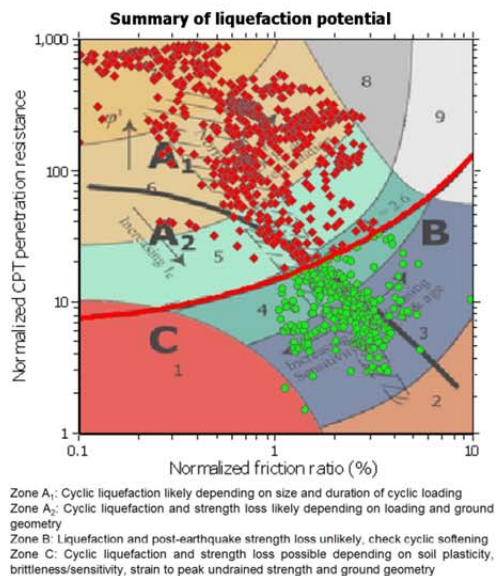
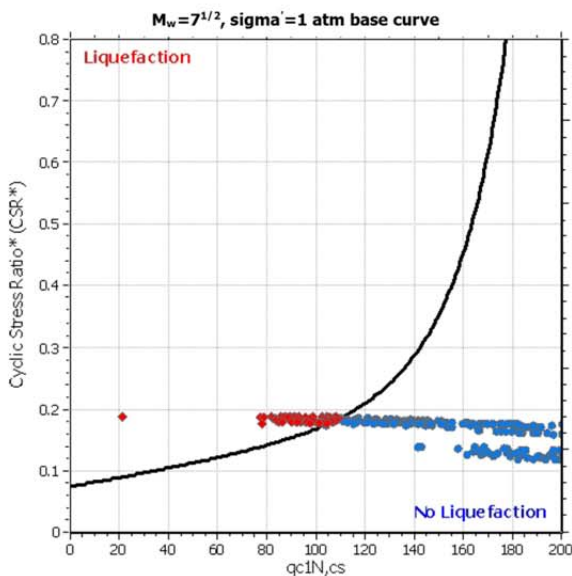
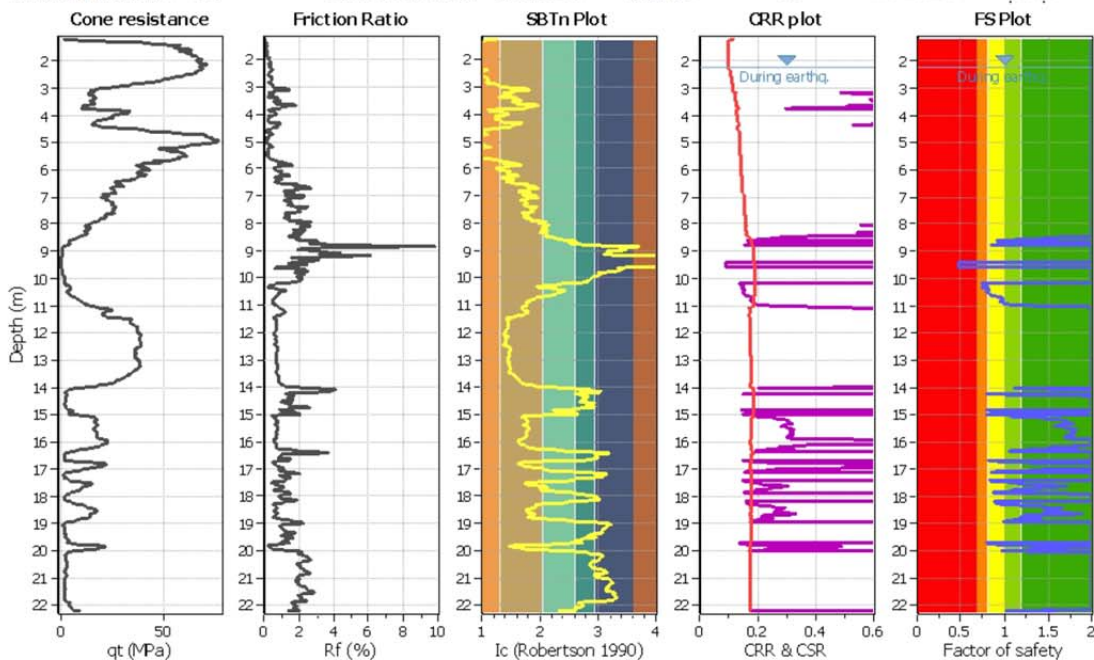
Project title : C Building Event: Darfield

Location : Christchurch, NZ

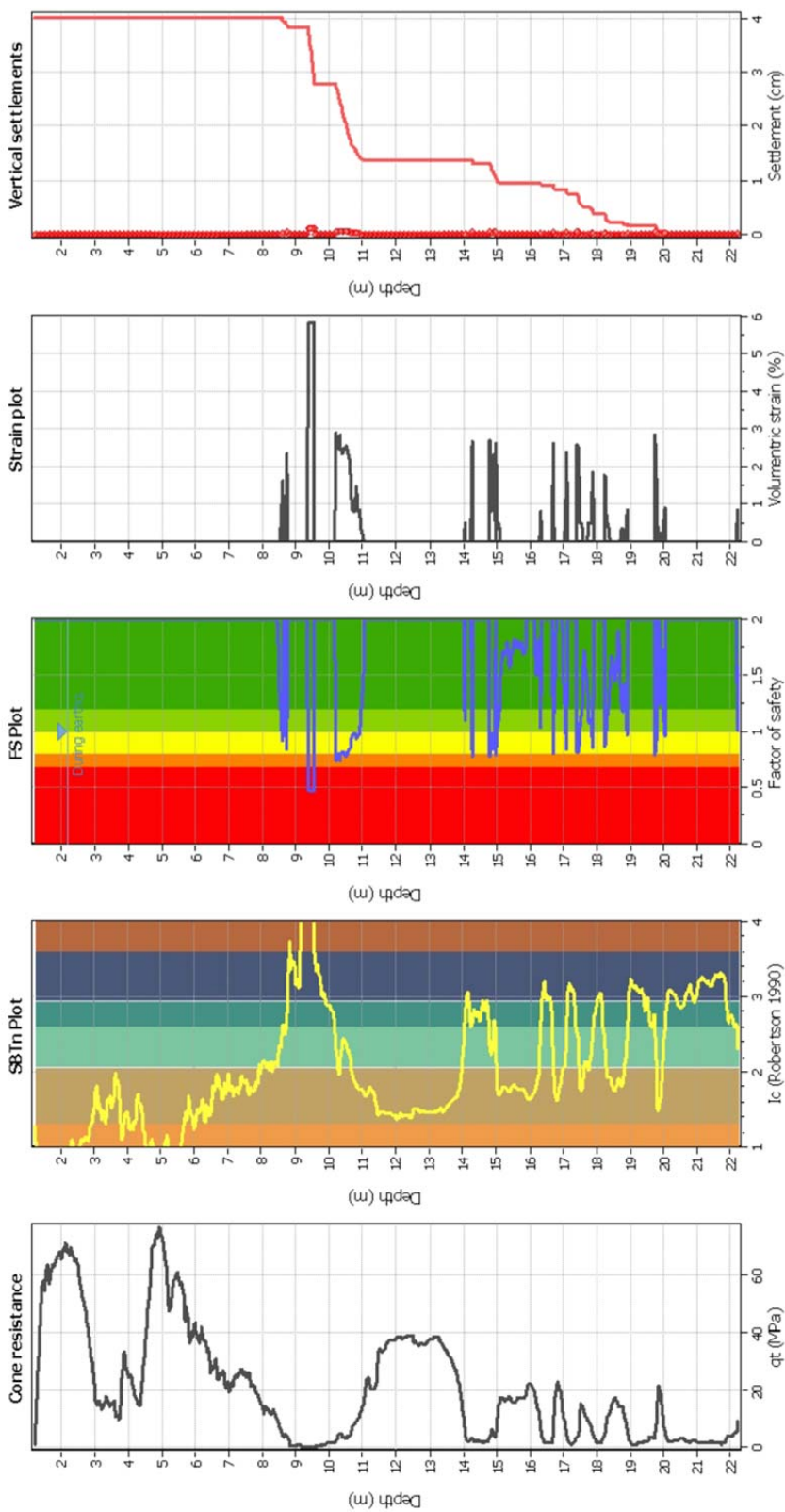
CPT file : R2B

Input parameters and analysis data

Analysis method:	B&I (2014)	G.W.T. (in-situ):	2.90 m	Use fill:	No	Clay like behavior applied:	Sands only
Fines correction method:	B&I (2014)	G.W.T. (earthq.):	2.20 m	Fill height:	N/A	Limit depth applied:	No
Points to test:	Based on Ic value	Average results interval:	3	Fill weight:	N/A	Limit depth:	N/A
Earthquake magnitude M_w :	7.10	Ic cut-off value:	2.60	Trans. detect. applied:	No	MSF method:	Method
Peak ground acceleration:	0.20	Unit weight calculation:	Based on SBT	K_s applied:	Yes		



Estimation of post-earthquake settlements



Abbreviations

- q_t: Total cone resistance (cone resistance q_c corrected for pore water effects)
- I_c: Soil Behaviour Type Index
- FS: Calculated Factor of Safety against liquefaction
- Volumetric strain: Post-liquefaction volumetric strain

Roberto Luque
 University of California, Berkeley
 435 Davis Hall
 Berkeley, CA, 94720

LIQUEFACTION ANALYSIS REPORT

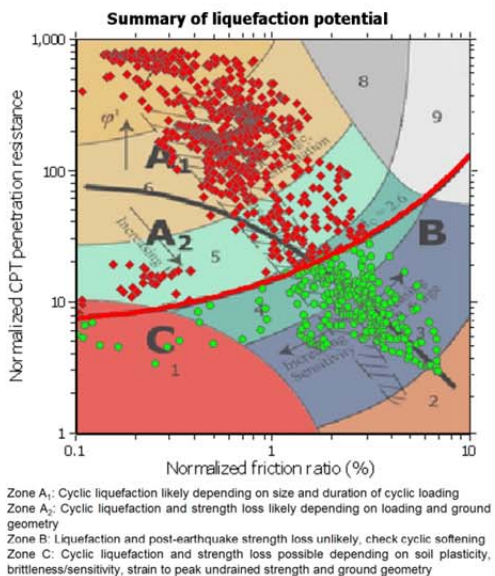
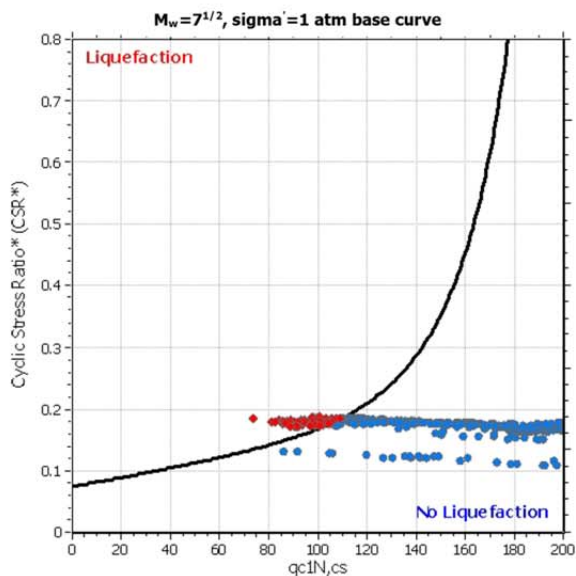
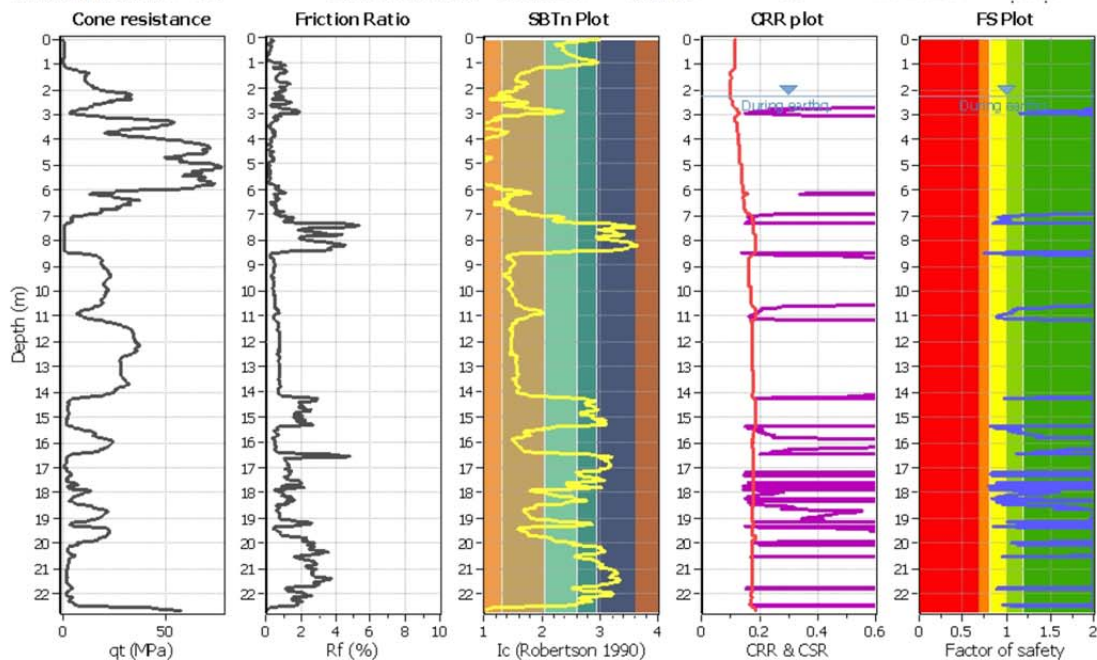
Project title : C Building Event: Darfield

Location : Christchurch, NZ

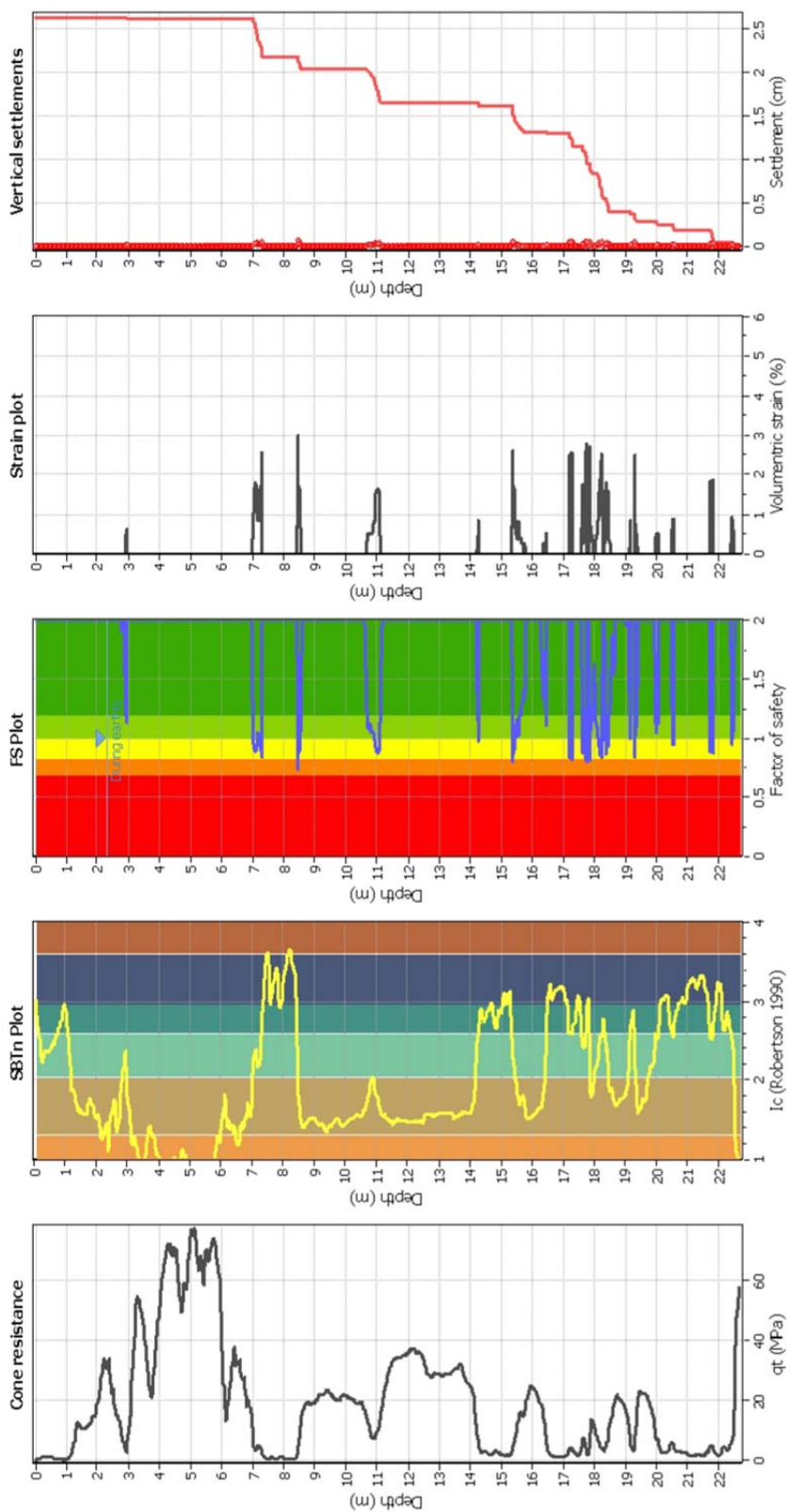
CPT file : R5

Input parameters and analysis data

Analysis method:	B&I (2014)	G.W.T. (in-situ):	2.90 m	Use fill:	No	Clay like behavior applied:	No	Sands only
Fines correction method:	B&I (2014)	G.W.T. (earthq.):	2.30 m	Fill height:	N/A	Limit depth applied:	No	
Points to test:	Based on Ic value	Average results interval:	3	Fill weight:	N/A	Limit depth:	N/A	
Earthquake magnitude M_w :	7.10	Ic cut-off value:	2.60	Trans. detect. applied:	No	MSF method:	Method	
Peak ground acceleration:	0.20	Unit weight calculation:	Based on SBT	K_s applied:	Yes			



Estimation of post-earthquake settlements



Abbreviations

- q_t: Total cone resistance (cone resistance q_c corrected for pore water effects)
- I_c: Soil Behaviour Type Index
- FS: Calculated Factor of Safety against liquefaction
- Volumetric strain: Post-liquefaction volumetric strain

Roberto Luque
 University of California, Berkeley
 435 Davis Hall
 Berkeley, CA, 94720

LIQUEFACTION ANALYSIS REPORT

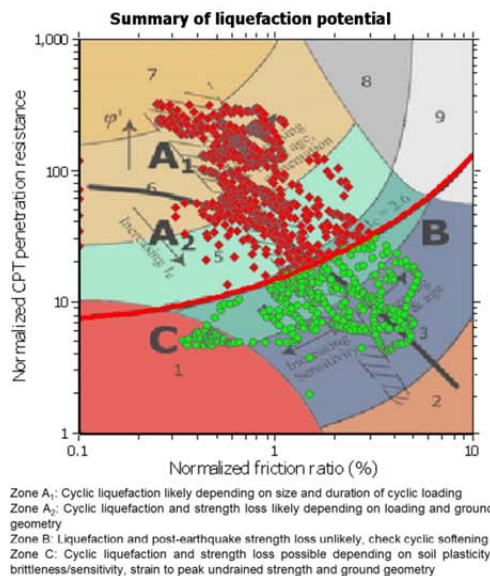
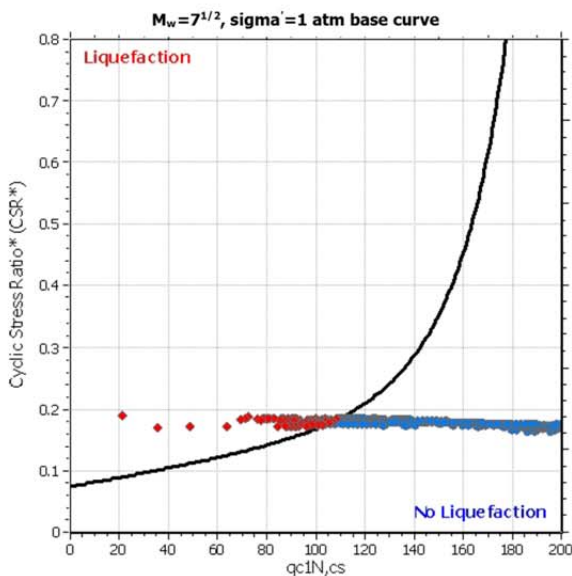
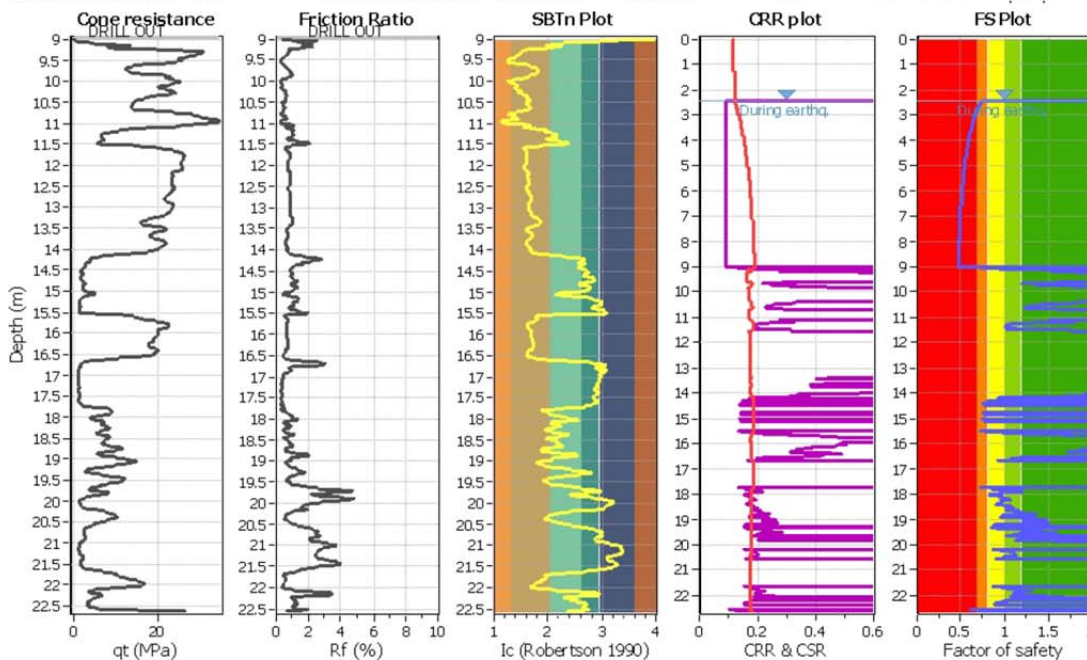
Project title : C Building Event: Darfield

Location : Christchurch, NZ

CPT file : CPT-02

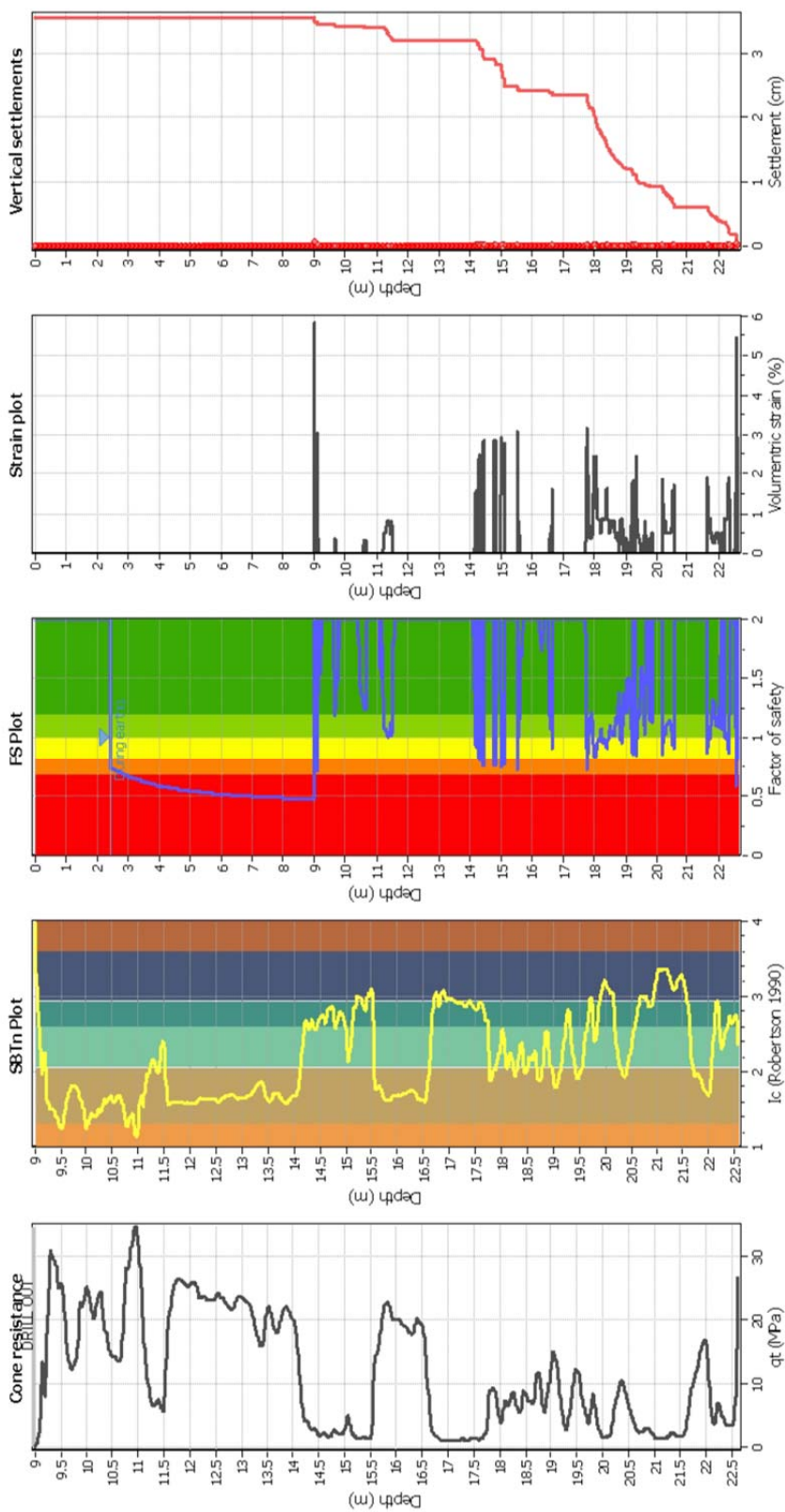
Input parameters and analysis data

Analysis method:	B&I (2014)	G.W.T. (in-situ):	3.00 m	Use fill:	No	Clay like behavior applied:	No	Sands only
Fines correction method:	B&I (2014)	G.W.T. (earthq.):	2.44 m	Fill height:	N/A	Limit depth applied:	No	
Points to test:	Based on Ic value	Average results interval:	3	Fill weight:	N/A	Limit depth:	N/A	
Earthquake magnitude M_w :	7.10	Ic cut-off value:	2.60	Trans. detect. applied:	No	MSF method:	N/A	
Peak ground acceleration:	0.20	Unit weight calculation:	Based on SBT	K_s applied:	Yes			



Zone A₁: Cyclic liquefaction likely depending on size and duration of cyclic loading
 Zone A₂: Cyclic liquefaction and strength loss likely depending on loading and ground geometry
 Zone B: Liquefaction and post-earthquake strength loss unlikely, check cyclic softening
 Zone C: Cyclic liquefaction and strength loss possible depending on soil plasticity, brittleness/sensitivity, strain to peak undrained strength and ground geometry

Estimation of post-earthquake settlements



Abbreviations

- q_t : Total cone resistance (cone resistance q_c corrected for pore water effects)
- I_c : Soil Behaviour Type Index
- FS: Calculated Factor of Safety against liquefaction
- Volumetric strain: Post-liquefaction volumetric strain

Roberto Luque
 University of California, Berkeley
 435 Davis Hall
 Berkeley, CA, 94720

LIQUEFACTION ANALYSIS REPORT

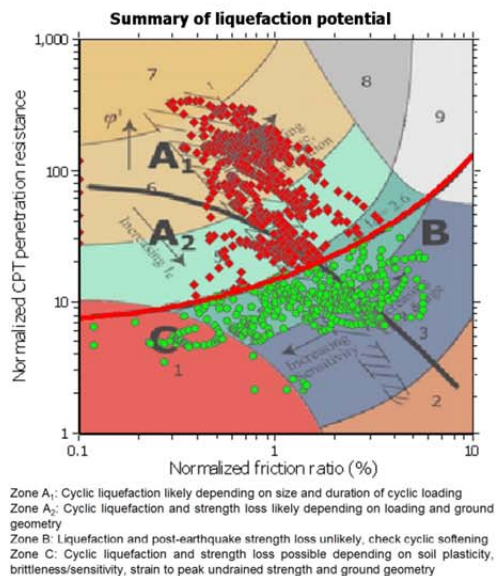
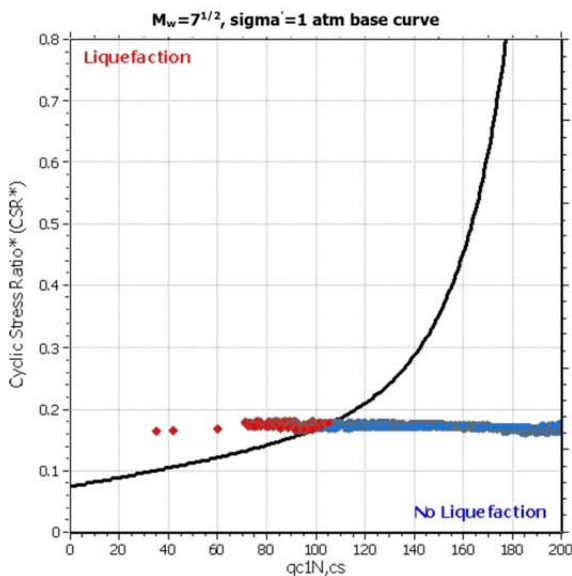
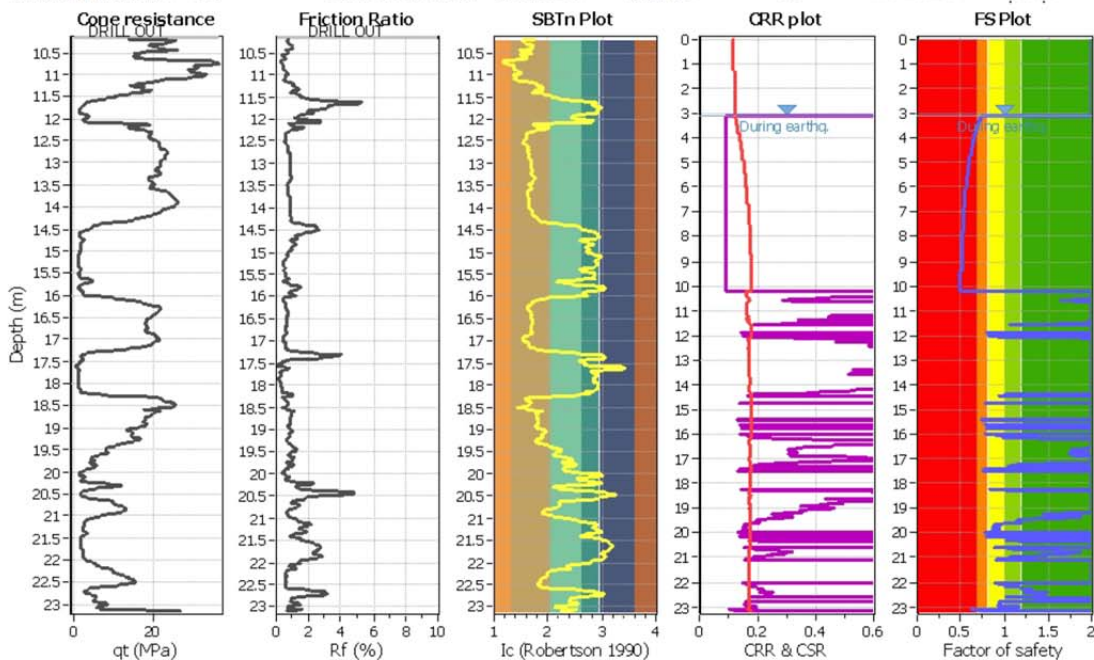
Project title : C Building Event: Darfield

Location : Christchurch, NZ

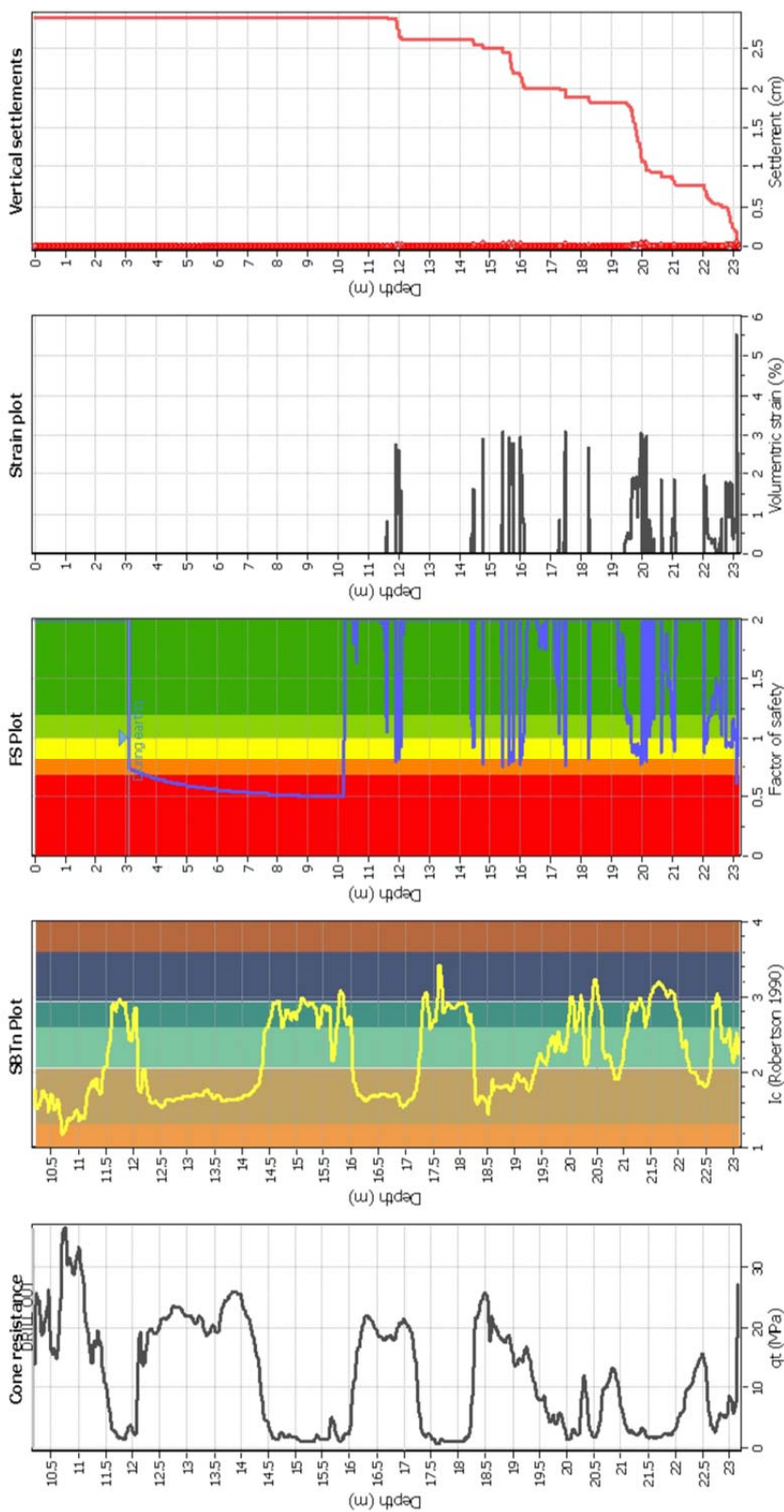
CPT file : CPT-03

Input parameters and analysis data

Analysis method:	B&I (2014)	G.W.T. (in-situ):	3.00 m	Use fill:	No	Clay like behavior applied:	No	Sands only
Fines correction method:	B&I (2014)	G.W.T. (earthq.):	3.10 m	Fill height:	N/A	Limit depth applied:	No	
Points to test:	Based on Ic value	Average results interval:	3	Fill weight:	N/A	Limit depth:	N/A	
Earthquake magnitude M_w :	7.10	Ic cut-off value:	2.60	Trans. detect. applied:	No	MSF method:	N/A	
Peak ground acceleration:	0.20	Unit weight calculation:	Based on SBT	K_s applied:	Yes			



Estimation of post-earthquake settlements



Abbreviations

- q: Total cone resistance (cone resistance q_c corrected for pore water effects)
- I_c: Soil Behaviour Type Index
- FS: Calculated Factor of Safety against liquefaction
- Volumetric strain: Post-liquefaction volumetric strain

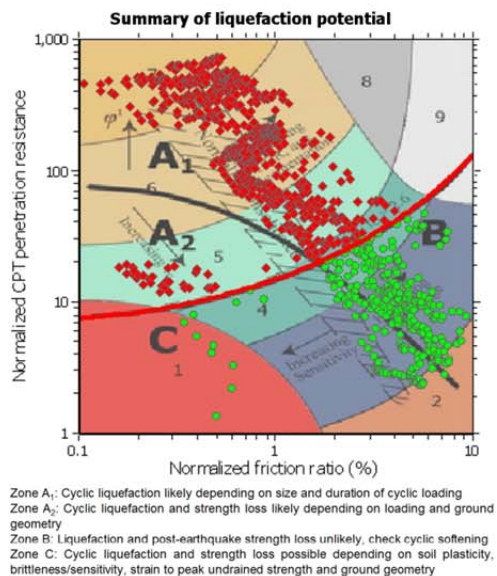
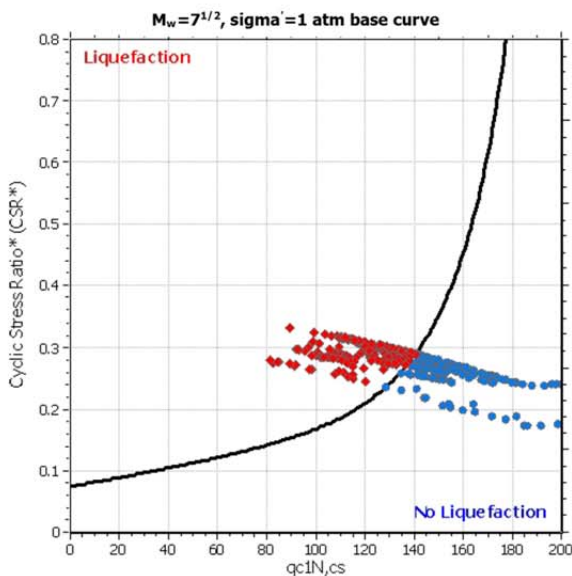
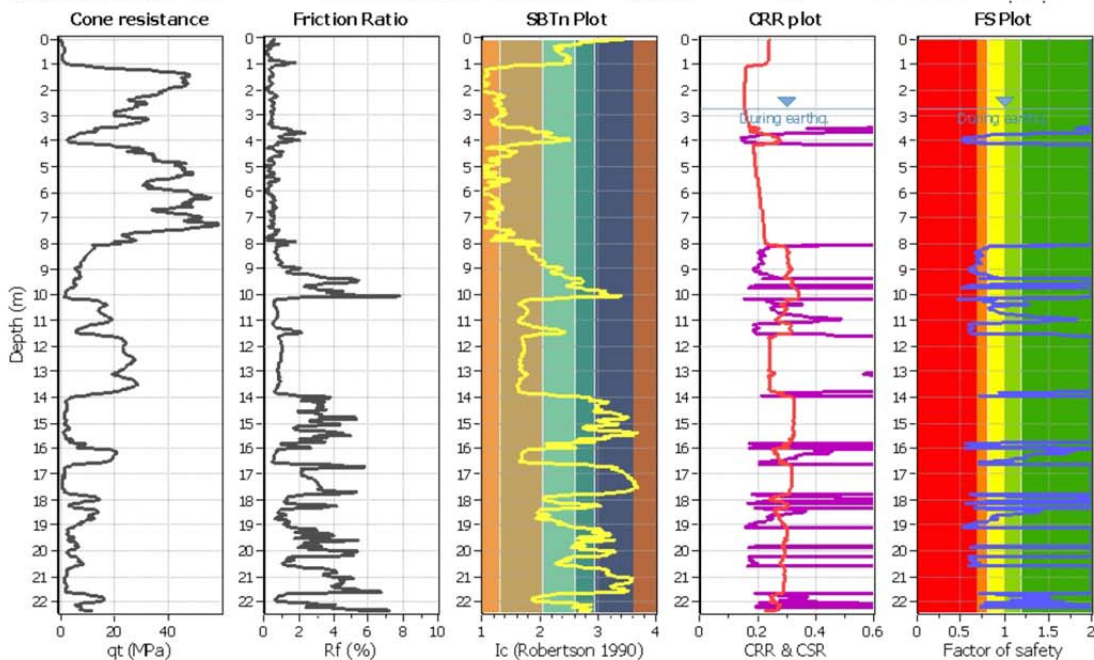
Roberto Luque
 University of California, Berkeley
 435 Davis Hall
 Berkeley, CA, 94720

LIQUEFACTION ANALYSIS REPORT

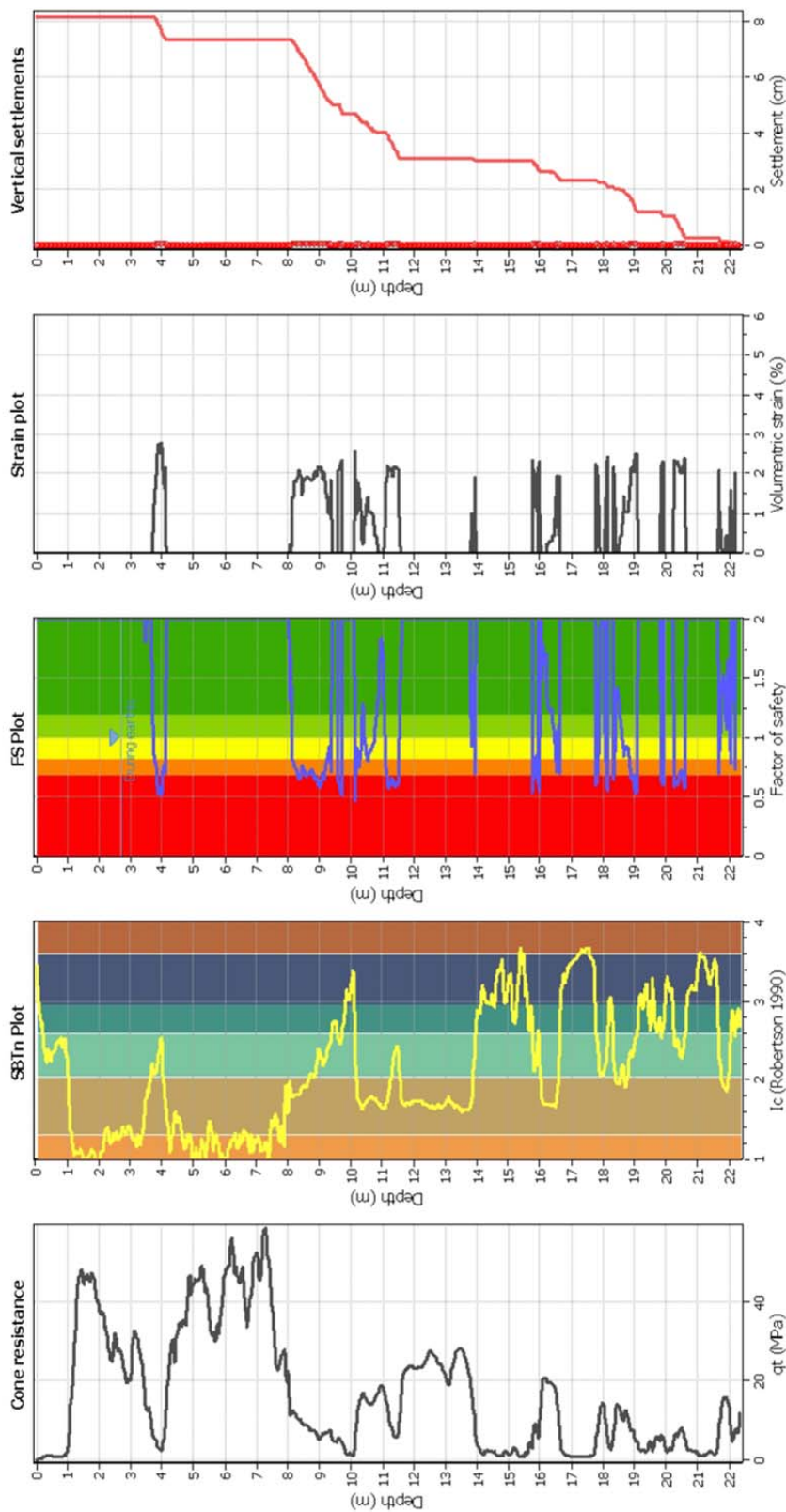
Project title : C Building Event: Christchurch Location : Christchurch, NZ
CPT file : R7B

Input parameters and analysis data

Analysis method:	B&I (2014)	G.W.T. (in-situ):	3.70 m	Use fill:	No	Clay like behavior applied:	No	Sands only
Fines correction method:	B&I (2014)	G.W.T. (earthq.):	2.70 m	Fill height:	N/A	Limit depth applied:	No	
Points to test:	Based on Ic value	Average results interval:	3	Fill weight:	N/A	Limit depth:	N/A	
Earthquake magnitude M_w :	6.20	Ic cut-off value:	2.60	Trans. detect. applied:	No	MSF method:	Method	
Peak ground acceleration:	0.43	Unit weight calculation:	Based on SBT	K_s applied:	Yes			



Estimation of post-earthquake settlements



Abbreviations

- q_t: Total cone resistance (cone resistance q_c corrected for pore water effects)
- I_c: Soil Behaviour Type Index
- FS: Calculated Factor of Safety against liquefaction
- Volumetric strain: Post-liquefaction volumetric strain

Roberto Luque
 University of California, Berkeley
 435 Davis Hall
 Berkeley, CA, 94720

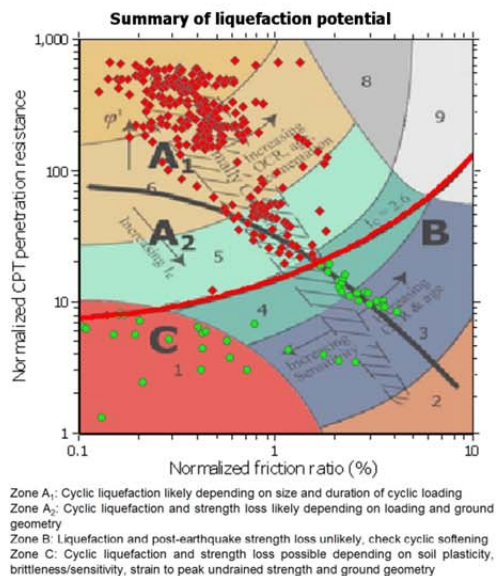
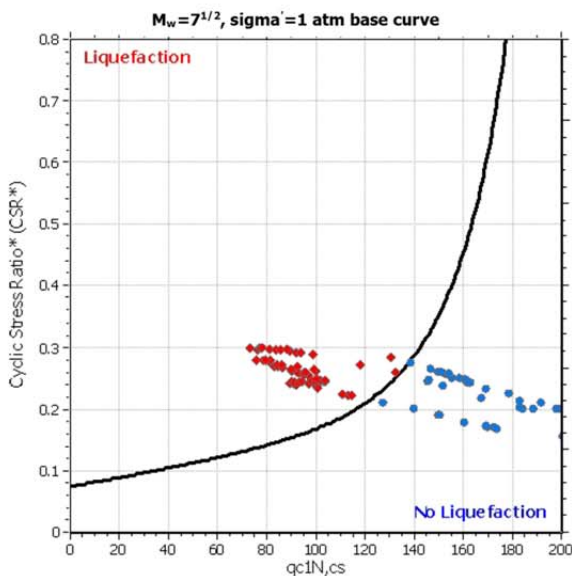
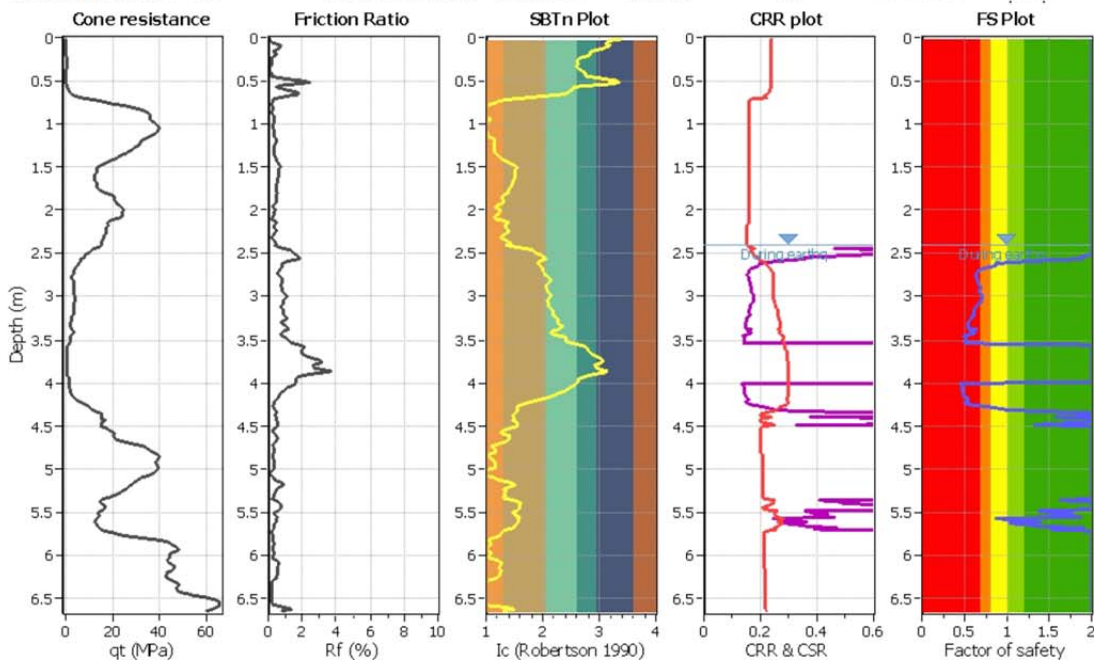
LIQUEFACTION ANALYSIS REPORT

Project title : C Building Event: Christchurch Location : Christchurch, NZ

CPT file : R6

Input parameters and analysis data

Analysis method:	B&I (2014)	G.W.T. (in-situ):	3.20 m	Use fill:	No	Clay like behavior applied:	No	Sands only
Fines correction method:	B&I (2014)	G.W.T. (earthq.):	2.40 m	Fill height:	N/A	Limit depth applied:	No	
Points to test:	Based on Ic value	Average results interval:	3	Fill weight:	N/A	Limit depth:	N/A	
Earthquake magnitude M_w :	6.20	Ic cut-off value:	2.60	Trans. detect. applied:	No	MSF method:	Method	
Peak ground acceleration:	0.43	Unit weight calculation:	Based on SBT	K_σ applied:	Yes			



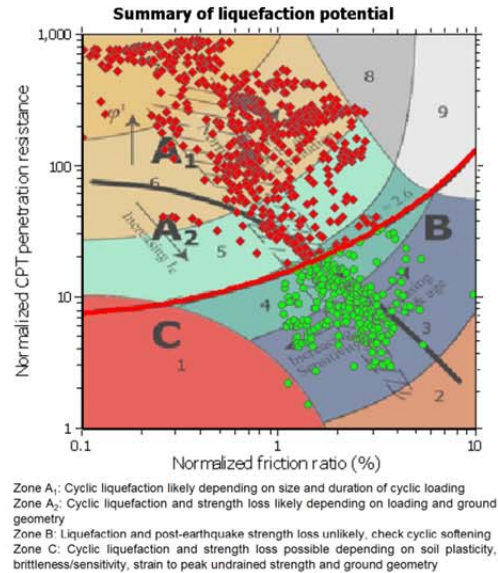
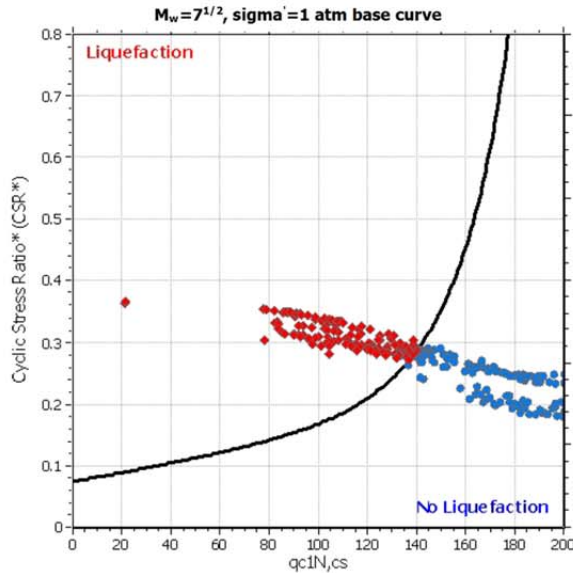
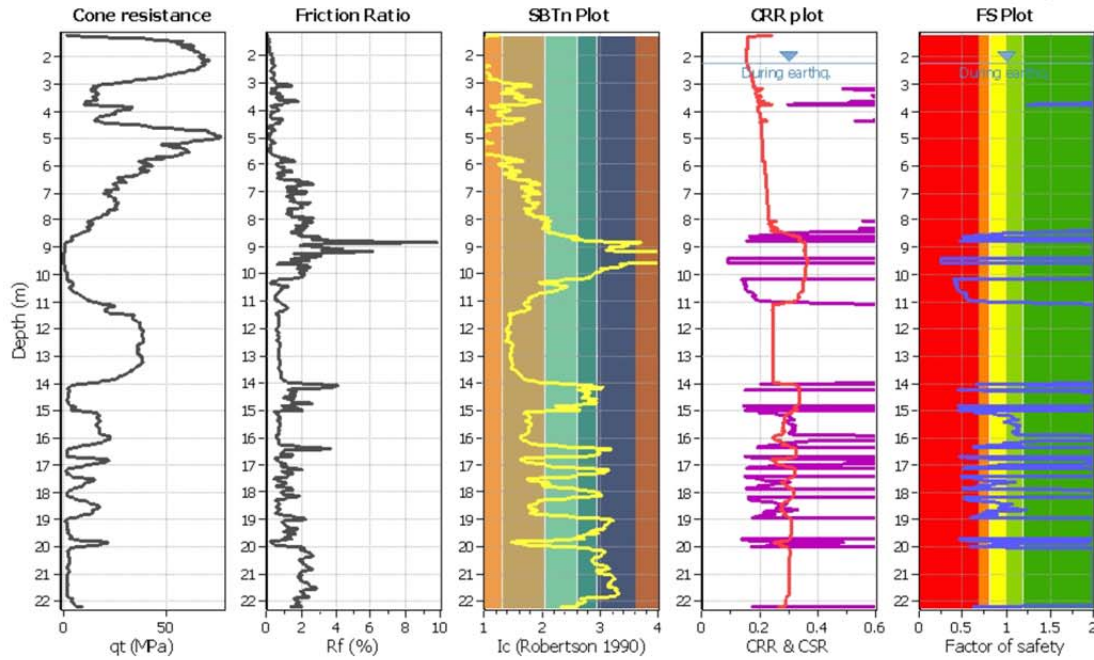
Roberto Luque
 University of California, Berkeley
 435 Davis Hall
 Berkeley, CA, 94720

LIQUEFACTION ANALYSIS REPORT

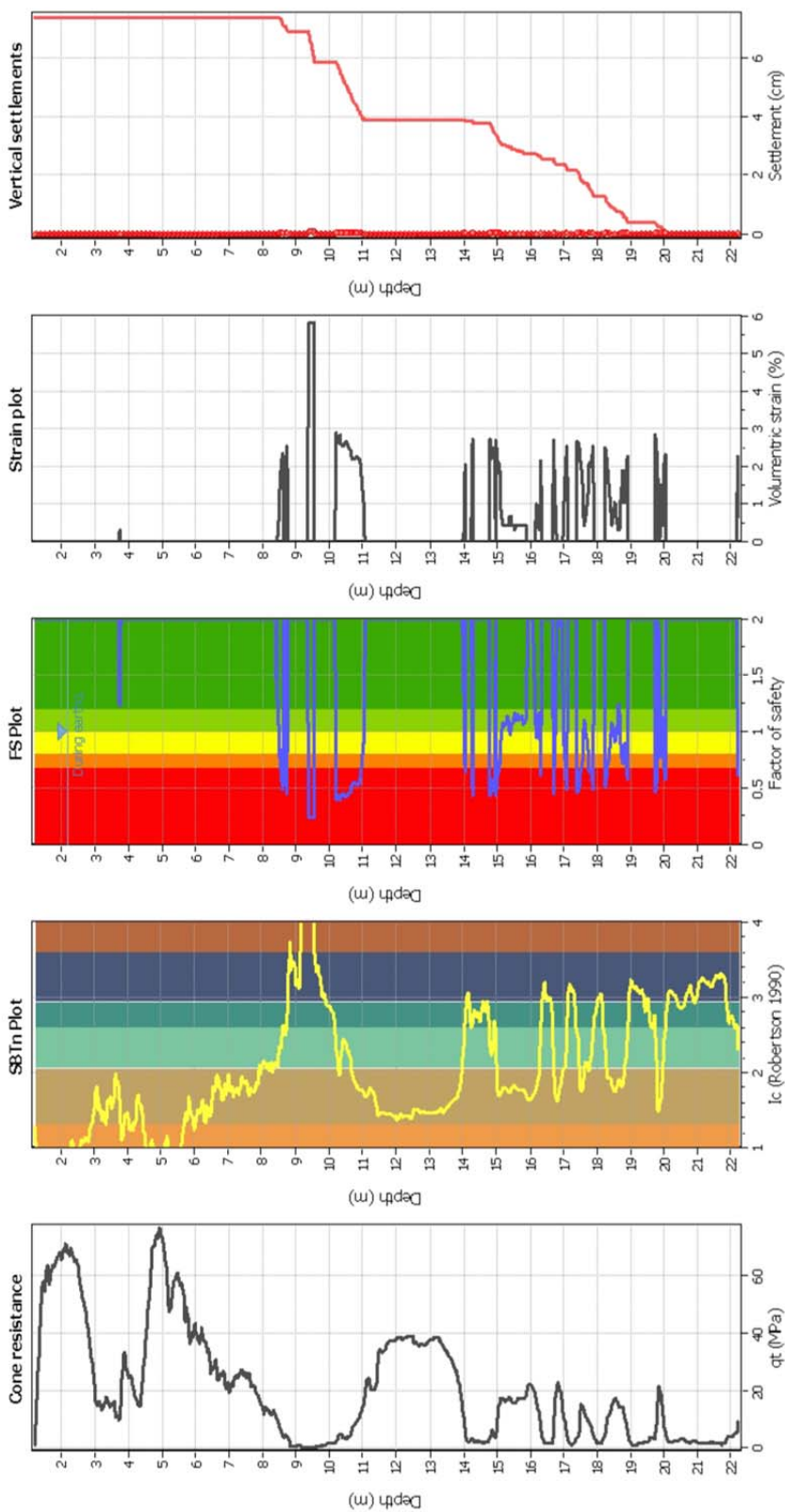
Project title : C Building Event: Christchurch Location : Christchurch, NZ
CPT file : R2B

Input parameters and analysis data

Analysis method:	B&I (2014)	G.W.T. (in-situ):	2.90 m	Use fill:	No	Clay like behavior applied:	Sands only
Fines correction method:	B&I (2014)	G.W.T. (earthq.):	2.20 m	Fill height:	N/A	Limit depth applied:	No
Points to test:	Based on Ic value	Average results interval:	3	Fill weight:	N/A	Limit depth:	N/A
Earthquake magnitude M_w :	6.20	Ic cut-off value:	2.60	Trans. detect. applied:	No	MSF method:	Method
Peak ground acceleration:	0.43	Unit weight calculation:	Based on SBT	K_σ applied:	Yes		



Estimation of post-earthquake settlements



Abbreviations

- q_t : Total cone resistance (cone resistance q_c corrected for pore water effects)
- I_c : Soil Behaviour Type Index
- FS: Calculated Factor of Safety against liquefaction
- Volumetric strain: Post-liquefaction volumetric strain

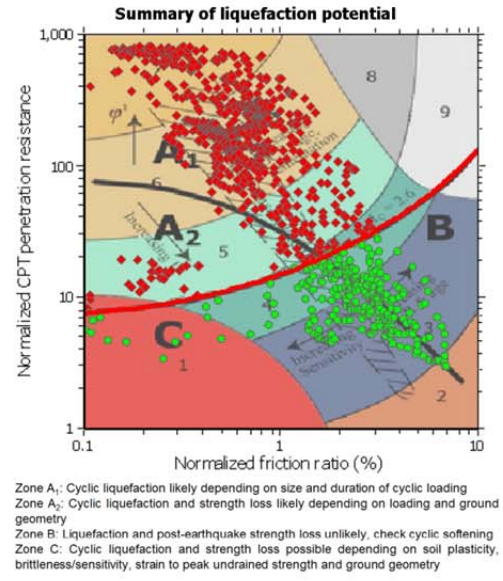
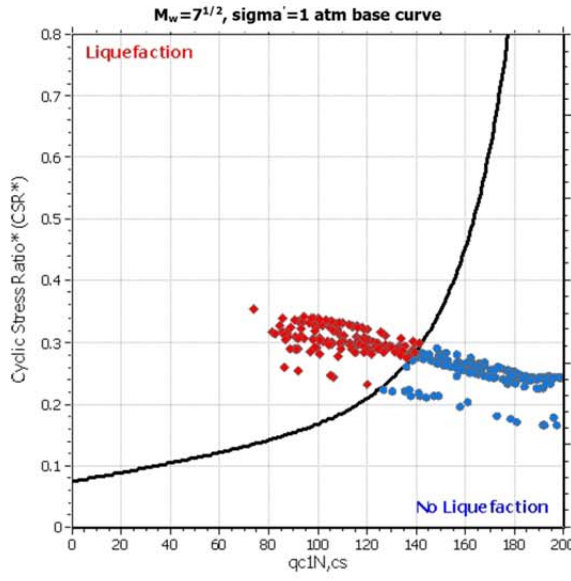
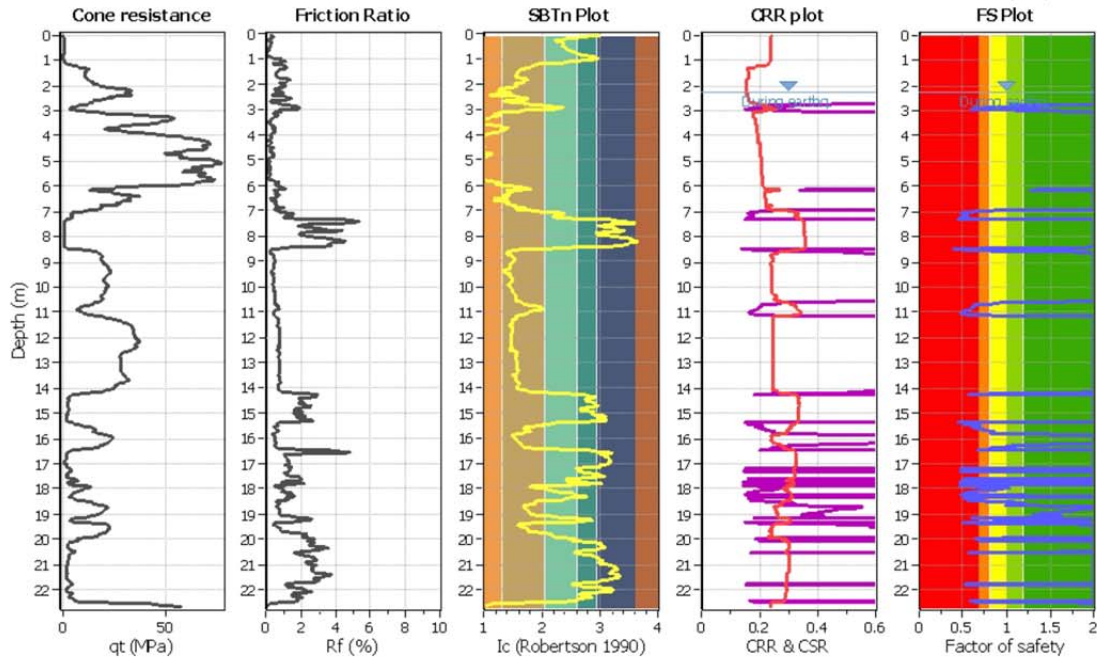
Roberto Luque
 University of California, Berkeley
 435 Davis Hall
 Berkeley, CA, 94720

LIQUEFACTION ANALYSIS REPORT

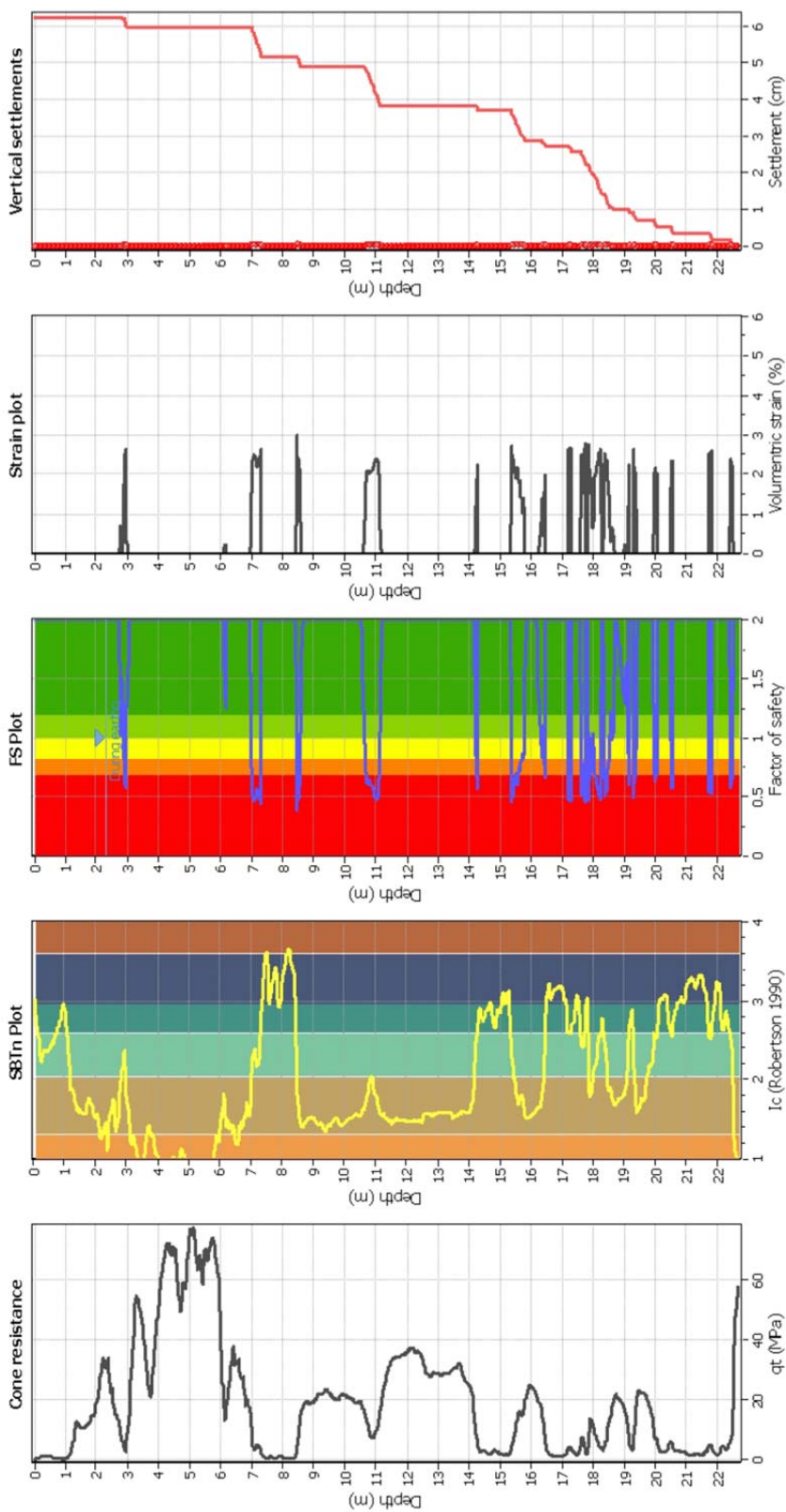
Project title : C Building Event: Christchurch Location : Christchurch, NZ

Input parameters and analysis data

Analysis method:	B&I (2014)	G.W.T. (in-situ):	2.90 m	Use fill:	No	Clay like behavior applied:	No	Sands only
Fines correction method:	B&I (2014)	G.W.T. (earthq.):	2.30 m	Fill height:	N/A	Limit depth applied:	No	
Points to test:	Based on Ic value	Average results interval:	3	Fill weight:	N/A	Limit depth:	N/A	
Earthquake magnitude M_w :	6.20	Ic cut-off value:	2.60	Trans. detect. applied:	No	MSF method:	Method	
Peak ground acceleration:	0.43	Unit weight calculation:	Based on SBT	K_p applied:	Yes			



Estimation of post-earthquake settlements



Abbreviations

- q: Total cone resistance (cone resistance q_c corrected for pore water effects)
- I_c : Soil Behaviour Type Index
- FS: Calculated Factor of Safety against liquefaction
- Volumetric strain: Post-liquefaction volumetric strain

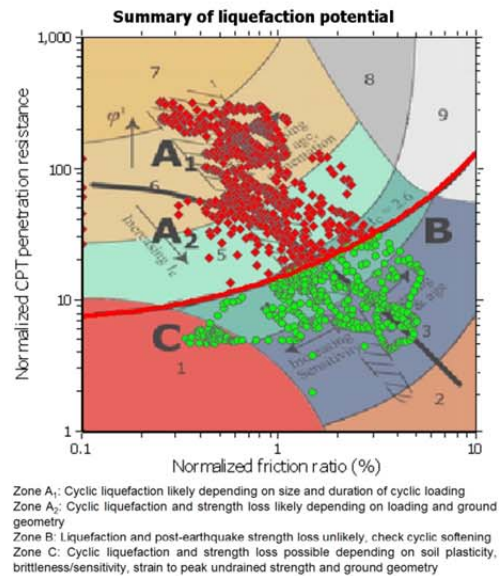
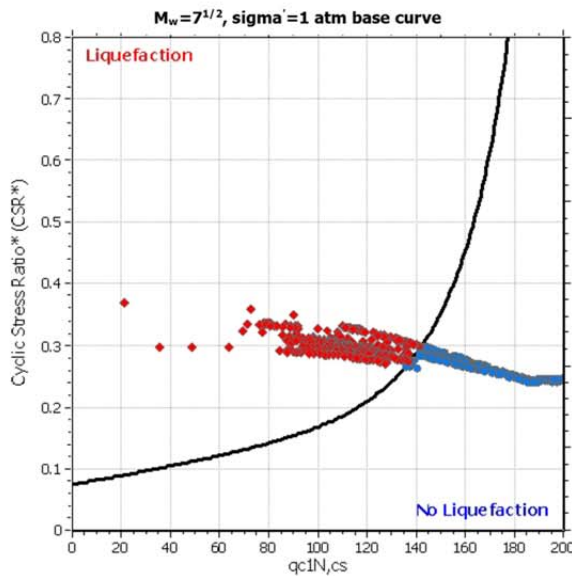
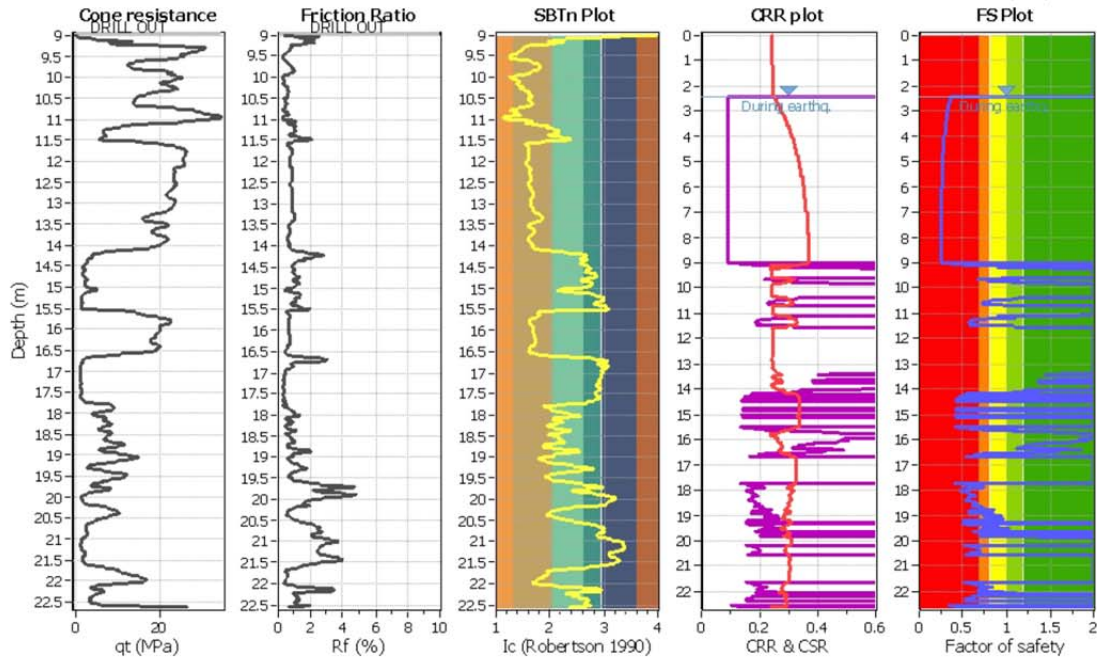
Roberto Luque
 University of California, Berkeley
 435 Davis Hall
 Berkeley, CA, 94720

LIQUEFACTION ANALYSIS REPORT

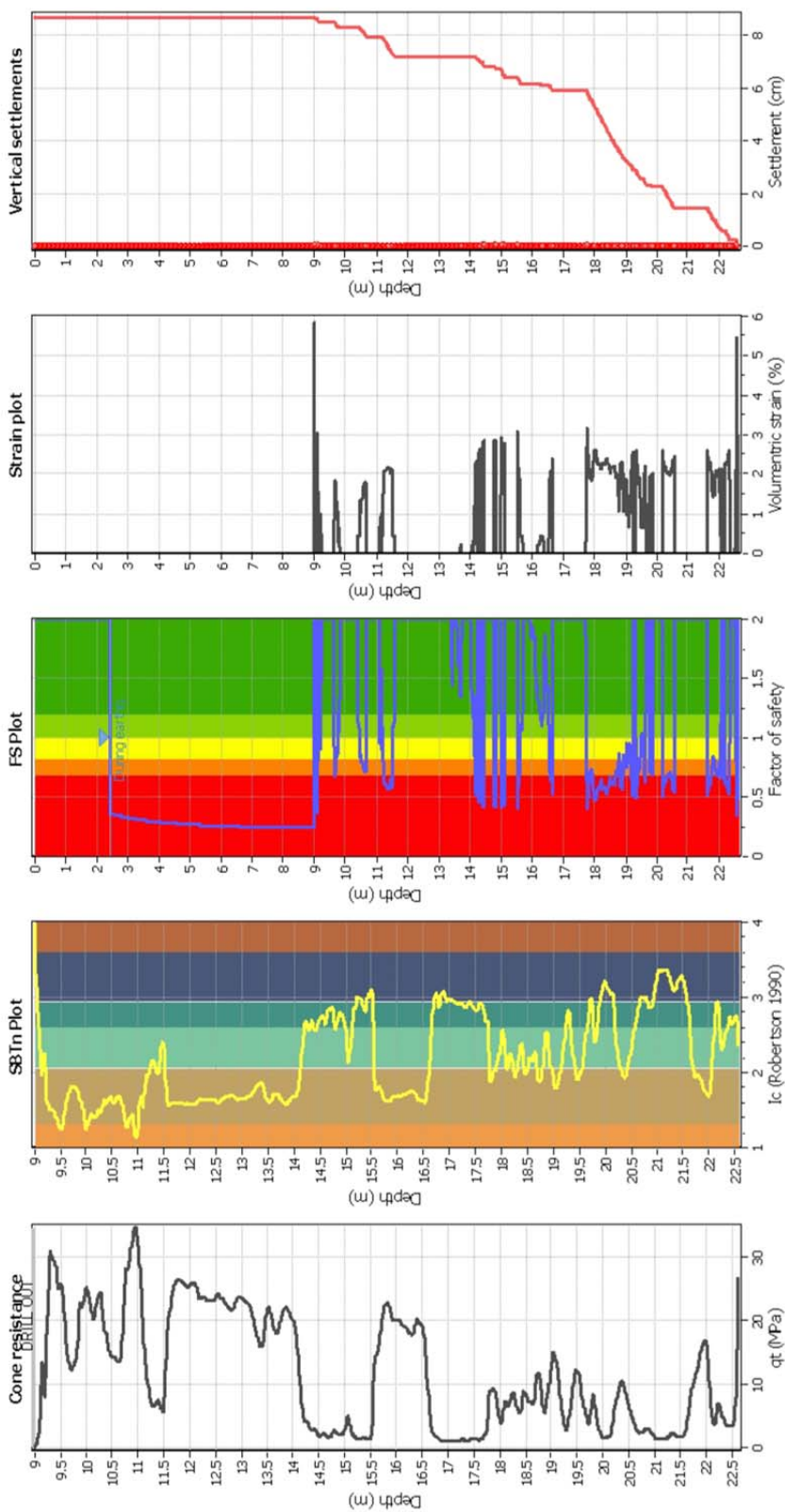
Project title : C Building Event: Christchurch Location : Christchurch, NZ
CPT file : CPT-02

Input parameters and analysis data

Analysis method:	B&I (2014)	G.W.T. (in-situ):	3.00 m	Use fill:	No	Clay like behavior applied:	No	Sands only
Fines correction method:	B&I (2014)	G.W.T. (earthq.):	2.44 m	Fill height:	N/A	Limit depth applied:	No	
Points to test:	Based on Ic value	Average results interval:	3	Fill weight:	N/A	Limit depth:	N/A	
Earthquake magnitude M_w :	6.20	Ic cut-off value:	2.60	Trans. detect. applied:	No	MSF method:	N/A	
Peak ground acceleration:	0.43	Unit weight calculation:	Based on SBT	K_s applied:	Yes			



Estimation of post-earthquake settlements



Abbreviations

- q_t: Total cone resistance (cone resistance q_c corrected for pore water effects)
- I_c: Soil Behaviour Type Index
- FS: Calculated Factor of Safety against liquefaction
- Volumetric strain: Post-liquefaction volumetric strain

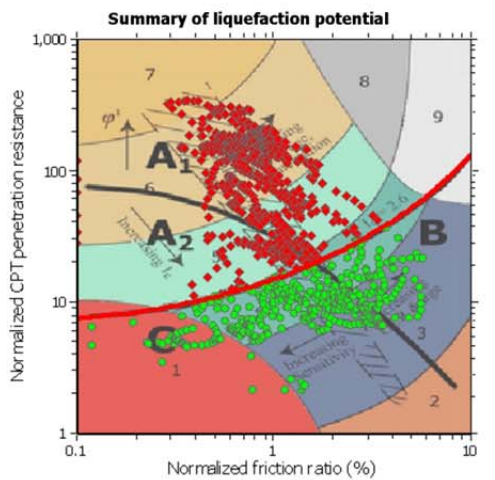
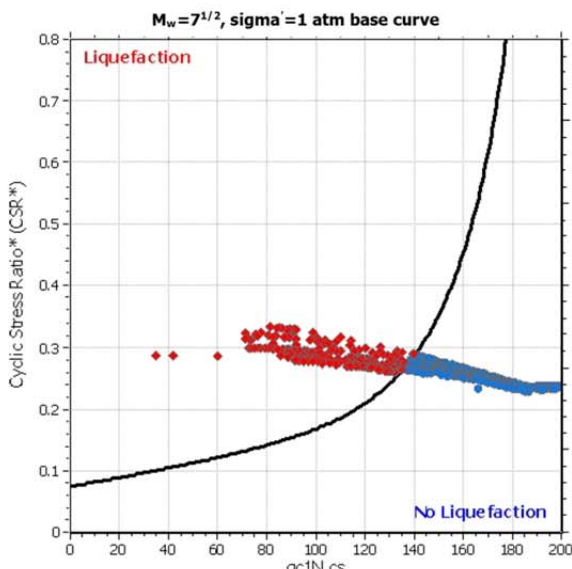
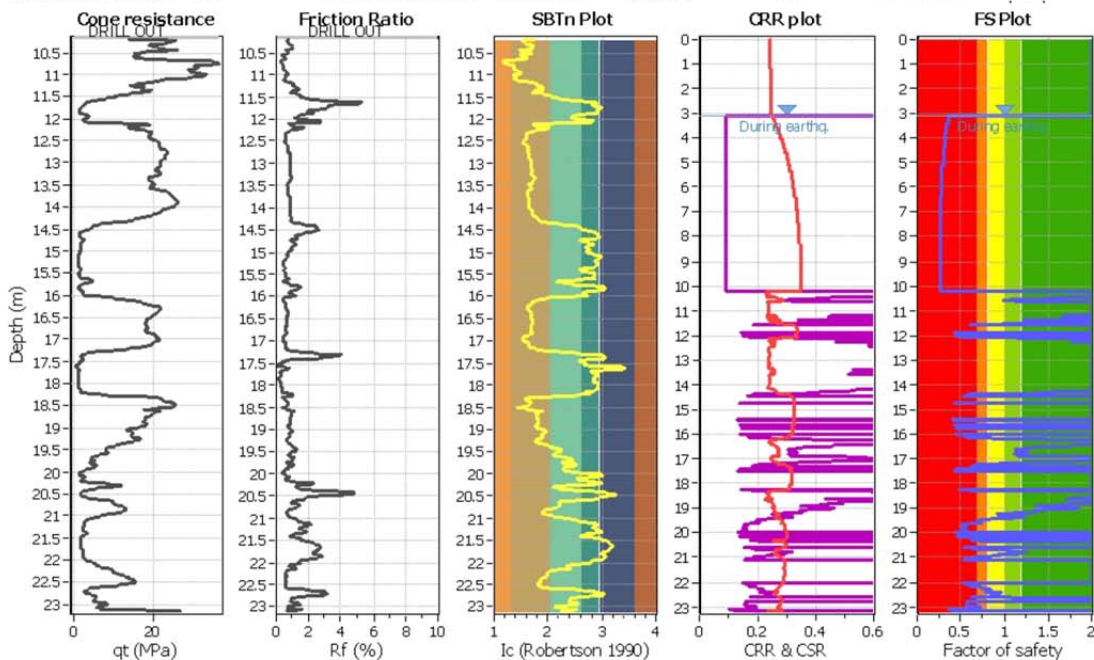
Roberto Luque
 University of California, Berkeley
 435 Davis Hall
 Berkeley, CA, 94720

LIQUEFACTION ANALYSIS REPORT

Project title : C Building Event: Christchurch Location : Christchurch, NZ
CPT file : CPT-03

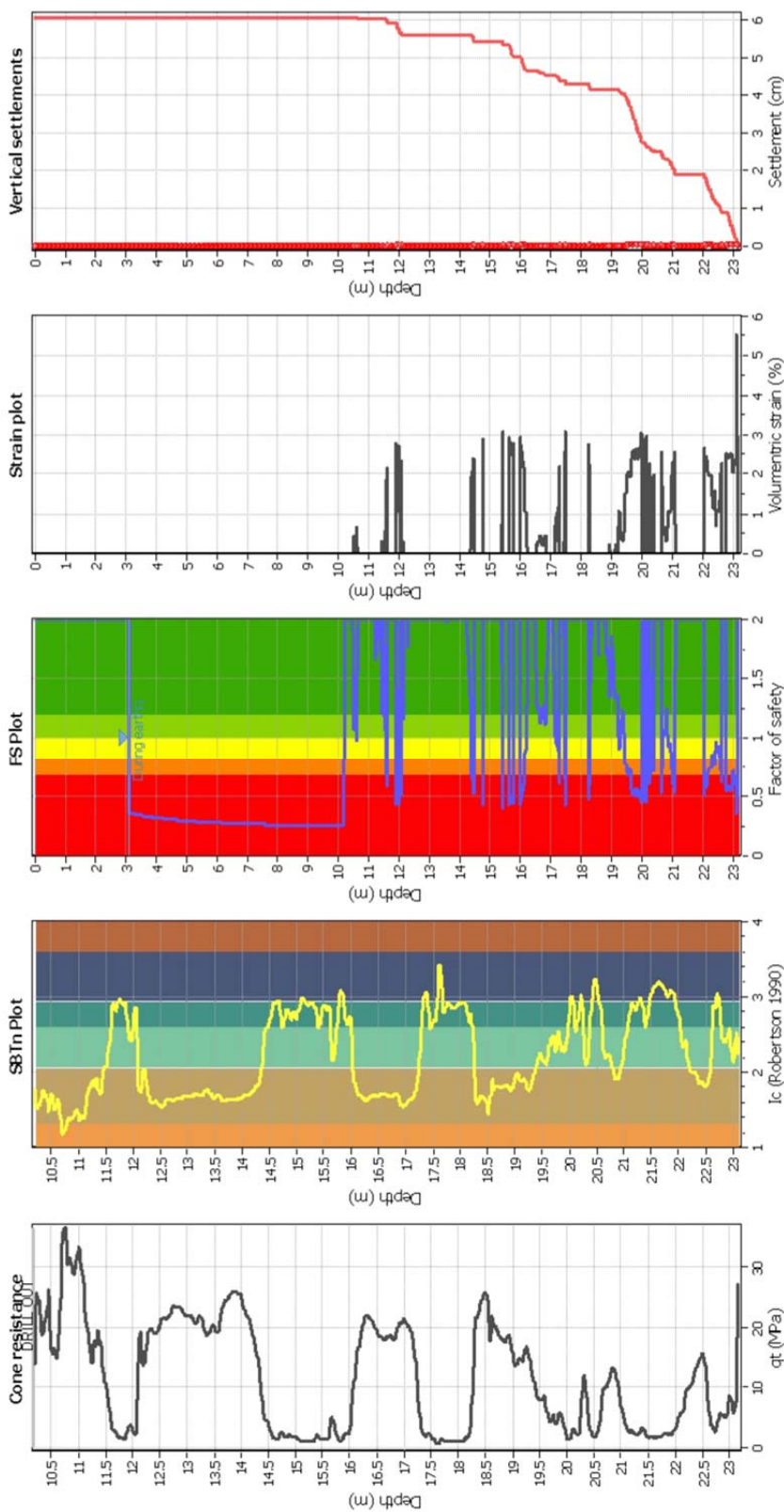
Input parameters and analysis data

Analysis method:	B&I (2014)	G.W.T. (in-situ):	3.00 m	Use fill:	No	Clay like behavior applied:	No	Sands only
Fines correction method:	B&I (2014)	G.W.T. (earthq.):	3.10 m	Fill height:	N/A	Limit depth applied:	No	
Points to test:	Based on Ic value	Average results interval:	3	Fill weight:	N/A	Limit depth:	N/A	
Earthquake magnitude M_w :	6.20	Ic cut-off value:	2.60	Trans. detect. applied:	No	MSF method:	N/A	
Peak ground acceleration:	0.43	Unit weight calculation:	Based on SBT	K_s applied:	Yes			



Zone A₁: Cyclic liquefaction likely depending on size and duration of cyclic loading
 Zone A₂: Cyclic liquefaction and strength loss likely depending on loading and ground geometry
 Zone B: Liquefaction and post-earthquake strength loss unlikely, check cyclic softening
 Zone C: Cyclic liquefaction and strength loss possible depending on soil plasticity, brittleness/sensitivity, strain to peak undrained strength and ground geometry

Estimation of post-earthquake settlements



Abbreviations

- q: Total cone resistance (cone resistance q_c corrected for pore water effects)
- I_c: Soil Behaviour Type Index
- FS: Calculated Factor of Safety against liquefaction
- Volumetric strain: Post-liquefaction volumetric strain

Roberto Luque
 University of California, Berkeley
 435 Davis Hall
 Berkeley, CA, 94720

LIQUEFACTION ANALYSIS REPORT

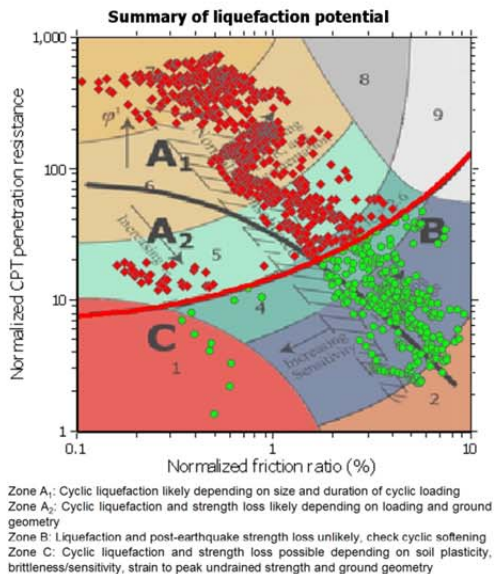
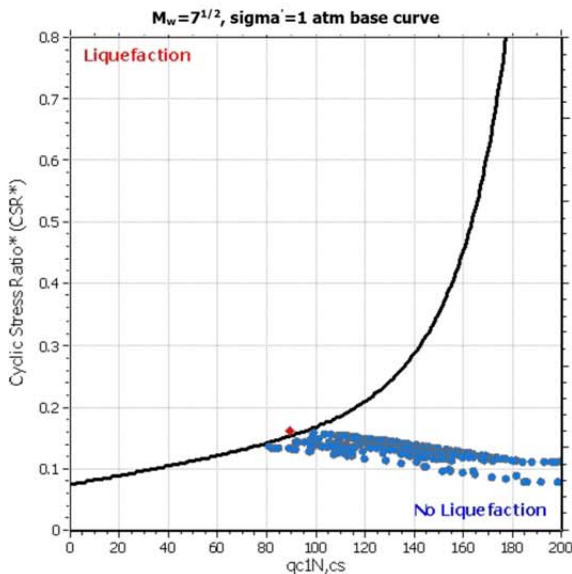
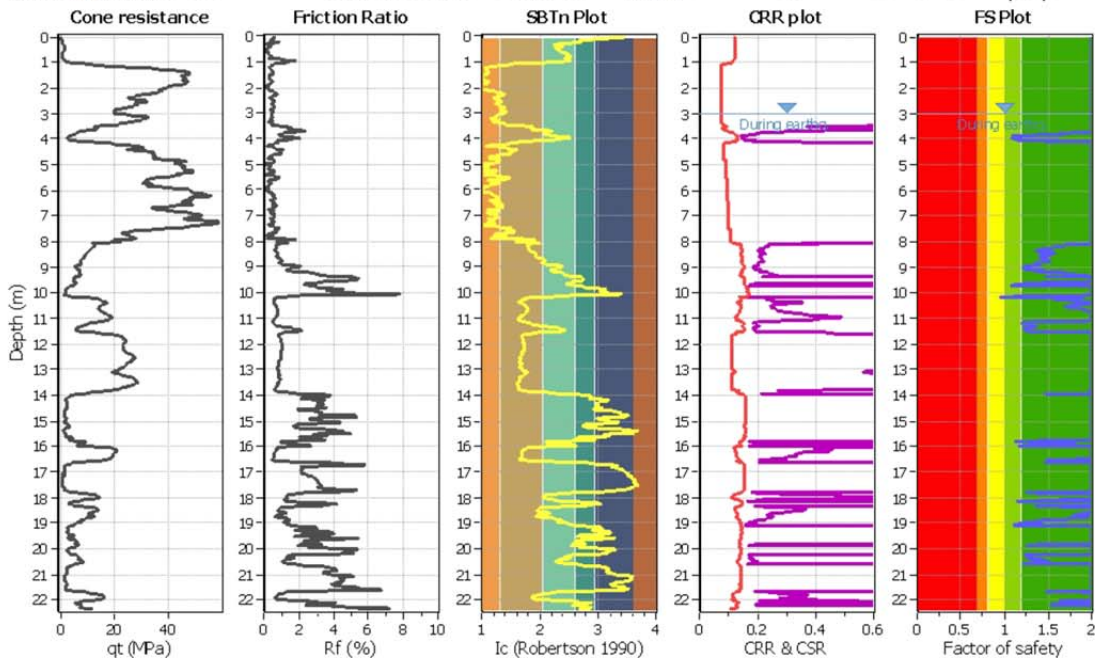
Project title : C Building Event: 13Jun2011

Location : Christchurch, NZ

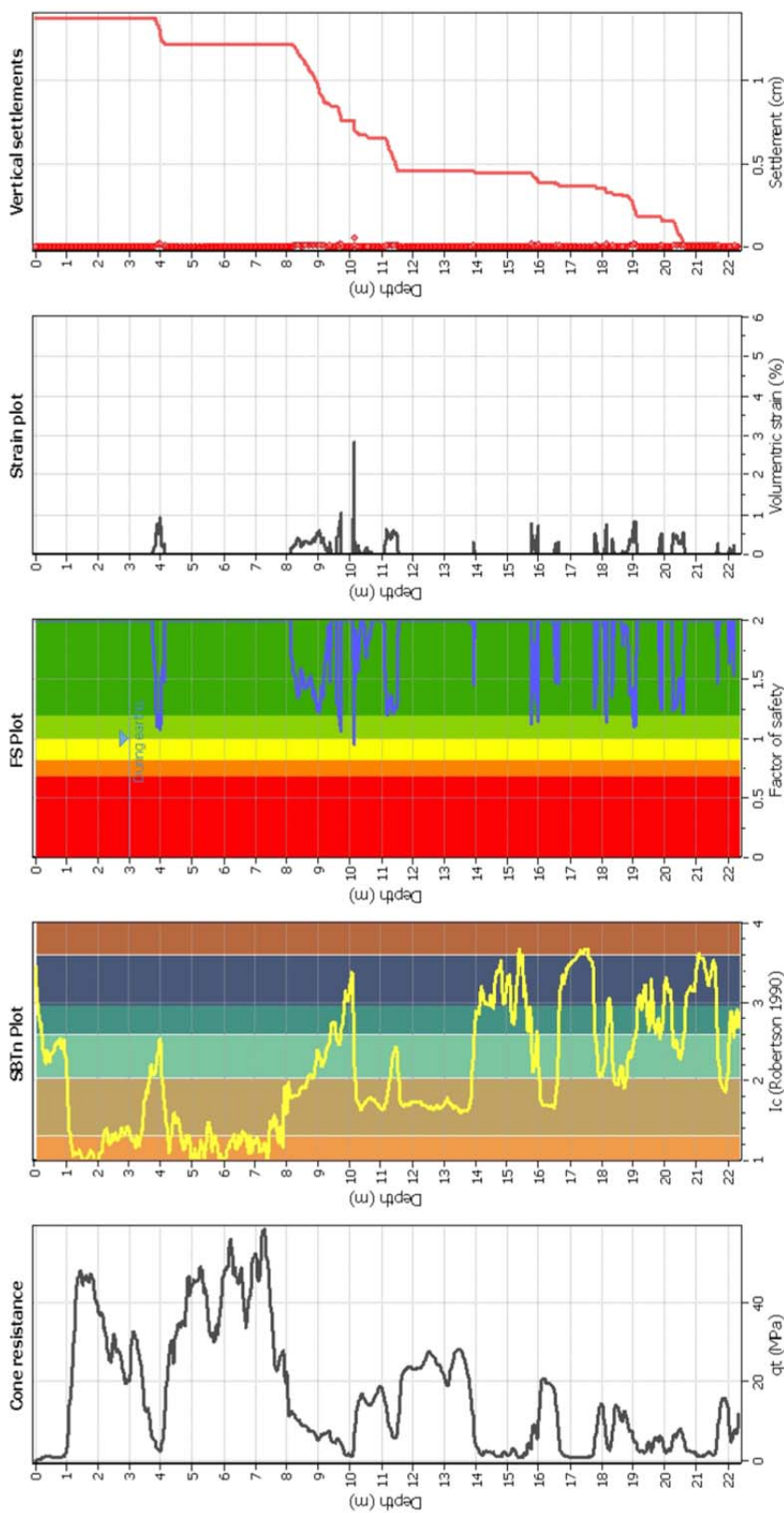
CPT file : R7B

Input parameters and analysis data

Analysis method:	B&I (2014)	G.W.T. (in-situ):	3.70 m	Use fill:	No	Clay like behavior applied:	Sands only
Fines correction method:	B&I (2014)	G.W.T. (earthq.):	3.00 m	Fill height:	N/A	Limit depth applied:	No
Points to test:	Based on Ic value	Average results interval:	3	Fill weight:	N/A	Limit depth:	N/A
Earthquake magnitude M_w :	6.00	Ic cut-off value:	2.60	Trans. detect. applied:	No	MSF method:	Method
Peak ground acceleration:	0.22	Unit weight calculation:	Based on SBT	K_σ applied:	Yes		



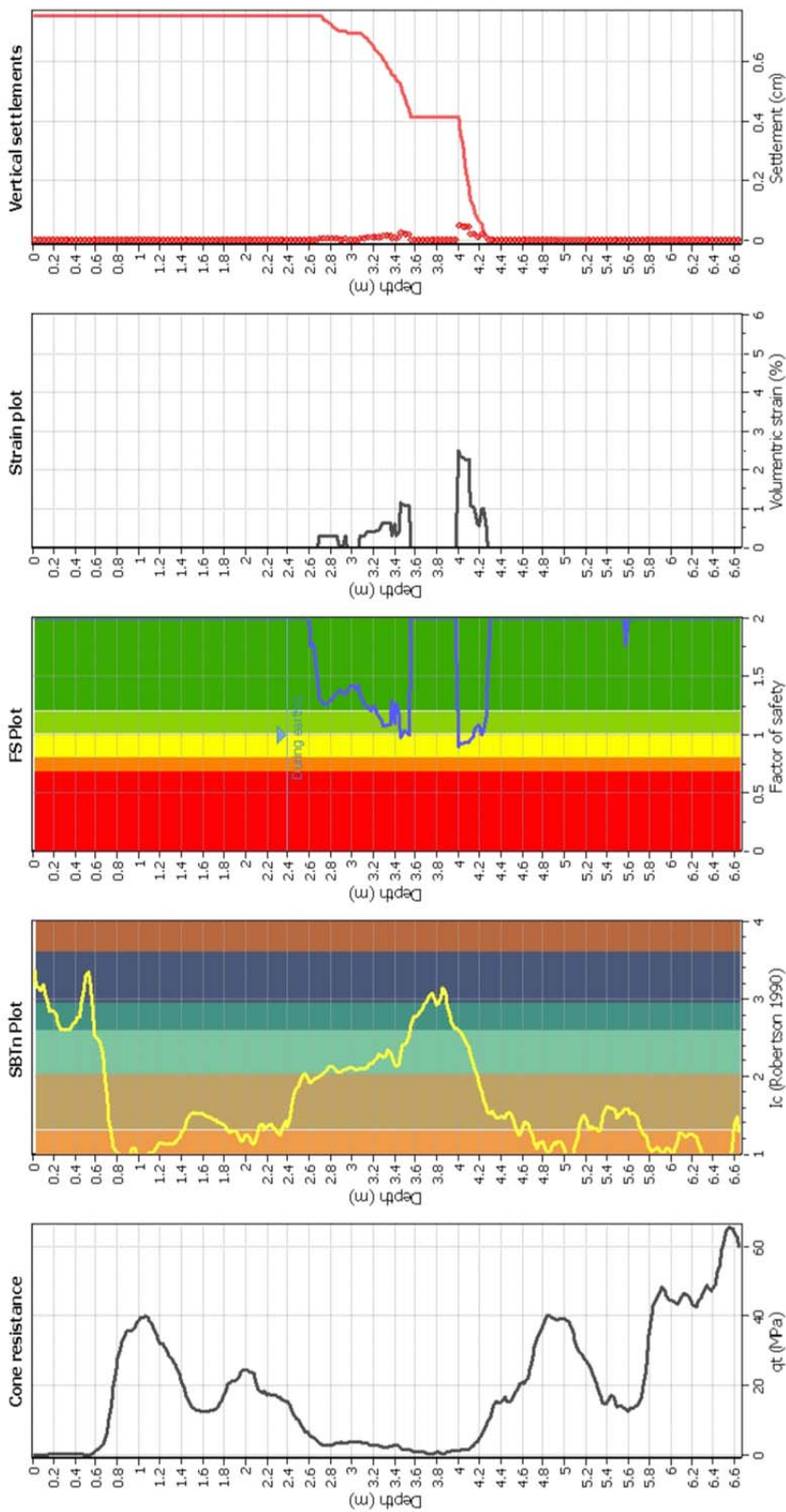
Estimation of post-earthquake settlements



Abbreviations

- qt: Total cone resistance (cone resistance q_c corrected for pore water effects)
- I_c: Soil Behaviour Type Index
- FS: Calculated Factor of Safety against liquefaction
- Volumetric strain: Post-liquefaction volumetric strain

Estimation of post-earthquake settlements



Abbreviations

- q_t: Total cone resistance (cone resistance q_c corrected for pore water effects)
- I_c: Soil Behaviour Type Index
- FS: Calculated Factor of Safety against liquefaction
- Volumetric strain: Post-liquefaction volumetric strain

Roberto Luque
 University of California, Berkeley
 435 Davis Hall
 Berkeley, CA, 94720

LIQUEFACTION ANALYSIS REPORT

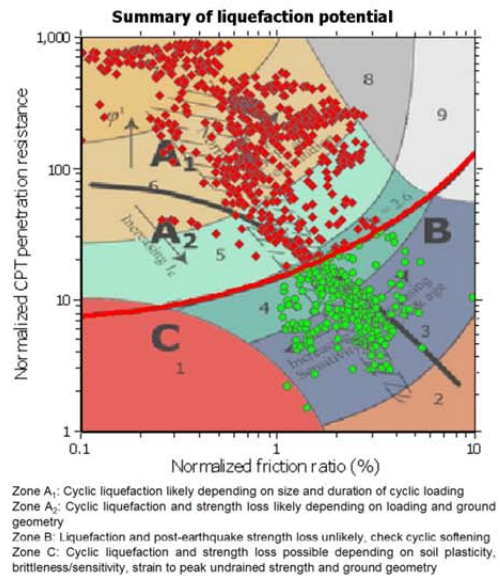
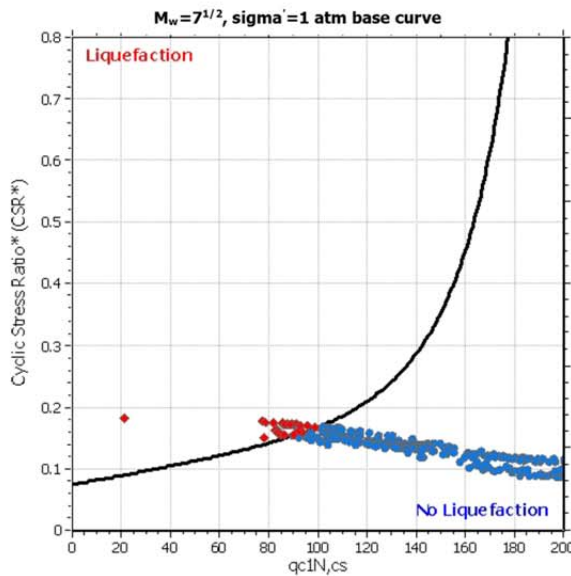
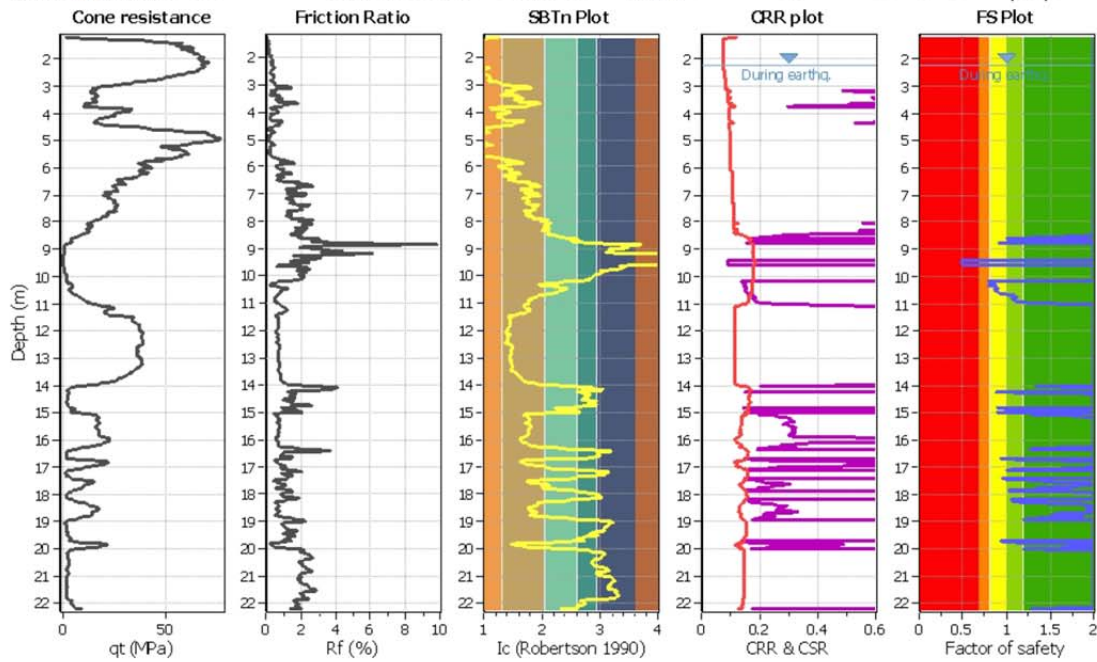
Project title : C Building Event: 13Jun2011

Location : Christchurch, NZ

CPT file : R2B

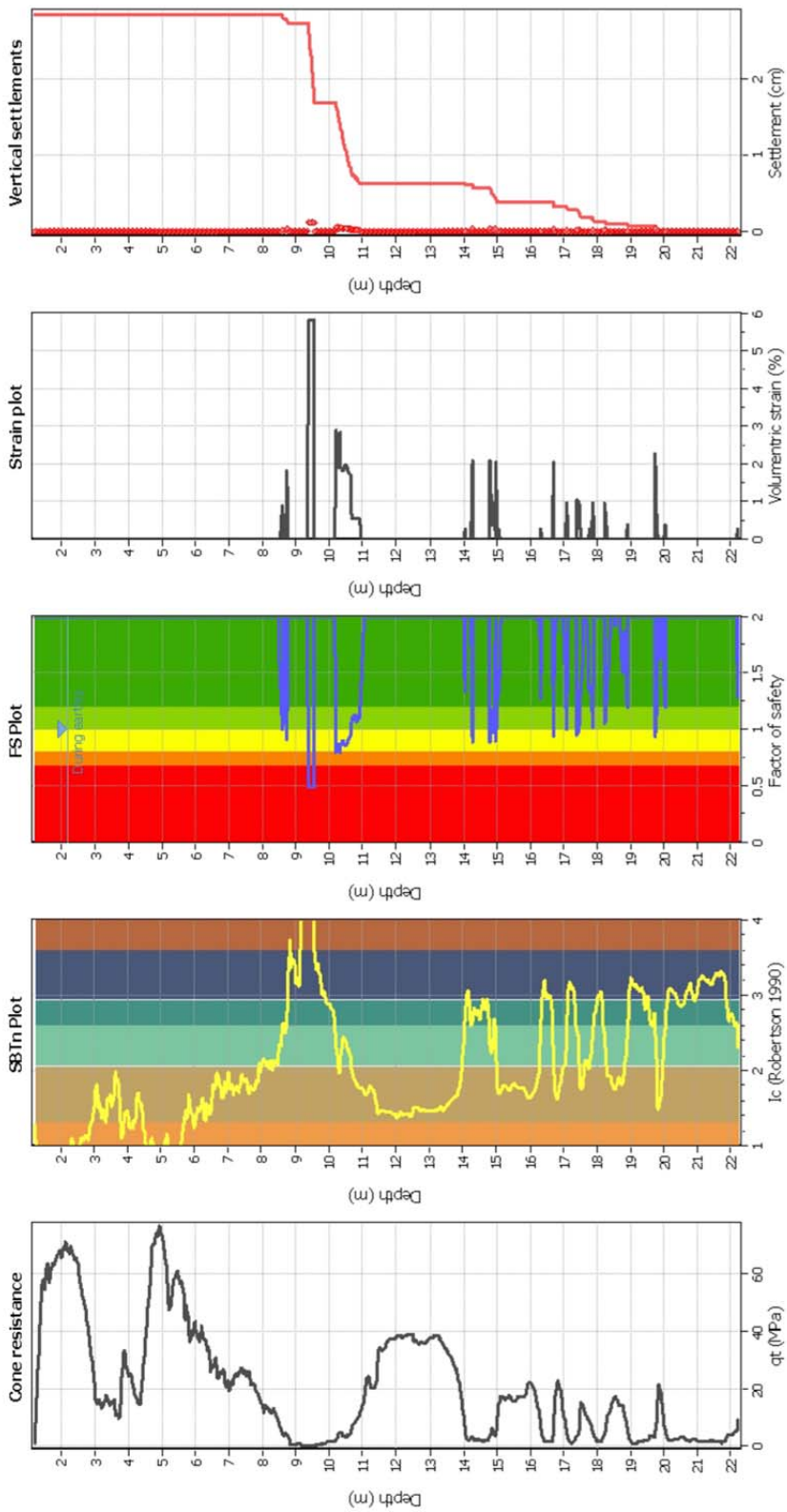
Input parameters and analysis data

Analysis method:	B&I (2014)	G.W.T. (in-situ):	2.90 m	Use fill:	No	Clay like behavior applied:	No	Sands only
Fines correction method:	B&I (2014)	G.W.T. (earthq.):	2.20 m	Fill height:	N/A	Limit depth applied:	No	
Points to test:	Based on Ic value	Average results interval:	3	Fill weight:	N/A	Limit depth:	N/A	
Earthquake magnitude M_w :	6.00	Ic cut-off value:	2.60	Trans. detect. applied:	No	MSF method:	Method	
Peak ground acceleration:	0.22	Unit weight calculation:	Based on SBT	K_s applied:	Yes			



Estimation of post-earthquake settlements

This software is licensed to: Roberto Luque



Abbreviations

- q_t : Total cone resistance (cone resistance q_c corrected for pore water effects)
- I_c : Soil Behaviour Type Index
- FS: Calculated Factor of Safety against liquefaction
- Volumetric strain: Post-liquefaction volumetric strain

Roberto Luque
 University of California, Berkeley
 435 Davis Hall
 Berkeley, CA, 94720

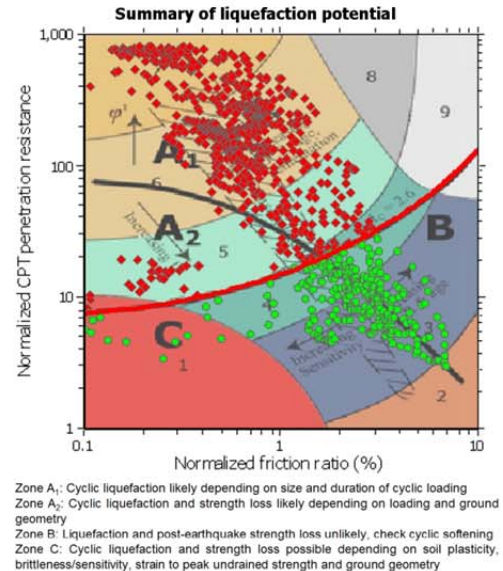
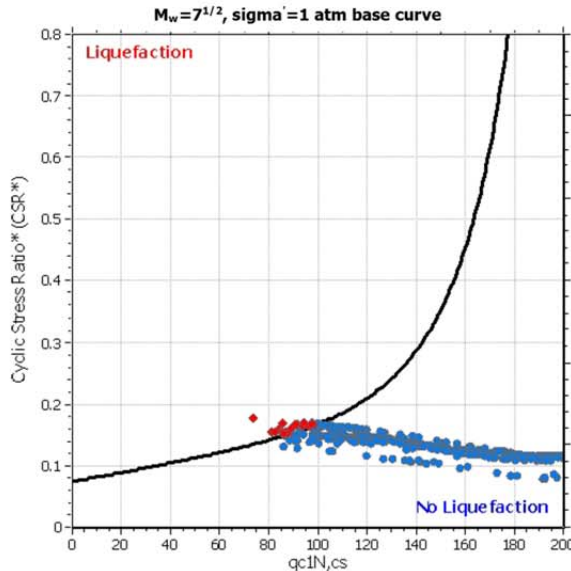
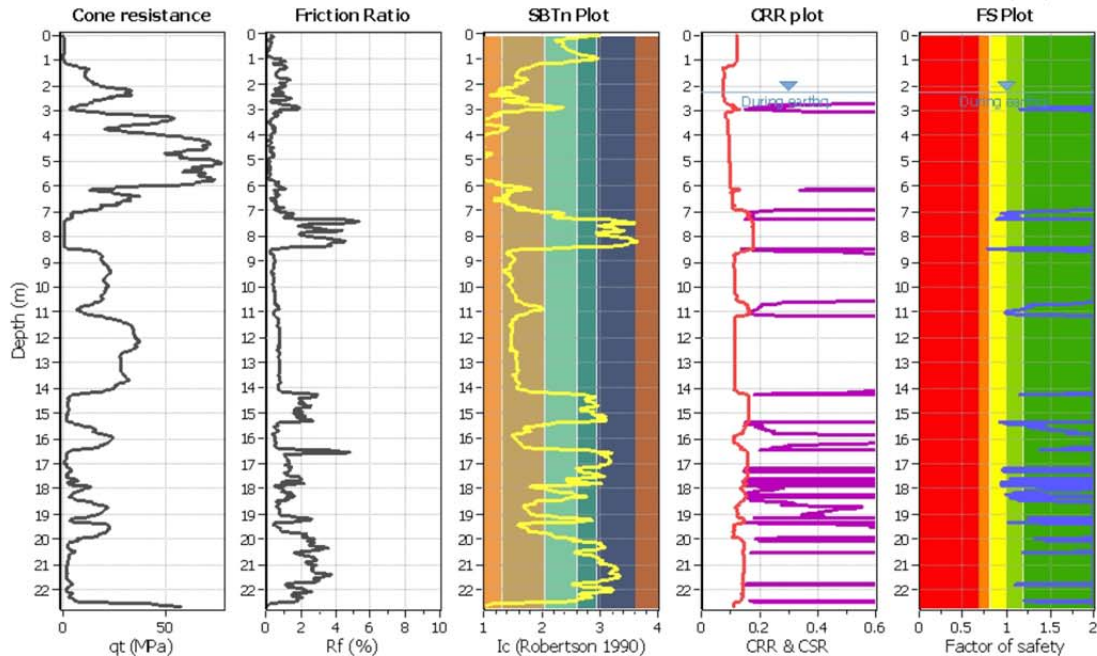
LIQUEFACTION ANALYSIS REPORT

Project title : C Building Event: 13Jun2011 Location : Christchurch, NZ

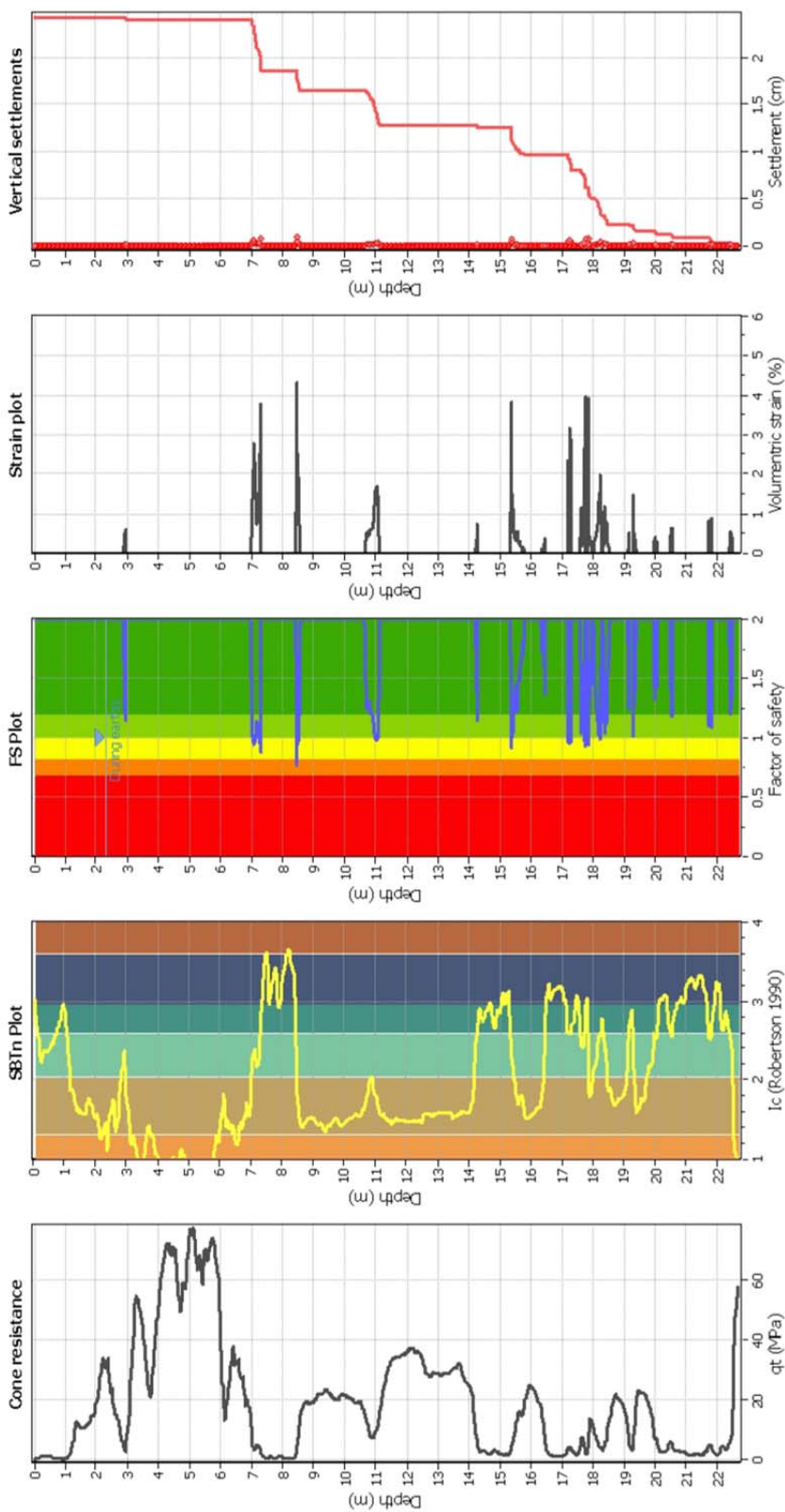
CPT file : R5

Input parameters and analysis data

Analysis method:	B&I (2014)	G.W.T. (in-situ):	2.90 m	Use fill:	No	Clay like behavior applied:	No	Sands only
Fines correction method:	B&I (2014)	G.W.T. (earthq.):	2.30 m	Fill height:	N/A	Limit depth applied:	No	
Points to test:	Based on Ic value	Average results interval:	3	Fill weight:	N/A	Limit depth:	N/A	
Earthquake magnitude M_w :	6.00	Ic cut-off value:	2.60	Trans. detect. applied:	No	MSF method:	Method	
Peak ground acceleration:	0.22	Unit weight calculation:	Based on SBT	K_σ applied:	Yes			



Estimation of post-earthquake settlements



Abbreviations

- q_t: Total cone resistance (cone resistance q_c corrected for pore water effects)
- I_c: Soil Behaviour Type Index
- FS: Calculated Factor of Safety against liquefaction
- Volumetric strain: Post-liquefaction volumetric strain

Roberto Luque
 University of California, Berkeley
 435 Davis Hall
 Berkeley, CA, 94720

LIQUEFACTION ANALYSIS REPORT

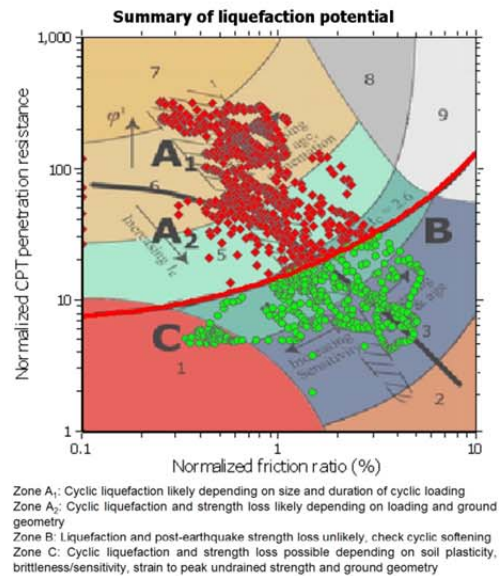
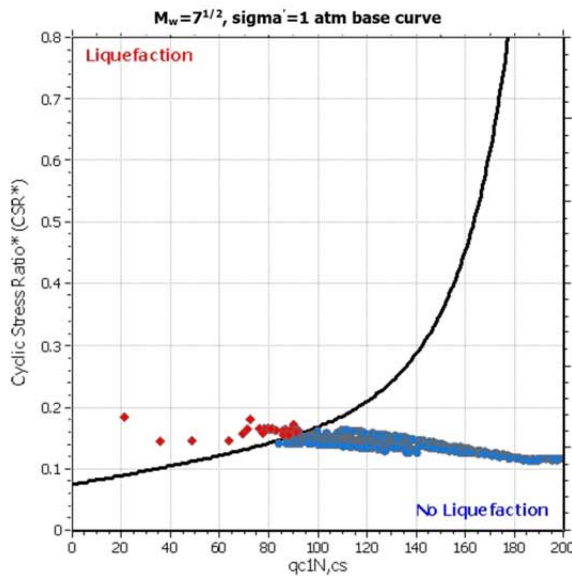
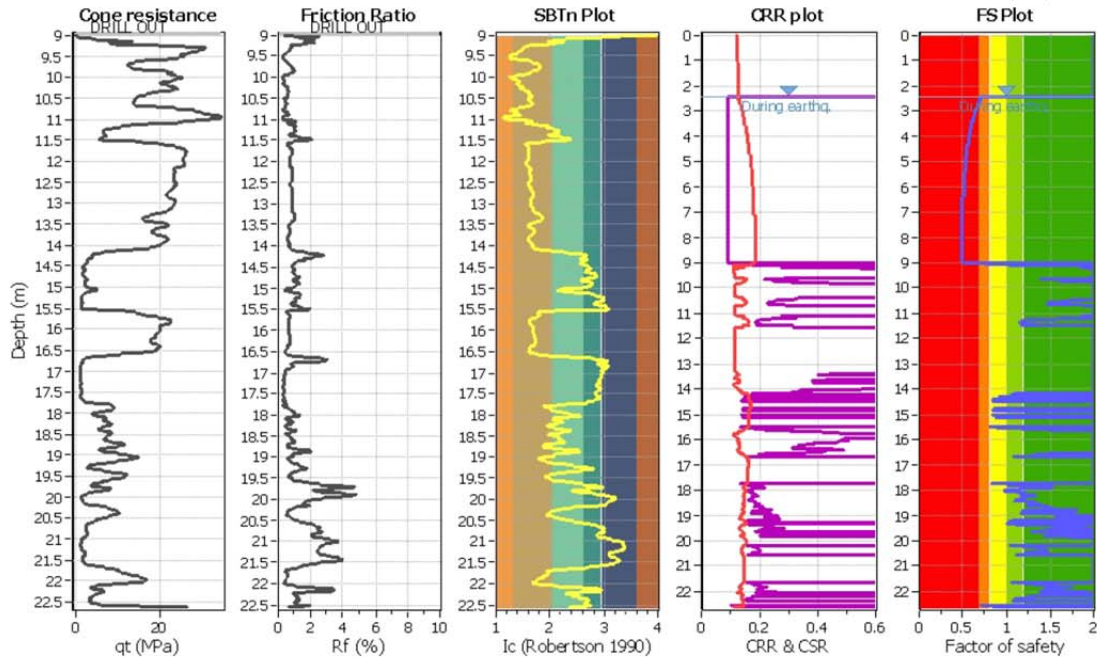
Project title : C Building Event: 13Jun2011

Location : Christchurch, NZ

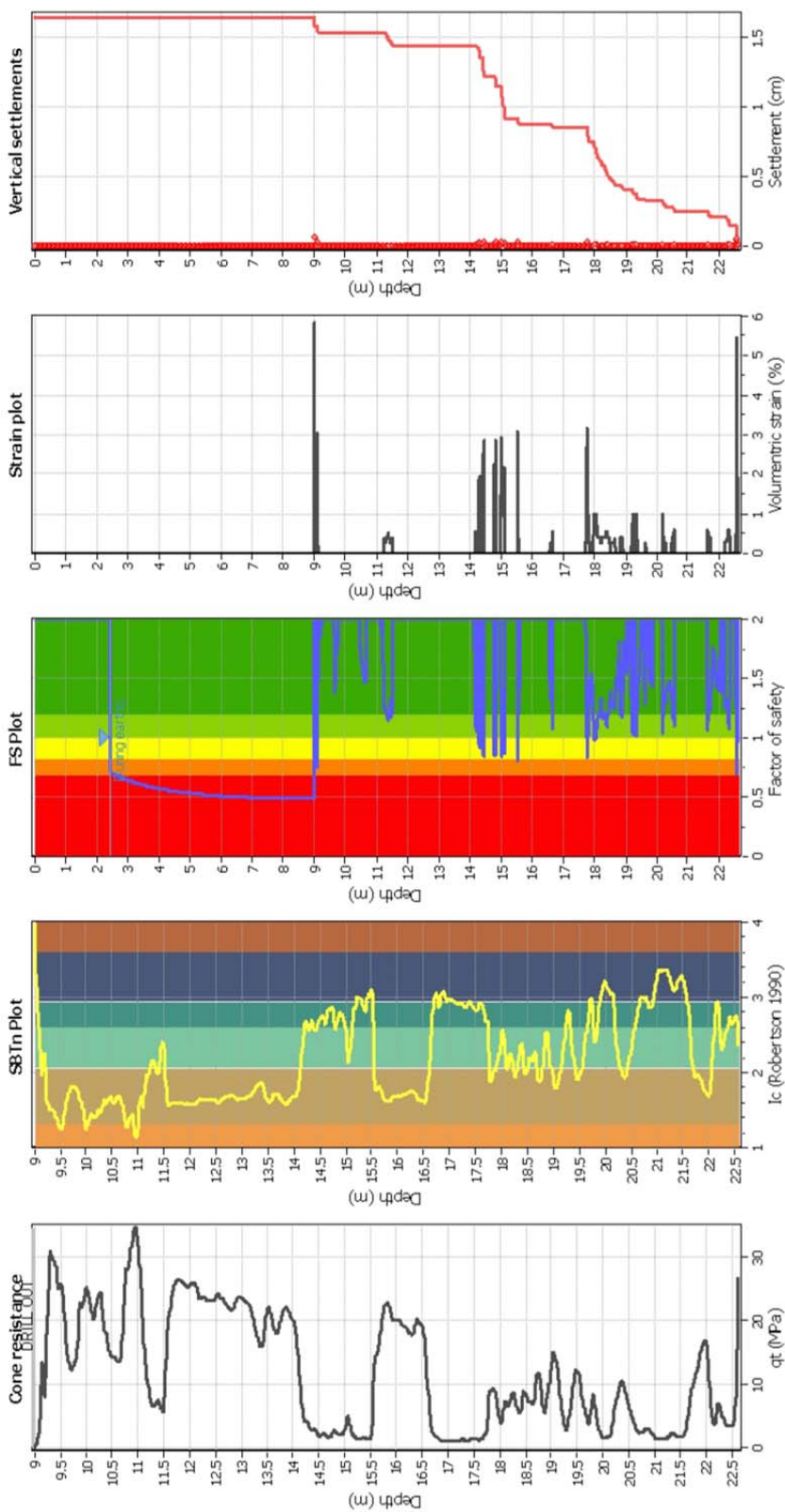
CPT file : CPT-02

Input parameters and analysis data

Analysis method:	B&I (2014)	G.W.T. (in-situ):	3.00 m	Use fill:	No	Clay like behavior applied:	No	Sands only
Fines correction method:	B&I (2014)	G.W.T. (earthq.):	2.44 m	Fill height:	N/A	Limit depth applied:	No	
Points to test:	Based on Ic value	Average results interval:	3	Fill weight:	N/A	Limit depth:	N/A	
Earthquake magnitude M_w :	6.00	Ic cut-off value:	2.60	Trans. detect. applied:	No	Limit depth:	N/A	
Peak ground acceleration:	0.22	Unit weight calculation:	Based on SBT	K_s applied:	Yes	MSF method:	Method	



Estimation of post-earthquake settlements



Abbreviations

- q_t: Total cone resistance (cone resistance q_c corrected for pore water effects)
- I_c: Soil Behaviour Type Index
- FS: Calculated Factor of Safety against liquefaction
- Volumetric strain: Post-liquefaction volumetric strain

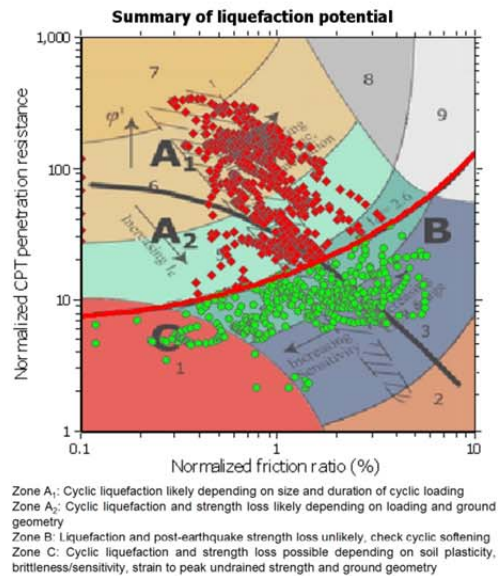
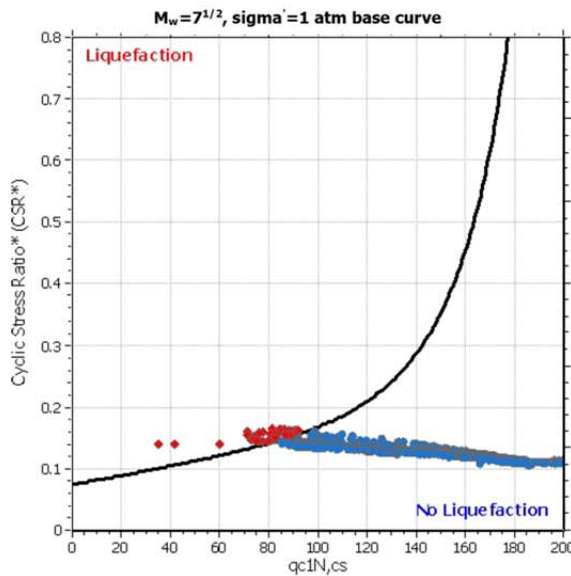
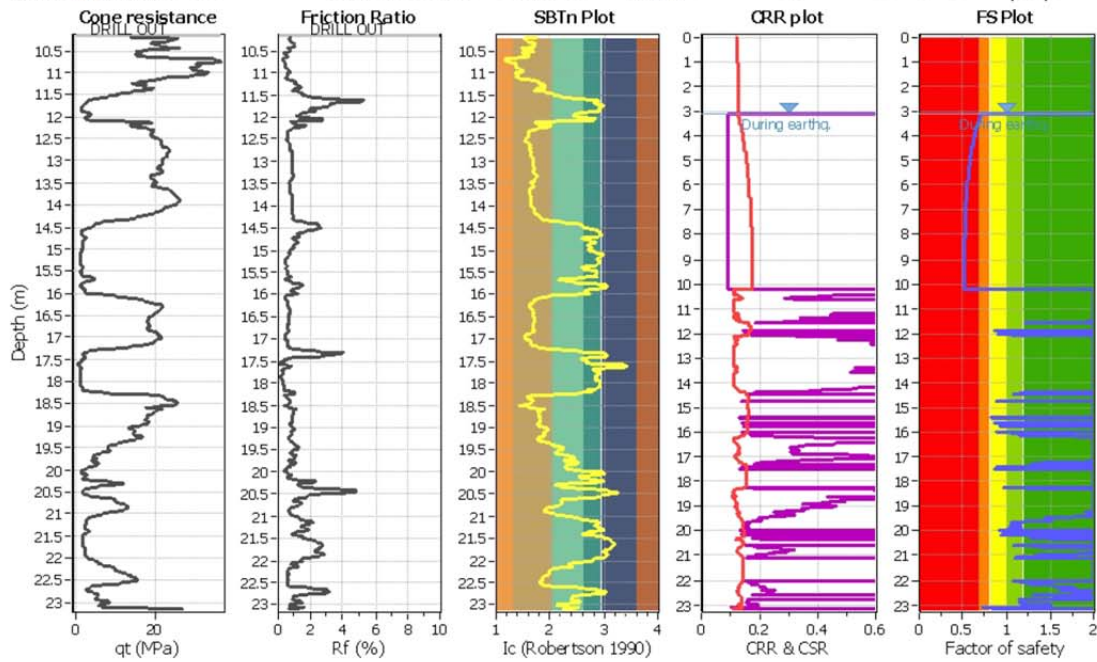
Roberto Luque
 University of California, Berkeley
 435 Davis Hall
 Berkeley, CA, 94720

LIQUEFACTION ANALYSIS REPORT

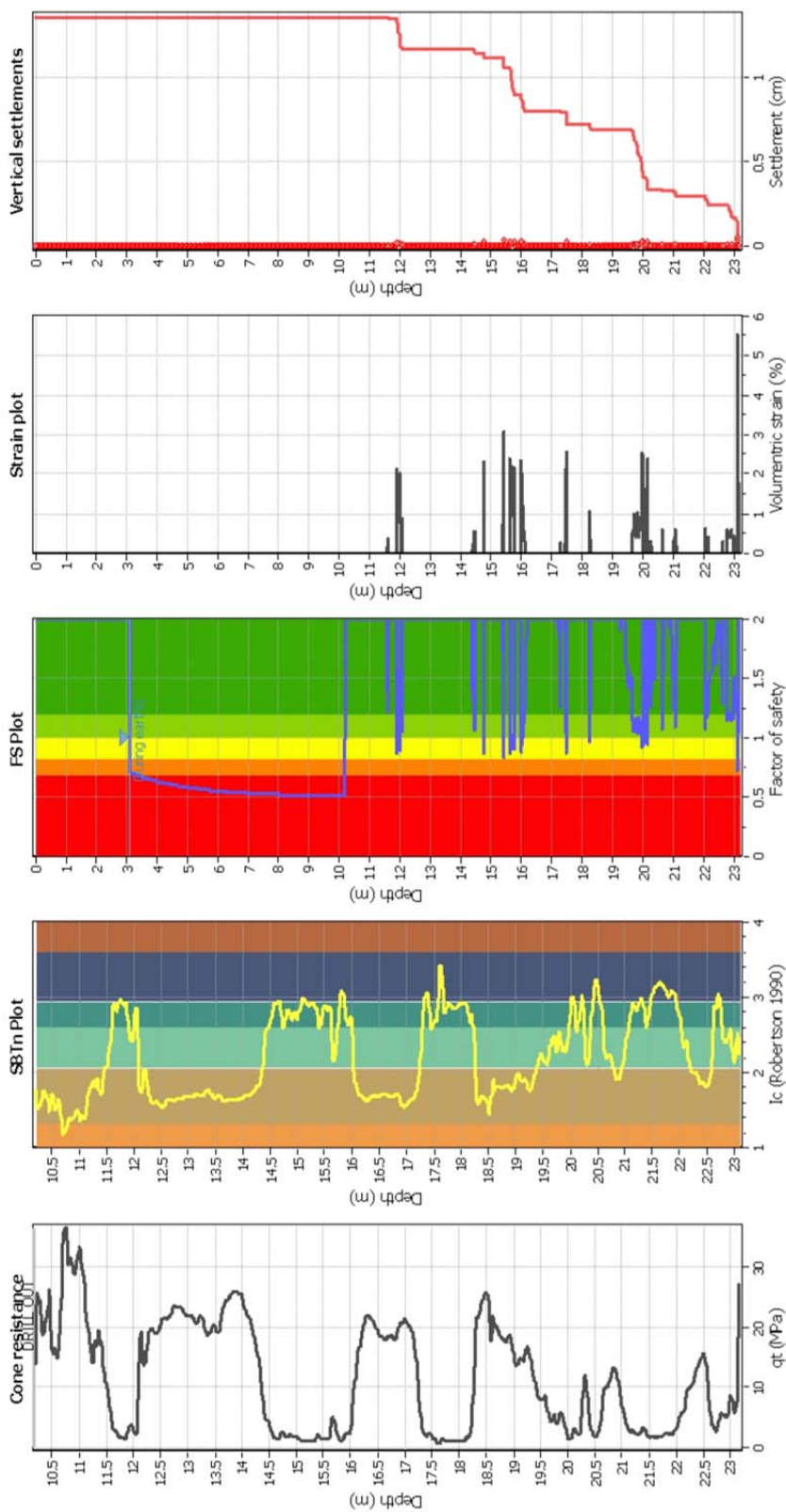
Project title : C Building Event: 13Jun2011 Location : Christchurch, NZ
CPT file : CPT-03

Input parameters and analysis data

Analysis method:	B&I (2014)	G.W.T. (in-situ):	3.00 m	Use fill:	No	Clay like behavior applied:	No	Sands only
Fines correction method:	B&I (2014)	G.W.T. (earthq.):	3.10 m	Fill height:	N/A	Limit depth applied:	No	
Points to test:	Based on Ic value	Average results interval:	3	Fill weight:	N/A	Limit depth:	N/A	
Earthquake magnitude M_w :	6.00	Ic cut-off value:	2.60	Trans. detect. applied:	No	Limit depth:	N/A	
Peak ground acceleration:	0.22	Unit weight calculation:	Based on SBT	K_s applied:	Yes	MSF method:	Method	



Estimation of post-earthquake settlements



Abbreviations

- q_t: Total cone resistance (cone resistance q_c corrected for pore water effects)
- I_c: Soil Behaviour Type Index
- FS: Calculated Factor of Safety against liquefaction
- Volumetric strain: Post-liquefaction volumetric strain

Appendix B - Condominium “Los Presidentes”: Case History Documentation

APPENDIX B: CONDOMINIUM LOS PRESIDENTES: CASE HISTORY DOCUMENTATION

B.1. INTRODUCTION

The Condominium “Los Presidentes” consists of four 8-story buildings, which names are *Bulnes* (NW building), *Montt* (NE building), *Riesco* (SW building) and *Errazuriz* (SE building) located in the city of Concepcion, Chile. In February 27th 2010 the Maule earthquake ($M_w=8.8$) resulted in severe damage in infrastructure in the city of Concepcion. The performance of the four buildings was different, even though they were 14 and 25 m away from each other. This feature makes this case an excellent case history to evaluate the effect of liquefaction on the performance of buildings on shallow foundations.

This appendix will present the case history by giving a description of the structures, the site conditions, the likely ground shaking and the performance observations. The site investigation performed in this site varies widely between SPT for the design phase, dynamic cone (DCPT) and Spectral Analyses of Surface Waves (SASW) during the reconnaissance efforts and Swedish Weight Sounding (SWS) and Cone Penetration Testing (CPT) later. Simplified liquefaction assessments have been performed for the different tests available. Further details on this building can be found in Bray et al. (2012).

B.2. SEISMOLOGICAL AND GROUND MOTIONS ASPECTS

The $M_w = 8.8$ February 27th 2010 Maule earthquake occurred in a subduction zone in which the Nazca plate subducts beneath the South American plate. The rate of convergence of the plates is estimated to be 70 mm/yr. The event occurred at 3:34 am local time and its epicenter was located at $36^{\circ}17'23.20''$ $73^{\circ}14'20.00''$ W, according to Renadic (Chilean National Network of Accelerometers from the Universidad of Chile).

The USGS moment tensor solution gives a seismic moment of 1.8×10^{22} N·m, a moment magnitude $M_w=8.8$ and a hypocentral distance of 30 km. It was estimated that the critical nodal plane for the moment tensor solution strikes at an azimuth of 14° and dips at 19° to the east. The aftershock distribution indicates an approximation of the rupture area of 95.000 km^2 (530 km long by 180 km wide). Figure B.1 shows a map with the rupture area, aftershock distribution and the epicenter.

The site studied herein (Condominium Los Presidentes, $36^{\circ}47'26.74''$ S, $73^{\circ} 4'53.22''$ W) is located 57 km away from the epicenter at an azimuth of 166° approximately (Figure B.2.a). The site is located between the cities of Talcahuano (North-West from the site) and Concepcion (South-east from the site). The nearest seismic station is called SMA-1 and is located in Concepcion, at about 5 km southwest from the site, as shown in Figure B.2.b.

Figure B.3 shows the acceleration time-histories for the three channels (longitudinal, vertical and transversal) for seismic station SMA-1. The peak accelerations are 0.4, 0.284 and 0.398 for the longitudinal, transversal and vertical directions respectively. The peak acceleration that will be used for the liquefaction evaluation is the geometric mean of both horizontal components, which is $PGA_{GM} = (PGA_L \cdot PGA_T)^{0.5} = 0.34 \text{ g}$.

B.3. SITE INVESTIGATION

Site investigation in this site has been performed in five stages at different times:

1. Site investigation for the design of the building (February 2006): Consisted of three Standard Penetration Tests (SPT) without energy measurements and without any information about type of hammer used.
2. Site investigation performed after the earthquake (March 2010) as part of the GEER report (GEER, 2010). Consists of two Dynamic Cone Penetration Tests (DCPT) and Shear Wave Velocity measurement using Spectral Analysis of Surface Waves (SASW).
3. Site investigation performed by the owners of the building after the earthquake (October 2011). Consisted of two SPTs without energy measurements or information about the type of hammer used.
4. Site investigation performed in December 2013. Consists of eleven Swedish Weight Sounding (SWS) Tests.
5. Site investigation performed in July 2016. Consisted of six Cone Penetration Tests (CPT), one of them with shear wave velocity measurements.

The geotechnical design of the buildings included soil replacement because the site consisted of marshy ground before being developed. Also, the site was susceptible to flooding and it had been used previously to deposit low quality earth materials that were not adequate for construction (Empro, 2006). This replacement was to be performed in an area equal to the area of the building plus two meters in each direction and the slopes of the excavation was specified to be 1:1.5 (H:V). The material for replacement was specified to be Bio Bio river sand to be compacted to a relative density equal or greater than 75% (Empro, 2006). Because the site had different conditions before the development of the buildings, the two cases will be presented herein; the pre-construction and post-construction conditions. Figure B.4 shows a plan view of the four buildings and other two buildings that were planned and designed but not constructed together with the site investigation (three SPTs) prior to construction. Although no energy measurements were taken or any information about the type of hammer used was given, engineers in the area affirmed that it is very standard in practice in Concepcion to do the SPT with the donut hammer. So the assumption of donut hammer was taken and the measured N values were multiplied by a C_E value of 0.75 to obtain N_{60} . Section A-A from Figure B.5 is shown in Figure B.5, which shows the general site conditions prior to construction, consisting of: 1) A loose sand layer (SP) with N_{60} values between 6 and 10 with a thickness of 1.5 to 2 m. 2) A low plasticity silt (ML) with very low N_{60} values (< 5) and a thickness of about 1 m. 3) A medium dense to dense coarse sand with some gravel content and with very small fines content, classifying as SP-SM with thickness of about 1.5 to 3 m. 4) A medium stiff low plasticity silt (ML) with N_{60} values in the order of 10-15 and thickness of 1 to 3 m. 5) A dense sand layer (SP/SM/SW) is encountered with N_{60} in the order of 40. Within this layer, towards the south a low plasticity silty/sand sandy/silt is encountered with N_{60} values below 10.

Figure B.6 shows the plan view of the four constructed buildings together with the site investigations performed after the earthquake. The cross sections A'-A', to D'-D' depicted in Figure B.6 are shown in Figures B.7 to B.10 respectively. Similarly, the cross sections 1-1 and 2-2 are shown in Figures B.11 and B.12 respectively. For the SPTs performed after the earthquake the same assumption of a donut hammer was made to estimate N_{60} . In Figures B.7 to B.12, the SPTs are shown in terms of N_{60} and also shown is the fine contents (FC). The SPTs went to a

depth of about 15 m each. For the SWS testing it is shown the measured N_{SW} value and also N_{60} , which was obtained through a correlation between N_{SW} and N_{60} (Tsukamoto et al. 2004). Test SWS-11, in cross section C-C shows also the W_{SW} value because this value it is important for soft soils, which were encountered in this particular test. Most of the SWS tests had a depth of 3 to 5 m, but the deepest test was SWS-9, which reached a depth of 6 m. The CPTs in Figures B.7 to B.11 are shown in terms of the normalized tip resistance (Q_{tn}) and the soil behavior type index (I_C). The CPTs were performed to a depth of 10 m, with the exception of CPT-1 which reached a depth of 30 m.

The water table was founded a different depths depending on the site investigation. The GEER team that went to the site on March 17th 2010 observed the water table at 0.5 meters depth. The GEER team that went on March 25th 2010 to perform the DCPT and Shear Wave Velocity Testing encountered water at 1.7 meters depth. The SPTs performed in October 2011 report the groundwater table at a depth of 1.25 m for S-1 and 1.4 for S-2. The site investigation that took place in December 2013 measured water tables at depth ranging from 0.9 to 1.4 meters. Finally in July 2011, the water table was found at depths ranging from 2.7 to 3.5 m. The likely water table at the time of the earthquake is 1 m.

B.4. DESCRIPTION OF THE BUILDINGS

The four buildings have identical floor plans and structural details. The construction of the southern buildings (Riesco and Errazuriz) was around 2006-2007. The other two buildings were constructed two years later and were not fully occupied at the time of the earthquake. The two buildings constructed later (Montt and Bulnes) had a different contractor than the previous built structures. Riesco and Errazuriz towers were demolished as the result of the earthquake damage. The footprint of the building was about 25 m long and 13.6 m wide with a height of 21 m.

The structural system of the 8-story buildings consisted generally of several reinforced concrete (RC) shear walls with thickness of 0.15 m tied to each other with RC coupling beams of different sizes depending on the location of the beams within the building. The floor units consisted of a RC slab with thickness of 0.14 m with the exception of the 8th story which had a thickness of 0.12 m. The foundation system is complex, but is mainly composed of 0.6 m thick strip footings that receive the shear walls. The width of the footing is variable across the entire footprint of the building as shown in Figure B.13, but it ranges between 1.40 and 2 m. The embedment depth of the foundation is specified in the building plans as being minimum 1 m below the ground surface and the embedment depth of the strip footings for the elevator shear walls is 1.8 m.

In Figure B.13 is also shown in red the shear walls of the building. Some of these shear walls are 19.8 high and 0.15 meters thick. The perimeter walls parallel to the longitudinal axis of the building are connected by coupling beams with varying depth depending on where the shear walls are connected. The middle wall parallel to the longitudinal axis of the building consists of two different shear walls of 9.6 m length, which in the center is separated by the entrance hall to the apartments. The perimeter walls parallel to the transverse axis of the building are shear walls of 6.3 m length over all the height of the building. This shear wall arrives to a 0.6 m deep, 2 m wide strip footing. The distance between floors is 2.3 m and the total height of the building is 21 m.

B.5. PERFORMANCE OBSERVATIONS AND ANALYSES

Details about the seismic performance of the building are found in Bray et al. (2012) with additional details given herein. Near the buildings, there were observations of sediment ejecta, ground cracking, ground and building settlements. These observations were particular to this site. Nearby areas such as streets or adjacent one- and two-story homes did not show evidence of soil liquefaction. The ejecta observed in the site was primarily composed of well-graded silty sand with approximately 10-15% non-plastic fines (Bray et al., 2012). Sediment ejecta and water stains were observed in the NE corner of the Riesco building, where also most of the building settlement was measured.

The performance of the building has been evaluated based on measurements taken during the reconnaissance efforts (summarized in Bray and Frost, 2010 and Bray et al. 2012), which included in-situ measurements of settlements and tilting and also LiDAR data collected from the GEER team. During the reconnaissance, settlement measurements were taken relative to the ground adjacent to the Bulnes Building, which did not appear to settle relative to the surrounding ground. The northeast corner of the Riesco Building displaced downward about 40 cm with respect to the ground adjacent to the Bulnes Building. In contrast, the southern end of the Riesco Building settled only 10 cm, while the ground surrounding the building settled about 20 to 25 cm in the southern section. The northern end of the Riesco Building tilted approximately 1° to the east and 1° to the north as a result of the differential movement across the building. Figure B.14 (a) shows the sand ejecta and water stains in the NE corner of Riesco Building. Figure B.14 (b) shows that same corner and it clearly shows a sharp settlement in the ground where the “improved” soil was placed. Figure B.15 shows the measured settlements and tilt in the Riesco Building based on data collected in-situ. Structural damage within the buildings included shear failure of coupling beams due to differential settlements, shear cracking of structural walls. Non-structural damage in partition walls was also observed.

LiDAR data was later collected and the results agree in general with observed measurements taken (Kayen, 2016). Figure B.16 shows a shot from the LiDAR where it is observed a sharp settlement that clearly corresponds to the boundary where the “soil improvement” was located during the construction of the buildings. Table B.2 provides the results of the LiDAR-based building settlements using as a datum the top of the Bulnes Building which appear to not have displaced. It can be seen that the Montt building either settled uniformly about 2 cm or it was constructed 2 cm lower or shorter. Errazuriz building settled differentially towards the North by an amount of 1.5 to 2 cm approximately. Riesco’s NE corner settled about 35 cm compared to the Bulnes building. Differential settlement in the NS direction was about 15 to 20 cm.

Simplified liquefaction evaluation and volumetric settlements estimation have been performed for the different in-situ tests. In general, more weight has been given to the results of the CPT because of its numerous advantages in respect to the other tests. In Appendix B.1 the results of simplified liquefaction evaluations are shown for the testing described in Section B.3. Table B.2 summarizes the results for the CPT in terms of volumetric-induced settlements obtained from the Zhang et al. (2002) method and based on the Boulanger and Idriss (2016) liquefaction triggering evaluation and also the Liquefaction Severity Number (van Ballegooy et al., 2014).

B.6. CONCLUSIONS

The Condominium Los Presidentes, located in the city of Concepcion, Chile, consisted of four identical buildings located at close proximity. Before the development of the project, the site was subjected to flooding and the soil consisted of marsh deposits. Thus, the design of the building included soil replacement in the area below the buildings to a depth of 6 m. The soil was replaced with Bio Bio River Sand, and it was specified to be compacted to relative density greater than 75%. In February 27th, 2010, the Maule earthquake resulted in high ground motions in the area of Concepcion. As a result, the four buildings had different performance despite their identical structural configuration and ground motion intensity (the buildings are only separated 25 m away from each other). The difference in performance is attributed to the ground modification performed; poor compaction of the soil that was replaced in the two southern buildings (Riesco and Errazuriz) resulted in significant settlement and tilting of the structure with the consequence of severe damage in structural elements. The damage ultimately resulted in the demolition of the two buildings.

B.7. REFERENCES

- Bray, J.D. and Frost, D. (2010). "Geo-engineering Reconnaissance of the 2010 Maule, Chile Earthquake". GEER Association Report No. GEER-022.
- Bray, J.D., Rollins, K., Hutchinson, T., Verdugo, R., Ledezma, C., Mylonakis, G., Assimaki, D., Montalva, G., Arduino, P., Olson, S.M., Kayen, R., Hashash, Y.M.A, and Candia, G. (2012). "Effects of Ground Failure on Buildings, Ports, and Industrial Facilities". *Earthquake Spectra*: June 2012, Vol. 28, No. S1, pp. S97-S118.
- Idriss, I.M. and Boulanger, R. "Soil Liquefaction during Earthquakes". Oakland, CA: EERI, 2008.
- Instituto de Investigaciones Tecnológicas - Soil Mechanics Laboratory Concepcion University (2011) "Soil Mechanics Report". Concepcion, October, 2011.
- Kayen, R. (2016), personal communication.
- Ltda., EMPRO (2006) "Soil Mechanics Report for Santa Maria Valley". Concepcion, February, 2006.
- Japanese Industrial Standard (1983) "Method of swedish weight sounding" Japanese Standards Association, 1983 (revised in 1995)
- Tsukamoto, Y., Ishihara, K., Sawada, S. (2004) "Correlation between penetration resistance of swedish weight sounding tests and SPT blow counts in sandy soils". *Soils and Foundations*, Vol. 44, No.3, pp 13-24
- van Ballegooy, S., Malan, P., Lacrosse, V., Jacka, M.E., Cubrinovski, M., Bray, J.D., O'Rourke, T.D., Crawford, S.A., and Cowan, H. (2014). "Assessment of Liquefaction-Induced Land Damage for Residential Christchurch." *Earthquake Spectra Journal*, Earthquake Engineering Research Institute, 30(S1), 31-55.
- Universidad de Chile, Facultad de Ciencias Físicas y Matemáticas, Departamento de Ingeniería Civil (2010) "Registros del Terremoto de Maule Mw=8.8 27 de Febrero 2010" Rev. 2: Octubre, 2010.
- Zhang, G., Robertson, P.K. and Brachman, R.W.I. (2002). "Estimating Liquefaction Induced Ground Settlements from CPT for Level Ground." *Canadian Geotechnical Journal*, Ottawa, 39(5):1168-1180.

Table B.1. LiDAR-based settlements from the four buildings in the Condominium Los Presidentes.

Building	NE	NW	SE	SW
Bulnes	0	0	0	0
Montt	1.9	1.8	2.2	2.0
Errazuriz	9.0	10.7	8.8	7.6
Riesco	34.5	19.7	12.8	6.9

Table B.2. Results of CPT-based analyses

Test	Settlement (cm)	LSN
CPT-1	10	25
CPT-2	6	25
CPT-3	10	48
CPT-4	19	69
CPT-5	17	77
CPT-6	11	46

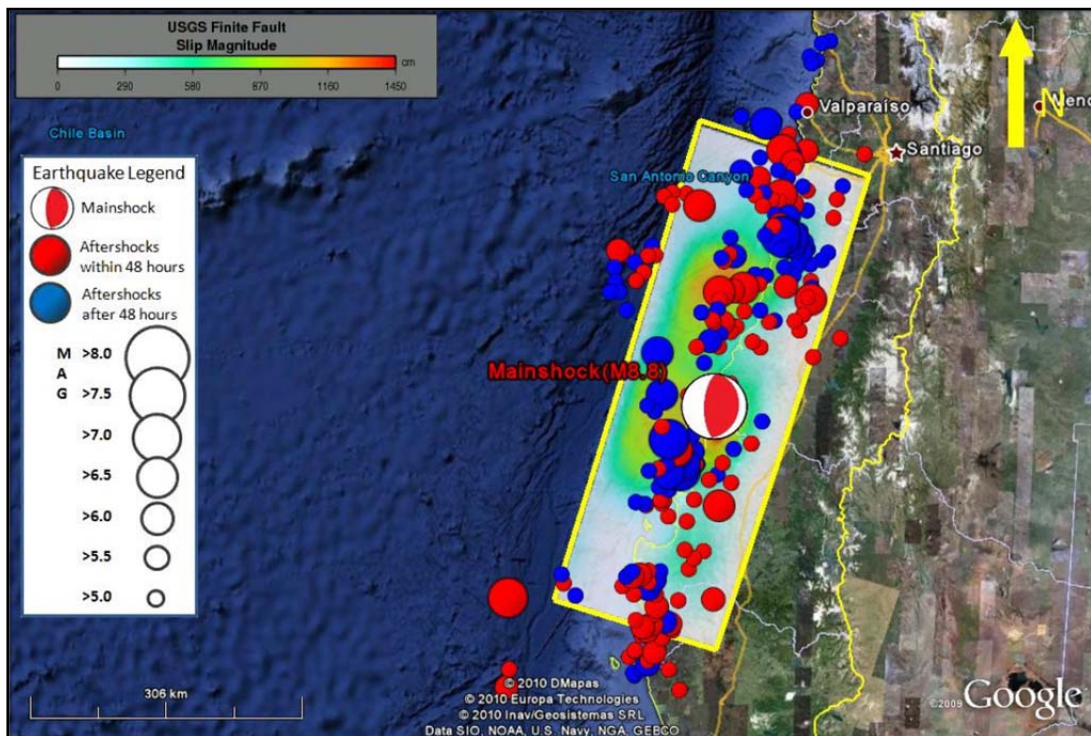


Figure B.1. Map with rupture area (yellow line), aftershock distribution (red and blue circles) and epicenter (moment tensor solution) from Bray and Frost, 2010



Figure B.2. Location of Condominium Los Presidentes respect to the earthquake epicenter and location of the condominium respect to the near strong ground motion station SMA-1.

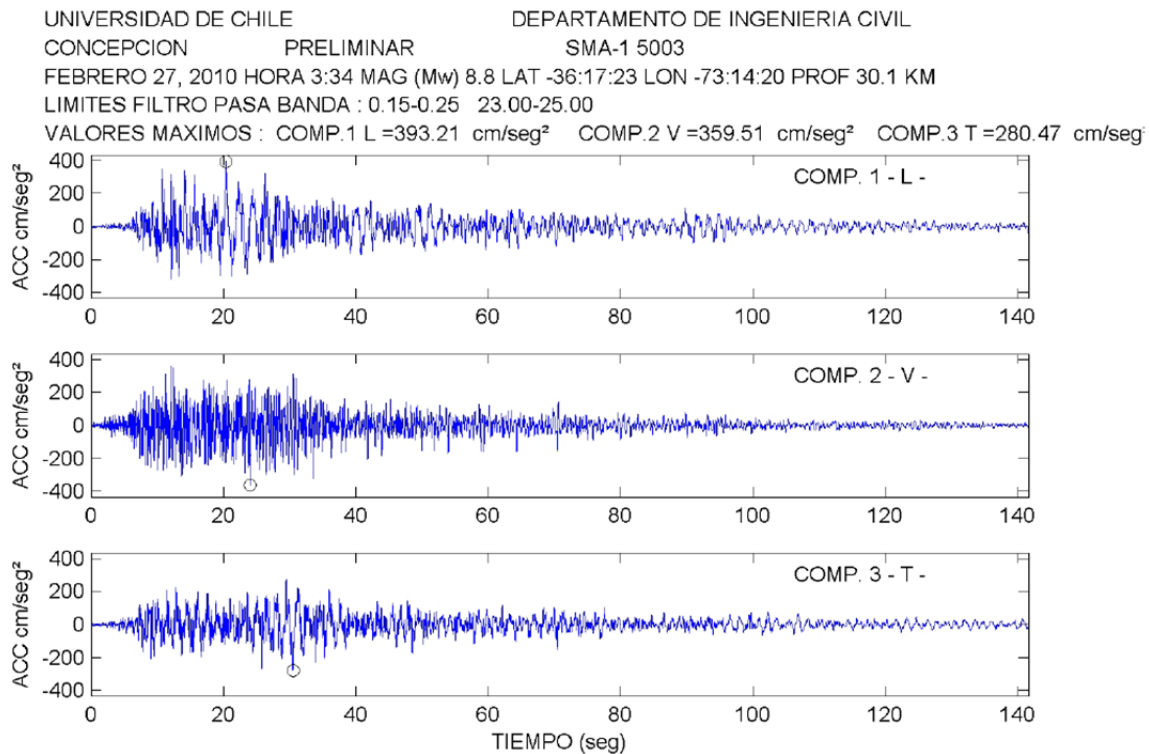


Figure B.3. Seismic records of the tree components in seismic station located in Concepcion

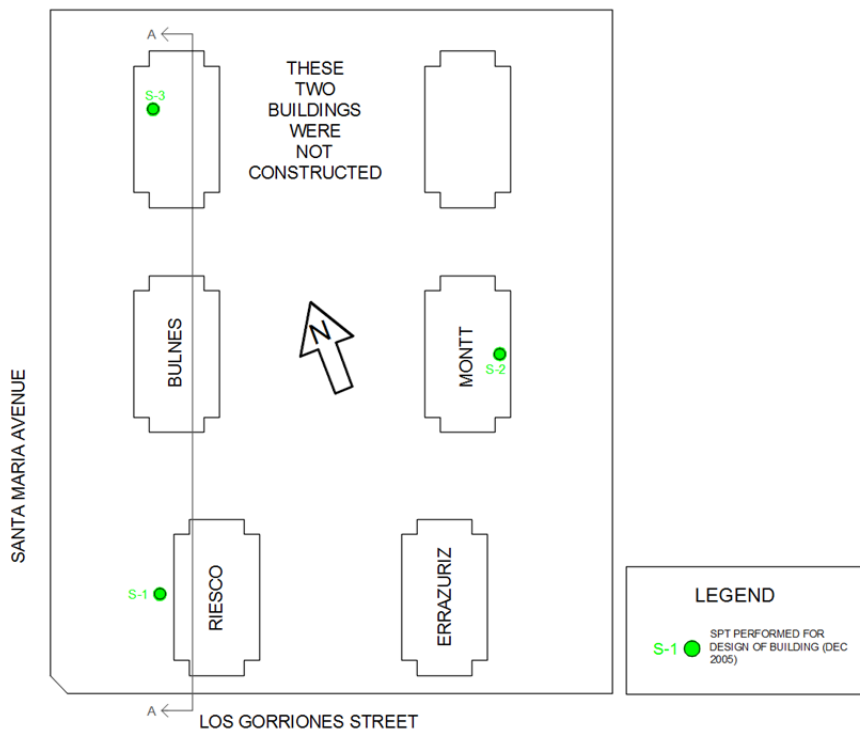


Figure B.4. Plan view of the site investigation performed prior to construction of the buildings during the design phase.

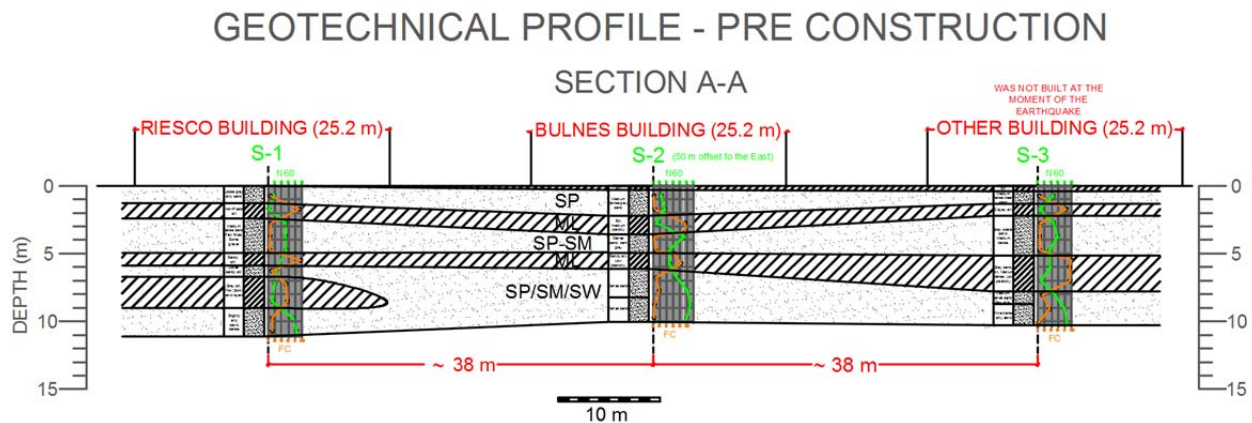


Figure B.5. Site conditions based on investigation performed prior to construction of the buildings during the design phase.

POST EARTHQUAKE FIELD INVESTIGATION

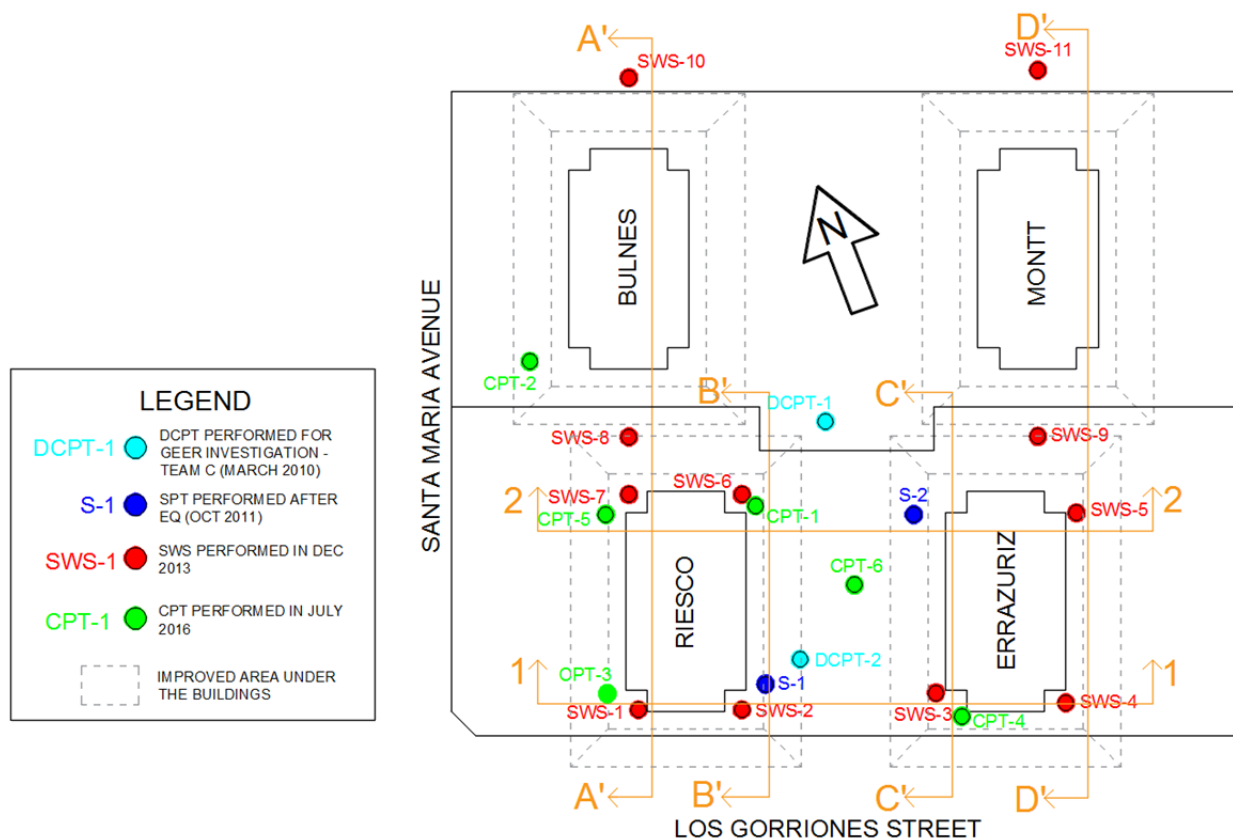


Figure B.6. Plan view of the four buildings together with the site investigation performed after the earthquake, showing also the area of replaced soil as specified in the geotechnical design report.

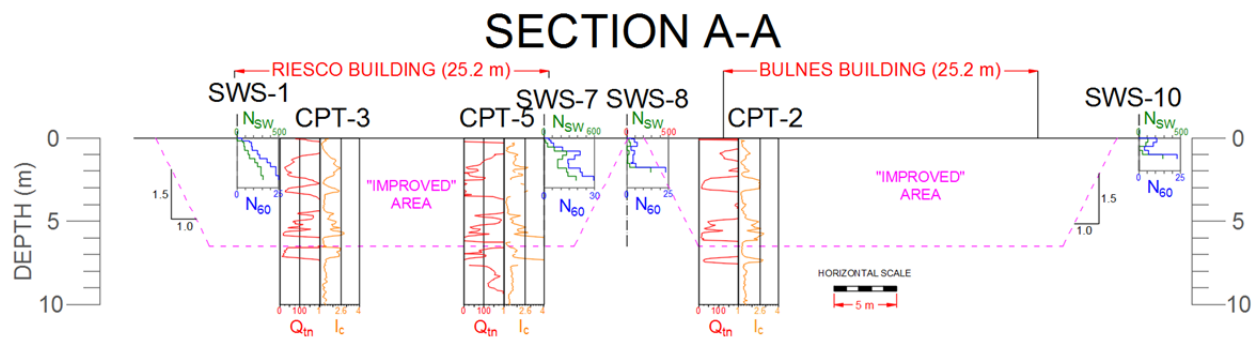


Figure B.7. Section A-A through the west side of buildings Riesco and Bulnes.

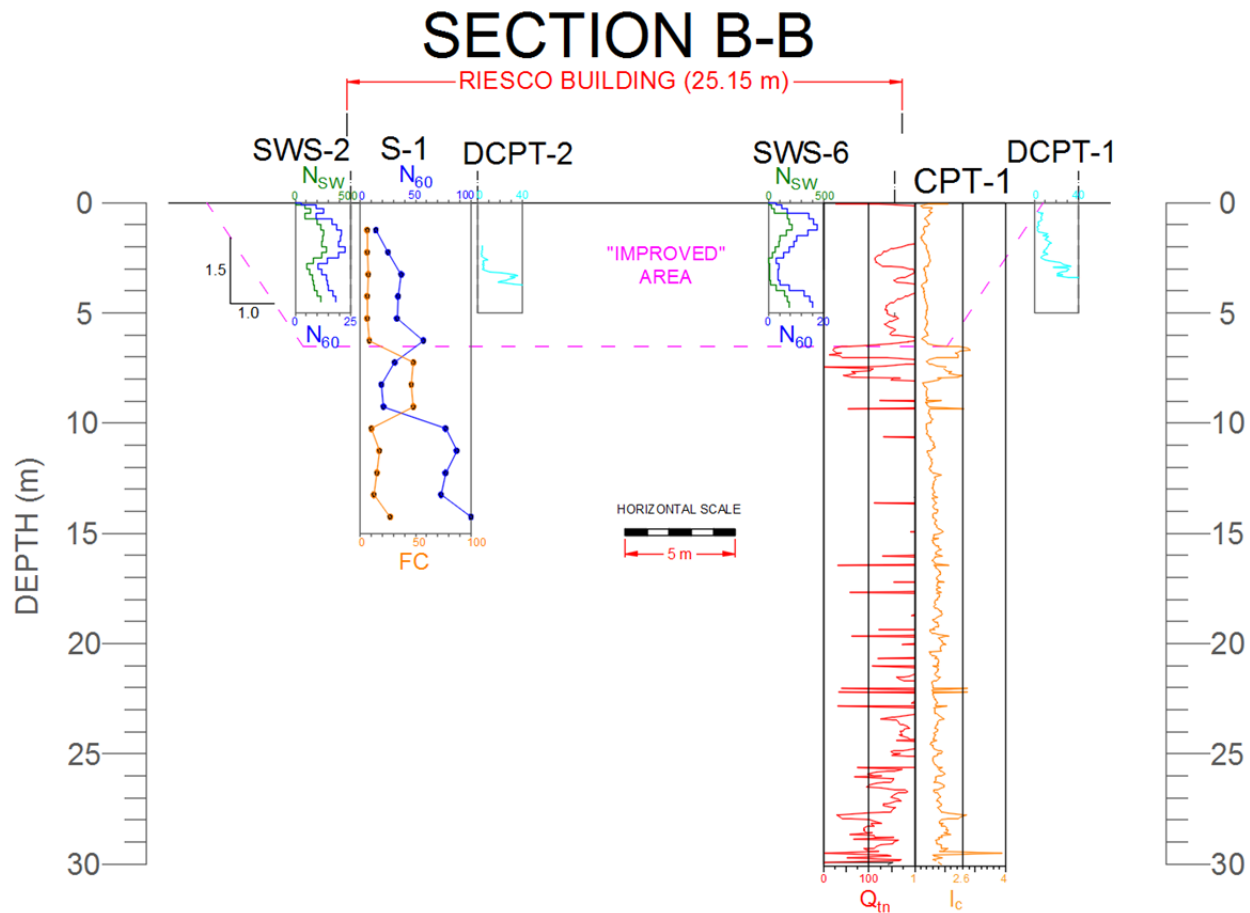


Figure B.8. Section B-B through the east side of Riesco Building.

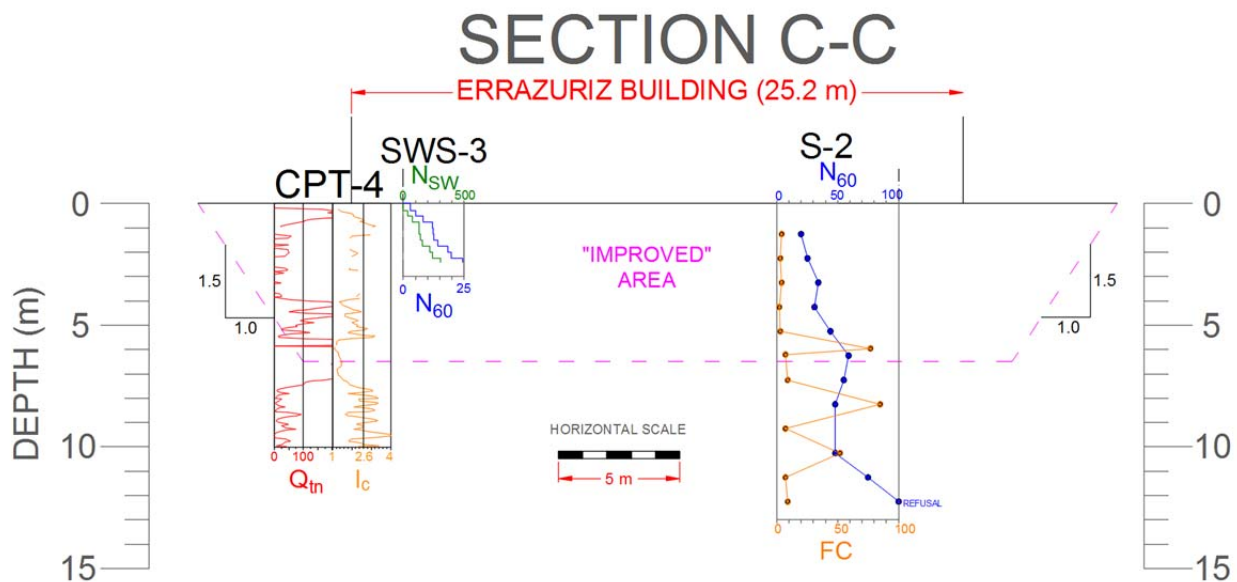


Figure B.9. Section C-C through west side of Errazuriz and Montt Buildings.

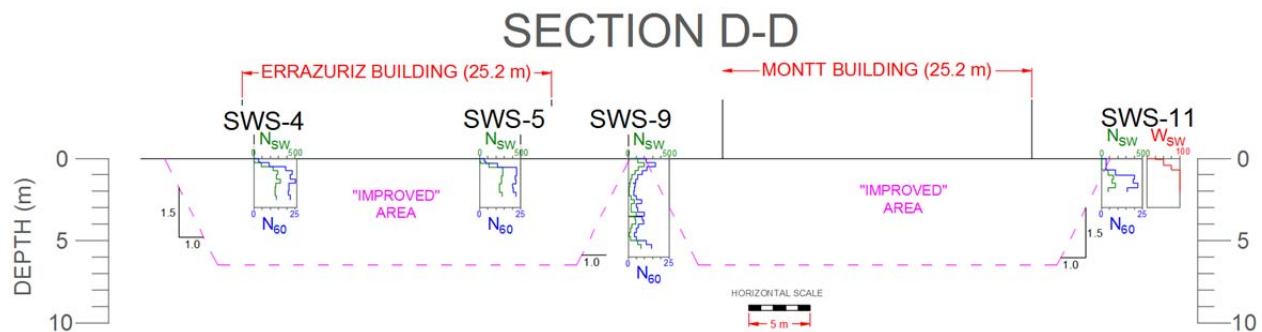


Figure B.10. Section D-D through east side of Errazuriz and Montt Buildings.

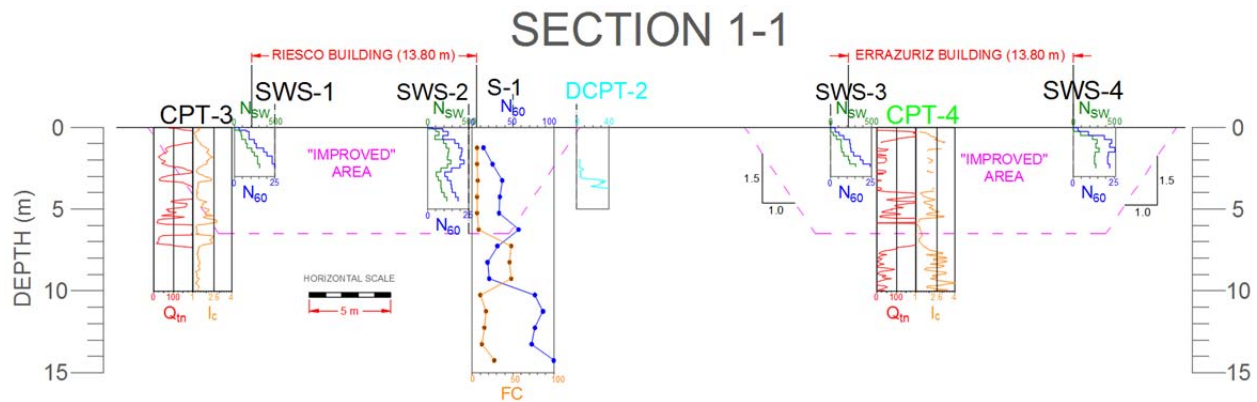


Figure B.11. Section 1-1 through the south side of Buildings Riesco and Errazuriz

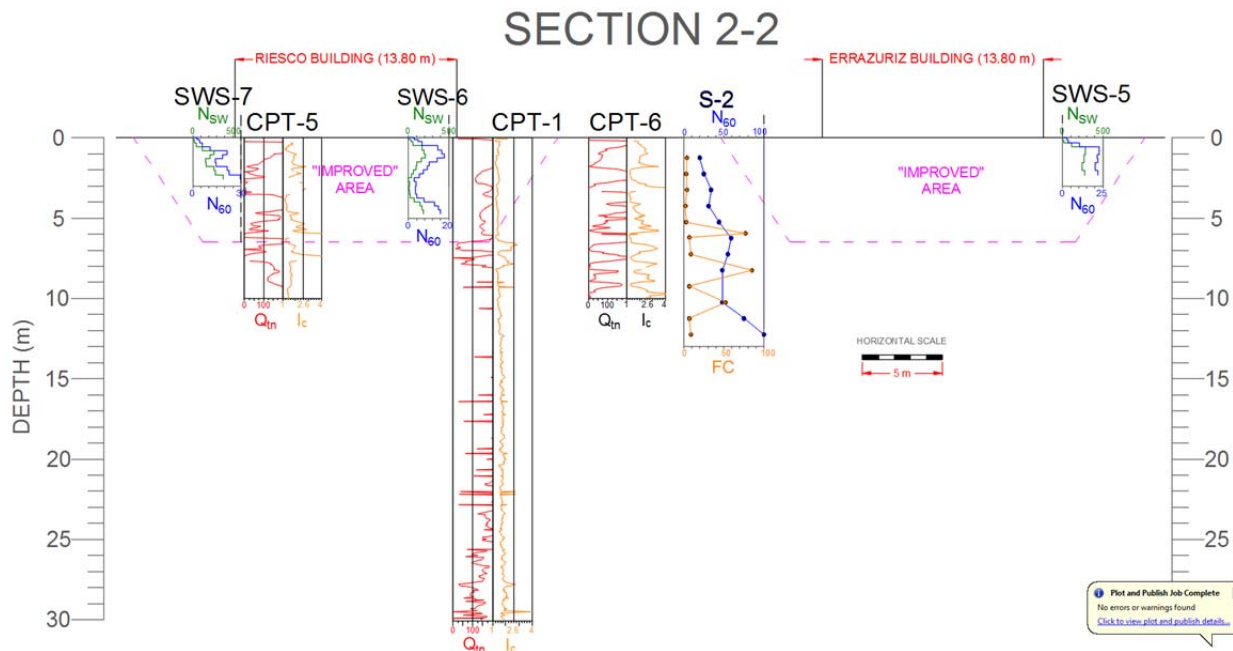


Figure B.12. Section 2-2 through the north side of Buildings Riesco and Errazuriz

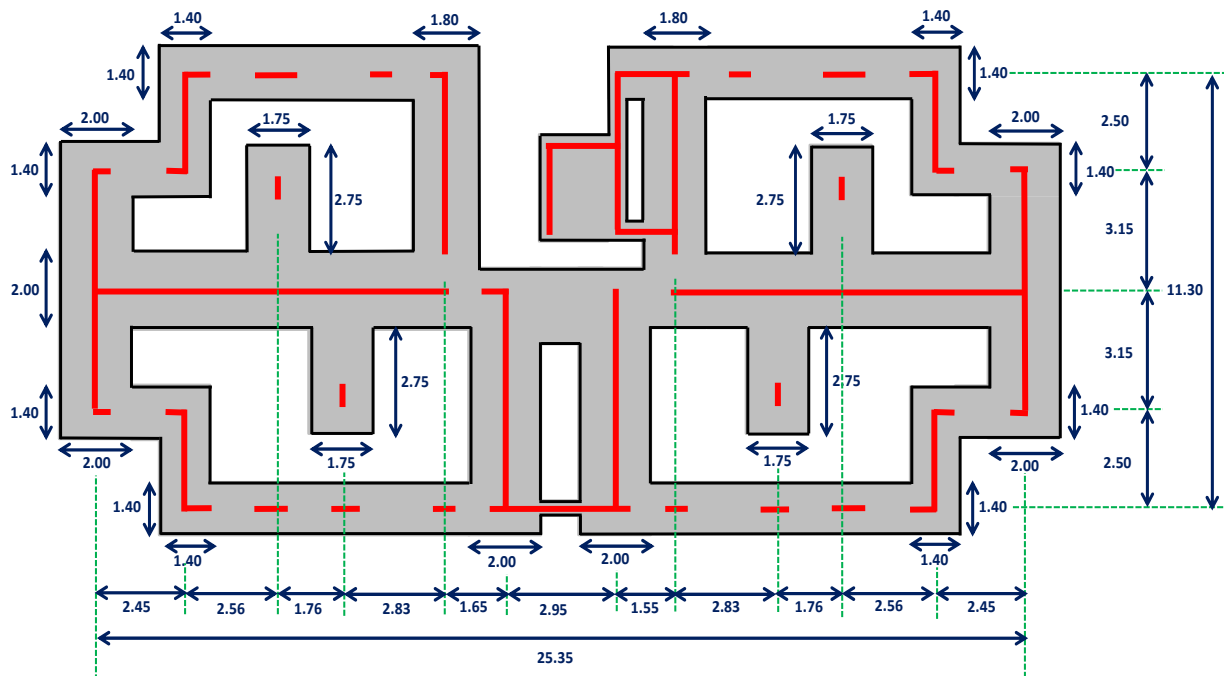


Figure B.13. Plan view of the foundation system of the four buildings.



Figure B.14. Sediment ejecta and water stains in the wall located in the NE corner of the Riesco Building (From Bray et al., 2012)

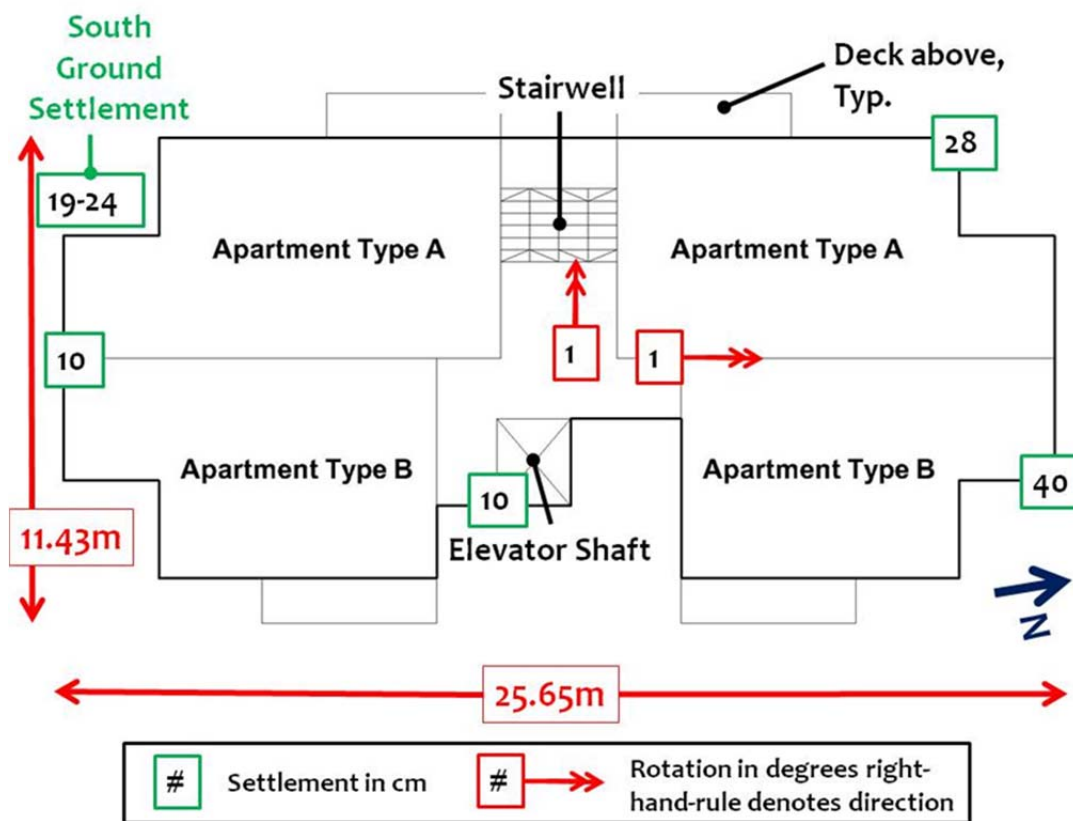


Figure B.15. Settlement and tilting measurements from the Riesco Building (From Bray et al. (2012))



Figure B.16. LiDAR photography for Riesco Building from Kayen (2016), personal communication.

Appendix C - Ground Motions for use in
Numerical Soil-Structure-Interaction (SSI)
Dynamic Analyses of case histories in
Christchurch, New Zealand

APPENDIX C: GROUND MOTIONS FOR USE IN NUMERICAL SOIL-STRUCTURE-INTERACTION (SSI) DYNAMIC ANALYSES OF CASE HISTORIES IN CHRISTCHURCH, NEW ZEALAND

C.1. DESCRIPTION OF PROCEDURE

Digital files provided by Markham (2015) were given. The files correspond to deconvolved within acceleration records to the Riccarton Gravel at two stations (RHSC and CASC) for two components (fault normal and parallel) and for three earthquakes (Darfield, Christchurch and June 2011). The acceleration records are going to be modified to be used in the numerical analyses at five sites of interest:

- FTG-7 building (Chapter 3)
- CTUC building (Chapter 3)
- PWC building (Chapter 4)
- CTH building (Chapter 4)
- C building (Appendix A)

The direction of the frames of the five buildings coincides with the NS and EW directions. Thus, the accelerations records were rotated to have these components instead of fault normal and fault parallel. These ground motions need also to be scaled such that they have a representative source – site distance for each event and also representative site conditions. The scaling factor was estimated based on Bradley (2012) GMPE. The approach for estimating the scale factor is described:

1. Calculate the 5% damping response spectra using the GMPE for each station where the motions were deconvolved (RHSC and CASC) using the corresponding source-to-site distance (R_{RUP}) and the shear wave velocity (V_S) of the Riccarton Gravel at that site.
2. Calculate the 5% damping response spectra using the same GMPE for each site (FTG7, CTUC, PWC, CTH and C buildings) using the corresponding R_{RUP} and the V_S of the Riccarton gravel at that site.
3. Divide the two spectra and calculate an average scaling factor

C.2. SOURCE PARAMETERS FOR EACH EVENT

Bradley (2012) GMPE requires the following source parameters to be used: magnitude (M_W), reverse fault flag (F_{RV}), normal fault flag (F_{NM}), depth to top of the rupture (Z_{TOR}) and dip angle (δ). These were obtained from Bradley Metadata files (Bradley, personal communication). Table C.1 shows the source parameters used.

C.3. SITE PARAMETERS FOR EACH SITE

The site parameters to be used for the GMPE are the shear wave velocity in the upper 30 m (V_{S30}) and the depth at which the shear wave velocity is equal to 1 km/s ($Z_{1.0}$). In this case, instead of the actual V_{S30} for each site, the V_S of the Riccarton Gravel has been used as we want to get the difference between the stations where the deconvolution was performed and the actual sites where the Riccarton Gravel will be used as a rigid base in the numerical model. The best estimates of shear wave velocities for the Riccarton Gravel at the stations RHSC and CASC as well as for the buildings are specified in Table C.2. When specific data for the estimation of V_S for the Riccarton Gravel was not available, the data available in the NZGD was used and also data provided by Bradley (personal communication). The parameter $Z_{1.0}$ was taken from Bradley's Metadata and was found to be 332 for all stations near the CBD including RHSC and CASC, so this value was not changed for the sites in the CBD.

C.4. PATH PARAMETERS: SOURCE TO SITE DISTANCE (R_{RUP})

The source – site distance for the seismic stations have been taken from Bradley (2014). The R_{RUP} for the sites has been interpolated from the R_{RUP} of the several seismic stations in Christchurch. The R_{RUP} used for the stations has been obtained from Bradley's Metadata. Table C.3 shows R_{RUP} for each station and site for each of the three events investigated.

C.5. SCALING FACTOR

With all the parameters described above, the GMPE can be used and the procedure described above can be used. The results of the average scaling factor are shown for the five sites and the two seismic stations in Table C.4. In total, for each building, this procedure will give a total of twelve ground motions (2 components, 2 deconvolved stations, three earthquakes).

Table C.1. Source parameters for each event

PARAMETER	DARFIELD	CHRISTCHURCH	13-JUN-2011
M_W	7.1	6.2	6.0
F_{RV}	0	1	0
F_{NM}	0	0	0
Z_{TOR}	0	0.50	1.41
Dip angle	82.2	69	67

Table C.2. Shear wave velocity (V_S) of the Riccarton Gravel for the stations RHSC and CASC and for the sites.

PARAMETER	Buildings						
	RHSC	CASC	FTG-7	CTUC	PWC	CTH	C
V_S (m/s)	460	460	350	400	400	400	350

Table C.3. R_{RUP} (km) for stations where deconvolution was performed for each earthquake and for the analyzed sites

Event	RHCS	CACS	FTG7	CTUC	PWC	CTH	C
Darfield	10	11.7	15.9	16.2	15.8	15.7	15.3
Christchurch	6.5	12.8	4.2	3.8	4.1	4.4	4.3
13-Jun-11	11.8	16.2	6.3	6	6.32	6.5	6.75

Table C.5. Average scaling factors for each earthquake, for the two seismic stations and for the five buildings.

Event	FTG7/RHSC, FTG/CASC	CTUC/RHSC, CTUC/CASC	PWC/RHSC, PWC/CASC	CTH/RHSC, CTH/CASC	C/RHSC, C/CASC
Darfield	0.686, 0.711	0.674, 0.758	0.742, 0.831	0.747, 0.836	0.721, 0.806
Christchurch	1.31, 2.367	1.378, 2.491	1.367, 2.414	1.321, 2.331	1.392, 2.462
13-Jun-11	1.748, 2.483	1.811, 2.573	1.800, 2.529	1.766, 2.480	1.804, 2.535